



HAL
open science

Thermochemical energy storage on "salt/supports" composites

Minh Hoang Nguyen

► **To cite this version:**

Minh Hoang Nguyen. Thermochemical energy storage on "salt/supports" composites. Material chemistry. Université de Haute Alsace - Mulhouse, 2022. English. NNT : 2022MULH5666 . tel-04128297

HAL Id: tel-04128297

<https://theses.hal.science/tel-04128297>

Submitted on 14 Jun 2023

HAL is a multi-disciplinary open access archive for the deposit and dissemination of scientific research documents, whether they are published or not. The documents may come from teaching and research institutions in France or abroad, or from public or private research centers.

L'archive ouverte pluridisciplinaire **HAL**, est destinée au dépôt et à la diffusion de documents scientifiques de niveau recherche, publiés ou non, émanant des établissements d'enseignement et de recherche français ou étrangers, des laboratoires publics ou privés.

Année 2022

N° d'ordre : (attribué par le SCD)

UNIVERSITÉ DE HAUTE-ALSACE
UNIVERSITÉ DE STRASBOURG

THESE

Pour l'obtention du grade de

DOCTEUR DE L'UNIVERSITÉ DE HAUTE-ALSACE

ECOLE DOCTORALE : Chimie et Chimie Physique (ED 182)

Discipline : Chimie des matériaux

Présentée et soutenue publiquement

par

Minh-Hoang NGUYEN

Le 14 Novembre 2022

Stockage de chaleur thermochimique sur des composites « sel/supports »

Sous la direction de Mme Simona BENNICI, Directrice de recherche, CNRS,
Et de M. Patrick DUTOURNIÉ, Professeur, Université de Haute-Alsace.

Jury :

M. Jerzy ZAJAC, Professeur, Université de Montpellier (Rapporteur)

M. Loïc FAVERGEON, Maître de conférences, École des Mines de Saint-Étienne (Rapporteur)

M. Simone MANCIN, Maître de conférences, Université de Padoue, Italie (Examineur)

Mme Simona BENNICI, Directrice de recherche, IS2M, Mulhouse (Directrice de thèse)

M. Patrick DUTOURNIÉ, Professeur, Université de Haute-Alsace (co-Directeur de thèse)

TABLE OF CONTENTS

General Introduction	1
Chapter I. The State-of-the-art of Thermochemical Heat Storage	13
Chapter II. Methods, experimental techniques and materials	55
Chapter III. Thermochemical sorption heat storage: Investigate the heat released from activated carbon beads used as porous host matrix for MgSO ₄ salt.....	66
Chapter IV. Toward new low-temperature thermochemical heat storage materials: Investigation of hydration/dehydration behaviors of MgSO ₄ /hydroxyapatite composite.....	81
Chapter V. Heat storage: Hydration investigation of MgSO ₄ /active carbon composites, from material development to domestic applications scenarios	96
Chapter VI. ‘Corn cobs’ biochar as a macroporous host of salt hydrates for heat storage applications.....	111
Chapter VII. Fast hydration kinetics and remarkable heat storage capacity of new binary salt materials for heat storage applications	132
General Conclusion	166
RÉSUMÉ	172

PRODUCTION SCIENTIFIQUE

Liste des publications

- **Nguyen, M.H.**; Bennici, S. Recent progresses in Thermochemical Heat Storage: materials and applications M. Jeguirim Ed. Recent Advances in Renewable Energy Technologies 1st edition, Elsevier 2021, ISBN 978-0-323-91093-4, Chapter 8, p.281-310., doi:10.1016/B978-0-323-91093-4.00008-1.
- Bennici, S.; Dutournié, P.; Cathalan, J.; Zbair, M.; **Nguyen, M.H.**; Scuiller, E.; Vaultot, C. Heat storage: Hydration investigation of MgSO₄/active carbon composites, from material development to domestic applications scenarios. *Renew. Sustain. Energy Rev.* **2022**, *158*, 112197, doi:10.1016/j.rser.2022.112197.
- **Nguyen, M.H.**; Zbair, M.; Dutournié, P.; Gervasini, A.; Vaultot, C.; Bennici, S. Toward new low-temperature thermochemical heat storage materials: Investigation of hydration/dehydration behaviors of MgSO₄/Hydroxyapatite composite. *Sol. Energy Mater. Sol. Cells* **2022**, *240*, 111696, doi:10.1016/j.solmat.2022.111696.
- **Nguyen, M.H.**; Zbair, M.; Dutournié, P.; Bennici, S. Thermochemical sorption heat storage: Investigate the heat released from activated carbon beads used as porous host matrix for MgSO₄ salt. *J. Energy Storage* **2023**, *59*, 106452, doi:10.1016/j.est.2022.106452
- Zbair, M.; **Nguyen, M.H.**; Dutournié, P.; Bennici, S. Fast hydration kinetics and remarkable heat storage capacity of new binary salt materials for heat storage applications. (*submitted to Applied Energy*).
- **Nguyen, M.H.**; Zbair, M.; Dutournié, P.; Bennici, S. “Corn cobs” biochar as a macroporous host of salt hydrates for heat storage applications. (*submitted to Biochar*).

Liste des présentations orales

- **M.H. Nguyen**, S. Bennici, P. Dutournié. Hydration behavior of MgSO₄/HAP composites for thermochemical heat storage. 3rd Young Scientists Day, videoconference, 04/02/2021.
- **M.H. Nguyen**, M. Zbair, S. Bennici, P. Dutournié. Thermochemical heat storage: potential materials of different porous support impregnated with MgSO₄. Calorimetry and Thermal Analysis days – 52nd edition, Colmar (France), 16/06/2022.
- **M.H. Nguyen**, M. Zbair, S. Bennici, P. Dutournié. Hydration behavior of MgSO₄ impregnated in different porous support as potential long-term heat storage materials. 9th International Conference on Engineering for Waste and Biomass Valorization, Copenhagen (Denmark), 27/06/2022.
- **M.H. Nguyen**, M. Zbair, P. Dutournié, S. Bennici. Thermochemical sorption heat storage using activated carbon beads as a porous host matrix for MgSO₄ salt. 14th International Green Energy Conference, videoconference, 07/07/2022.
- S. Bennici, **M.H. Nguyen**, M. Zbair, P. Dutournié, C. Vaultot. Stockage de la chaleur par des composites MgSO₄/support carboné : du développement des matériaux aux scénarios d'applications domestiques. Matériaux 2022, 26/10/2022.
- P. Dutournié, **M.H. Nguyen**, E. Scullier, S. Bennici. Stockage thermochimique de la chaleur : des résultats de calorimétrie à la simulation d'une installation pour le chauffage domestique individuel. 51^{ème} journées de Calorimétrie et d'Analyse Thermique, vidéoconférence, 23/06/2021.
- M. Zbair, **M.H. Nguyen**, S. Bennici, P. Dutournié. Heat storage: a new benchmark material based on binary salts impregnated into activated carbon for low thermochemical heat storage. Calorimetry and Thermal Analysis days – 52nd edition, Colmar (France), 16/06/2022.
- M. Zbair, **M.H. Nguyen**, S. Bennici, P. Dutournié. Binary salts impregnation into activated carbon for thermochemical heat storage: fast kinetic and enhanced released energy. 9th International Conference on Engineering for Waste and Biomass Valorization, Copenhagen (Denmark), 27/06/2022.

GENERAL INTRODUCTION

Energy is of the utmost importance to the advancement of society. For thousands of years, humans have progressed beyond the simple conversion of energy from food to several different forms that are used in daily activities. However, they all fall back to the same principle that is one of sustainability. Energy originates from different sources with the most common being fossil fuels. In 2019, the world energy consumption is about 13.9 billion TOE (Ton Oil Equivalent) and over 84.3 % of this consumption was supplied by fossil fuels (Oil, Natural gas and Coal), nuclear (4.3 %) and renewable energies (11.4 %) [1]. Even though fossil fuels are still the main resources for the world energy supply, they are non-renewable and so the question is when they will be exhausted. Shafiee and Topal [2] calculated the proven reserves of fossil fuels (proven reserves available with current technologies and price) and reported that coal will be the only fossil fuel remaining after 2042 and will be available up to 2112. Being aware of the urgency of transition towards renewable energy sources, multiple international policies have been designed by the United Nations in 2015: Sustainable Development Goal 7 (Affordable and Clean Energy), Goal 13 (Climate Action) [3] and Paris Climate Agreement signed by 196 countries aiming to reduce CO₂ emissions by half by 2030. According to IAE [4] (International Energy Agency), the amount of renewable energies generated in 2019 was 11.4 % (1600 million TOE) compared to 9 % a decade ago which demonstrate the efforts in saving the planet suffered from the increase of global energy consumption and the fossil fuels use. One of the major constraints on renewable energy development is the intermittency and the availability of these resources, especially for producing heat. The amount of renewable heat supplied by geothermal and solar heater (IAE data) is about 70 million TOE and the low-grade waste heat recovered are very underexploited regarding the huge available resources.

Several main uses of solar energy are in domains of transportation, electronic devices, but the most well-known are the building applications. Cabeza et al. [5] stated that buildings are a substantial source of CO₂ emissions and make up more than one-third of the world's total final energy consumption. The production of hot water, space heating and cooling are now projected to count for around half of the energy used in buildings worldwide. These end-uses have a significant potential to lower energy consumption, increase energy security, and lower CO₂ emissions because they are heavily dependent on fossil fuels. Space and water heating, and cooling demand are rising quickly in countries with very carbon-intensive power grids. By 2050, CO₂ emissions might be reduced by using building heating and cooling systems with low or no carbon footprints and great energy efficiency. In Europe, residential buildings account for 75 % of the total building heritage and 38 % of them were built before 1970 [6]. Despite the

widespread adoption of energy-saving measures, only 12 % of the EU residential built stock has been renovated to fulfill climate change objectives. Therefore, sustainable buildings can be obtained by shifting away from fossil fuels dependence and going toward renewable energy sources, such as solar energy. The most serious problem of solar energy is the intermittency of the effective solar gain. Solar power can only operate throughout the day, and no electricity or heat is produced after nightfall, which creates a huge gap between supply and demand [7] (**Figure 1**). In 2019, the residential sector accounted for around 36 % (170 TWh) of total energy consumption in France, second highest share in the country [8,9]. Among the various residential usages, space heating and domestic hot water (DHW) accounted for 40 % in total of those 170 TWh consumed. Tonellato [10] reviewed that the residential sector in the EU is the largest energy consumer with the most part used for space heating and DHW. In Canada, these two usages accounted for over 80 % [11,12]. This data can confirm that this sector has a significant impact in reducing our dependence from fossil fuels. A larger integration of renewable energy, particularly solar thermal energy, is required.

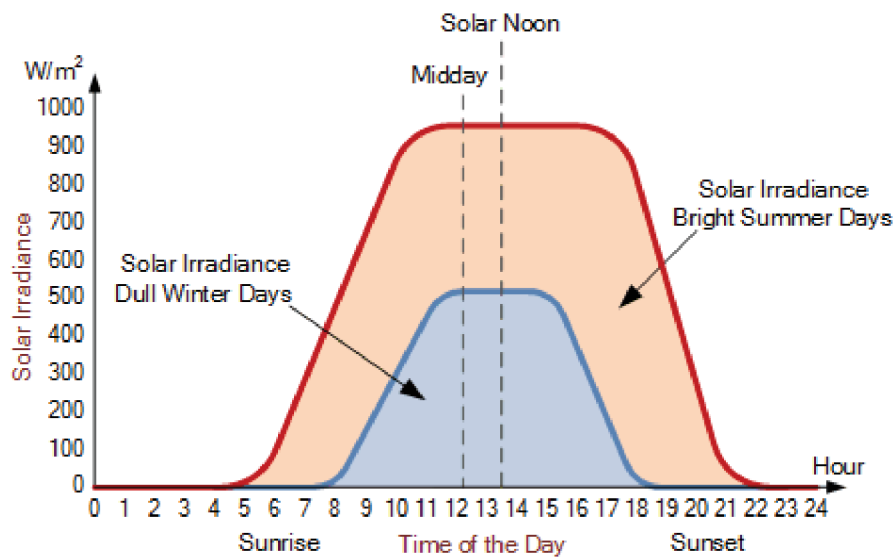


Figure 1. Average solar irradiation during the day per m^2 (horizontal panel) [13].

During on-sun hours, the best-performed concentrated solar cell is reported to have an efficiency up to 38.9 % [14]. Thermal energy storage (TES) systems are then critical and complementary solutions to mitigate climate changes effectively and to enhance global energy performance. TES technologies allow to the excess thermal energy to be stored and used hours (short-term) or months later (seasonal). These technologies can be divided into three separate categories: sensible heat storage (SHS), latent heat storage (LHS) and thermochemical heat storage (TCHS) [15].

Sensible Heat Storage system (SHS)

The most prevalent kind of thermal energy storage is SHS, which employs solid or liquid materials such as rock, sand, water, and oil (**Figure 2**). SHS is the process of storing energy by increasing the temperature of a medium possessing a high heat capacity, such as water or rock [16,17]. The heat is then extracted from the storage whenever it is required, such as for space heating or DHW. A sensible heat storage medium, despite its various variations, always presents the following components: an insulated container, heat storage material, and a device for supplying and releasing heat [18]. The fundamental equation for calculating the amount of heat stored in SHS is as follows:

$$Q_s = mC_p\Delta T \quad \text{Equation 1}$$

where Q_s is the amount of sensible heat stored (J), m is the mass of the storage medium (kg), C_p is the specific heat capacity (J/kg.K) and ΔT is the difference between the storage medium's input and output temperatures.

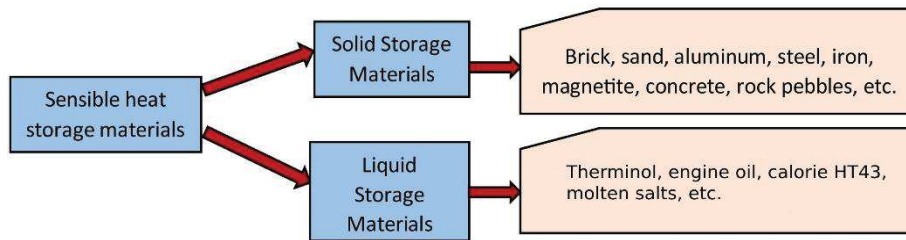


Figure 2. Classification of SHS materials [19].

Solid sensible storage materials can offer higher storage capacity than liquid storage materials since they can sustain higher temperature change. Shah wrote in the “Thermal Energy” book [20] that a general guideline for space heating applications is to use up to 500 kg of solid material per m² of collector surface and that a solid-bed storage may resist greater temperatures of up to 1000 °C. Compared to solid, liquid sensible storage materials have a restricted temperature range because of their boiling point. The temperature at which the heat needs to be stored has an impact on the type of liquid selected as a storage medium. Water is the most frequently employed storage medium below 100 °C due to its high specific heat. For higher temperature applications (> 100 °C), oils such as therminol or engine oil can be adapted. Unfortunately, at high temperatures, oils are vulnerable to cracking, polymerization, and the generation of volatile chemicals [21]. The thermal capabilities of several types of storage media are listed in **Table 1**.

Table 1. Thermal capacities of sensible storage materials.

Material	Temperature range (°C)	Density (kg/m ³)	Specific thermal capacity (kJ/kg.K)	Reference
Brick	≤ 1000	1400-1900	0.84	[22]
Wood	≤ 80	700	2.39	[23]
Glass	≤ 450	2710	0.84	[24]
Sand	≤ 500	1555	0.80	[25]
Massive Soapstone	≤ 1000	2980	0.98	[26]
Concrete	≤ 1000	2000	0.88	[27]
Thermal oil	≤ 400	850-900	1.60-2.10	[28]
Water	0-100	1000	4.18	
Engine oil	≤ 160	885	1.88	
Molten salts	150-550	1800	1.56	[29,30]

Latent Heat Storage system (LHS)

Latent heat storage systems (LHS) aim to use the stored heat by changing the physical state of a substance from one state to another via melting or vaporization (solid to liquid or liquid to gas and vice versa) in a desired operating temperature range. The temperature variation is minimal and it is one of the benefits of LHS [31]. This is why LHS is also called “isothermal process” (for pure compound). The heat recovery and release take part when a storage material goes through a phase change. The heat associated with the melting of a solid material or of a frozen liquid is known as latent heat of fusion. The heat associated with the vaporization of a liquid or the condensation of a vapor is known as latent heat of vaporization [32]. The fundamental equation for calculating the amount of heat stored in LHS is as follows:

$$Q_L = mL \quad \text{Equation 2}$$

where Q_L is the amount of latent heat stored (J), m is the mass of the storage medium (kg) and L is the latent heat associated with the transition (J/kg).

There are three forms of LHS: solid-solid, solid-liquid, and liquid-vapor phase transition. Most LHS research focuses on solid-liquid phase change in order to avoid the problems connected to the volume variation of the gas-liquid phase change process [33]. The solid-liquid phase change materials (PCMs) are classified as organic, inorganic and eutectic materials (**Figure 3**).

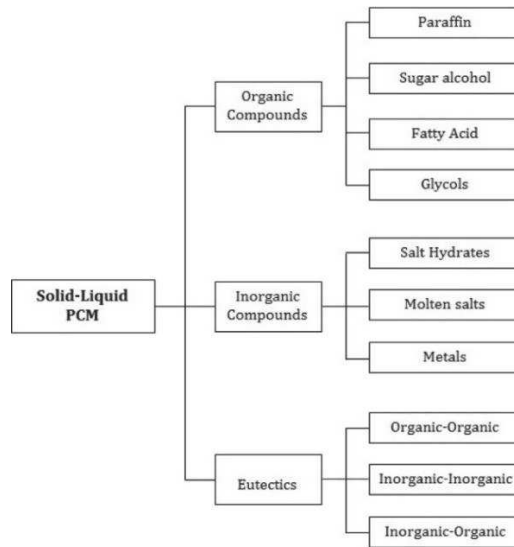


Figure 3. Classification of the solid-liquid PCMs [34].

The organic PCMs offer the benefits of easy implementation in the process, good molding, relative low price, little corrosion, and no supercooling phenomena or phase separation. On the other hand, they present some disadvantages as a low thermal conductivity (TC), a rapid volume change, and a low melting point that make them difficult to be applied in high temperature systems [35]. The inorganic PCMs include molten salts, metals and alloys that are mainly used in medium and high temperature applications. Pure molten salts have a low TC and produce leaks in the installations due to corrosion. On the other hand, metal and alloy have a high TC, high latent heat value per volume, but they are also corrosive [36,37]. Eutectic PCMs are mixtures of two or three inorganic salts. They are mostly utilized in the field of solar thermal applications at medium/high temperatures because of their high density and stability [38]. **Figure 4** shows the performance of different types of PCMs based on their temperatures range.

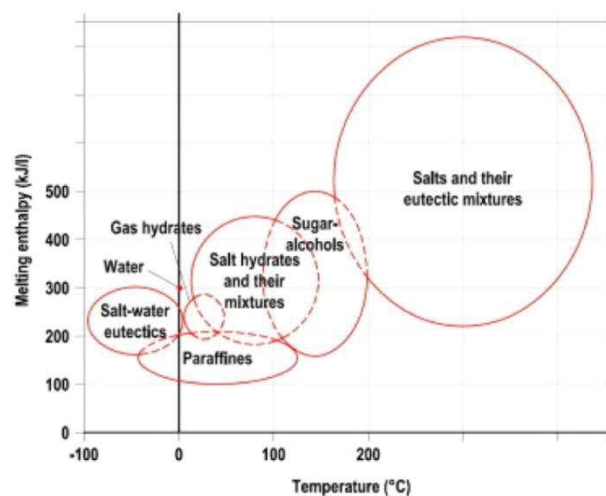


Figure 4. Classes of PCMs based on their melting temperatures range and enthalpy [39].

Thermochemical heat storage system

Thermochemical heat storage (TCHS) is based on reversible exo-/endo-thermic reactions. The systems offer a much higher storage density than the SHS and LHS systems. Consequently, a much smaller volume of the installation. Moreover, once charged, TCHS present a theoretical very low heat loss during the storage time. Further details on TCHS are described in chapter I of this thesis.

The objective of the thesis

The main objective of this work concerns the research and the study of potential materials for long-term heat storage applications. A variety of material composites were synthesized and studied. The thesis focuses on evaluating and improving the performance of the selected materials for thermochemical heat storage by water adsorption. In order to attain this objective, our research direction has gone through these following steps:

- Selection of porous adsorbents as hosts for hygroscopic salts (MgSO_4 , MgCl_2)
- Synthesis of novel composite storage material (salt impregnation into porous hosts)
- Analysis and study of the influence of the porous adsorbents on the heat storage performance
- Evaluation of the energy density storage and sorption capacity of different materials
- Evaluation of kinetic adsorption and the stability of the material upon cycling
- Study of the influence of coupling different salt hydrates on the hydration capacity and kinetics of the composites

This thesis is composed of the results presented in peer reviewed papers published or submitted and divided into several sections (described below):

Chapter I presents a bibliographic study and a state-of-the-art relating to thermochemical heat storage. It consists of a published book chapter focused on the material storage properties and technological solutions. The bibliography is completed by a section focused on the use of two highly potential hydrate salts for long-term heat storage material application (MgSO_4 and MgCl_2), deposited alone or coupled on different supports. Recent research and findings on composites made by impregnating one or the two salts onto a porous matrix host have also been discussed.

Chapter II presents the methods and experimental techniques which were used during this work.

The preparation of the 5 different series of composites is reported. They are synthesized by depositing MgSO_4 onto various porous supports (beads activated carbon, hydroxyapatite, two types of granular activated carbon and a biochar corncob).

Chapter III presents a series of MgSO_4 /carbon-based composites prepared on a microporous supports constituted of beads of activated carbon with a high specific surface area. 3 composites with different salt content were prepared and here described. Energy storage density and adsorption kinetic rates were then evaluated.

Chapter IV describes the heat storage behavior of composites prepared on a mesoporous inorganic support: hydroxyapatite. This work takes origin from a collaboration with the University of Milano (hydroxyapatite synthesis).

Chapter V presents the results of composites of MgSO_4 deposited on a second micro/mesoporous, a commercial granular activated carbon.

Chapter VI is dedicated to the study of composites prepared on a biomass derived carbon material: a biochar obtained by pyrolysis of corncobs. This biochar presents the usual micro and ultramicroporosity of this family of carbon materials. In addition, it presents also a macroporous structure according to the analysis of the Hg intrusion porosimetry. This material was chosen for such characteristic, allowing the deposition of higher amount of the salt in the macrostructure. The influence of the presence of macropores on the hydration kinetics and heat storage capacity is here reported. Moreover, the sustainable origin of the support helps to further decrease the carbon footprint of the overall storage system.

Chapter VII presents a solution to avoid mass transfer limitations due to the difficult diffusion of water molecules towards the MgSO_4 layer. The solution to add a second hydrate salt as MgCl_2 is here investigated.

And finally, a general conclusion presents the essential results of this thesis research. The perspectives, which need to be considered in order to design an efficient and durable heat storage system, are here analyzed.

References

1. Statistical Review of World Energy | Energy economics | Home Available online: <https://www.bp.com/en/global/corporate/energy-economics/statistical-review-of-world-energy.html> (accessed on Jul 15, 2021).

2. Shafiee, S.; Topal, E. When will fossil fuel reserves be diminished? *Energy Policy* **2009**, *37*, 181–189, doi:10.1016/j.enpol.2008.08.016.
3. Izam, N.S.M.N.; Itam, Z.; Sing, W.L.; Syamsir, A. Sustainable Development Perspectives of Solar Energy Technologies with Focus on Solar Photovoltaic—A Review. *Energies* **2022**, *15*, 2790, doi:10.3390/en15082790.
4. bp Statistical Review of World Energy. **2022**.
5. Cabeza, L.F.; de Gracia, A.; Pisello, A.L. Integration of renewable technologies in historical and heritage buildings: A review. *Energy Build.* **2018**, *177*, 96–111, doi:10.1016/j.enbuild.2018.07.058.
6. Romano, E. *Technology options for earthquake resistant, eco-efficient buildings in Europe: Research needs*; 2014; ISBN 9789279354243.
7. Han, Y.; Sun, Y.; Wu, J. A low-cost and efficient solar/coal hybrid power generation mode: Integration of non-concentrating solar energy and air preheating process. *Energy* **2021**, *235*, 121367, doi:10.1016/j.energy.2021.121367.
8. Fitó, J.; Dimri, N.; Ramousse, J. Competitiveness of renewable energies for heat production in individual housing: A multicriteria assessment in a low-carbon energy market. *Energy Build.* **2021**, *242*, 110971, doi:10.1016/j.enbuild.2021.110971.
9. Fitó, J.; Dimri, N.; Ramousse, J. Improving Thermo-economic and Environmental Performance of District Heating via Demand Pooling and Upscaling. *Energies* **2021**, *14*, 8546, doi:10.3390/en14248546.
10. Tonellato, G.; Heidari, A.; Pereira, J.; Carnieletto, L.; Flourentzou, F.; De Carli, M.; Khovalyg, D. Optimal design and operation of a building energy hub: A comparison of exergy-based and energy-based optimization in Swiss and Italian case studies. *Energy Convers. Manag.* **2021**, *242*, 114316, doi:10.1016/j.enconman.2021.114316.
11. Emamjome Kashan, M.; Fung, A.S.; Swift, J. Integrating Novel Microchannel-Based Solar Collectors with a Water-to-Water Heat Pump for Cold-Climate Domestic Hot Water Supply, Including Related Solar Systems Comparisons. *Energies* **2021**, *14*, 4057, doi:10.3390/en14134057.
12. Hailu; Fung Optimum Tilt Angle and Orientation of Photovoltaic Thermal System for Application in Greater Toronto Area, Canada. *Sustainability* **2019**, *11*, 6443,

- doi:10.3390/su11226443.
13. Solar Irradiance. Available online: <https://www.alternative-energy-tutorials.com/solar-power/solar-irradiance.html> (accessed on Jul 21, 2022).
 14. Sharma, D.; Mehra, R.; Raj, B. Comparative analysis of photovoltaic technologies for high efficiency solar cell design. *Superlattices Microstruct.* **2021**, *153*, 106861, doi:10.1016/j.spmi.2021.106861.
 15. Zbair, M.; Bennici, S. Survey Summary on Salts Hydrates and Composites Used in Thermochemical Sorption Heat Storage: A Review. *ENERGIES* **2021**, *14*, doi:10.3390/en14113105.
 16. De Rosa, M.; Afanaseva, O.; Fedyukhin, A. V.; Bianco, V. Prospects and characteristics of thermal and electrochemical energy storage systems. *J. Energy Storage* **2021**, *44*, 103443, doi:10.1016/j.est.2021.103443.
 17. Ramos, A.; López, E.; del Cañizo, C.; Datas, A. Cost-effective ultra-high temperature latent heat thermal energy storage systems. *J. Energy Storage* **2022**, *49*, 104131, doi:10.1016/j.est.2022.104131.
 18. Kalidasa Murugavel, K.; Srithar, K. Performance study on basin type double slope solar still with different wick materials and minimum mass of water. *Renew. Energy* **2011**, *36*, 612–620, doi:10.1016/j.renene.2010.08.009.
 19. Khatod, K.J.; Katekar, V.P.; Deshmukh, S.S. An evaluation for the optimal sensible heat storage material for maximizing solar still productivity: A state-of-the-art review. *J. Energy Storage* **2022**, *50*, 104622, doi:10.1016/j.est.2022.104622.
 20. Shah, Y.T. *Thermal Energy*; CRC Press, 2018; ISBN 9781315305950.
 21. Dincer, I. Evaluation and selection of energy storage systems for solar thermal applications. *Int. J. Energy Res.* **1999**, *23*, 1017–1028, doi:10.1002/(SICI)1099-114X(19991010)23:12<1017::AID-ER535>3.0.CO;2-Q.
 22. RAVICHANDRAN, L.; RUSOV, D.; ARJUNAN, T.V.; VIJAYAN, S.; MATHESWARAN, M. EXPERIMENTAL STUDY OF BRACKISH WATER DISTILLATION IN SINGLE SLOPE SOLAR STILL USING SENSIBLE HEAT STORAGE MATERIALS. In Proceedings of the Proceedings of International Scientific Conference “RURAL DEVELOPMENT 2017”; Aleksandras Stulginskis

- University, 2018.
23. Jamil, B.; Akhtar, N. Effect of specific height on the performance of a single slope solar still: An experimental study. *Desalination* **2017**, *414*, 73–88, doi:10.1016/j.desal.2017.03.036.
 24. Attia, M.E.H.; Driss, Z.; Kabeel, A.E.; Alagar, K.; Athikesavan, M.M.; Sathyamurthy, R. Phosphate bags as energy storage materials for enhancement of solar still performance. *Environ. Sci. Pollut. Res.* **2021**, *28*, 21540–21552, doi:10.1007/s11356-020-12018-x.
 25. Panchal, H.; Patel, D.K.; Patel, P. Theoretical and experimental performance analysis of sandstones and marble pieces as thermal energy storage materials inside solar stills. *Int. J. Ambient Energy* **2018**, *39*, 221–229, doi:10.1080/01430750.2017.1298059.
 26. Skreiberg, Ø.; Georges, L. Wood stove material configurations for increased thermal comfort. *Energy Procedia* **2017**, *142*, 488–494, doi:10.1016/j.egypro.2017.12.076.
 27. Dumka, P.; Mishra, D.R. Performance evaluation of single slope solar still augmented with the ultrasonic fogger. *Energy* **2020**, *190*, 116398, doi:10.1016/j.energy.2019.116398.
 28. Hailu, G. Seasonal Solar Thermal Energy Storage. In *Thermal Energy Battery with Nano-enhanced PCM*; IntechOpen, 2019.
 29. MARVILLET, C. Fluides caloporteurs - Propriétés. *Therm. pour l'industrie* **2015**, doi:10.51257/a-v2-be9571.
 30. Roche, M. L' utilisation d' un m' elange de sels fondus pour le stockage de chaleur
To cite this version : *Rev. Phys. Appliquée* **1980**, *15*, 895–902.
 31. Zeinelabdein, R.; Omer, S.; Gan, G. Critical review of latent heat storage systems for free cooling in buildings. *Renew. Sustain. Energy Rev.* **2018**, *82*, 2843–2868, doi:10.1016/j.rser.2017.10.046.
 32. Anand, A.; Shukla, A.; Sharma, A. Recapitulation on latent heat hybrid buildings. *Int. J. Energy Res.* **2020**, *44*, 1370–1407, doi:10.1002/er.4920.
 33. Feng, P.H.; Zhao, B.C.; Wang, R.Z. Thermophysical heat storage for cooling, heating, and power generation: A review. *Appl. Therm. Eng.* **2020**, *166*, 114728,

- doi:10.1016/j.applthermaleng.2019.114728.
34. Su, W.; Darkwa, J.; Kokogiannakis, G. Review of solid–liquid phase change materials and their encapsulation technologies. *Renew. Sustain. Energy Rev.* **2015**, *48*, 373–391, doi:10.1016/j.rser.2015.04.044.
 35. Liu, W.; Bie, Y.; Xu, T.; Cichon, A.; Królczyk, G.; Li, Z. Heat transfer enhancement of latent heat thermal energy storage in solar heating system: A state-of-the-art review. *J. Energy Storage* **2022**, *46*, 103727, doi:10.1016/j.est.2021.103727.
 36. Lin, Y.; Alva, G.; Fang, G. Review on thermal performances and applications of thermal energy storage systems with inorganic phase change materials. *Energy* **2018**, *165*, 685–708, doi:10.1016/j.energy.2018.09.128.
 37. Liu, M.; Sun, Y.; Bruno, F. A review of numerical modelling of high-temperature phase change material composites for solar thermal energy storage. *J. Energy Storage* **2020**, *29*, 101378, doi:10.1016/j.est.2020.101378.
 38. Bell, S.; Steinberg, T.; Will, G. Corrosion mechanisms in molten salt thermal energy storage for concentrating solar power. *Renew. Sustain. Energy Rev.* **2019**, *114*, 109328, doi:10.1016/j.rser.2019.109328.
 39. Baetens, R.; Jelle, B.P.; Gustavsen, A. Phase change materials for building applications: A state-of-the-art review. *Energy Build.* **2010**, *42*, 1361–1368, doi:10.1016/j.enbuild.2010.03.026.

Chapter I

The State-of-the-Art of Thermochemical Heat Storage

Résumé

La chaleur sensible, la chaleur latente et la chaleur thermochimique sont les trois types d'énergies utilisées dans les systèmes de stockage de la chaleur. Les systèmes basés sur le stockage thermochimique de la chaleur sont les plus attractifs en termes de densité énergétique et donc d'un volume de stockage limité. Le principe du stockage thermochimique se base sur un procédé réversible constitué d'une réaction endothermique (charge), dans laquelle les réactifs stockant la chaleur sous forme de potentiel chimique sont séparés et une réaction exothermique (décharge), durant laquelle la chaleur est libérée grâce à la recombinaison des réactifs. Ce premier chapitre présentera une étude bibliographique et un état de l'art du stockage de la chaleur thermochimique. Il se constitue d'une part d'un chapitre de livre publié qui se concentre sur les systèmes de réaction solide-gaz comme les systèmes basés sur la formation d'hydroxydes, les systèmes à sorption utilisant l'ammoniac ou l'eau. D'autre part, l'étude est complétée par une partie consacrée à l'utilisation de deux sels hydratés à haut potentiel pour une application de stockage de chaleur à long terme (MgSO_4 et MgCl_2), déposés seuls ou couplés sur des différents supports. Des recherches et des résultats récents sur des composites fabriqués par imprégnation d'un ou des deux sels sur un hôte à structure poreuse ont également été discutés.

Recent progress in thermochemical heat storage: materials and applications

Minh Hoang Nguyen^{1,2}, Simona Bennici^{1,2}

¹Université de Haute-alsace, CNRS, IS2M UMR 7361, Mulhouse, France; ²Université de Strasbourg, Strasbourg, France

1. Introduction

Over the past few decades, we have faced an uncontrolled increase in energy consumption worldwide. The world population has reached 7.8 billion people and will continue to grow with an estimation of over 9 billion by 2050 [1], which makes providing energy for the long-term needs of future generations a colossal problem of the 21st century. Fig. 8.1 shows the world energy sources used in 2019 (data collected from Ref. [2]). Primary fossil energy sources (petroleum, coal, and natural gas) represent 84% of global energy consumption. This acceleration of fossil fuel utilization has led to a serious and negative impact on the environment (global warming and pollution), and consequently on human health. Acceptance of the Paris Agreement imposes on each signatory to take action to reduce greenhouse gas emissions and to enhance the use of renewable energy [3]. Renewable energies can be produced from biomass, wind, water, earth (geothermic), and sun. Among others, solar irradiation appears to be the most adapted thermal energy source, due to its vast availability and relatively easy collection. However, in many places in the world, due to the intermittent and location-dependent nature of the sun, an important mismatch between supply and demand of energy affects implemented solar technologies in both the short and long term. As a consequence, integrating an adequate thermal energy storage system (TESS) could be the promising solution to tackle this seasonal energy difference [4–7]. A TESS works as a collector and storage of excess solar energy during the hours of sunshine. The stored energy can then be released for use when needed (for heating buildings as an example). Sensible heat storage (SHS), latent heat storage (LHS), and thermochemical heat storage (TCHS) are three types of

World Energy Supply in 2019

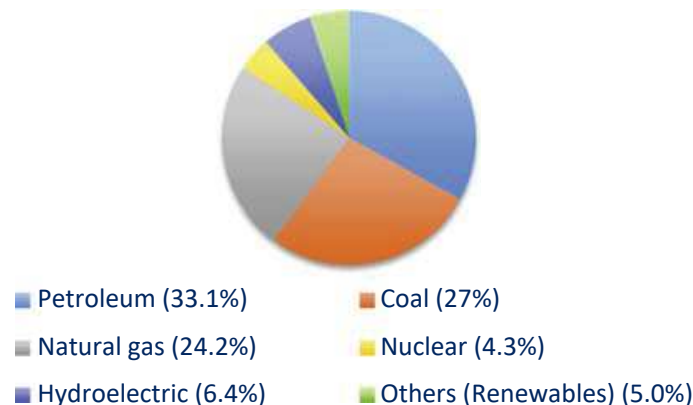


FIGURE 8.1 Illustration of world energy supply sources in 2019.

TESS that have been investigated and widely discussed in the literature up to now [7–12]. The SHS system stores energy by exchanging the temperature within the storage medium. A variation of 50°C can generate an energy storage density (ESD) of 200 MJ/m³ [13]. The advantages of this system are its simplicity and low-price implementation since the maturity of this technology is already at the industrial scale. Major drawbacks of SHS systems are the low energy density, large volume of installation, and heat perditions (which lead to a significant and relatively fast loss of the stored energy) [14]. LHS systems operate in a small temperature range and the storage materials are phase change materials (PCMs). These systems present a higher energy density than SHS with an ESD up to 500 MJ/m³ [13]. Nevertheless, PCMs suffer from low thermal stability, which leads to uncertain behavior in the long term [14].

TCHS systems are based on reversible exo-/endothermic reactions. The thermal energy is stored as chemical potential by separating the reactants through endothermic reaction (charging process). Reversely, the discharge process happens during exothermic reaction when the reactants are put in contact (Fig. 8.2). The TCHS system offers a much higher storage density than the other two systems, resulting in a smaller volume of storage material. Another clear advantage of this system is the very low heat loss during the time when the charged material is kept isolated from the environment. Similar to the other technologies, TCHS systems also present some limitations such as installation complexity and heat and mass transfer limitations due to the low thermal conductivity (TC) of the storage materials [4,15,16]. Recent research has focused on solving these drawbacks and extending the application panel to the industrial scale. On this point, Farulla et al. [10] discussed the recent advancements in power-to-heat technologies, and Liu et al. [12] reviewed the potential of storage materials for electricity production in concentrated solar power (CSP) plants using a high-temperature storage material system. The storage capacity of the TCHS system depends on the involved reversible

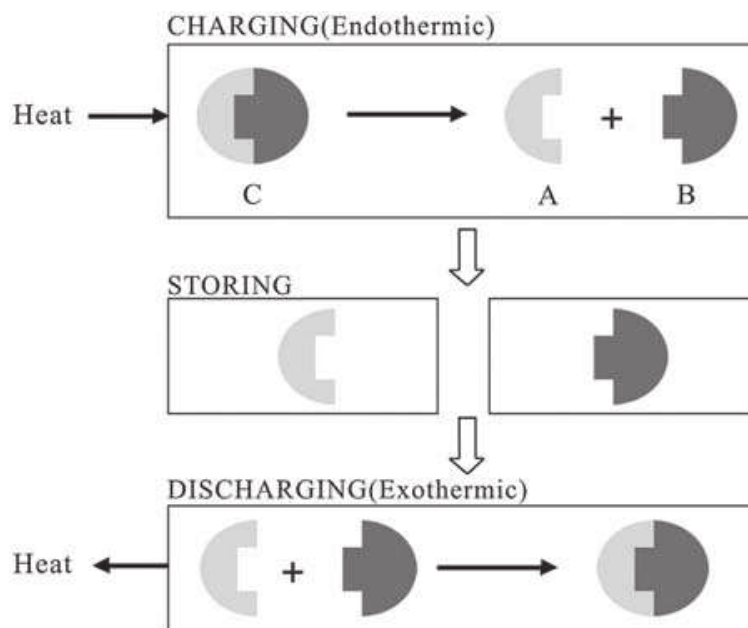


FIGURE 8.2 Principal steps in a thermochemical heat storage cycle: charging, storing, and discharging. From A.H. Abedin, M.A. Rosen, *Closed and open thermochemical energy storage: energy- and exergy-based comparisons*, *Energy* 41 (2012) 83–92. <https://doi.org/10.1016/j.energy.2011.06.034>.

reaction: a high reaction enthalpy corresponds to a high heat storage capacity. Thermochemical materials (TCMs) are also selected by their intrinsic properties and by matching the process conditions [4,7]:

- High reaction enthalpy and high ESD under operating working conditions;
- Appropriate TC to increase mass and heat transfer;
- Completely reversible reaction and no secondary reactions;
- Low cost and abundancy;
- Nontoxic and noncorrosive materials; and
- Regeneration temperature compatible with the specific application (for example, a charging temperature below 150°C for applications in the building sector and up to 1000°C for applications in electricity production in power plants).

Based on the foregoing selection criteria, potential TCMs, such as metal hydride [17–22], redox system [23–27], and methane reforming [28–30], have caught the attention of various research groups. Among them, most studies favor the development and application of hydroxide-based materials and sorption material systems because of their properties, as listed earlier. André et al. [31] pointed out that the $\text{Ca}(\text{OH})_2/\text{CaO}$ couple shows great potential as a storage system due to the high enthalpy of reaction, low cost, and easy implementation in industrial applications. Among the others, Kyaw et al. [32] studied the CaO/CO_2 working pair at high temperature to store thermal energy. Frazzica and Freni [33] concluded in their study that employing

ammonia as a working fluid can exploit lower evaporator temperatures, even if the performance is still limited. Donkers et al. [34] reported that salt hydrates are very promising storage materials for domestic seasonal heat storage, but not realistic for a large-scale implementation.

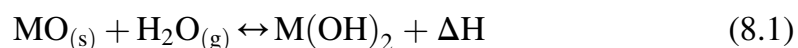
Due to the extent of the heat storage domain, in this review only the latest research (since 2018) is focused on: hydroxide for CSP technologies and sorption materials for residential space heating applications, focusing on three main fluids (CO₂, NH₃, and H₂O). Challenges and future perspectives in the research of new materials will also be given.

2. Solid–gas TCHS reaction systems

TCHS reactions are categorized into solid–gas reactions, liquid–gas reactions, and gas–gas reactions [8,35,36]. This review is mainly focused on solid–gas reactions: hydroxide-based systems (Ca(OH)₂/CaO or Mg(OH)₂/MgO) and sorption systems with different working fluids (NH₃, CO₂, H₂O). Their storage properties will also be discussed in this section.

2.1 Hydroxide-based reactions

Reversible hydration/dehydration reactions of metal oxides (Eq. 8.1, where M represents the metal) have been of key interest in recent years. Original articles can be traced back to the 1980s [35,37]. Ca(OH)₂/CaO and Mg(OH)₂/MgO are the most studied hydroxides and considered potential candidates for thermal energy storage systems at medium and high temperatures (up to about 500°C). Their potential is also due to their abundance, their high ESD (up to 800 kJ/kg_{composite}), and their high reaction enthalpy ($\Delta H = 104 \text{ kJ/mol}_{\text{H}_2\text{O}}$ for Ca(OH)₂ and $\Delta H = 81 \text{ kJ/mol}_{\text{H}_2\text{O}}$ for Mg(OH)₂, respectively) [38].



2.1.1 Ca(OH)₂/CaO systems

The dehydration reaction of Ca(OH)₂ occurs between 400 and 508°C, so the Ca(OH)₂/CaO system can be used for high-temperature thermal energy storage. Samms and Evans [39] and Schmidt et al. [40] concluded that the optimal operating conditions of the system (Fig. 8.3) corresponded to a temperature of 510°C and a water vapor pressure of 1 bar. This system has attracted enormous attention especially in CSP [41]. In this study, Takham and Tippayawong developed a small TCHS unit using charged Ca(OH)₂ powder as a reactant and analyzed the hydration behavior of the material. The hydration rate was high; a rapid increase in temperature was observed. Energy efficiency was relatively high, in the 60%–83% range. The agglomeration of the powder after

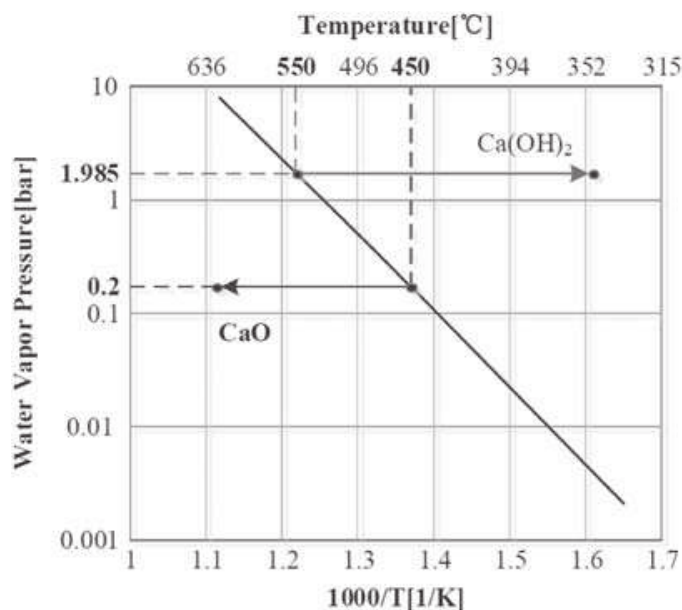


FIGURE 8.3 Equilibrium line for the $\text{Ca}(\text{OH})_2/\text{CaO}$ reaction system. From M. Schmidt, C. Szczukowski, C. Roßkopf, M. Linder, A. Worner, *Experimental results of a 10-kW high temperature thermochemical storage reactor based on calcium hydroxide*, *Appl. Therm. Eng.* 62 (2) (2014) 553–559. <https://doi.org/10.1016/j.applthermaleng.2013.09.020>.

hydration was also observed, causing mass transfer issues due to the nonuniform diffusion of water in the bed. At 510°C and 1 bar, another TCHS setup was built by Dai et al. [42] to monitor the thermal cycling stability of the system. Their results suggested that there was no decrease in performance of the material after 20 cycles, but technical problems, because of powder agglomeration and the poor TC, had yet to be overcome. Yan et al. [43] investigated the influence of the dehydration temperature on the performance of the $\text{Ca}(\text{OH})_2/\text{CaO}$ system. They verified that by choosing a higher dehydration temperature and a thinner sample layer, the overall kinetics, as well as the energy efficiency, could be improved. Xia et al. [44] ameliorated the mass transfer through the CaO bed by integrating a fractal porous medium. Effective gas diffusion coefficients of 0.228 and 0.188 cm^2/s were respectively measured for CaO and $\text{Ca}(\text{OH})_2$. For comparison, these values are higher than that of oxygen diffusion in air at 25°C (0.176 cm^2/s).

Recently, Xia et al. [25] presented a novel composite made from CaO, sodium carboxymethyl cellulose, and vermiculite to overcome the problems related to pure CaO powders (mass transfer issues and low TC). The composite was structurally stable during several cycles of dehydration/hydration and a significant improvement of the heat storage rate was observed when compared to the natural product. In 2020, another group in Japan, Funayama et al. [45], developed a new composite material prepared by depositing $\text{Ca}(\text{OH})_2$ on a Si–SiC ceramic honeycomb support with the aim of enhancing the heat transfer through the reaction bed. A heat output rate of 1.6 kW/L-bed was

recorded, being two times higher than that of the pure $\text{Ca}(\text{OH})_2$ pellet bed. It should be noted that the Si–SiC ceramic honeycomb is an inert support and that no side products were formed during the cycling experiment.

Huang et al. [46] investigated the dehydration of hexagonal boron nitride (HBN)-doped $\text{Ca}(\text{OH})_2$. The composites were better performing than the pure calcium hydroxide. First, the dehydration rate of the 15%wt HBN-doped composite was much higher than that of the pure $\text{Ca}(\text{OH})_2$ (Fig. 8.4A). Fig. 8.4B illustrates the enhancement of TC (improvement of 13.2% at 17°C and nearly of 23% at 300°C) of the material after being doped with different contents of HBN. The same research group [47] synthesized a spindle-shaped $\text{Ca}(\text{OH})_2$ nanomaterial and evaluated its performance. The study proved that the spindle-shaped material increased the specific surface area of the storage bed, resulting in a better heat storage capacity (up to 1300 kJ/kg_{composite}). The newly synthesized material also provided a faster reaction kinetic and higher cycling stability than the “normal-shaped” commercial calcium hydroxide. This indicated that morphology of the material selected could play a crucial role in the development of TCHS.

2.1.2 $\text{Mg}(\text{OH})_2/\text{MgO}$ systems

Even though presenting a lower ESD than the $\text{Ca}(\text{OH})_2/\text{CaO}$ systems, the $\text{Mg}(\text{OH})_2/\text{MgO}$ systems are still largely studied. Piperopoulos et al. and Yan et al. [48,49] synthesized magnesium hydroxide in the presence of a cationic surfactant, cetyl trimethyl ammonium bromide (CTAB), to diminish the material’s natural tendency to aggregate. At specific operating conditions (150°C for 6 h at pH 11) and at the identified optimal concentration of 2 mM of CTAB, the resulting $\text{Mg}(\text{OH})_2$ particles aggregated less easily. The composite exhibited a better volumetric heat capacity, almost double that of the material without CTAB and presented very good stability after 13 cycles of dehydration/hydration.

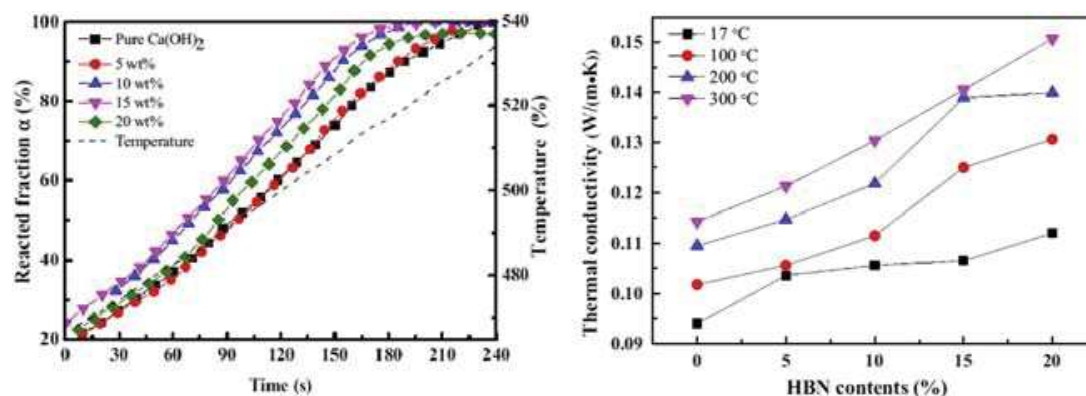


FIGURE 8.4 $\text{Ca}(\text{OH})_2$ conversion (dehydration) (A) and thermal conductivity (B) as a function of hexagonal boron nitride (HBN) content. From C. Huang, M. Xu, X. Huai, *Experimental investigation on thermodynamic and kinetic of calcium hydroxide dehydration with hexagonal boron nitride doping for thermochemical energy storage*, *Chem. Eng. Sci.* 206 (2019) 518–526. <https://doi.org/10.1016/j.ces.2019.06.002>.

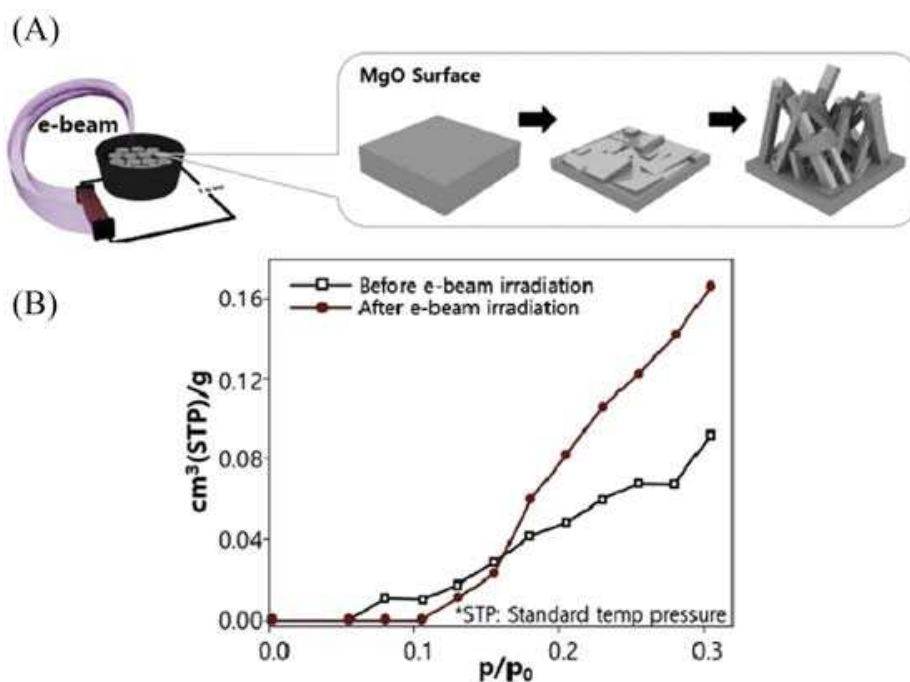


FIGURE 8.5 Illustration of the irradiation of the electron beam on a MgO pellet (A) and pore volume evolution before and after beam irradiation (B). From Y. Kim, N. Kim, T.S. Kim, G.J. Park, Y. Kwon, H.K. Yu, *Mg(OH)₂ nano-sheet decorated MgO micro-beams by electron beam irradiation for thermochemical heat storage*, *Ceram. Int.* 45 (2019) 18908–18913. <https://doi.org/10.1016/j.ceramint.2019.06.126>.

Kim et al. [50] irradiated MgO pellets with an electron beam (Fig. 8.5A) and used the obtained microbeamed MgO in the Mg(OH)₂/MgO TCHS working pair. Electron beam irradiation seems to have an impact on the specific surface area, which doubled after treatment (Fig. 8.5B). The Mg(OH)₂ flakes synthesized from these microbeamed MgO dehydrated much faster than the common MgO-based materials.

2.1.3 Application

Both Ca(OH)₂/CaO and Mg(OH)₂/MgO systems operate at high temperature (up to 500°C), so they are applied at large scale, in particular in CSP. In a recent review, Prasad et al. [8] reported on the inertia of MgO toward hydration in a highly superheated steam. For this reason, the Mg(OH)₂/MgO system is considered less attractive than Ca(OH)₂/CaO. Laboratory- and pilot-scale systems have been tested to explore their potential in electricity production. Angerer et al. [51] researched the design of an MW-scale Ca(OH)₂/CaO TCHS reactor, including a bubbling fluidized bed. A reactor volume of 100 m³ was estimated to be capable of generating 15 MW of heat power. In 2016, Schmidt et al. [52] mixed the reaction material with nano-additives to facilitate fluidization and to ameliorate the low TC of Ca(OH)₂. The final material was then used in an innovative moving-bed reactor (Fig. 8.6). Ugo et al. [53] modeled and simulated a TCHS system integrated in a CSP plant using Ca(OH)₂ coupled to a Rankine power cycle. The integration of the

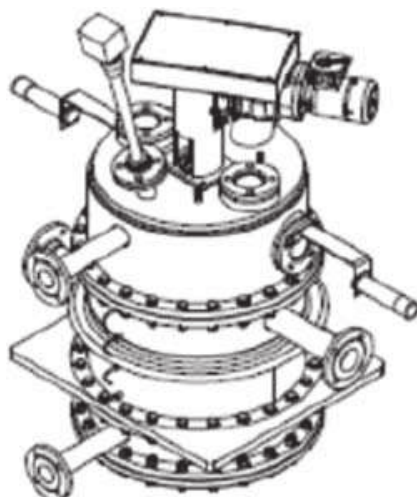


FIGURE 8.6 Moving-bed reactor used in pilot plant using $\text{Ca(OH)}_2/\text{CaO}$ modified with nano-additives. From M. Schmidt, M. Gollsch, F. Giger, M. Grun, M. Linder, *Development of a moving bed pilot plant for thermochemical energy storage with $\text{CaO}/\text{Ca(OH)}_2$* , AIP Conf. Proc. 2016 1734. <https://doi.org/10.1063/1.4949139>.

TCHS system could increase the overall efficiency of the CSP plant of more than 10%. Moreover, an efficiency slightly higher than 30% could be stably maintained over 1 year by using the turbine integration concept.

2.2 Sorption systems

2.2.1 Ammonia sorption/desorption

Metal halide amines have been reported to have exceptionally good cycling stability and high ESD [54], thus they are viable material options for TCHS applications. Eq. (8.2) represents the reversible sorption reaction of metal halide salts (MX) with ammonia gas as a working fluid. The reaction is endothermic, so heat needs to be supplied to separate ammonia and the halide salt. The ammonia gas can then be condensed as a liquid in a storage tank. As a result, this system works mainly as a heat storage system, but can also indirectly store ammonia.



Recently, Berdiyeva et al. [55] analyzed spatiotemporal development of $\text{SrCl}_2 \cdot 8\text{NH}_3$ powder within a reactor using in situ neutron imaging. This method allows them “to study simultaneously NH_3 spatial distribution and the structural changes.” They stated that the stainless-steel honeycomb used to embed the powder did not ameliorate the heat transfer during the desorption process as expected. A volume expansion of 10% was also observed during NH_3 absorption. The study provided crucial information for improving the safety and efficiency of TCHS reactors.

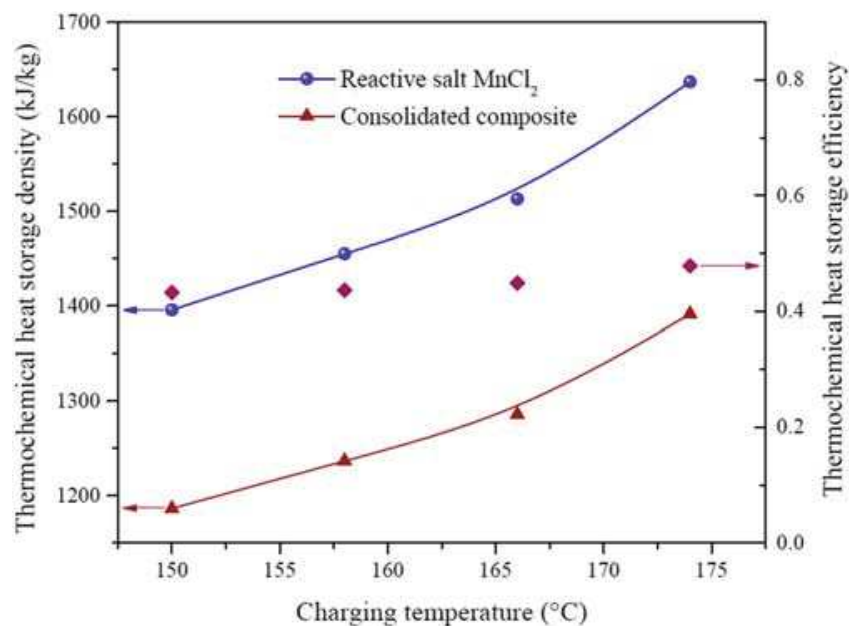


FIGURE 8.7 Evolution of energy storage density with the charging temperatures of pure salt MnCl_2 and composite $\text{MnCl}_2/\text{NH}_3$. From T. Yan, R.Z. Wang, T.X. Li, *Experimental investigation on thermochemical heat storage using manganese chloride/ammonia*. *Energy* 143 (2018) 562–574. <https://doi.org/10.1016/j.energy.2017.11.030>.

Intensive experimental research was conducted by Yan et al. [56], at laboratory scale, to study the $\text{MnCl}_2/\text{NH}_3$ storage system. With the presence of expanded graphite (EG), the heat and mass transfer properties of the composite material were significantly enhanced with an energy efficiency of 48%. Fig. 8.7 shows a surprisingly high ESD of $1391 \text{ kJ/kg}_{\text{composite}}$, recorded at a very low charging temperature of $150\text{--}180^\circ\text{C}$. This temperature range is compatible with solar collectors in summer and for industrial applications for reducing waste heat in factories.

More recently, instead of working on a single salt/ammonia composite, Yan et al. [54] decided to develop a composite containing a mixture of salts. MnCl_2 and SrCl_2 were used for the reversible sorption reaction with ammonia. The double salts/ammonia composite material generated 45% more of ESD ($2 \text{ MJ/kg}_{\text{composite}}$) than the single salt/ammonia composite (Fig. 8.8). The latest research article [57] from the same authors refers to another double salts/ammonia composite. This time, they investigated an $\text{NiCl}_2\text{--SrCl}_2/\text{NH}_3$ storage system. They obtained a significant heat efficiency of 0.978 with a relatively high ESD of $2.1 \text{ MJ/kg}_{\text{composite}}$.

2.2.2 CO_2 sorption/desorption

In the 1970s Baker [58] suggested an energy storage system based on the reversible carbonation/decomposition reaction (Eq. 8.3). One of the most common and studied systems is the CaCO_3/CaO couple integrated in CSP technologies, and also called the “calcium looping (CaL) process.” In this

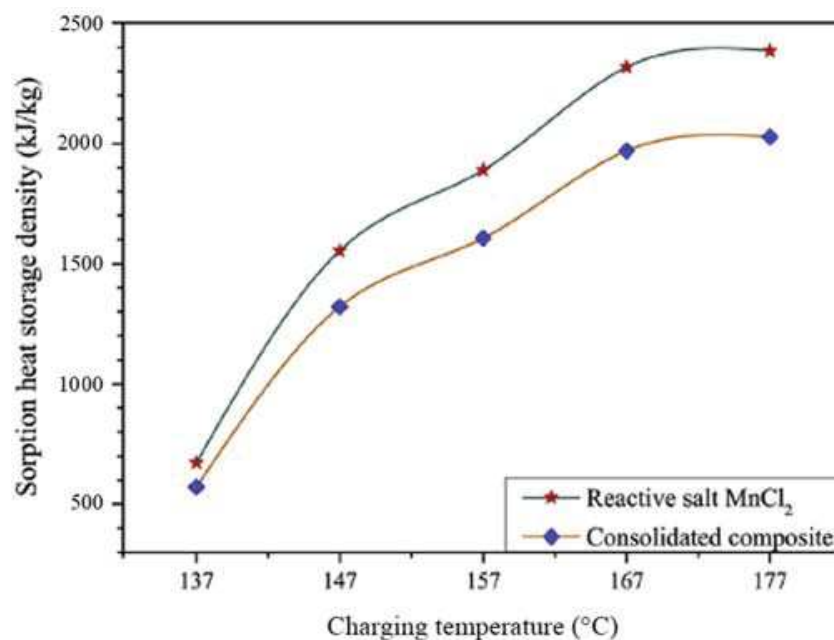
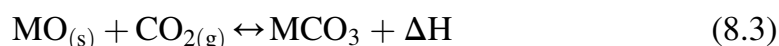


FIGURE 8.8 Evolution of energy storage density with the charging temperature of a pure salt MnCl_2 and $\text{MnCl}_2\text{-SrCl}_2/\text{NH}_3$ composite. From T. Yan, Z.H. Kuai, S.F. Wu, *Experimental investigation on a $\text{MnCl}_2\text{-SrCl}_2/\text{NH}_3$ thermochemical resorption heat storage system*, *Renew. Energy* 147 (2020) 874–883. <https://doi.org/10.1016/j.renene.2019.09.033>.

system, CO_2 and CaO are stored separately and the stored energy is released when needed by combining the two products following the exothermic reaction reported in Eq. (8.3). The CaL process presents advantages in terms of low cost, availability of the used products, and zero risk toward the environment because of the use of natural compounds (CaO and CO_2) [59].



The CaCO_3/CaO system works at a very high temperature, at least 700°C . Addition of doping agent has been investigated to decrease the working temperature. This enlarges the working temperature domain, and avoids certain drawbacks, such as the sintering of CaO , that slow down the reaction kinetics. To avoid sintering, the carbonation of CaCO_3 needs to be carried out at temperatures below 925°C . Khosa and Zhao [60] analyzed the heat storage/release performance of the system before and after doping with SiO_2 . After being doped, the decarbonation temperature was reduced to 800°C and the reaction rate improved thanks to the easier diffusion of CO_2 in the smaller CaO particles. The addition of SiO_2 helped improve the cyclic stability of the CaCO_3 by 13%.

As an alternative to calcined limestone (natural CaO), Li et al. [61] used CaO pellets under high pressure carbonation (up to 13 bar). When the pressure of the carbonation reaction is increased to 5 bar (Fig. 8.9), the heat storage density is reported to increase up to $1400 \text{ kJ/kg}_{\text{composite}}$ after 10 cycles, and increasing the pressure over 5 bar does not seem to increase the energy stored.

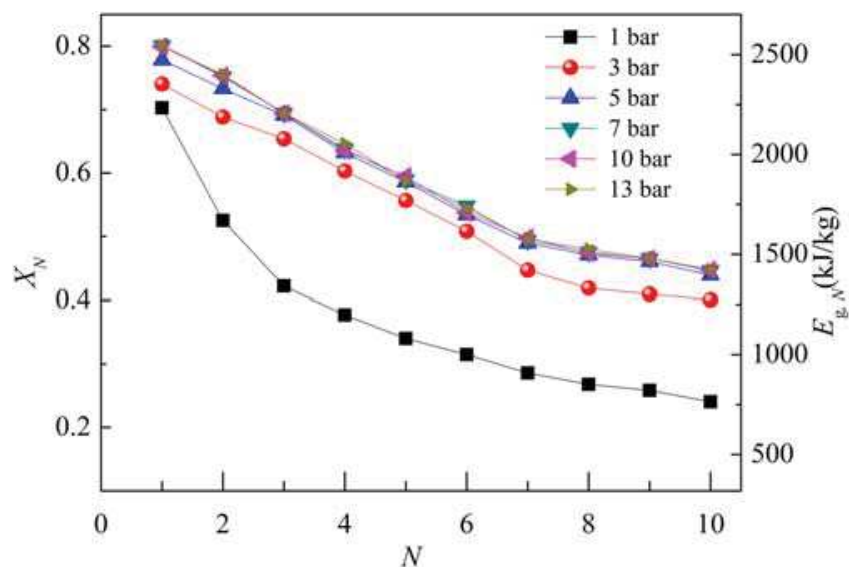


FIGURE 8.9 Effect of carbonation pressure on heat storage density of CaO pellets at 800°C. From B. Li, Y. Li, H. Sun, Y. Wang, Z. Wang, *Thermochemical heat storage performance of CaO pellets fabricated by extrusion-spheronization under harsh calcination conditions*, *Energy Fuels* 34 (5) (2020) 6462–6473. <https://doi.org/10.1021/acs.energyfuels.0c00644>.

The addition of biomass (5%wt bagasse or 5%wt pine) in the CaO pellets was also investigated with the aim of inhibiting the decrease in heat storage capacity after multiple cycling.

In a more recent article about CaL system materials, Teng et al. [62] succeed in enhancing the solar absorptance of CaCO₃ in the conventional CaL–CSP system. They applied particle doping and ion doping by using Mn–Fe (MnFe₂O₄) oxide composite. At a molar ratio of 100:6:12 (Ca:Mn:Fe), the solar absorptance of CaCO₃ increased significantly from 11% to 90%. The energy efficiency was also found to be stable at 93% (1438 kJ/kg_{composite}) over 60 cycles, compared to 20% for the commercial CaCO₃.

A similar energy storage system to CaCO₃/CaO is SrCO₃/SrO. This system operates at extremely high temperature, up to 1200°C at atmospheric pressure. The same sintering problem detected for CaO was also observed for SrO. So, to overcome this issue, Bagherisereshki et al. [63] used a polymorphic spacer to produce sintering-resistant sorbents. CaSO₄ and Sr₃(PO₄)₂ are two potential sintering inhibitors and were added to the parent material to maintain the particle size when reaching high temperatures (Fig. 8.10). Compared to calcium sulfate (only 350 kJ/kg_{composite} after 10 cycles), strontium phosphate appears to be more promising since it seemed to maintain a higher energy density (500 kJ/kg_{composite}) after 10 cycles. The addition of 25%wt of Sr₃(PO₄)₂ seems to be the best compromise to obtain the highest performance.

Gigantino et al. [64] investigated another aspect of the system. They wanted to maintain (or even improve) the cycling stability by mixing strontium acetate hemihydrate and porous MgO to the SrO-based materials. They

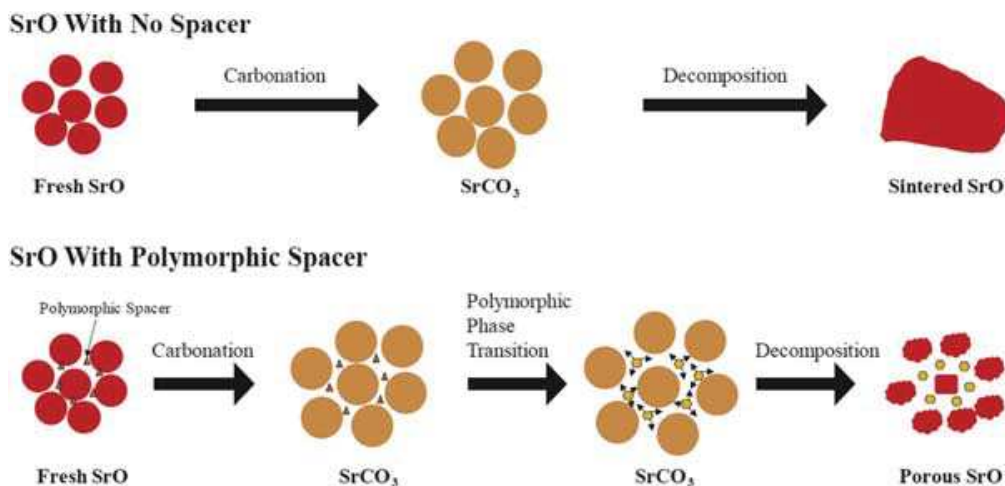


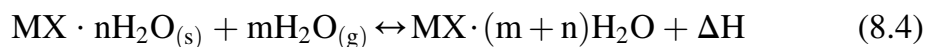
FIGURE 8.10 Illustration of the effect of the polymorphic spacer added to precarbonated SrO. From E. Bagherisereshki, J. Tran, F. Lei, N. AuYeung, *Investigation into SrO/SrCO₃ for high temperature thermochemical energy storage*, *Sol. Energy* 160 (2018) 85–93. <https://doi.org/10.1016/j.solener.2017.11.073>.

concluded that the composite containing 40%wt of SrO maintained the same carbonation–decomposition performance during 100 consecutive cycles with an ESD of 810 kJ/kg_{composite}. A year later, Ammendola et al. [65] studied another oxide as an additive for the SrCO₃/SrO system. Investigations of different Al₂O₃/SrO composite compositions were carried out to understand the effect on sintering limitation and energy storage capacity. The optimum content of the aluminum oxide to achieve the best compromise between the lowering of sintering and the maintaining of a high heat storage performance was identified to be around 34%wt. A higher content will not increase the reactivity, but only reduce the overall energy density due to the lack of the reactive phase SrO. On the other hand, a lower amount would not avoid the sintering and agglomeration of the SrO particles.

2.2.3 H₂O sorption/desorption

Wu et al. [9] presented different properties of a number of selected working fluids (H₂O, NH₃, CO₂, C₂H₅OH, CH₃OH, etc.) especially concerning the safety issues. Methanol, ethanol, and ammonia are flammable in air. Ammonia vapors can be extremely toxic if inhaled or if contacted with eyes and skin. Carbon dioxide (higher than 10% concentration in air) presents long-term toxicity, which is harmful to the cardiovascular system. Water is the best candidate because of its high accessibility and nontoxicity to humans and the environment. Consequently, water is the most adapted and investigated working fluid for TCHS. Freed water does not need to be stored, which reduces the complexity of the system, thus reducing the cost of the overall ESD. Reversible hydration/dehydration (Eq. 8.4) reaction systems with

various sorbents (especially hydrate salts and composites) are the subject of numerous research works.



Padamurthy et al. [66] explored the characteristics of sodium thiosulfate pentahydrate ($\text{Na}_2\text{S}_2\text{O}_3 \cdot 5\text{H}_2\text{O}$) for TCHS. The temperature to reach total dehydration is around 130°C , which is appropriate for solar collector applications. In a single cycle test, the hydration process was performed at 30°C for 2 h to attain complete dehydration, and the corresponding reaction enthalpy was $1012 \text{ J/g}_{\text{material}}$, corresponding to an ESD of 1.81 GJ/m^3 . Erlund and Zevenhoven [67] evaluated the thermal behavior of an inorganic carbonate. They set up a lab-scale reactor design using MgCO_3 /silica gel (SG) as reactive material and matrices support, respectively. At 50%wt salt content, the hydration enthalpy was $410 \text{ J/g}_{\text{composite}}$. A slight decrease in storage capacity was observed by increasing the MgCO_3 content to 10%. This behavior can be explained by mass transfer limitations.

Another inorganic carbonate salt hydrate that has received a lot of attention in recent years is potassium carbonate. Detailed research was performed by Gaeini et al. [68] on K_2CO_3 in terms of cyclability, kinetics, and energy density. It is reported that the kinetics increases cycle after cycle because of the expansion of the material upon hydration. The authors also measured the ESD presenting a value of 0.75 GJ/m^3 . Shkatulov et al. [69] also investigated K_2CO_3 but mixed with expanded vermiculite. In this study, compact K_2CO_3 was used instead of granular material; the kinetics seemed ameliorated (about 2–5 times better). A composite containing 69%wt of K_2CO_3 can release up to 0.9 GJ/m^3 energy, 20% higher than for pure K_2CO_3 [68]. Moreover, the conversion was surprisingly stabilized at least for 47 cycles.

Due to the high ESD of $1440 \text{ kJ/kg}_{\text{composite}}$ and the low charging temperature ($\sim 100^\circ\text{C}$) [70,71], $\text{LiOH} \cdot \text{H}_2\text{O}$ is one of the most promising thermochemical materials for storage applications. Different LiOH -based composites were prepared and analyzed (Table 8.1). Kubota et al. [70] improved the hydration kinetics of LiOH by over five times by depositing LiOH (10%wt) on mesoporous carbon (MPC). Li et al. [72] modified LiOH with Ni-carbon nanotubes (Ni-CNT) and found improvements in the released energy and the TC. These two parameters could also be enhanced when LiOH was modified with graphene oxide [71] or multiwalled CNT [73]. EG was also used as a matrix support by Li et al. [74] to improve the heat and mass transfer of $\text{LiOH} \cdot \text{H}_2\text{O}$. Even if the heat storage capacity was 22% lower than that of the pure $\text{LiOH} \cdot \text{H}_2\text{O}$ salt, the composite containing EG presented a TC 6.5 times higher than the pure salt and an improved cycling stability. Another LiOH -based composite was synthesized and analyzed by Li et al. [75] using 13X zeolite as a hygroscopic support with an ESD 35% higher than that of the pure hydrate salt.

TABLE 8.1 Comparison of different LiOH-based composites with pure LiOH.

Composite	ESD (kJ/kg _{composite})	Thermal conductivity (W/mK)	References
LiOH	1440		[70,71]
LiOH (14%)/Ni-CNT	4000	3.78	[72]
LiOH/graphite oxide	1980	1.8	[71]
LiOH/MWCNT	1804	1.75	[73]
LiOH/EG (8%)	1120	6.52	[74]
LiOH/13X	1949		[75]

CNT, Carbon nanotube; *EG*, expanded graphite; *ESD*, energy storage density; *MWCNT*, multiwalled carbon nanotube.

Besides LiOH.H₂O and carbonate salts, hygroscopic chloride salts are also investigated as potential candidates for TCHS. CaCl₂ is one of the chosen materials due to its properties. CaCl₂ is cheap, easily available [76], and presents a high water absorption capacity of 0.9 g/g (at 25 °C and 1 atm) [77]. For these reasons, CaCl₂ is one of the most used and studied hydrate salts in industry and the building sector. Shi et al. [78] tried to employ metal–organic frameworks based on MIL-101(Cr) as porous matrices supports and they did not measure any significant loss in the heat storage capacity during 17 consecutive cycles (1274 kJ/kg_{composite} for MIL-101(Cr)–SO₃H/CaCl₂).

Different SG-based composite materials were also synthesized for long-term heat storage potential. Pierre D’ans et al. [79] encapsulated 43%wt CaCl₂ in mesoporous SG and measured TC in the 0.129–0.155 W/mK range. Skrylnyk et al. [80] evaluated the storage capacity of the same composite and reported an ESD up to 145 kWh/m³ in a laboratory-scale prototype reactor (Fig. 8.11).

Gaeini et al. [81] investigated three distinct porous supports: expanded natural graphite (ENG), vermiculite, and ethyl cellulose (used for microencapsulation). They were used as matrices for CaCl₂-based composite materials. Fig. 8.12 shows the results reported on the ESDs of these composite materials. Overhydration was observed in samples containing vermiculite and graphite, leading to agglomeration. Consequently, the storage performances are low compared to those of the pure CaCl₂. A second deposition was effected on the impregnated composites to verify a possible improvement in the heat storage capacity. As expected, the twice impregnated samples revealed higher performances: 1.5 GJ/m³ compared to 0.6 GJ/m³ in the case of graphite and 1.2 GJ/m³ compared to 0.5 GJ/m³ in the case of vermiculite. To avoid



FIGURE 8.11 Laboratory-scale prototype reactor used for cycling test of CaCl_2/SG . From O. Skrylnyk, E. Courbon, N. Heymans, M. Frere, J. Bougard, G. Descy, *Performance characterization of salt-in-silica composite materials for seasonal energy storage design*, *J. Energy Storage* 19 (2018) 320–336. <https://doi.org/10.1016/j.est.2018.08.015>.

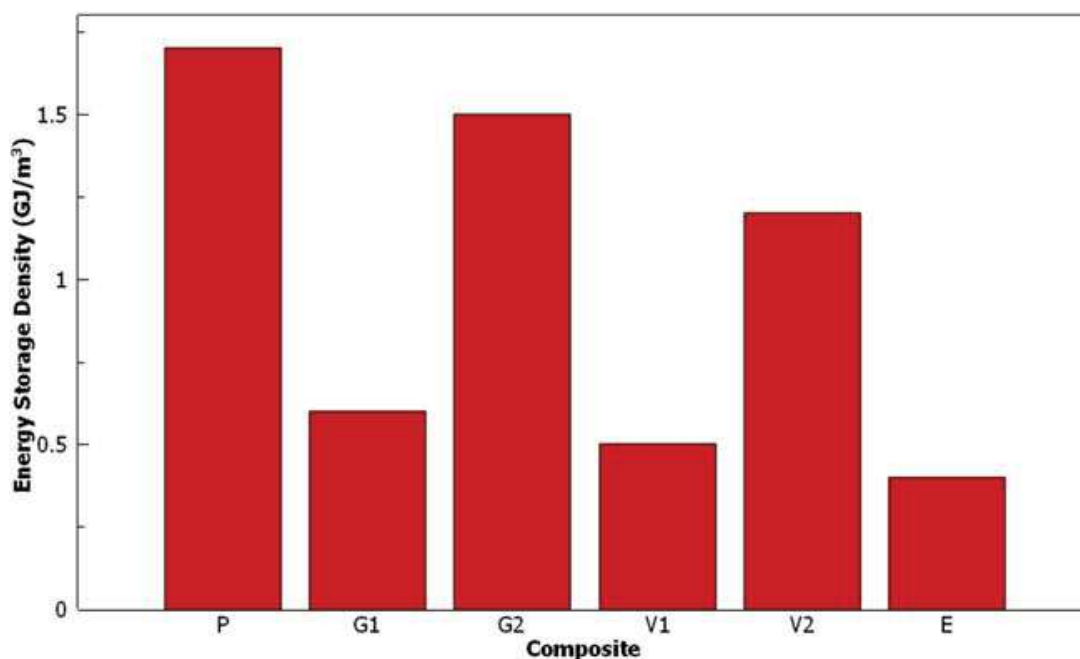


FIGURE 8.12 Energy storage density of CaCl_2 -based composite materials on different supports, where P is the pure CaCl_2 , G1, G2, V1, V2 are respectively the graphite and vermiculite-modified samples, and E the encapsulated sample. Data collected from M. Gaeini, A.L. Rouws, J.W.O. Salari, H.A. Zondag, C.C.M. Rindt, *Characterization of microencapsulated and impregnated porous host materials based on calcium chloride for thermochemical energy storage*, *Appl. Energy* 212 (2018) 1165–1177. <https://doi.org/10.1016/j.apenergy.2017.12.131>.

aggregation, CaCl_2 was encapsulated with ethyl cellulose. This sample showed good cycling stability, but unfortunately a lower ESD (0.4 GJ/m^3). This poor ESD of the CaCl_2 /vermiculite/composite was also confirmed by Nejhad and Aydin [82] and Yilmaz et al. [83].

Hygroscopic chlorides are claimed to coagulate even at low relative humidity (RH) during the discharge phase [84–86]. Efforts have been made on CaCl_2 modified by graphite or vermiculite to overcome the problem, but the expectations were too high. Mehrabadi and Farid [87] tried to use expanded clay and pumice as host matrices for $\text{SrCl}_2 \cdot 6\text{H}_2\text{O}$ for low-grade thermal energy storage applications. Despite having low dehydration temperature ($<150^\circ\text{C}$) and a high theoretical ESD (2.4 GJ/m^3), the synthesized composite materials presented a dramatically low ESD of 26.3 MJ/m^3 (pumice- SrCl_2 with 14%wt) and 100 MJ/m^3 (expanded clay- SrCl_2 with 40%wt). Besides the low composite salt content, salt leaching and agglomeration were found to be the main causes of the low power generation. Until 2017, the composite with the highest salt content reported in the literature was 70%wt of CaCl_2 deposited on activated carbons (ACs) [88]. Unfortunately, its thermal storage performance was not investigated. Later, Kallenberger et al. [89] successfully synthesized alginate-based matrix composites allowing the macroscopic structuring of the composite as beads. The shaping had the advantage of decreasing the pressure loss in packed beds. Table 8.2 shows the results, from calorimetric investigation, of the hydration carried out at 30°C on different composite materials with 86%wt salt content. High volumetric storage densities up to 1.5 GJ/m^3 (CaCl_2 composite sample) combined with relatively high water uptake were reported, proving the potentials of these composite materials for heat storage applications.

TABLE 8.2 Thermal storage performance (storage density and water uptake) of different alginate-based composite materials at different relative humidities.

Composite	Relative humidity at 30°C (%)	Storage density (GJ/m^3)	Water uptake (g/g)
MgSO_4 /alginate	84	1.32	0.65
MgCl_2 /alginate	30	1.27	0.93
	20	0.59	0.38
CaCl_2 /alginate	30	1.50	0.88
	20	1.10	0.64
SrCl_2 /alginate	60	1.05	0.55

In their studies, Posern and Osburg [90] concluded that crystalline salts or salt pellets of SrCl_2 (at 30°C and 60%RH) and MgSO_4 (at 30°C and 84%RH) generated similar amounts of heat of sorption, 2.04 and 1.70 kJ/g_{material}, respectively. Additionally, an evaluation of the temperature increase (for experiments carried out in the same conditions) was also done on composites made of SrCl_2 (35 and 49%wt) and AC. The results revealed that the hydration kinetics was improved thanks to the good dispersion of the salt in the porous support AC. Consequently, temperature increase was higher in the composite than in the pure salt. Instead of working with pure SrCl_2 or MgSO_4 , Li et al. [13] decided to mix them in different proportions varying from 10% to 50%wt of MgSO_4 . Hydration experiments were carried out at 30°C and 55%RH (value lower than the deliquescence relative humidity [DRH] of the highest hydrates from of each of the two salts) [90,91]. The composite containing 20% wt of MgSO_4 showed impressive ESD (595 kWh/m³) and a better dehydration (at 150°C) than both pure salts (Fig. 8.13). A higher cycling stability was also observed for this composite that, after 20 cycles, still presented a high heat storage capacity (equal to the 75% of the value measured for the first cycle).

Hydroscopic sulfate salts are thermally stable and have a relatively high DRH. So, MgSO_4 was recently investigated as a high potential material for TCHS [92,93]. The heptahydrated salt presents a very high theoretical ESD (2.8 GJ/m³), but this value could not be achieved due to only partial reversibility of the hydration reaction [94,95]. To solve this issue, the integration of host materials in the composite formulation seems to be a promising solution. MgSO_4 was among the most investigated salts of the last decade. More recently, it was impregnated on zeolite 13X by Hongois et al. [96]. The beneficial effect of the presence of zeolite was proved. After hydration and dehydration at 150°C, the 15%wt MgSO_4 /zeolite 13X composite could still store 80% of the original energy density (for experiments carried out on 10 mg of sample). When increasing the quantity of storage material (200 g) the heat storage density strongly decreased and represented only 45% of the original value after three cycles. Wang et al. [97] prepared a 15%wt MgSO_4 /zeolite 13X composite material by impregnation. At 80%RH and 25°C, hydration was not homogeneous, as observed by X-ray diffraction. Different hydrate forms were detected, but the $\text{MgSO}_4 \cdot 7\text{H}_2\text{O}$, the highest hydrated phase, was not detected, even at such a high RH. However, the composite showed a relatively good hydration energy of 632 J/g_{composite}. The deposition of MgSO_4 onto the zeolite 13X enhanced the stability to hydration/dehydration cycling. The presence of MgSO_4 seemed to protect the material surface from the air pollutant effect and to enhanced the long term material stability [98].

Another porous structure material was proposed by Brancato et al. [99], who made use of silicone foams. According to the authors, two water vapor-permeable silicones were chosen: poly(methylhydrosiloxane) and a silanol terminated polydimethylsiloxane to form a polymeric foam porous matrix. The composites containing MgSO_4 were observed by scanning electron

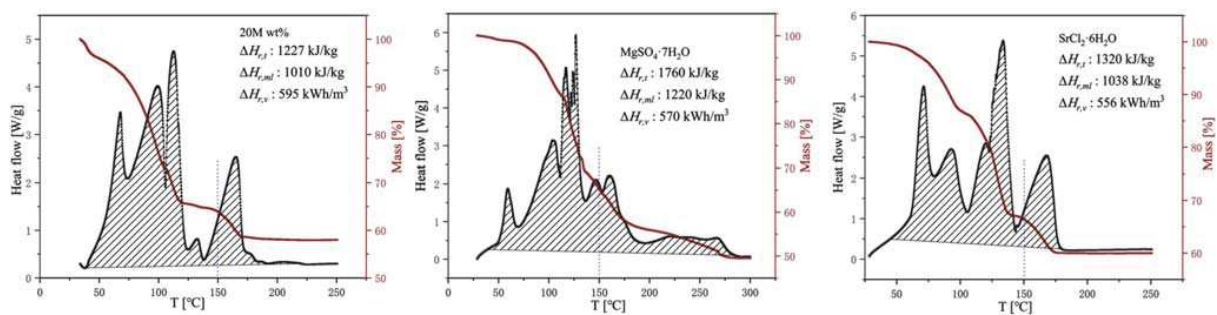


FIGURE 8.13 Comparison of the storage performance of the 20wt MgSO_4 composite and two pure salts. Adapted from W. Li, M. Zeng, Q. Wang, *Development and performance investigation of $\text{MgSO}_4/\text{SrCl}_2$ composite salt hydrate for mid-low temperature thermochemical heat storage*, *Sol. Energy Mater. Sol. Cell.* 210 (2020) 110509. <https://doi.org/10.1016/j.solmat.2020.110509>.

microscope. The salt was well dispersed into the porous structure. It is worth noting that the optimal salt content that the polymeric foam can host was around 60%wt of MgSO_4 . A year later, Calabrese et al. [100] performed mechanical tests on this novel material. Due to the hydrophobic nature of the silicone materials, only 87% of the salt was left after 50 hydration cycles. In early 2020, Piperopoulos et al. [101] performed experiments to evaluate the morphology and dehydration/hydration cycling process of the same composite. With the composite containing the optimum salt content (60%wt of MgSO_4), they found an ESD of $821 \text{ J/g}_{\text{composite}}$ (after a charging step, dehydration, performed by heating up the sample from 30 to 180°C at $5^\circ\text{C}/\text{min}$). No degradation of the silicone matrices was observed upon cycling, which suggests an improvement in terms of material durability. AC is another common TCHS porous support that shows some advantages when compared to zeolites. One of the reasons is the very high specific surface area of AC, which can offer a better water vapor sorption rate. Akcaoglu et al. [102] prepared pellets of MgSO_4 and AC. Expanded natural graphite was also added to enhance the TC. The $\text{MgSO}_4/\text{ENG} + \text{AC}$ (1:1) composite was hydrated at 20°C for 1 week and the hydration heat released was equal to $1395 \text{ J/g}_{\text{composite}}$. The presence of ENG improved the heat transfer of the composite by 86%. Recently, another sulfate hydrate salt, ZnSO_4 , received increased attention from researchers. In Ref. [103], Rehman et al. compared the hydration behavior at 100°C of three hydrated sulfate salts: MgSO_4 , FeSO_4 , and ZnSO_4 . They found that zinc sulfate is an interesting material for heating in buildings because it exhibits a relatively high ESD (1.26 GJ/m^3) when compared to MgSO_4 (0.52 GJ/m^3) and FeSO_4 (0.84 GJ/m^3). In Ref. [104], the authors highlighted the effect of RH on the water sorption ability. At 75%RH, the value of water sorption was 0.148 g/g for $\text{ZnSO}_4 \cdot 7\text{H}_2\text{O}$, but at 85%RH, this value decreased to 0.114 g/g after 10 h of hydration and eventually decreased to 0.001 g/g . The observed phenomena were related to the deliquescence of $\text{ZnSO}_4 \cdot 7\text{H}_2\text{O}$ when RH exceeded 75%.

A screening method was applied by Richter et al. [105] to 308 different inorganic salts to find the most suitable candidate for industrial waste heat recycling ($150\text{--}300^\circ\text{C}$) applications. It was concluded that SrBr_2 was the most promising material with some remarkable properties, as follows: harmless to humans, no decomposition up to 300°C , reversible hydration/dehydration reaction, and stability for at least 10 charging/discharging cycles. Furthermore, with a theoretical ESD of 628 kWh/m^3 [106] and a low dehydration temperature (100°C is sufficient to lose five water molecules going from hexahydrated to monohydrated), SrBr_2 is also considered a good candidate for applications in heating buildings. One of the main drawbacks of $\text{SrBr}_2 \cdot 6\text{H}_2\text{O}$ is corrosion of the materials constituting the reactor. Pierre D'ans et al. [107] studied the corrosion rate caused by $\text{SrBr}_2 \cdot 6\text{H}_2\text{O}$ in low carbon steel and copper at 80°C at different RH values (35% and 24%). In this condition, a severe corrosion of over 1 mm/year (estimated) was observed. This behavior was explained by the presence of SrCO_3 , identified as a coproduct of the

TABLE 8.3 Performance of SrBr₂ after being incorporated into inert matrices.

Composite	ESD	Other properties	References
63% SrBr ₂ /MIL-101(Cr)	233 kWh/m ³ at 30°C	Water sorption capacity 0.4 g/g	[109]
SrBr ₂ /40%-ENG	500 kJ/kg _{composite} (T _{charge} = 80°C) 600 kJ/kg _{composite} (T _{charge} = 150°C)	- Cp increased from 0.6 to 1.3 kJ/kg K - TC increased five times from 0.5 to 2.5 W/mK	[110]
SrBr ₂ /20%-ENG + 0.5%wt NH ₄ ⁺ polyelectrolyte	550 kJ/kg _{composite}	Hydration rate increased three times at 23°C, 50%RH	[111]

ENG, Expanded natural graphite; RH, relative humidity; TC, thermal conductivity.

reaction bringing the formation of HBr, which is extremely corrosive. A similar study was carried out with SrBr₂·6H₂O by Fernandez et al. [108], but this time the experiments were performed under vacuum at a pressure of 123 mbar and a temperature of 78°C. Corrosion was largely suppressed, and the carbon steel material showed a corrosion rate of only 0.038 mm/year. However, the materials presenting the higher resistance to corrosion were identified to be aluminum and stainless steel, with a corrosion rate of only 0.002 mm/year. Other solutions were also suggested to inhibit the corrosion problem, such as incorporating the salt in an inert matrix in contact with a metallic surface (Table 8.3).

3. Conclusion and perspectives

Promising sorption materials for thermochemical heat storage need to have certain properties, such as: environmental nontoxicity, relative cheapness, appropriate affinity between sorbents and sorbates, and high heat storage density. Sorption materials can be adapted to a wide temperature range for targeted applications, in particular for low-temperature building heating. Various drawbacks are currently stopping the implementation of these materials in commercial systems, and intensive research has been carried out to understand the mechanisms involved and find solutions. For example, in the high-temperature range, SiO₂ was added to CaO to reduce the sintering temperature and thus increase its durability, while white CaCO₃ was “blackened” to be able to absorb more efficiently the solar irradiance. Other candidates, such as metal halide amines, suffer from low heat transfer capacity, but by coupling them with graphite-based materials, the final composites could reach high ESD (such as, for example, MnCl₂/NH₃ with about 1400 J/g_{composite}).

Among others, salt hydrates and water are considered the most suitable couple for TCHS, especially for residential building heating applications, in relation to their high ESD. Additionally, water does not need to be stored, thus reducing the complexity of the system. Unfortunately, salt hydrate systems also present numerous drawbacks, including (1) deliquescence of the salts above a certain humidity (DRH), eventually leaking into the surrounding materials, and/or agglomeration during recrystallization, and (2) low TC and porosity, connected to poor heat transfer and low mass transfer respectively, and affecting the overall kinetics. The integration of salts into a porous matrix seems to be the most efficient way to answer these issues. Low cost and high water absorption capacity are the two main reasons why CaCl_2 is widely studied alone or in the presence of various types of host materials. SG, vermiculite, and graphite are employed as supports, but their corresponding composites did not improve their performance, and, in certain cases, even reduced the heat capacity. Embedding CaCl_2 in ethyl cellulose significantly reduced agglomeration and improved cycling stability, but a too low heat capacity was reported. Having the highest theoretical ESD and high DRH, MgSO_4 appears to be the most adapted salt for heat storage systems. Zeolites are the most widely studied support, often coupled to MgSO_4 to produce composites. A composite containing 15%wt of MgSO_4 deposited on zeolite 13X could release over $630 \text{ J/g}_{\text{composite}}$ with good cyclability. ENG was recently investigated to enhance the poor TC of salt hydrates; this parameter needs to be optimized for the implementation of storage systems.

To ensure future research in the building sector, the following points need be considered:

- Search for new composites to improve the heat storage capacity of the system;
- Ameliorate the heat and mass transfer of hydrated salt composites (which are the most promising candidates);
- Perform more consistent durability and cyclability tests;
- At the pilot scale, take into consideration the type of reactor material since corrosion in the presence of salt (hydrates) can impact the lifetime of the installation. Moreover, perform experiments for adapted upscaling simulation as disproportional results when increasing sample mass can falsify the final project.
- Lastly, take into consideration the material cost, energy price, and installation energy efficiency to facilitate the implementation of the technology at the industrial level.

Acronyms

AC activated carbon

CaL calcium looping

CNT carbon nanotube
CSP concentrated solar power
CTAB cetyl trimethyl ammonium bromide
DRH deliquescence relative humidity
EG expanded graphite
ENG expanded natural graphite
ESD energy storage density
HBN hexagonal boron nitride
LHS latent heat storage
MPC mesoporous carbon
PCM phase change material
RH relative humidity
SG silica gel
SHS sensible heat storage
TC thermal conductivity
TCHS thermochemical heat storage
TCM thermochemical material
TESS thermal energy storage system

Acknowledgments

The authors would like to thank the Carnot Institutes MICA (France) and the Region Grand Est (France) for financing the PhD internship of Mr. Minh Hoang Nguyen.

References

- [1] L. Wolfgang, G. Anne, K.C. Samir, S. Marcin, S. Nikolaos, Demographic and Human Capital Scenarios for the 21st Century: 2018 Assessment for 201 Countries, European Commission, Joint Research Centre, Publications Office of the European Union, Luxembourg, 2018, <https://doi.org/10.2760/417766>. ISBN 978-92-79-78024-0.
- [2] Statistical Review of World Energy, Energy Economics, 2019. <https://www.bp.com/en/global/corporate/energy-economics/statistical-review-of-world-energy.html>. (Accessed 10 January 2020).
- [3] Paris Climate Agreement, Government, 2016. <https://www.gouvernement.fr/en/paris-climate-agreement-0>. (Accessed 15 July 2020).
- [4] V. Palomba, A. Frazzica, Recent advancements in sorption technology for solar thermal energy storage applications, *Sol. Energy* 192 (2019) 69–105, <https://doi.org/10.1016/j.solener.2018.06.102>.
- [5] B. Fumey, R. Weber, L. Baldini, Sorption based long-term thermal energy storage - process classification and analysis of performance limitations: a review, *Renew. Sustain. Energy Rev.* 111 (2019) 57–74, <https://doi.org/10.1016/j.rser.2019.05.006>.
- [6] A.H. Abedin, M.A. Rosen, Closed and open thermochemical energy storage: energy- and exergy-based comparisons, *Energy* 41 (2012) 83–92, <https://doi.org/10.1016/j.energy.2011.06.034>.
- [7] H. Jarimi, D. Aydin, Z. Yanan, G. Ozankaya, X. Chen, S. Riffat, Review on the recent progress of thermochemical materials and processes for solar thermal energy storage and industrial waste heat recovery, *Int. J. Low Carbon Technol.* 14 (2019) 44–69, <https://doi.org/10.1093/ijlct/cty052>.

- [8] J.S. Prasad, P. Muthukumar, F. Desai, D.N. Basu, M.M. Rahman, A critical review of high-temperature reversible thermochemical energy storage systems, *Appl. Energy* 254 (2019) 113733, <https://doi.org/10.1016/j.apenergy.2019.113733>.
- [9] H. Wu, F. Salles, J. Zajac, A critical review of solid materials for low-temperature thermochemical storage of solar energy based on solid-vapour adsorption in view of space heating uses, *Molecules* 24 (2019) 945, <https://doi.org/10.3390/molecules24050945>.
- [10] G.A. Farulla, M. Cellura, F. Guarino, M. Ferraro, A review of thermochemical energy storage systems for power grid support, *Appl. Sci.* 10 (9) (2020) 3142, <https://doi.org/10.3390/app10093142>.
- [11] J. Lizana, R. Chacartegui, A. Barrios-Padura, C. Ortiz, Advanced low-carbon energy measures based on thermal energy storage in buildings: a review, *Renew. Sustain. Energy Rev.* 82 (2018) 3705–3749, <https://doi.org/10.1016/j.rser.2017.10.093>.
- [12] D. Liu, L. Xin-Feng, L. Bo, Z. Si-quan, X. Yan, Progress in thermochemical energy storage for concentrated solar power: a review, *Int. J. Energy Res.* 42 (2018) 4546–4561, <https://doi.org/10.1002/er.4183>.
- [13] W. Li, M. Zeng, Q. Wang, Development and performance investigation of $\text{MgSO}_4/\text{SrCl}_2$ composite salt hydrate for mid-low temperature thermochemical heat storage, *Sol. Energy Mater. Sol. Cell.* 210 (2020) 110509, <https://doi.org/10.1016/j.solmat.2020.110509>.
- [14] I. Sarbu, C. Sebarchievici, A comprehensive review of thermal energy storage, *Sustainability* 10 (1) (2018) 191, <https://doi.org/10.3390/su10010191>.
- [15] X. Chen, Z. Zhang, C. Qi, X. Ling, H. Peng, State of the art on the high-temperature thermochemical energy storage systems, *Energy Convers. Manag.* 177 (2018) 792–815, <https://doi.org/10.1016/j.enconman.2018.10.011>.
- [16] R.-J. Clark, A. Mehrabadi, M. Farid, State of the art on salt hydrate thermochemical energy storage systems for use in building applications, *J. Energy Storage* 27 (2020) 101145, <https://doi.org/10.1016/j.est.2019.101145>.
- [17] L. Poupin, T.D. Humphries, M. Paskevicius, C.E. Buckley, A thermal energy storage prototype using sodium magnesium hydride, *Sustain. Energy Fuels* 3 (4) (2019) 985–995, <https://doi.org/10.1039/c8se00596f>.
- [18] K. Manickam, P. Mistry, G. Walker, D. Grant, C.E. Buckley, T.D. Humphries, M. Paskevicius, T. Jensen, R. Albert, K. Peinecke, M. Felderhoff, Future perspectives of thermal energy storage with metal hydrides, *Int. J. Hydrogen Energy* 44 (15) (2019) 7738–7745, <https://doi.org/10.1016/j.ijhydene.2018.12.011>.
- [19] S.N. Nyamsi, I. Tolj, M. Lototskyy, Metal hydride beds-phase change materials: dual mode thermal energy storage for medium-high temperature industrial waste heat recovery, *Energies* 12 (20) (2019) 3949, <https://doi.org/10.3390/en12203949>.
- [20] S. Mellouli, F. Askri, A. Edacherian, T. Alqahtani, S. Algarni, J. Abdelmajid, P. Phelan, Performance analysis of a thermal energy storage system based on paired metal hydrides for concentrating solar power plants, *Appl. Therm. Eng.* 144 (2018) 1017–1029, <https://doi.org/10.1016/j.applthermaleng.2018.09.014>.
- [21] A. d'Entremont, C. Corgnale, B. Hardy, R. Zidan, Simulation of high temperature thermal energy storage system based on coupled metal hydrides for solar driven steam power plants, *Int. J. Hydrogen Energy* 43 (2) (2018) 817–830, <https://doi.org/10.1016/j.ijhydene.2017.11.100>.
- [22] D.A. Sheppard, C.E. Buckley, The potential of metal hydrides paired with compressed hydrogen as thermal energy storage for concentrating solar power plants, *Int. J. Hydrogen Energy* 44 (18) (2019) 9143–9163, <https://doi.org/10.1016/j.ijhydene.2019.01.271>.

- [23] S. Wu, C. Zhou, E. Doroodchi, B. Moghtaderi, A unique phase change redox cycle using CuO/Cu₂O for utility-scale energy storage, *Energy Convers. Manag.* 188 (2019) 366–380, <https://doi.org/10.1016/j.enconman.2019.03.055>.
- [24] G. Gravogl, C. Knoll, J.M. Welch, W. Artner, N. Freiberger, R. Nilica, E. Eitenberger, G. Friedbacher, M. Harasek, A. Werner, K. Hradil, H. Peterlik, P. Weinberger, D. Müller, R. Miletich, Cycle stability and hydration behavior of magnesium oxide and its dependence on the precursor-related particle morphology, *Nanomaterials* 8 (10) (2018) 795, <https://doi.org/10.3390/nano8100795>.
- [25] B.Q. Xia, C.Y. Zhao, J. Yan, A.A. Khosa, Development of granular thermochemical heat storage composite based on calcium oxide, *Renew. Energy* 147 (2020) 969–978, <https://doi.org/10.1016/j.renene.2019.09.065>.
- [26] M. Silakhori, M. Jafarian, M. Arjomandi, G.J. Nathan, Experimental assessment of copper oxide for liquid chemical looping for thermal energy storage, *J. Energy Storage* 21 (2019) 216–221, <https://doi.org/10.1016/j.est.2018.11.033>.
- [27] M. Silakhori, M. Jafarian, M. Arjomandi, G.J. Nathan, Thermogravimetric analysis of Cu, Mn, Co, and Pb oxides for thermochemical energy storage, *J. Energy Storage* 23 (2019) 138–147, <https://doi.org/10.1016/j.est.2019.03.008>.
- [28] J. Ding, Y. Wang, R. Gu, W. Wang, J. Lu, Thermochemical storage performance of methane reforming with carbon dioxide using high temperature slag, *Appl. Energy* 45 (2019) 1270–1279, <https://doi.org/10.1016/j.apenergy.2019.05.064>.
- [29] R. Gu, J. Ding, Y. Wang, Q. Yuan, W. Wang, J. Lu, Heat transfer and storage performance of steam methane reforming in tubular reactor with focused solar simulator, *Appl. Energy* 233 (2019) 789–801, <https://doi.org/10.1016/j.apenergy.2018.10.072>.
- [30] B.G. Lougou, Y. Shuai, G. Chaffa, H. Xing, H. Tan, H. Du, Analysis of CO₂ utilization into synthesis gas based on solar thermochemical CH₄-reforming, *J. Energy Chem.* 28 (2019) 61–72, <https://doi.org/10.1016/j.jechem.2018.01.011>.
- [31] L. André, S. Abanades, G. Flamant, Screening of thermochemical systems based on solid-gas reversible reactions for high temperature solar thermal energy storage, *Renew. Sustain. Energy Rev.* 64 (2016) 703–715, <https://doi.org/10.1016/j.rser.2016.06.043>.
- [32] K. Kyaw, T. Shibata, F. Watanabe, H. Matsuda, M. Hasatani, Applicability of zeolite for CO₂ storage in a CaO-CO₂ high temperature energy storage system, *Energy Convers. Manag.* 38 (10–13) (1997) 1025–1033, [https://doi.org/10.1016/S0196-8904\(96\)00132-X](https://doi.org/10.1016/S0196-8904(96)00132-X).
- [33] A. Frazzica, A. Freni, Adsorbent working pairs for solar thermal energy storage in buildings, *Renew. Energy* 110 (2017) 87–94, <https://doi.org/10.1016/j.renene.2016.09.047>.
- [34] P.A. J Donkers, L.C. Sögütöglü, H.P. Huinink, H.R. Fischer, O.C.G. Adan, A review of salt hydrates for seasonal heat storage in domestic applications, *Appl. Energy* 199 (2017) 45–68, <https://doi.org/10.1016/j.apenergy.2017.04.080>.
- [35] G. Ervin, Solar heat storage using chemical reactions, *J. Solid State Chem.* 22 (1) (1977) 51–61, [https://doi.org/10.1016/0022-4596\(77\)90188-8](https://doi.org/10.1016/0022-4596(77)90188-8).
- [36] T. Yan, R.Z. Wang, T.X. Li, L.W. Wang, I.T. Fred, A review of promising candidate reactions for chemical heat storage, *Renew. Sustain. Energy Rev.* 43 (2015) 13–31, <https://doi.org/10.1016/j.rser.2014.11.015>.
- [37] I. Fujii, K. Tsuchiya, M. Higano, J. Yamada, Studies of an energy storage system by use of the reversible chemical reaction: CaO + H₂O ⇌ Ca(OH)₂, *Sol. Energy* 34 (4–5) (1985) 367–377, [https://doi.org/10.1016/0038-092X\(85\)90049-0](https://doi.org/10.1016/0038-092X(85)90049-0).

- [38] J. Yan, C.Y. Zhao, Z.H. Pan, The effect of CO₂ on Ca(OH)₂ and Mg(OH)₂ thermochemical heat storage systems, *Energy* 124 (2017) 114–123, <https://doi.org/10.1016/j.energy.2017.02.034>.
- [39] J.A.C. Samms, B.E. Evans, Thermal dissociation of Ca(OH)₂ at elevated pressures, *J. Appl. Chem.* 18 (1968) 5–8, <https://doi.org/10.1002/jctb.5010180102>.
- [40] M. Schmidt, C. Szczukowski, C. Roßkopf, M. Linder, A. Worner, Experimental results of a 10-kW high temperature thermochemical storage reactor based on calcium hydroxide, *Appl. Therm. Eng.* 62 (2) (2014) 553–559, <https://doi.org/10.1016/j.applthermaleng.2013.09.020>.
- [41] N. Takham, N. Tippayawong, Experimental investigation of hot water generation from small CaO/Ca(OH)₂ thermochemical energy storage system, *IOP Conf. Ser. Earth Environ. Sci.* 159 (1) (2018) 012002, <https://doi.org/10.1088/1755-1315/159/1/012002>.
- [42] L. Dai, X.F. Long, B. Lou, J. Wu, Thermal cycling stability of thermochemical energy storage system Ca(OH)₂/CaO, *Appl. Therm. Eng.* 133 (2018) 261–268, <https://doi.org/10.1016/j.applthermaleng.2018.01.059>.
- [43] J. Yan, C.Y. Zhao, B.Q. Xia, T. Wang, The effect of dehydration temperatures on the performance of the Ca(OH)₂/CaO thermochemical heat storage system, *Energy* 186 (2019) 115837, <https://doi.org/10.1016/j.energy.2019.07.167>.
- [44] B.Q. Xia, Z.H. Pan, J. Yan, C.Y. Zhao, Mesoscopic exploration on mass transfer in porous thermochemical heat storage materials, *Int. J. Heat Mass Tran.* 135 (2019) 52–61, <https://doi.org/10.1016/j.ijheatmasstransfer.2019.01.108>.
- [45] S. Funayama, H. Takasu, S.T. Kim, Y. Kato, Thermochemical storage performance of a packed bed of calcium hydroxide composite with a silicon-based ceramic honeycomb support, *Energy* 201 (2020) 117673, <https://doi.org/10.1016/j.energy.2020.117673>.
- [46] C. Huang, M. Xu, X. Huai, Experimental investigation on thermodynamic and kinetic of calcium hydroxide dehydration with hexagonal boron nitride doping for thermochemical energy storage, *Chem. Eng. Sci.* 206 (2019) 518–526, <https://doi.org/10.1016/j.ces.2019.06.002>.
- [47] C. Huang, M. Xu, X. Huai, Synthesis and performances evaluation of the spindle-shaped calcium hydroxide nanomaterials for thermochemical energy storage, *J. Nano Res.* 21 (12) (2019) 262, <https://doi.org/10.1007/s11051-019-4694-z>.
- [48] E. Piperopoulos, E. Mastronardo, M. Fazio, M. Lanza, S. Galvagno, C. Milone, Enhancing the volumetric heat storage capacity of Mg(OH)₂ by the addition of a cationic surfactant during its synthesis, *Appl. Energy* 215 (2018) 512–522, <https://doi.org/10.1016/j.apenergy.2018.02.047>.
- [49] H. Yan, X. Zhang, J. Wu, L. Wei, X. Liu, B. Xu, The use of CTAB to improve the crystallinity and dispersibility of ultrafine magnesium hydroxide by hydrothermal route, *Powder Technol.* 188 (2008) 128–132, <https://doi.org/10.1016/j.powtec.2008.04.024>.
- [50] Y. Kim, N. Kim, T.S. Kim, G.J. Park, Y. Kwon, H.K. Yu, Mg(OH)₂ nano-sheet decorated MgO micro-beams by electron beam irradiation for thermochemical heat storage, *Ceram. Int.* 45 (2019) 18908–18913, <https://doi.org/10.1016/j.ceramint.2019.06.126>.
- [51] M. Angerer, M. Becker, S. Harzschel, K. Kroper, S. Gleis, A. Vandersickel, H. Spliethoff, Design of a MW-scale thermo-chemical energy storage reactor, *Energy Rep.* 4 (2018) 507–519, <https://doi.org/10.1016/j.egy.2018.07.005>.
- [52] M. Schmidt, M. Gollsch, F. Giger, M. Grun, M. Linder, Development of a moving bed pilot plant for thermochemical energy storage with CaO/Ca(OH)₂, *AIP Conf. Proc.* (2016) 1734, <https://doi.org/10.1063/1.4949139>.

- [53] P. Ugo, L. Lingai, F. Yilin, S. Driss, Dynamic modeling and simulation of a concentrating solar power plant integrated with a thermochemical energy storage system, *J. Energy Storage* 28 (2020) 101164. <https://doi.org/10.1016/j.est.2019.101164>.
- [54] T. Yan, Z.H. Kuai, S.F. Wu, Experimental investigation on a $\text{MnCl}_2\text{-SrCl}_2/\text{NH}_3$ thermochemical resorption heat storage system, *Renew. Energy* 147 (2020) 874–883, <https://doi.org/10.1016/j.renene.2019.09.033>.
- [55] P. Berdiyeva, A. Karabanova, M.G. Makowska, R.E. Johnsen, D. Blanchard, B.C. Hauback, S. Deledda, *In-situ* neutron imaging study of NH_3 absorption and desorption in SrCl_2 within a heat storage prototype reactor, *J. Energy Storage* 29 (2020) 101388, <https://doi.org/10.1016/j.est.2020.101388>.
- [56] T. Yan, R.Z. Wang, T.X. Li, Experimental investigation on thermochemical heat storage using manganese chloride/ammonia, *Energy* 143 (2018) 562–574, <https://doi.org/10.1016/j.energy.2017.11.030>.
- [57] T. Yan, Z.H. Kuai, S.F. Wu, Multi-mode solid-gas thermochemical resorption heat transformer using $\text{NiCl}_2\text{-SrCl}_2/\text{NH}_3$, *Appl. Therm. Eng.* 167 (2020) 114800, <https://doi.org/10.1016/j.applthermaleng.2019.114800>.
- [58] R. Baker, The reactivity of calcium oxide towards carbon dioxide and its use for energy storage, *J. Appl. Chem. Biotechnol.* 24 (4–5) (1974) 221–227, <https://doi.org/10.1002/jctb.2720240405>.
- [59] C. Ortiz, J.M. Valverde, R. Chacartegui, L.A. Perez-Maqueda, P. Giménez, The Calcium-Looping (CaCO_3/CaO) process for thermochemical energy storage in concentrating solar power plants, *Renew. Sustain. Energy Rev.* 113 (2019) 109252, <https://doi.org/10.1016/j.rser.2019.109252>.
- [60] A.A. Khosa, C.Y. Zhao, Heat storage and release performance analysis of CaCO_3/CaO thermal energy storage system after doping nano silica, *Sol. Energy* 188 (2019) 619–630, <https://doi.org/10.1016/j.solener.2019.06.048>.
- [61] B. Li, Y. Li, H. Sun, Y. Wang, Z. Wang, Thermochemical heat storage performance of CaO pellets fabricated by extrusion-spheronization under harsh calcination conditions, *Energy Fuels* 34 (5) (2020) 6462–6473, <https://doi.org/10.1021/acs.energyfuels.0c00644>.
- [62] L. Teng, Y. Xuan, Y. Da, X. Liu, Y. Ding, Modified Ca-Looping materials for directly capturing solar energy and high-temperature storage, *Energy Storage Mater.* 25 (2020) 836–845, <https://doi.org/10.1016/j.ensm.2019.09.006>.
- [63] E. Bagherisereshki, J. Tran, F. Lei, N. AuYeung, Investigation into SrO/SrCO_3 for high temperature thermochemical energy storage, *Sol. Energy* 160 (2018) 85–93, <https://doi.org/10.1016/j.solener.2017.11.073>.
- [64] M. Gigantino, D. Kiwic, A. Steinfeld, Thermochemical energy storage via isothermal carbonation-calcination cycles of MgO -stabilized SrO in the range of 1000–1100°C, *Sol. Energy* 188 (2019) 720–729, <https://doi.org/10.1016/j.solener.2019.06.046>.
- [65] P. Ammendola, F. Raganati, F. Miccio, A.N. Murri, E. Landi, Insights into utilization of strontium carbonate for thermochemical energy storage, *Renew. Energy* 157 (2020) 769–781, <https://doi.org/10.1016/j.renene.2020.05.048>.
- [66] A. Padamurthy, J. Nandanavanam, P. Rajagopalan, Evaluation of reaction characteristics of $\text{Na}_2\text{S}_2\text{O}_3 \cdot 5\text{H}_2\text{O}$ for thermochemical energy storage, *Mater. Today Proc.* 17 (2019) 239–245, <https://doi.org/10.1016/j.matpr.2019.06.425>.
- [67] R. Erlund, R. Zevenhoven, Thermal energy storage (TES) capacity of a lab scale magnesium hydro carbonates/silica gel system, *J. Energy Storage* 25 (2019), <https://doi.org/10.1016/j.est.2019.100907>. UNSP 100907.

- [68] M. Gaeini, S.A. Shaik, C.C. M Rindt, Characterization of potassium carbonate salt hydrate for thermochemical energy storage in buildings, *Energy Build.* 196 (2019) 178–193, <https://doi.org/10.1016/j.enbuild.2019.05.029>.
- [69] A.I. Shkatulov, J. Houben, H. Fischer, H.P. Huinink, Stabilization of K_2CO_3 in vermiculite for thermochemical energy storage, *Renew. Energy* 150 (2020) 990–1000, <https://doi.org/10.1016/j.renene.2019.11.119>.
- [70] M. Kubota, S. Matsumoto, H. Matsuda, Enhancement of hydration rate of LiOH by combining with mesoporous carbon for low-temperature chemical heat storage, *Appl. Therm. Eng.* 150 (2019) 858–863, <https://doi.org/10.1016/j.applthermaleng.2019.01.049>.
- [71] X.X. Yang, H.Y. Huang, Z.H. Wang, M. Kubota, Z.H. Nea, N. Koboyashi, Facile synthesis of graphene oxide-modified lithium hydroxide for low-temperature chemical heat storage, *Chem. Phys. Lett.* 644 (2016) 31–34, <https://doi.org/10.1016/j.cplett.2015.11.033>.
- [72] S. Li, H. Huang, J. Li, N. Koboyashi, Y. Osaka, Z. He, H. Yuan, The effect of 3D carbon nanoadditives on lithium hydroxide monohydrate based composite materials for highly efficient low temperature thermochemical heat storage, *RSC Adv.* 8 (15) (2018) 8199–8208, <https://doi.org/10.1039/c8ra00269j>.
- [73] X.X. Yang, S.J. Li, H.Y. Huang, J. Li, N. Kobayashi, M. Kubota, Effect of carbon nano-additives on lithium hydroxide monohydrate-based composite materials for low temperature chemical heat storage, *Energies* 10 (5) (2017) 644–653, <https://doi.org/10.3390/en10050644>.
- [74] W. Li, J.J. Klemes, Q. Wang, M. Zeng, Development and characteristics analysis of salt-hydrate based composite sorbent for low-grade thermochemical energy storage, *Renew. Energy* 157 (2020) 920–940, <https://doi.org/10.1016/j.renene.2020.05.062>.
- [75] S. Li, H. Huang, X. Yang, Y. Bai, J. Li, N. Kobayashi, M. Kubota, Hydrophilic substance assisted low temperature LiOH.H₂O based composite thermochemical materials for thermal energy storage, *Appl. Therm. Eng.* 128 (2018) 706–711, <https://doi.org/10.1016/j.applthermaleng.2017.09.050>.
- [76] S.D. Sharma, H. Kitano, K. Sagara, Phase change materials for low temperature solar thermal applications, *Res. Rep. Fac. Eng. Meiji Univ.* 29 (2004) 31–64.
- [77] C.Y. Tso, C.Y.H. Chao, Activated carbon, silica-gel and calcium chloride composite adsorbents for energy efficient solar adsorption cooling and dehumidification systems, *Int. J. Refrig.* 35 (6) (2012) 1626–1638, <https://doi.org/10.1016/j.ijrefrig.2012.05.007>.
- [78] W. Shi, Y. Zhu, C. Shen, J. Shi, G. Xu, X. Xiao, R. Cao, Water sorption properties of functionalized MIL-101(Cr)-X (X = -NH₂, -SO₃H, H, -CH₃, -F) based composites as thermochemical heat storage materials, *Microporous Mesoporous Mater.* 285 (2019) 129–136, <https://doi.org/10.1016/j.micromeso.2019.05.003>.
- [79] P. D'ans, O. Skrylnyk, W. Hohenauer, E. Courbon, L. Malet, M. Degrez, G. Descy, M. Frere, Humidity dependence of transport properties of composite materials used for thermochemical heat storage and thermal transformer appliances, *J. Energy Storage* 18 (2018) 160–170, <https://doi.org/10.1016/j.est.2018.04.027>.
- [80] O. Skrylnyk, E. Courbon, N. Heymans, M. Frere, J. Bougard, G. Descy, Performance characterization of salt-in-silica composite materials for seasonal energy storage design, *J. Energy Storage* 19 (2018) 320–336, <https://doi.org/10.1016/j.est.2018.08.015>.
- [81] M. Gaeini, A.L. Rouws, J.W.O. Salari, H.A. Zondag, C.C.M. Rindt, Characterization of microencapsulated and impregnated porous host materials based on calcium chloride for thermochemical energy storage, *Appl. Energy* 212 (2018) 1165–1177, <https://doi.org/10.1016/j.apenergy.2017.12.131>.

- [82] M.K. Nejhad, D. Aydin, Synthesize and hygro-thermal performance analysis of novel APC-CaCl₂ composite sorbent for low-grade heat recovery, storage, and utilization, *Energy Sources, Part A Recovery, Util. Environ. Eff.* (2019) 1–21, <https://doi.org/10.1080/15567036.2019.1666187>.
- [83] B. Yilmaz, B. Yuksel, G. Orhan, D. Aydin, Z. Utlu, Synthesis and characterization of salt-impregnated anodic aluminum oxide composites for low-grade heat storage, *Int. J. Miner. Metall. Mater.* 27 (1) (2020) 112–118, <https://doi.org/10.1007/s12613-019-1890-x>.
- [84] H. Zondag, B. Kikkert, S. Smeding, R. Boer, M. Bakker, Prototype thermochemical heat storage with open reactor system, *Appl. Energy* 109 (2013) 360–365, <https://doi.org/10.1016/j.apenergy.2013.01.082>.
- [85] B. Michel, N. Mazet, S. Mauran, D. Stitou, J. Xu, Thermochemical process for seasonal storage of solar energy: characterization and modeling of a high density reactive bed, *Energy* 47 (2012) 553–563, <https://doi.org/10.1016/j.energy.2012.09.029>.
- [86] B. Michel, P. Neuve, N. Mazet, Comparison of closed and open thermochemical processes, for long term thermal energy storage applications, *Energy* 72 (2014) 702–716, <https://doi.org/10.1016/j.energy.2014.05.097>.
- [87] A. Mehrabadi, M. Farid, New salt hydrate composite for low-grade thermal energy storage, *Energy* 164 (2018) 194–203, <https://doi.org/10.1016/j.energy.2018.08.192>.
- [88] K. Okada, M. Nakanome, Y. Kameshima, T. Isobe, A. Nakajima, Water vapor adsorption of CaCl₂-impregnated activated carbon, *Mater. Res. Bull.* 45 (11) (2010) 1549–1553, <https://doi.org/10.1016/j.materresbull.2010.07.027>.
- [89] P. Kallenberger, K. Posern, K. Linnow, F.J. Brieler, M. Steiger, M. Froeba, Alginate-derived salt/polymer composites for thermochemical heat storage, *Adv. Sustain. Syst.* 2 (7) (2018), <https://doi.org/10.1002/adsu.201700160>. UNSP 1700160.
- [90] K. Posern, A. Osburg, Determination of the heat storage performance of thermochemical heat storage materials based on SrCl₂ and MgSO₄, *J. Therm. Anal. Calorim.* 131 (3) (2018) 2769–2773, <https://doi.org/10.1007/s10973-017-6861-8>.
- [91] A. Apelbat, E. Korin, Vapour pressures of saturated aqueous solutions of ammonium iodide, potassium iodide, potassium nitrate, strontium chloride, lithium sulphate, sodium thiosulphate, magnesium nitrate, and uranyl nitrate from T= (278 to 323) K, *J. Chem. Thermodyn.* 30 (1998) 459–471.
- [92] K. Posern, C. Kaps, Humidity controlled calorimetric investigation of the hydration of MgSO₄ hydrates, *J. Therm. Anal. Calorim.* 92 (2008) 905–909, <https://doi.org/10.1007/s10973-007-8640-4>.
- [93] V. M Essen, H.A. Zondag, J.C. Gores, L.P. Bleijendaal, M. Bakker, R. Schuitema, W.G.J. Helden, Z. He, C.C.M. Rindt, Characterization of MgSO₄ hydrate for thermochemical seasonal heat storage, *J. Sol. Energy Eng.* 131 (7) (2009) 0410141, <https://doi.org/10.1115/1.4000275>.
- [94] K. Linnow, M. Niermann, P. Bonatz, K. Posern, M. Steiger, Experimental study of the mechanism and kinetics of hydration reactions, *Energy Proc.* 48 (2014) 394–404, <https://doi.org/10.1016/j.egypro.2014.02.046>.
- [95] L. Okhrimenko, L. Favergeon, K. Johannes, F. Kuznik, New kinetic model of the dehydration reaction of magnesium sulfate hexahydrate: application for heat storage, *Thermochim. Acta* 687 (2020) 178569, <https://doi.org/10.1016/j.tca.2020.178569>.

- [96] S. Hongois, F. Kuznik, P. Stevens, J.J. Roux, Development and characterization of a new MgSO_4 zeolite composite for long-term thermal energy storage, *Sol. Energy Mater. Sol. Cell.* 95 (2011) 1831–1837, <https://doi.org/10.1016/j.solmat.2011.01.050>.
- [97] Q. Wang, Y. Xie, B. Ding, G. Yu, F. Ye, C. Xu, Structure and hydration state characterizations of MgSO_4 -zeolite 13x composite materials for long-term thermochemical heat storage, *Sol. Energy Mater. Sol. Cell.* 200 (2019), <https://doi.org/10.1016/j.solmat.2019.110047>. UNSP 110047.
- [98] S. Bennici, T. Polimann, M. Ondarts, E. Gonze, C. Vaultot, N. Le Pierres, Long-term impact of air pollutants on thermochemical heat storage materials, *Renew. Sustain. Energy Rev.* 117 (2020) 109473, <https://doi.org/10.1016/j.rser.2019.109473>.
- [99] V. Brancato, L. Calabrese, V. Palomba, A. Frazzica, M. Fullana-Puig, A. Sole, L.F. Cabeza, $\text{MgSO}_4 \cdot 7\text{H}_2\text{O}$ filled macro cellular foams: an innovative composite sorbent for thermochemical energy storage applications for solar buildings, *Sol. Energy* 173 (2018) 1278–1286, <https://doi.org/10.1016/j.solener.2018.08.075>.
- [100] L. Calabrese, V. Brancato, V. Palomba, A. Frazzica, L.F. Cabeza, Magnesium sulphate-silicone foam composites for thermochemical energy storage: assessment of dehydration behaviour and mechanical stability, *Sol. Energy Mater. Sol. Cell.* 200 (2019), <https://doi.org/10.1016/j.solmat.2019.109992>. UNSP 109992.
- [101] E. Piperopoulos, L. Calabrese, P. Bruzzaniti, V. Brancato, V. Palomba, A. Capri, A. Frazzica, L.F. Cabeza, E. Proverbio, C. Milone, Morphological and structural evaluation of hydration/dehydration stages of MgSO_4 filled composite silicone foam for thermal energy storage applications, *Appl. Sci. Basel* 10 (2) (2020) 453, <https://doi.org/10.3390/app10020453>.
- [102] S.C. Akcaoglu, Z. Sun, S.C. Moratti, G. Martinopoulos, Investigation of novel composite materials for thermochemical heat storage systems, *Energies* 13 (5) (2020) 1042, <https://doi.org/10.3390/en13051042>.
- [103] A.U. Rehman, A. Hayat, A. Munis, T. Zhao, M. Israr, M. Zheng, Characterisation of magnesium, zinc and iron sulfates for thermochemical storage, *Proc. Inst. Civ. Eng. Energy* 173 (2) (2020) 60–67, <https://doi.org/10.1680/jener.19.00018>.
- [104] A. U Rehman, M. Zheng, A. Hayat, Hydration performance and cycling stability of three TCM: MgSO_4 , ZnSO_4 and FeSO_4 , *Int. J. Energy Res.* 44 (8) (2020) 6981–6990, <https://doi.org/10.1002/er.5470>.
- [105] M. Richter, E.-M. Habermann, E. Siebecke, M. Linder, A systematic screening of salt hydrates as materials for a thermochemical heat transformer, *Thermochim. Acta* 659 (2018) 136–150, <https://doi.org/10.1016/j.tca.2017.06.011>.
- [106] F.-L. Armand, G.T. Jean, A review on the use of $\text{SrBr}_2 \cdot 6\text{H}_2\text{O}$ as a potential material for low temperature energy storage systems and building applications, *Sol. Energy Mater. Sol. Cell.* 164 (2017) 175–187, <https://doi.org/10.1016/j.solmat.2017.02.018>.
- [107] P. D'ans, E. Courbon, M. Frere, G. Descy, T. Segato, M. Degrez, Severe corrosion of steel and copper by strontium bromide in thermochemical heat storage reactors, *Corrosion Sci.* 138 (2018) 275–283, <https://doi.org/10.1016/j.corsci.2018.04.020>.
- [108] A.G. Fernandez, M. Fullana, L. Calabrese, V. Palomba, A. Frazzica, L.F. Cabeza, Corrosion assessment of promising hydrated salts as sorption materials for thermal energy storage systems, *Renew. Energy* 150 (2020) 428–434, <https://doi.org/10.1016/j.renene.2020.01.001>.

- [109] P. D'ans, E. Courbon, A. Permyakova, F. Nouar, C. Simonnet-Jegat, F. Bourdreux, L. Malee, C. Serre, M. Frere, N. Steunou, A new strontium bromide MOF composite with improved performance for solar energy storage application, *J. Energy Storage* 25 (2019), <https://doi.org/10.1016/j.est.2019.100881>. UNSP 100881.
- [110] A. Cammarata, V.V.A. Sciacovelli, Y. Ding, Hybrid strontium bromide-natural graphite composites for low to medium temperature thermochemical energy storage: formulation, fabrication and performance investigation, *Energy Convers. Manag.* 166 (2018) 233–240, <https://doi.org/10.1016/j.enconman.2018.04.031>.
- [111] S. Salviati, F. Carosio, G. Saracco, A. Fina, Hydrated salt/graphite/polyelectrolyte organic-inorganic hybrids for efficient thermochemical storage, *Nanomaterials* 9 (3) (2019) 420, <https://doi.org/10.3390/nano9030420>.

State of the art on MgSO₄, - MgCl₂- mono and binary systems.

As discussed in the book chapter, incorporating salt particles into porous host materials to produce composites would help in improving the storage capacity potential of these salts. MgSO₄ and MgCl₂ are two salt candidates with high potential for long-term heat storage. The following section is a mini-review regarding the performance of the composites synthesized from those two salts.

MgSO₄-based composites

Zeolite is the most common as well as the most investigated host porous material for impregnation of hygroscopic salts. Xu et al. [1] conducted a comprehensive investigation of 13X-MgSO₄ composite after that zeolite 13X was chosen as the best porous matrix compared to zeolite 3A and 4A. At 25 °C and 85 % RH, the composite containing 20 % MgSO₄ performed best, with a saturation adsorption amount of 0.26 g/g. This represents an enhancement of 40 % compared with pure zeolite 13X in the same conditions. The air temperature lift and the hydration rate were further investigated in a macro-scale reactor and both displayed an improvement by increasing the air flow rate or the inlet air RH. An energy efficiency of 81.34 % was recorded at 25 °C, 65 % RH, and a flow rate of 0.3 m³/h, indicating that the tested composite has a potential as a thermochemical storage material. Zeolite 13X was also employed by Rehman et al. [2] to prepare two composites (13X-MgSO₄) with 5 and 10 wt% salt content. The salt deposited on the zeolite (composites) absorbed 5.1 and 6 molecules of water, respectively. Additionally, the energy stored (dehydration heat) at 150 °C and ambient pressure by the synthesized composite with 10 % of MgSO₄ (1985 J/g) was improved by around 10 % compared with the pure MgSO₄ hydrate (1817 J/g). The cyclability of the composite was also increased. The rehydration heat of MgSO₄ decreased of 58 % after 100 cycles compared with the first cycle, while the heat released (at 25 °C and 75 % RH) by the 10 % of MgSO₄ composite, after 100 cycles (1397 J/g), still corresponded to 87 % of the heat released during the first cycle (1603 J/g), which increases the lifetime of the material. Xu et al. [3] added a third component into the parent 13X/MgSO₄ composite: expanded natural graphite treated with sulfuric acid (ENG-TSA). This component acts as a packing material, in the purpose of filling the voids among the host matrix pellets, thus increasing the thermal conductivity. ENG-TSA was previously reported to improve the heat and mass transfer of the salt hydrates, but it did not influence the water uptake of the material [4–6].

Miao et al. [7] prepared several high MgSO₄ content composites containing 50 to 80 % expanded graphite (EG). The optimal salt content of the composite at 25 °C and 85 % RH was 60 wt% MgSO₄, with saturation adsorption achieved after approximately 8 hours of hydration time. Moreover, thanks

to the use of EG, the thermal conductivity was greatly enhanced by over 80 %. For instance, the thermal conductivity of the composite with 60 wt% MgSO_4 was measured to be 0.73 W/mK.

Recently, a novel composite made from MgSO_4 and diatomite was synthesized and characterized by Zhang et al. [8]. They prepared two tablet-formed composites by impregnating 30 and 60 wt% of MgSO_4 into diatomite. At 25 °C and 85 % RH, the composite with 60 % of MgSO_4 showed an energy storage density of 773 J/g and an adsorption capacity of 0.37 g/g. Although improvement in terms of heat released was not observed, the mass transfer was greatly enhanced, as the composite supported more charge/discharge cycles than the pure MgSO_4 . Tabard et al. [9] manufactured a 3-scale porosity host material with pore diameters spread from 200 nm to 200 μm with the aim of maximizing the amount of salt that can be deposited. The composites were then obtained by impregnating different ratios of MgSO_4 (**Figure 5**). An energy density 420 $\text{kWh}\cdot\text{m}^{-3}$ high was recorded and represents the highest performance of these composites, with a remarkable stability over time proven after 10 cycles of charge/discharge.

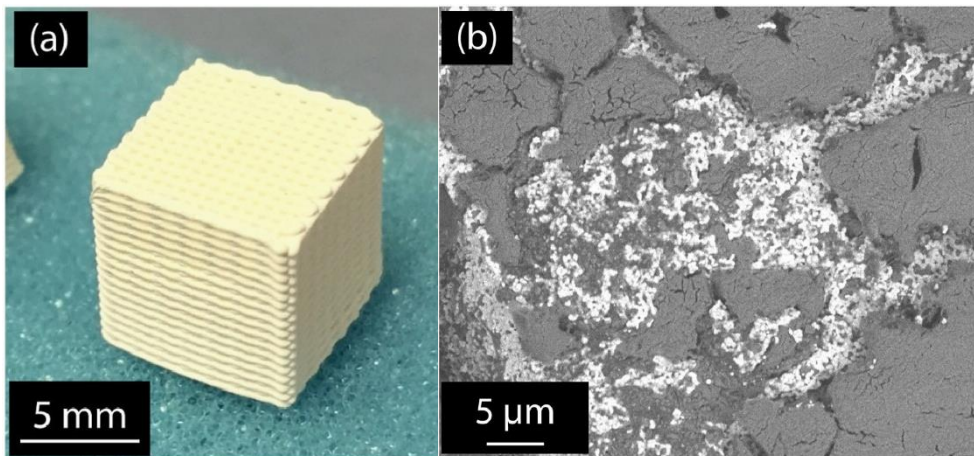


Figure 5. a) Zirconia ceramic matrix after manufacturing and b) Homogenous infiltration of salt inside the porosity of the zirconia structure [9].

Zambotti et al. [10] for the first time used a polymer-derived SiOC ceramic aerogel as a porous host for the deposition of MgSO_4 as a long-term thermal storage material. With a tunable pore volume that can constitute up to 80 % of the material. MgSO_4 was successfully infiltrated by vacuum impregnation. 60 wt% is the maximum content of salt that can be confined into the porous network of this newly employed host matrix. The composites were characterized by a good cyclability and a fast hydration rates (less than 50 min). Another novel porous matrix that was introduced by Kallenberger et al. [11] is an alginate-based material that permits to obtain macroscopically structured composites (beads), assuring a low pressure loss in packed bed reactors. At 30 °C and 84 % RH, the composite embedded with MgSO_4 delivered a heat of hydration just over 1000 J/g with an adsorption

capacity of 0.65 g/g. The authors also claimed that the synthesis approach is scalable and inexpensive. Moreover, the material is nontoxic, which makes it simple to adapt the synthesis to the commercial scale.

MgCl₂-based composites

Zeolite is also a promising porous support candidate for the confinement of hygroscopic chloride salts. Taking into account the hydrophilicity of zeolite 13X and the highly hygroscopic character of salt hydrates (i.e., chloride with DRH of 33 % RH at 30 °C [12]), Xu et al. [13] proposed a multi-step sorption process that included the physisorption of water on the zeolite 13X, the chemisorption onto the hygroscopic salts, and the salt dissolution followed by deliquescence (**Figure 6**).

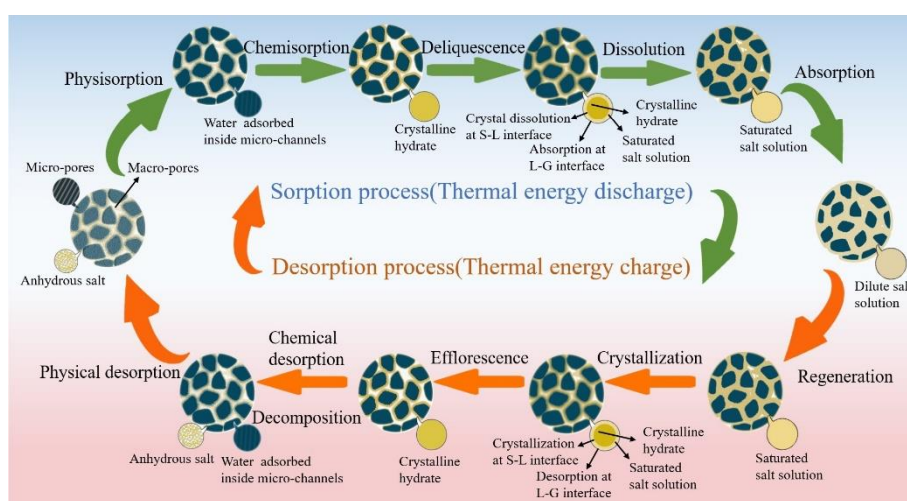


Figure 6. Working principle of multi-form thermochemical energy storage based on multi-step sorption/desorption processes [13].

The composites were prepared by ion-exchange procedure followed by impregnation of MgCl₂ (up to 25 wt%). The water vapor adsorption isotherm of the composite with the highest salt loading suggested that the solution leakage occurs when the relative humidity exceeds 65 % and that the sorption capacity can reach 0.8 g/g at 85 % RH. According to the authors, avoiding solution leaking at a RH higher than 65 % is possible, if the content of MgCl₂ in the composite does not exceed 13 wt%. By controlling the operating conditions, the salt content, and the hydration time, it is possible to achieve an adsorption capacity at 0.55 g/g at a high RH of 80 % with the composite with the highest salt content (25 wt%). The dehydration heat of the composite was reported to be around 1368 J/g with a good stability over 20 cycles.

Zhou and Zhang [14] prepared MgCl₂-based composites with graphene oxide aerogel (GOA) by hydrothermal and freeze-drying methods. GOA has an outstanding feature in the dehydration

behavior which has not been found in any other porous matrices. The charging temperature moves to a lower temperature gradually with the decrease of MgCl_2 content, thus providing a new method to manipulate the dehydration process. GOA is able to confine a very high amount of $\text{MgCl}_2 \cdot 6\text{H}_2\text{O}$ (up to 90 wt%) thus producing composites with a high energy density (up to about 1600 J/g). As a result, these composites are expected to play an important role in low-medium temperature heat storage applications. Three years later, Zhou and Zhang reached another milestone by improving the salt content in the composite, this time up to 97 %, by playing on the reduction degree of the GOA [15]. The reduction of the graphene oxide is referred to the reduction of the O-rich groups such as hydroxyl, carboxyl or ether. Thus, it is possible to insert more or less salt particles depending on the presence of the listed o-containing groups that act on the distance between the carbon planes. The highest reported water uptake at 25 °C and 95 % RH is 1.16 g/g, with an energy density of more than 2.2 kJ/g. The heat storage capacity of the composite sorbent after 5 dehydration-hydration cycles remained above 95 % of the original, which reinforces the viability of the material for long-term heat storage.

Jiand et al. [16] measured the thermal conductivities of MgCl_2 hydrates and found that they range from 0.15 to 0.96 W/mK at temperatures ranging from 15 to 70 °C, while MgSO_4 hydrates range from 0.29 to 0.68 W/mK at temperatures ranging from 20 to 45 °C. To improve the thermal properties of the hydrate salt, the authors confined MgCl_2 particles inside ENG. With salt loadings of 70-80 wt%; the thermal conductivities of the composites were measured and improved in the 0.97-2.92 W/mK (at 20 °C) range.

Binary systems including at least MgCl_2 or MgSO_4 .

Recent challenges revealed that the use of mono-salt hydrate materials brings to some major limitations, such as limitation on the water sorption and a low hydration heat. These drawbacks can be by-passed by adding a second inorganic salt hydrate to form binary composites.

In 2019, Rehman et al. [17] prepared a novel composite material containing two inorganic salt hydrates: 90 % MgSO_4 and 10 % ZnSO_4 , labelled MZx. The composite presented a lower dehydration temperature (120 °C) and a capacity of storing thermal energy (1422 J/g) much higher than its pure constituents. Under constant temperature, the water uptake capacity of the composite improved by increasing the humidity (below 80 % RH). On the other hand, at constant RH of 75 %, the hydration rate was significantly increased by increasing the discharge temperature up to 45 °C (**Figure 7**). A similar method was approached by Khan et al. [18] that prepared another binary system called ZM2

composed of 80 % ZnSO_4 and 20 % MgCl_2 . This composite was also reported to have a high heat storage capacity of over 1400 J/g at a low charging temperature.

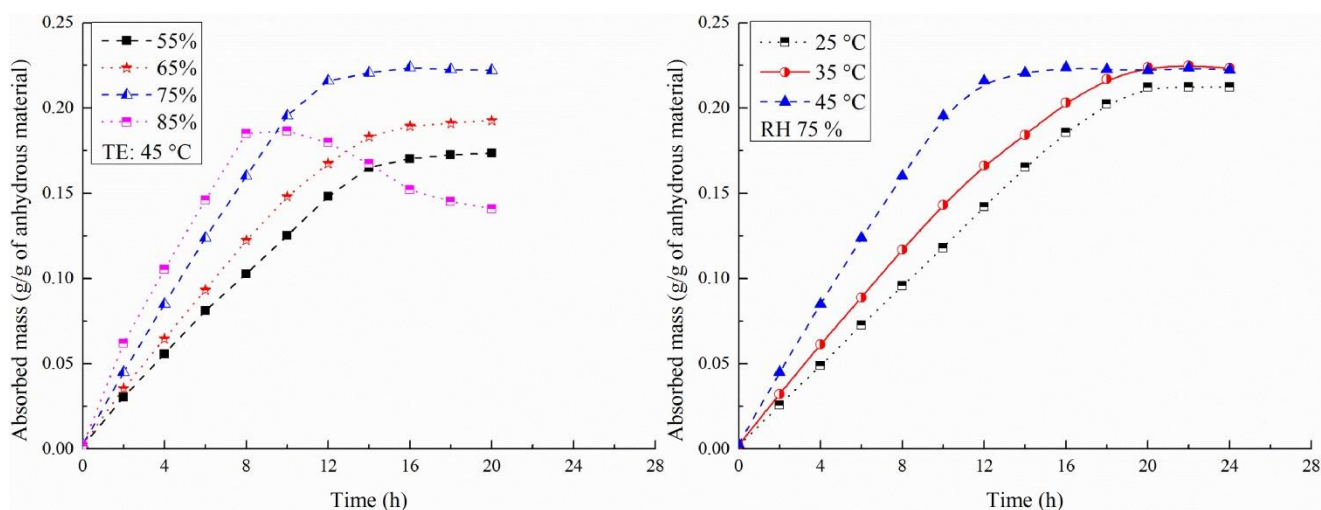


Figure 7. Variation of adsorbed mass with time under different operating conditions [17].

Zhang et al. [19] mixed a “strong” hygroscopic salt like CaCl_2 with a “medium” one like MgSO_4 prior to the insertion into zeolite 13X (“strong” and “medium” were used in the to describe the easy deliquescence of the hydrated salt). The best ratio for preparing the binary salt was found to be 60 % CaCl_2 and 40 % MgSO_4 ; this composite was characterized by an enhanced hydration heat, more than double than that of samples containing only MgSO_4 or only CaCl_2 . The authors performed a deep investigation to determine the optimal working conditions and the optimal configuration when using zeolite 13X as support. The results showed that the presence of 10 wt% of zeolite 13X and a salt ratio of 60 % CaCl_2 and 40 % MgSO_4 is the best configuration for synthesizing the composites. The sorption behavior of this optimized material (10 % 13X: 36 % MgSO_4 : 54 % CaCl_2) was studied and an outstanding adsorption capacity of 0.45 g/g was recorded. The heat storage capacity was 1414 J/g, accompanied by a remarkable stability during 20 cycles.

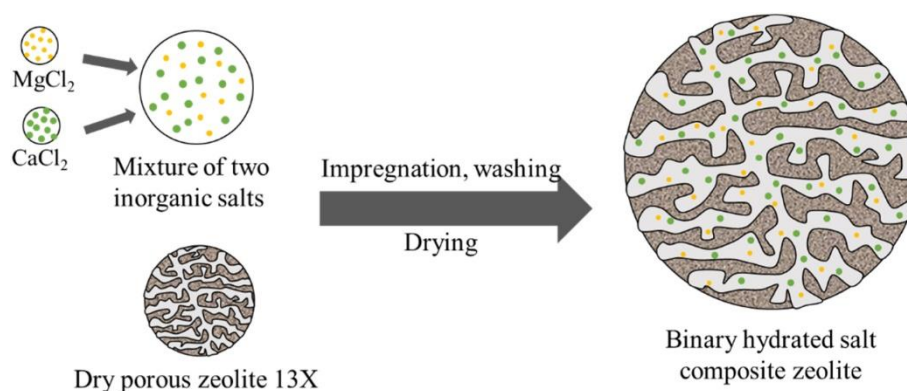


Figure 8. The preparation process of the binary hydrated salt composite zeolite [20].

Later, Ji et al. [20] mixed two chloride hygroscopic salts, CaCl_2 , and MgCl_2 right before impregnating them on a dry porous zeolite 13X (**Figure 8**). Even though the authors experienced a better performance when depositing more salt, they reported that for salt concentration above 15 wt%, the zeolite particles began to break. When the mass ratio of MgCl_2 to CaCl_2 was 1:1.5, the synthesized composite presented a storage density of 719 J/g. To further improve the heat and mass transfer, especially for the study of the composite in a reactor, the authors placed the hydrated salt zeolite mixture in an Al cube mesh (5 cm edge) (**Figure 9**) and the storage density recorded was improved to 918 J/g.

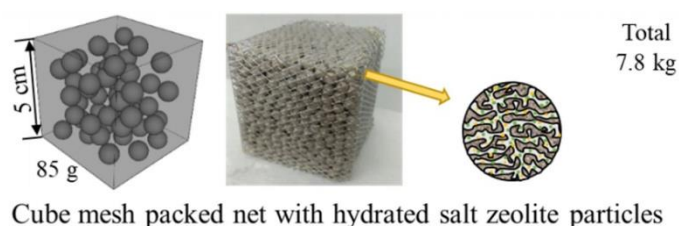


Figure 9. Representation of the Al cube mesh of 5 cm edge [20].

Ousaleh et al. [22] employed a mass ratio of MgSO_4 to MgCl_2 of 1:1 in their research, but the host matrix, instead of 85 wt%, represented only 20 wt% of the composite; 80 wt% being the salt mixture. The porous material used was a synthesized graphene sheets (Gr). It was stated that the incorporation of hydrated mixed salt into graphene sheets was successful. Even though the storage density is slightly lower than in the case when there was no porous support (**Figure 10**), the energy maintained after the cyclability test was impressively improved. Indeed, the Gr-MgSC composite presented great stability over 60 cycles of charging/discharging with nearly 91 % of the 1st cyclic energy still available (968.3 J/g compared to 1065.9 J/g) compared to only 38.6 % in absence of graphene sheets (553.1 J/g compared to 1433.1 J/g).

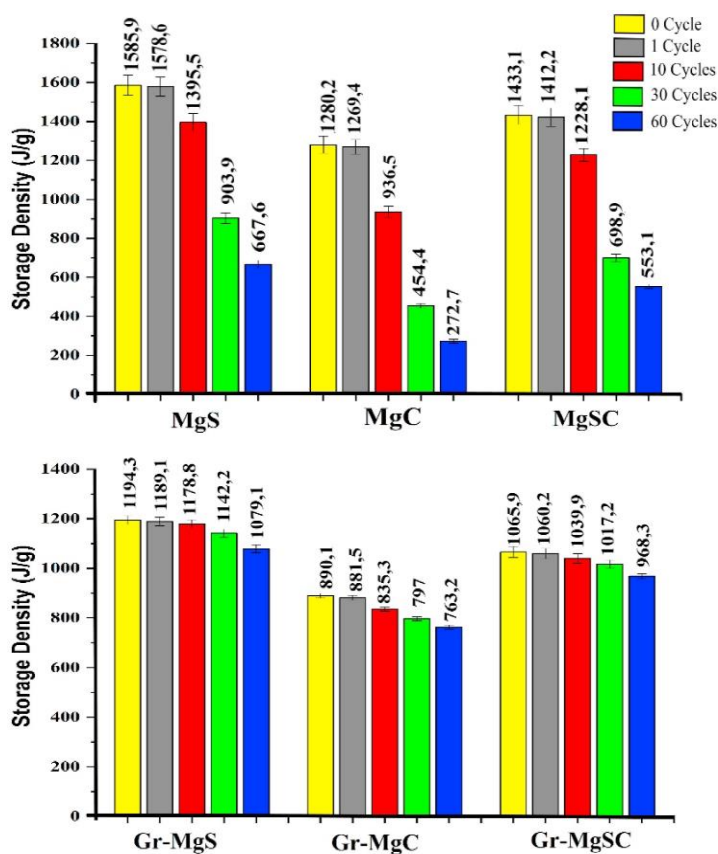


Figure 10. Heat storage density of different materials during the cyclability test [22].

Conclusion

As evidenced, MgSO_4 and MgCl_2 are undeniably two promising salts for heat storage applications. Thus, these two salts have been chosen for further investigation in this thesis. MgSO_4 , a hygroscopic salt with a strong potential because of its high theoretical energy density, will be the main hydrate salt considered during all the research work. MgCl_2 , a highly hygroscopic salt, will be used as a secondary salt to be added to MgSO_4 to form binary-salt composites that will be discussed in chapter VI of the thesis manuscript.

References

- Xu, C.; Yu, Z.; Xie, Y.; Ren, Y.; Ye, F.; Ju, X. Study of the hydration behavior of zeolite- MgSO_4 composites for long-term heat storage. *Appl. Therm. Eng.* **2018**, *129*, 250–259, doi:10.1016/j.applthermaleng.2017.10.031.
- Rehman, A.U.; Shah, M.Z.; Rasheed, S.; Afzal, W.; Arsalan, M.; Rahman, H.U.; Ullah, M.; Zhao, T.Y.; Ullah, I.; Din, A.U.; et al. Inorganic salt hydrates and zeolites composites studies for thermochemical heat storage. *ZEITSCHRIFT FUR Phys. CHEMIE-INTERNATIONAL J. Res. Phys. Chem. Chem. Phys.* **2021**, *235*, 1481–1497, doi:10.1515/zpch-2021-3012.

3. Xu, S.Z.; Wang, R.Z.; Wang, L.W.; Zhu, J. Performance characterizations and thermodynamic analysis of magnesium sulfate-impregnated zeolite 13X and activated alumina composite sorbents for thermal energy storage. *ENERGY* **2019**, *167*, 889–901, doi:10.1016/j.energy.2018.10.200.
4. Jiang, L.; Gao, J.; Wang, L.; Wang, R.; Lu, Y.; Roskilly, A.P. Investigation on performance of multi-salt composite sorbents for multilevel sorption thermal energy storage. *Appl. Energy* **2017**, *190*, 1029–1038, doi:10.1016/j.apenergy.2017.01.019.
5. Jiang, L.; Roskilly, A.P.; Wang, R.Z.; Wang, L.W.; Lu, Y.J. Analysis on innovative modular sorption and resorption thermal cell for cold and heat cogeneration. *Appl. Energy* **2017**, *204*, 767–779, doi:10.1016/j.apenergy.2017.07.041.
6. Zhao, Y.J.; Wang, R.Z.; Zhang, Y.N.; Yu, N. Development of SrBr₂ composite sorbents for a sorption thermal energy storage system to store low-temperature heat. *Energy* **2016**, *115*, 129–139, doi:10.1016/j.energy.2016.09.013.
7. Miao, Q.; Zhang, Y.; Jia, X.; Tan, L.; Ding, Y. MgSO₄-expanded graphite composites for mass and heat transfer enhancement of thermochemical energy storage. *Sol. Energy* **2021**, *220*, 432–439, doi:10.1016/j.solener.2021.03.008.
8. Zhang, Y.; Miao, Q.; Jia, X.; Jin, Y.; Li, Z.; Tan, L.; Ding, Y. Diatomite-based magnesium sulfate composites for thermochemical energy storage: Preparation and performance investigation. *Sol. ENERGY* **2021**, *224*, 907–915, doi:10.1016/j.solener.2021.05.054.
9. Tabard, L.; Prud'Homme, E.; Garnier, V.; Gremillard, L. Hierarchical salt-ceramic composites for efficient thermochemical energy storage. *Appl. Mater. Today* **2020**, *20*, 100658, doi:10.1016/j.apmt.2020.100658.
10. Zambotti, A.; Valentini, F.; Lodi, E.; Pegoretti, A.; Tyrpekl, V.; Kohúteková, S.; Sorarù, G.D.; Kloda, M.; Biesuz, M. Thermochemical heat storage performances of magnesium sulphate confined in polymer-derived SiOC aerogels. *J. Alloys Compd.* **2022**, *895*, doi:10.1016/j.jallcom.2021.162592.
11. Kallenberger, P.A.; Posern, K.; Linnow, K.; Brieler, F.J.; Steiger, M.; Froeba, M. Alginate-Derived Salt/Polymer Composites for Thermochemical Heat Storage. *Adv. Sustain. Syst.* **2018**, *2*, doi:10.1002/adsu.201700160.
12. Yu, N.; Wang, R.Z.; Wang, L.W. Sorption thermal storage for solar energy. *Prog. Energy*

- Combust. Sci.* **2013**, *39*, 489–514, doi:10.1016/j.pecs.2013.05.004.
13. Xu, J.X.; Li, T.X.; Chao, J.W.; Yan, T.S.; Wang, R.Z. High energy-density multi-form thermochemical energy storage based on multi-step sorption processes. *Energy* **2019**, *185*, 1131–1142, doi:10.1016/j.energy.2019.07.076.
 14. Zhou, H.; Zhang, D. Effect of graphene oxide aerogel on dehydration temperature of graphene oxide aerogel stabilized MgCl₂ center dot 6H(2)O composites. *Sol. ENERGY* **2019**, *184*, 202–208, doi:10.1016/j.solener.2019.03.076.
 15. Zhou, H.; Zhang, D. Investigation on pH/temperature-manipulated hydrothermally reduced graphene oxide aerogel impregnated with MgCl₂ hydrates for low-temperature thermochemical heat storage. *Sol. Energy Mater. Sol. Cells* **2022**, *241*, 111740, doi:10.1016/j.solmat.2022.111740.
 16. Jiang, L.; Lin, Y.C.; Liu, W.; Ma, Z.W.; Wang, R.Q.; Zhang, X.J.; Roskilly, A.P. Thermophysical characterization of magnesium chloride and its application in open sorption thermal energy storage system. *Sol. ENERGY Mater. Sol. CELLS* **2022**, *236*, doi:10.1016/j.solmat.2021.111528.
 17. Rehman, A.U.; Khan, M.; Maosheng, Z. Hydration behavior of MgSO₄–ZnSO₄ composites for long-term thermochemical heat storage application. *J. Energy Storage* **2019**, *26*, 101026, doi:10.1016/j.est.2019.101026.
 18. Khan, A.R.; Khan, M.; Rehman, A.U.; Zhao, T.Y.; Zheng, M. Novel Synthesis and Structural Investigations of ZnSO₄/MgCl₂ Composite Hydrated Salt for Enhanced Thermochemical Heat Storage Applications. *Russ. J. Inorg. Chem.* **2022**, *67*, 1125–1134, doi:10.1134/S0036023622070129.
 19. Zhang, X.L.; Wang, F.F.; Zhang, Q.; Lei, X.D.; Wang, Y.L.; Zhang, Y.Q.; Cheng, C.X.; Jin, T.X. Heat storage performance analysis of ZMS-Porous media/CaCl₂/MgSO₄ composite thermochemical heat storage materials. *Sol. ENERGY Mater. Sol. CELLS* **2021**, *230*, doi:10.1016/j.solmat.2021.111246.
 20. Ji, W.J.; Zhang, H.; Liu, S.L.; Wang, Z.H.; Deng, S.H. An experimental study on the binary hydrated salt composite zeolite for improving thermochemical energy storage performance. *Renew. ENERGY* **2022**, *194*, 1163–1173, doi:10.1016/j.renene.2022.06.024.
 21. Shere, L.; Trivedi, S.; Roberts, S.; Sciacovelli, A.; Ding, Y.L. Synthesis and Characterization

- of Thermochemical Storage Material Combining Porous Zeolite and Inorganic Salts. *HEAT Transf. Eng.* **2019**, *40*, 1176–1181, doi:10.1080/01457632.2018.1457266.
22. Ousaleh, H.A.; Sair, S.; Mansouri, S.; Abboud, Y.; Faik, A.; El Bouari, A. New hybrid graphene/inorganic salt composites for thermochemical energy storage: Synthesis, cyclability investigation and heat exchanger metal corrosion protection performance. *Sol. ENERGY Mater. Sol. CELLS* **2020**, *215*, doi:10.1016/j.solmat.2020.110601.

Chapter II

**Methods, experimental techniques
and materials**

Résumé

Pendant ces travaux de thèse, des matériaux composites ont été synthétisés par la méthode d'imprégnation par voie humide pour assurer l'homogénéité de la distribution du sel au sein de la matrice poreuse. Après un séchage à 150 °C, les composites finaux ont été caractérisés par différentes méthodes physico-chimiques afin de connaître leur composition élémentaire, le type de phases présentes, leur surface spécifique ainsi que la distribution de taille des pores. Ces analyses couplées aux mesures de sorption de la vapeur d'eau nous ont permis d'évaluer le potentiel de ces matériaux pour des applications de stockage de la chaleur et de comprendre les phénomènes d'adsorption associés. Ce chapitre décrit brièvement le principe de toutes les méthodes utilisées pour la caractérisation de ces matériaux composites. Egalement, à la fin de ce chapitre est présentée une liste de tous les matériaux (supports et composites synthétisés) qui ont été étudiés au cours de ce travail de thèse.

1. Methods and experimental techniques

This thesis work consists mainly of synthesizing new composites salt-in-matrix and studying the performance of these materials in terms of water uptake capacity and energy heat released upon the hydration. Consequently, following the selection process of salt hydrates and porous host support, optimizing the protocol of synthesis is a crucial step. As-synthesized composites are then characterized by various techniques to grasp an understanding of underlying structures, surface chemistry and different physicochemical properties. A list of composite materials during this thesis work is presented at the end of this chapter.

1.1. Protocol of synthesis

Wet Impregnation (WI) is the most widely-used method to incorporate salt hydrates particles within the porous structure of the chosen support; it has been then selected as the impregnation method. Firstly, a suitable amount of salt hydrates is totally dissolved in deionized water. The porous support (sieved) is then gently added to the saline solution with continuous agitation. After a certain time, long enough to impregnate the salt homogeneously inside the structure, the mixture is then oven-dried at up to 150 °C under atmospheric pressure with the aim of slowly vaporizing the excess water. The final dry-composites are then obtained and the material properties were investigated using characterization techniques. Detailed information about impregnation and drying time are to be found in following chapters.

1.2. Characterization techniques

A variety of experimental techniques was used during these three years of thesis to characterize different composites. The porous structures, the surface properties as well as the compositions of the composites were investigated. N₂ and CO₂ adsorption isotherms are useful to characterize the pore distribution and to measure the porous surface of the studied materials. Scanning electron microscopy (SEM) coupling with EDX (a local elementary analysis of any element) permit to obtain information on the morphology of the samples. Other techniques as the X-ray diffraction (XRD) gives useful information for identifying the crystallographic phases. X-ray fluorescence (XRF) provides the atomic composition of the samples. X-ray photoelectron spectroscopy (XPS) gives the distribution of the atoms on the surface and the type of the chemical bounds, as well as information of the redox state of the atoms. These above-mentioned techniques are briefly described in the following paragraphs within the characteristics of the devices and the measurement conditions.

X-ray diffraction (XRD) is a non-destructive technique used to determine the crystallographic structure of the materials. XRD works by irradiating the material with a monochromatic beam X-rays. As a result of this interaction, X-rays are scattered through the atoms located at different crystallographic planes and are re-emitted elastically producing an X-ray spectrum. The phenomenon of diffraction is then produced by the constructive interference between the different rays emitted. The interference is constructive when the Bragg's law conditions are met (**Figure 11**):

$$n\lambda = 2d_{hkl} \cdot \sin \theta \quad \text{Equation 3}$$

where n is an integer, λ is the wavelength of in the incident X-ray beam, d_{hkl} is the distance between two crystallographic planes and θ is the incident angle of the X-ray beam.

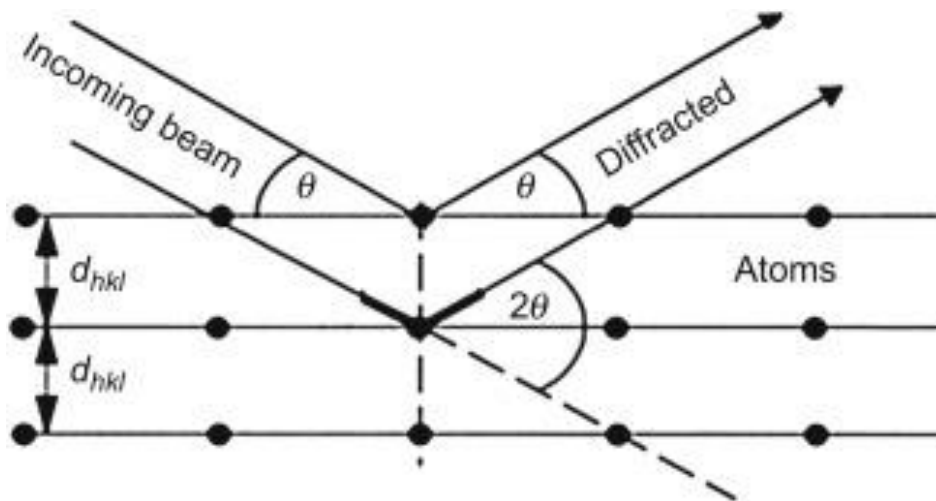


Figure 11. Geometrical condition for diffraction from lattice planes [1].

In this work, the X-ray powder diffraction was used for phase identification. The samples were prior finely ground and homogenized. The diffractogram of the analyzed sample was obtained by varying the incident angle and measuring the intensity of the characteristic beam. The XRD analyses were obtained on a diffractometer PANalytical MPD X'Pert Pro, equipped with a Pixcel real-time multiple strip detector, operating with an angular aperture of $3.347^\circ 2\theta$ in 3° – $80^\circ 2\theta$ range, and using $\text{CuK}\alpha$ radiation with 0.15418 nm wavelength. Diffractograms were recorded at 22°C with a step size of $0.013^\circ 2\theta$ and a scan time of 220 s per step.

X-ray fluorescence (XRF) is a non-destructive technique used to determine the elemental composition of the materials. Similar to XRD, XRF also works by irradiating a sample with high-energy X-rays beam. When an atom is excited, one of the electron is dislocated and became an unstable quantum state. To stabilize the atom, one electron from a higher energy

orbital drops to fill the vacancy. As a result, a fluorescent X-ray is emitted with an energy equals to the difference in energy between two quantum states of the electron. This energy is measured and is unique to the specific atom in question. Each atom has a unique set of characteristic fluorescent X-ray which allow one to quantify the composition of the atom (**Figure 12**).

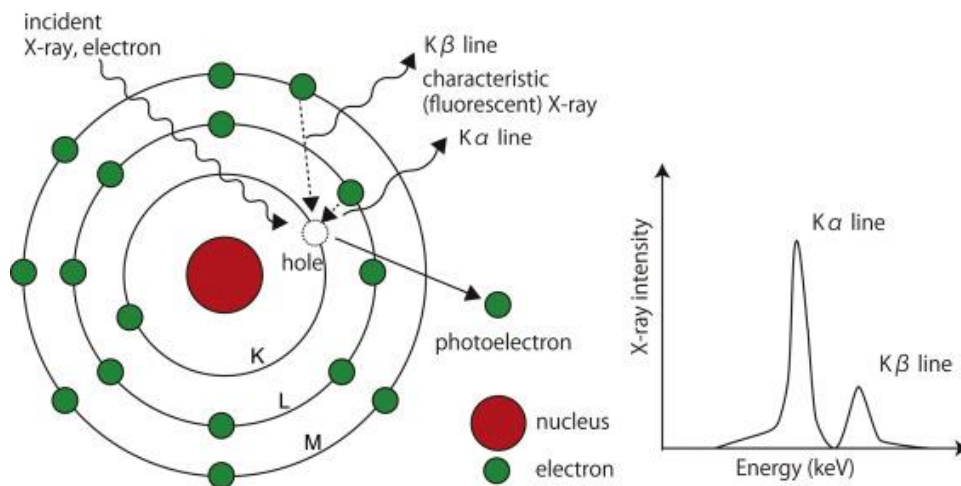


Figure 12. The mechanism of X-ray fluorescence [2].

In this thesis, XRF analyses were performed on a spectrometer PANalytical Zetium. Previous to analysis, for hydroxyapatite 0.2 g of the sample was formed in a pellet and for carbonated materials 0.1 g of the sample was mixed with 0.2 g of boric acid (H_3BO_3) as binding agent before being formed in pellets.

Scanning Electron Microscopy (SEM) is an imagery method that uses an electron beam to image samples with a resolution at the nanometer scale. The surface of the samples is bombarded with an electron beam emitted from a filament. As a result of the interaction between electrons and the surface sample, different types of signal are generated: backscattered electrons (BSE), secondary electrons (SE) and characteristic X-rays. BSE are high-energy electrons that reflected from the sample by elastic scattering. They emerge from the “bulk” of the sample (a few microns deep) and they provide information about the chemical composition. SE are electrons come from within a few nanometers of the sample surface and possess lower energy compared to BSE. Thus, SE provide a topographical contrast and therefore to observe the morphology of the sample. These two types of signal allow one to obtain the SEM images.

Characteristic X-rays are emitted when the electron beam removes an electron from the inner orbital of the sample. Then, an electron from a higher energy orbital fills the vacancy and release energy. This energy can be measured by **Energy-Dispersive X-ray (EDX)** spectroscopy which

can be used coupled to SEM. This measurement allows to identify the different elements and map their distribution (**Figure 13**).

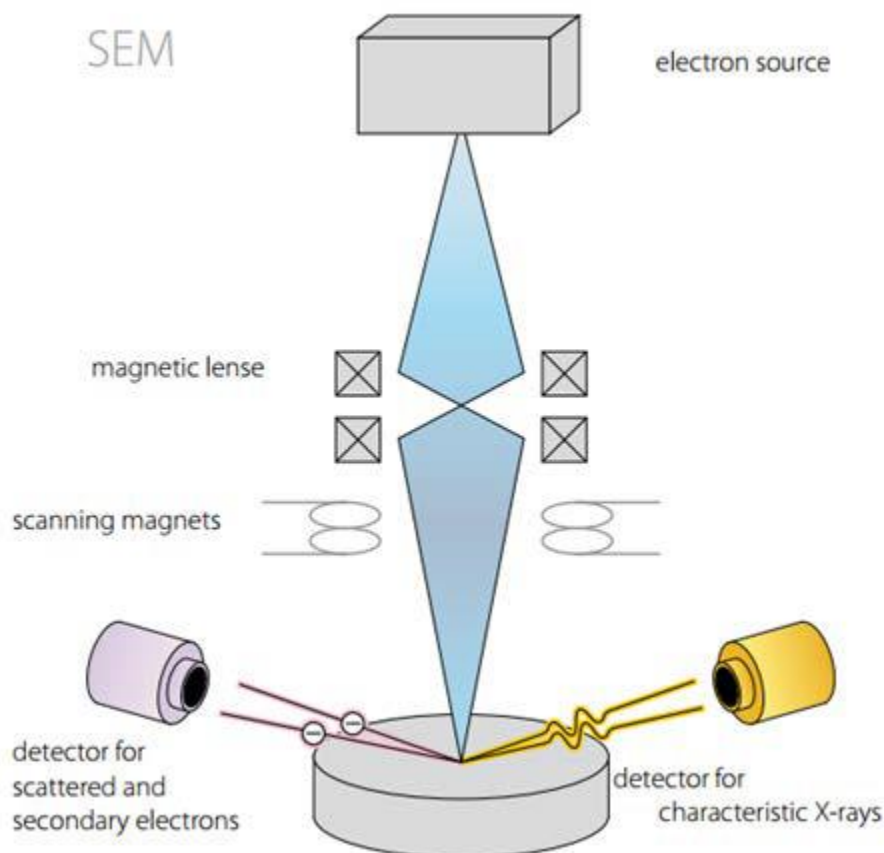


Figure 13. Schematic of the principle of SEM equipped with EDX [3].

All the high-resolution micrographics of different materials studied in this thesis work were acquired by a SEM from JEOL, JSM-7900F model. The semi-quantitative chemical analysis and atomic composition mapping of the sample was performed by means of EDX.

N₂ or CO₂ adsorption/desorption isotherm is a method which allows to determine the specific surface area as well as to probe the porosity of solid materials. The principle of the method is based on the physical adsorption of the gas molecules (N₂ or CO₂) on the surface of the material to constitute a monolayer. This method consists of plotting adsorption/desorption isotherms of the material by calculating the volume of the adsorbed gas in function of the gas relative pressure (p/p°) with p the equilibrium pressure and p° the saturated vapor pressure.

In order to study the porous structure of different materials, N₂ adsorption/desorption isotherms of support and composites were obtained at -196°C . CO₂ adsorption/desorption isotherms

were obtained at 0 °C. The experiments were performed in a ASAP 2420 device from Micrometrics (Micromeritics, Norcross, GA, USA). The samples were previously degassed at 150 °C for 12 h and then, again at 150 °C for 2 h directly in the cell on the analysis emplacement. The specific surface area was then calculated applying the Brunauer, Emmett and Teller (BET) equation (S_{BET}) in different p/p° range, depending on the characteristic of the material: microporous or mesoporous. The mesoporous volumes (V_m), external surface (ext) and microporous surface (S_m) were determined by applying the t-plot method (thickness range: 0.35–0.50). Finally, the pore size distribution (PSD) (from the N_2 adsorption isotherms) was determined using Barrett, Joyner and Halenda (BJH) method applied on the desorption branch of the isotherms or Density Functional Theory (DFT) method.

Mercury Intrusion Porosimetry is based on the penetration principle of a non-wetting and non-reactive liquid into a porous material. Liquid mercury is ideal since it does not spontaneously penetrate the pores by capillarity, thus it is necessary to apply pressure. The mechanism of intrusion is described by Equation 4 with d the pore diameter in which liquid mercury intruded, γ the surface tension of mercury, θ the contact angle and P the applied pressure. Liquid mercury therefore penetrates under a pressure that is inversely proportional to the pore diameter. In this thesis, this characterization was performed by **FiLab** on the biochar support and its synthesized composites.

$$d = \frac{-4\gamma\cos\theta}{P} \quad \text{Equation 4}$$

Thermal conductivity is one important parameter that needs to be considered for the performance of the storage process. **Hot Disk TPS 500 Analyzer** allows to determine the thermal conductivity of the sample. It is constituted of a plane Kapton sensor (**Figure 14**) sandwiched between two samples halves. The measurement starts when a constant electric power is sent through the conducting Ni-spiral, increasing the sensor temperature. The heat generated dissipates into the sample on both sides of the sensor, at a rate depending on the intrinsic material properties [4]. By recording the sensor temperature versus time response $\Delta T(t) = f(t)$, the thermal conductivity (λ) and heat capacity (ρC_p) of the material can be evaluated. Thus, the thermal diffusivity (α) can be calculated with Equation 5.

$$\alpha = \frac{\lambda}{\rho C_p} \quad \text{Equation 5}$$

The experiments were conducted at 20 °C for 160 s at a heating power of 100 mW. Each measurement was repeated at least 5 times.



Figure 14. Kapton sensor with a double spiral conducting.

To understand the behavior and the performance of different storage materials during the reversible reactions, thermogravimetry coupled to differential scanning calorimetry (TG-DSC) was used to determine the water sorption capacity as well as the heat released. These two properties are used to evaluate different salt hydrates, pure supports and also their composites.

1.3. Temperature and Humidity profiles

To be able to run experiments of water sorption heat storage (open system), the TG-DSC was coupled to a Wetsys – humidity generator (**Figure 15**) through a heated transfer line, in order to send into the calorimeter a gas flow with fixed relative humidity. The DSC allows to measure the heat stored (charged) or released (discharged) during the sorption process, while the TG (equipped with a microbalance) is used to evaluate the water uptake/loss of the samples. The temperature and humidity profiles could be programmed and optimized (**Figure 16**) in order to assure the completion of the dehydration process as well as the hydration process.

First, the samples were gradually dehydrated from 30 °C to 150 °C (5 °C/min) with a dried-air flow rate at 30 mL/min followed by an isotherm at 150 °C for at least 3 hours. Once the sample was cooled down to 30 °C and the DSC baseline was stable, the relative humidity was increased to 60 % (or a vapor pressure of 2.55 kPa) and the hydration process programmed during 8 hours for a completed reaction. The dehydration-hydration was repeated at least three times for each sample. These conditions were selected to replicate a real-life residential application: 150 °C is the temperature that can be reached using a flat-plate solar heat collectors and 30 °C is close to the indoor air temperature during the discharging phase.



Figure 15. TG-DSC apparatus with a microbalance connected to a humidity generator (Wetsys) through a thermal transfer line (Setaram).

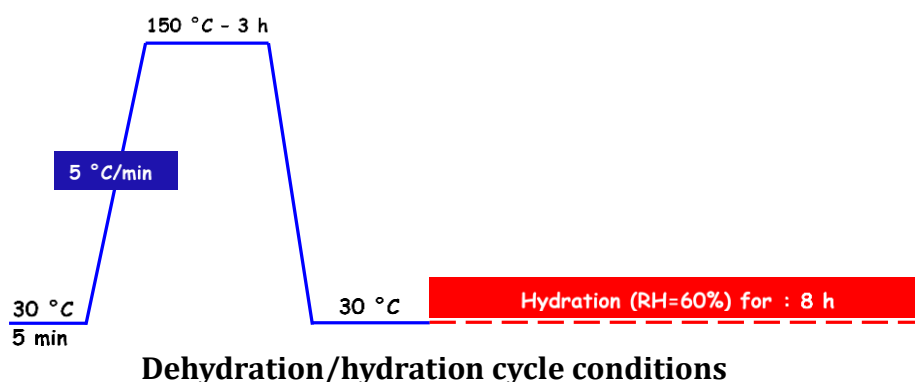


Figure 16. Example of a dehydration/hydration cycle with temperature and humidity.

2. List of materials

Here below is the **Table 2** that list the materials used and synthesized during this work thesis. Different types of porous host supports were employed to study the performance of different composites at various compositions. The host varies from mineral to carbon-based materials, with/or without a specific shaping (powder, granular, bead-formed). The main salt hydrates used was $\text{MgSO}_4 \cdot 7\text{H}_2\text{O}$ and a mixture constituted of MgSO_4 and MgCl_2 . Details on its properties are presented in Chapter VII. The composites are named as $x\text{-MgSO}_4/\text{support}$ with x - the actual mass content in the dried-composites.

Table 2. List of synthesized and studied materials during this work thesis.

Composite	Porous host support	Salt hydrates	Chapter/Publication
1.0-MgSO ₄ /BAC 5.2-MgSO ₄ /BAC 7.6-MgSO ₄ /BAC	Beads activated carbon (BAC)	MgSO ₄ .7H ₂ O	Chapter III/Publication 1 (Under reviewed)
5-MgSO ₄ /HAP 20-MgSO ₄ /HAP	Hydroxyapatite (HAP)	MgSO ₄ .7H ₂ O	Chapter IV/Publication 2 (Published)
5-MgSO ₄ /AC 10-MgSO ₄ /AC 20-MgSO ₄ /AC 30-MgSO ₄ /AC 40-MgSO ₄ /AC	Activated carbon L27W from Norit NV	MgSO ₄ .7H ₂ O	Chapter V/Publication 3 (Published)
5MgCC 10MgCC 15MgCC 20MgCC	Corncob biochar (CC)	MgSO ₄ .7H ₂ O	Chapter VI (article in preparation)
PC_20MgSO ₄ PC_40MgSO ₄ PC_60MgSO ₄ PC_20binary PC_40binary PC_60binary	Porous carbon (PC)	MgSO ₄ .7H ₂ O MgCl ₂ .6H ₂ O	Chapter VII/Publication 4 (submitted)

References

1. Epp, J. X-Ray Diffraction (XRD) Techniques for Materials Characterization. In *Materials Characterization Using Nondestructive Evaluation (NDE) Methods*; Elsevier Inc., 2016; pp. 81–124 ISBN 9780081000571.
2. Uo, M.; Wada, T.; Sugiyama, T. Applications of X-ray fluorescence analysis (XRF) to dental and medical specimens. *Jpn. Dent. Sci. Rev.* 2015, *51*, 2–9.
3. Mohamed, M.A.H.W. University of Southampton Research Repository. **2021**, 310.

4. Gustavsson, M.; Karawacki, E.; Gustafsson, S.E. Thermal conductivity, thermal diffusivity, and specific heat of thin samples from transient measurements with hot disk sensors. *Rev. Sci. Instrum.* **1994**, *65*, 3856–3859, doi:10.1063/1.1145178.

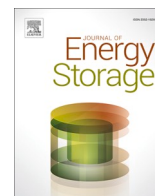
Chapter III

Thermochemical sorption heat storage: Investigate the heat released from activated carbon beads used as porous host matrix for MgSO₄ salt.

Journal of Energy Storage 59, 106452 (2023)

Résumé

Des billes de carbone activé dérivées de résidus pétroliers ont été choisies comme support pour préparer une première série de composites. Ces billes présentent une surface spécifique élevée, un faible coût et une non-toxicité. Trois composites avec des teneurs en sel MgSO_4 de 1, 5,2, et 7,6 % ont été préparés. Aucune phase secondaire n'a été détectée par DRX. L'analyse des isothermes adsorption d'azote a montré que les billes de carbone activé sont des matériaux microporeux avec une surface spécifique très élevée (de l'ordre de $1300 \text{ m}^2/\text{g}$). La distribution de tailles des pores se situe principalement entre 1 et 2 nm. Afin d'analyser plus finement la microporosité de ces échantillons, des analyses d'adsorption de CO_2 ($0 \text{ }^\circ\text{C}$) ont également été effectuées. Elles ont permis de détecter la présence d'ultra-micropores de tailles comprises entre 0,6 et 0,85 nm. Une taille de pores si petite peut empêcher les molécules de sel de rentrer dans la matrice pendant l'imprégnation. Le sel a ainsi tendance à rester sur la surface du support et bloquer l'accès des pores, ce qui affecte, pendant l'utilisation du matériau de stockage, le transfert de masse (migration des molécules d'eau pendant la phase d'hydratation). La cartographie EDX montre la dispersion homogène de MgSO_4 sur la surface du support, mais aucune information ne peut être déduite sur la présence de sel à l'intérieur des micropores. Les résultats de sorption d'eau montrent un bon niveau hydratation ($0,37 \text{ g}_{\text{eau}}/\text{g}_{\text{mat}}$) accompagné par des chaleurs d'hydratation de 920 J/g de composite, pour le matériau contenant 7,6 % en masse de sel. La stabilité suivant des cycles successifs d'hydratation/déshydratation a été démontrée pour 10 cycles.



Research papers

Thermochemical sorption heat storage: Investigate the heat released from activated carbon beads used as porous host matrix for MgSO₄ salt

Minh Hoang Nguyen, Mohamed Zbair, Patrick Dutournié, Simona Bennici*

Institut de Science des Matériaux de Mulhouse (IS2M), Université de Haute-Alsace, CNRS, IS2M UMR 7361, F-68100 Mulhouse, France
Université de Strasbourg, France



ARTICLE INFO

Keywords:

Thermochemical heat storage
Magnesium sulfate
Bead activated carbon
Water sorption
Adsorption kinetics

ABSTRACT

For sustainable and cost-effective thermal management and energy storage, sorption-based thermal storage has received a lot of attention. However, the low sorption capacity of sorbents has long been a barrier to high energy-density sorption-based thermal storage. We present a new promising composite with high heat release and sorption capacity. The use of MgSO₄/bead activated carbon composites in thermochemical sorption heat storage has been investigated. Because of the highly developed microporosity and high apparent specific surface area of about 1300 m²/g, bead activated carbon (BAC) is a potential candidate as support for salt/support composites for thermochemical heat storage. Also, the thermal conductivity of BAC has been measured and found to be 0.14 W/mK, which is higher than that of other materials like zeolites or alumina. This high thermal conductivity can influence the water sorption equilibrium, controlling the temperature of the solid, avoiding hot-spots, and thus preventing desorption during the hydration step. In stationary conditions (RH = 60 %, gas flow = 30 mL/min), the water sorption capacity of BAC was 0.138 g/g. This value was 2.32 times higher when the salt was dispersed into the BAC matrix, for the composite 7.6-MgSO₄/BAC. A water adsorption capacity, higher than the theoretical value, was observed and attributed to the condensation of water molecules within the porous structure, resulting in a high thermal energy density. The 7.6-MgSO₄/BAC composite achieved the highest heat of hydration of 920 J/g. The 10 hydration/dehydration cycles performed (dehydration at 150 °C and hydration at 30 °C with a RH of 60 %) confirmed the composite's excellent stability. This research provides a promising low-carbon pathway for the efficient capture, storage, and utilization of thermal energy.

1. Introduction

Energy supply, as an important global concern, is raising more awareness than ever, especially with the exponential expansion of the population. Fossil fuels have provided nearly 80 % of global energy since the mid-twentieth century [1], and the reserves are being exploited indiscriminately [2]. Transitioning to solar energy systems as an alternative source of energy is advocated as a way to reduce greenhouse gas emissions from fossil fuel consumption [3,4].

A large contribution of solar energy can be harvested and used in the built environment, as this sector is responsible for over one third of the world's energy consumption [5,6]. This natural source of energy, however, is weather dependent; energy is delivered during the day and none is produced during the night. Thermal energy storage (TES) is an advanced technology and an effective solution to resolve the mismatch

between supply and demand, as well as long-term solar energy use [7–9]. Latent heat storage, sensible heat storage, and thermochemical heat storage (TCHS) are three types of systems using TES technologies. While sensible heat storage is widely commercially known and latent heat storage is extensively studied [10,11], there has been less attention on TCHS, which is becoming a focal point in the domain due to its higher energy storage density and theoretically no heat loss over time [12–14]. The principle is based on the reversible sorption reaction, where the heat is stored during desorption (charge) and then released when needed during adsorption (discharge). To turn the system into a practical residential application (space heating and sanitary hot water), the TCHS material needs to be chosen with care. Certain properties, such as high energy density, low charging temperature, good mass and heat transfer [15,16], improved thermal conductivity [17] are used as criteria for choosing salt hydrates as the potential candidate [18–20]. Heat storage

* Corresponding author at: Institut de Science des Matériaux de Mulhouse (IS2M), Université de Haute-Alsace, CNRS, IS2M UMR 7361, F-68100 Mulhouse, France.
E-mail addresses: minh-hoang.nguyen@uha.fr (M.H. Nguyen), mohamed.zbair@uha.fr (M. Zbair), patrick.dutournie@uha.fr (P. Dutournié), simona.bennici@uha.fr (S. Bennici).

<https://doi.org/10.1016/j.est.2022.106452>

Received 19 July 2022; Received in revised form 9 December 2022; Accepted 15 December 2022

Available online 24 December 2022

2352-152X/© 2022 Elsevier Ltd. All rights reserved.

density is a crucial property of a storage material. There are two major formulations for this quantity in the literature, which relate to the amount of heat that can be stored in a unit of mass (gravimetric storage density, GSD) or a unit of volume (volumetric storage density, VSD). Both storage densities are critical for salt hydrate applications in buildings. VSD is the most important since it determines the volume of the final storage unit. Typical VSD values for bulk salt hydrates are 1–3 GJ/m³, allowing for long-term domestic heat storage of several cubic meters of salt for a typical European home [21]. The couple MgSO₄-H₂O is gaining popularity due to its high theoretical energy density (2.8 GJ/m³) and high deliquescence relative humidity (DRH) of 90 % [22,23]. Though the performance did not meet expectations due to the kinetic hindrance and the formation of aggregates.

The Borekov Institute of Catalysis in Russia came up with the idea of putting salt in a porous matrix (CSPM) to avoid or mitigate these problems [24]. In recent years, a lot of “salt in porous matrix” composite sorbents have been found by putting hygroscopic salts into zeolite, silica gel, hydrogels, MOFs, etc. [25–32]. A research team [30] embedded strontium bromide in a mesoporous MIL-101(Cr) Metal-Organic Framework, and a heat storage density of 233 kW h/m³ was achieved by employing water vapor at a partial pressure as low as 1.25 kPa. This is due in part to the high salt content (63 wt%), but also to unexpected changes in the SrBr₂ water sorption isotherms once encapsulated. Shkatulov and colleagues [31] present the domestic thermal energy storage core-shell composites “salt in hollow SiO₂ spheres with mesopores” (salt = LiCl·H₂O, CaCl₂·6H₂O, SrBr₂·6H₂O). The salt hydrates were enclosed in hollow SiO₂ (HS) capsules with a submicrometer size. The composites demonstrated a state-of-the-art energy storage density of up to 0.86 GJ/m³ for the bed of storage material and a high-temperature increasing of 32–47 °C. This system showed a high energy storage capacity and stability to hydration/dehydration cycling, and the mechanical integrity of the capsules was preserved for at least 50 cycles for LiCl@HS. A novel MgSO₄·7H₂O-filled silicone composite foam was examined [32]. The dehydration process of the composite foamed material was investigated in particular with variable filler quantity (40–70 wt% salt content). The thermogravimetric measurement of all salt-silicone foams revealed satisfactory dehydration capabilities, demonstrating that the silicone matrix does not decrease water vapor diffusion. Mechanical characterization using a static compression test revealed that the silicone cellular structure was stable even under high deformations. However, with higher compression cycles, a significant loss of salt was observed. A decrease of up to 13 % was reported after 50 cycles. Different kinds of zeolites were utilized by Hongois et al. [9] and Whiting et al. [13] for the wet impregnation of MgSO₄ salt into mineral supports. Similar to this, Posern et al. [33] impregnated a combination of MgSO₄ and MgCl₂ using attapulgite powders as matrix. In their study of CaCl₂ using three different matrices—silica gel, alumina, and bentonite—Jabbari-Hichri et al. [34] found that the silica gel-impregnated composite performed the best in terms of heat stored and released and water sorption capacity. A prototype was used by Xu et al. [8] to study the hydration behavior of MgSO₄ on zeolites for open sorption heat storage. The results demonstrated that zeolite-MgSO₄ composites were hydrated easier than pure zeolites, with zeolite 13X-MgSO₄ demonstrating the greatest performance. Up to five discharges were performed without observing any performance decrease, indicating that the material's cyclability may be considered adequate as a first approximation. Wang et al. [35] impregnated 15 wt% MgSO₄ onto a zeolite 13X and the heat released reached 632 J/g_{composite} after hydration at 25 °C using 80 % RH. As a result, it is possible to conclude that, in general, composites outperform pure salts in terms of thermo-physical and kinetic properties, allowing for improved thermochemical heat storage system performance [36]. However, the rigid structures of the examined matrices may suffer from long-term stability concerns because of the stress caused by salt solution expansion during the hydration phase. By confining calcium chloride (CaCl₂) within a graphene aerogel (GA) matrix (CaCl₂@GA), Yan et al. [25] developed a high-

performance graphene aerogel (GA)-based composite sorbent for sorption thermal batteries. The CaCl₂@GA composite sorbents possessed a high salt loading (96 wt%), rapid water uptake (2.89 g/g), good thermal stability, and quick sorption kinetics due to the 3D network porous structure and high porosity of the GA matrix. The researchers also showed a lab-scale CaCl₂@GA-based sorption thermal battery (STB) with a record energy density of 1580 Wh/kg and a power density of 815 W/kg for efficient thermal energy recovery and storage. Another interesting choice of porous support is activated carbon (AC). The AC is cheap and simple to produce from waste biomass, making it a more attractive option than MOFs and similar materials. AC is hydrophilic depending on the starting material and pyrolysis conditions, and it is also very porous and thermally stable. Since the AC's internal surface may be altered in a variety of ways, chemical modifications are also a realistic possibility. The good thermal conductivity and the extremely high specific surface will facilitate the water vapor sorption rate and offer a higher heat storage capacity. For this reason and for practical application, the beads of activated carbon (BAC) have been selected as a new porous support for the impregnation of MgSO₄ in this paper. Our main objective is to gain insight on the impact of MgSO₄ salt on the hydration behaviors when confined inside the beads activated carbon pores.

2. Materials and methods

2.1. Preparation of composites MgSO₄/BAC

Composite materials made of MgSO₄ and BAC (99.8 %, Kureha Corp.) (average particle radius of BAC is $R_p = 0.35$ mm) of different compositions were prepared using the wet impregnation method. Prior to impregnation, 3 g of BAC were dried in the oven at 150 °C to vaporize any traces of water residue. Then, 10 mL of an aqueous solution of MgSO₄·7H₂O (99.9 %, Sigma-Aldrich) at 3 different concentrations were added to the BAC. The solid-liquid mixture was mixed for 24 h so that the salt could be slowly deposited inside the BAC structure before being filtered through the Büchner funnel. The impregnated materials were finally oven-dried at 150 °C for 12 h. Fig. 1 summarizes schematically the preparation. Accordingly, three composites were prepared and then labelled as x-MgSO₄/BAC (1st column in Table 1) where x is the content of MgSO₄ in the composites, determined by X-ray Fluorescence.

2.2. Physicochemical characterizations methods

X-Ray Diffraction (XRD) analyses were performed on the powder of the samples (beads were ground into fine particles) on a diffractometer, PANalytical MPD X'Pert Pro, equipped with a Pixcel real-time multiple strip detector, operating with an angular aperture of 3.347° 2 θ in the 3° to 80° 2 θ range, and using CuK α radiation with a 0.15418 nm wavelength. Diffractograms were taken at 22 °C with a step size of 0.013° and a scan time of 220 s per step.

A wavelength dispersion X-Ray Fluorescence (WDXRF) spectrometer (from PANalytical, Zetium) was used to perform the XRF measurements on pellets made of 0.1 g of the sample and 0.2 g of binder boric acid (H₃BO₃).

High-resolution micrographics were acquired by a Scanning Electron Microscope (SEM) from JEOL, JSM-7900F model. The semi-quantitative chemical analysis and atomic composition mapping of the sample were performed by means of Energy Dispersive X-ray (EDX).

N₂ adsorption/desorption isotherms of support and composites at –196 °C were acquired in a ASAP 2420 device from Micrometrics. The samples were previously degassed at 150 °C for 12 h and then, again at 150 °C for 2 h directly on the analysis port before analysis. The apparent specific surface area was calculated by applying the Brunauer, Emmett, and Teller (BET) equation (S_{BET}). The microporous volumes (V_m) and surfaces (S_m) were determined by applying Dubinin-Astakhov's model. In this model, the exponent N was checked to be very close to 2. The external surface (S_{ext}) was considered the non-microporous surface,

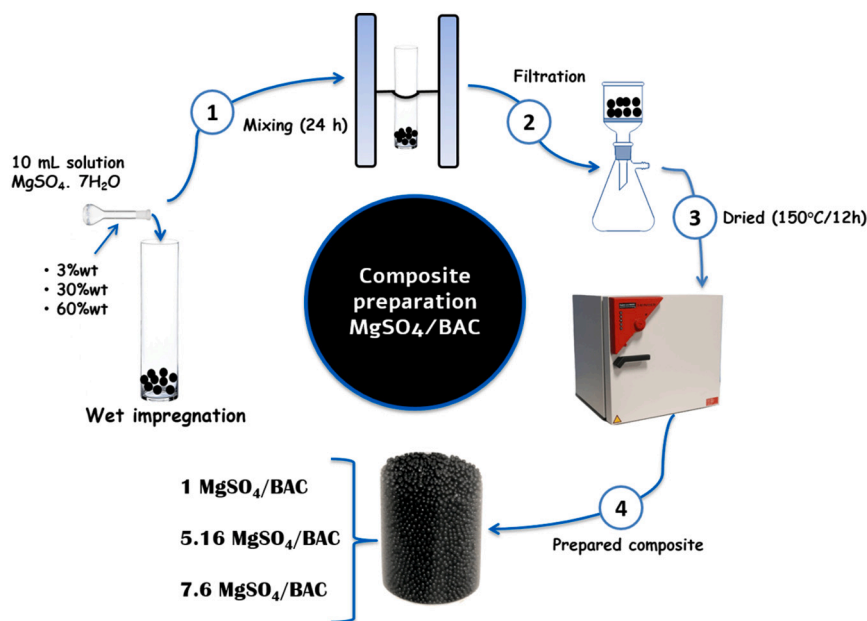


Fig. 1. Preparation of composite materials MgSO_4/BAC .

Table 1

Physicochemical characteristics of BAC support and MgSO_4/BAC composites obtained from N_2 (-196°C) adsorption isotherm data.

Sample	MgSO_4 content (wt%)	S_{BET} ($\text{m}^2\cdot\text{g}^{-1}$) ^a	S_{m} ($\text{m}^2\cdot\text{g}^{-1}$) ^b	S_{ext} ($\text{m}^2\cdot\text{g}^{-1}$) ^b	V_{p} ($\text{cm}^3\cdot\text{g}^{-1}$) ^c	V_{m} ($\text{cm}^3\cdot\text{g}^{-1}$) ^b	V_{meso} ($\text{cm}^3\cdot\text{g}^{-1}$) ^b
BAC	–	1295	1096	199	0.55	0.43	0.11
1.0- MgSO_4/BAC	1.0	1293	1099	194	0.55	0.43	0.11
5.2- MgSO_4/BAC	5.2	1210	1036	174	0.52	0.41	0.10
7.6- MgSO_4/BAC	7.6	1123	991	132	0.48	0.39	0.08

^a Calculated using the BET equation in the range 0.01 – 0.1 p/p° (cross-sectional area of 0.162 nm^2).

^b Determined using the Dubinin-Astakhov equation in the range 10^{-4} – 0.01 p/p° .

^c Determined from the amount of N_2 adsorbed at $p/p^\circ = 0.99$.

which was calculated by the t-plot method. The mesoporous volume (V_{meso}) compare the total pore volume V_{p} with the V_{m} . Finally, the pore size distribution (PSD) was determined using Density Functional Theory (DFT) calculations. The best-fitting and most logical model for the DFT calculation was a geometry of slits and a carbon surface. CO_2 adsorption/desorption isotherms at 0°C were also performed with the same equipment to observe more efficiently the ultra-microporosity, which was not accessible to the N_2 molecules. The slit geometry and the CO_2 -DFT model were also applied to this last experiment.

The thermal conductivity of the support (BAC) was measured at room temperature and humidity (equilibrium) by using two different methods (hot wire and hot disk) for comparison. Moreover, from experiments performed with the hot disk, the thermal effusivity was estimated, and consequently, the specific heat was calculated. In conclusion, the thermal properties of the support were obtained (water balance with ambience at room temperature).

For these two transient methods, the following devices and conditions were used:

- Hot wire; the apparatus is a TLS-100 (Thermtest Inc., Fredericton, NB, Canada), with a 100 mm long probe. The diameter of the tested sample is >50 mm, and its depth is 120 mm, in agreement with the manufacturer's recommendations. The probe heats the sample at constant power (0.1 W) and records its temperature ($\Delta T < 2^\circ\text{C}$). The apparent thermal conductivity is calculated assuming one-dimensional heat transfer in an infinite solid.
- Hot Disk; a thermal constant analyzer (Hot Disk AB, Gothenburg, Sweden) with a "Kapton 8563 F1" sensor (disk radius: $a = 9.868$ mm)

was used. It provides an estimation of the thermal effusivity ($E = (\rho C_p \lambda)^{\frac{1}{2}}$, $\text{J K}^{-1} \text{m}^{-2} \text{s}^{-0.5}$) and the thermal conductivity. From these two results, it calculates the specific heat (ρC_p , in $\text{J m}^{-3} \text{K}^{-1}$) and the thermal diffusivity ($\alpha = \frac{\lambda}{\rho C_p}$, $\text{m}^2 \text{s}^{-1}$). The sample is in a cubic box (thickness: 60 mm, side length: 70 mm). The probe is horizontally placed in the middle of the bed and heats the material at constant power P_0 (W) and records its temperature increase ΔT for a few minutes.

Because of the small temperature difference (2°C) and the short duration of the experiments, the hydric equilibrium is assumed in both cases.

For the composites, the amount of prepared material was insufficient to perform hot disk and hot wire experiments. We agree that the measurement of specific heat capacity can be carried out by DSC, but the estimation of C_p as a function of water content is very difficult as detailed, in our study described in Ref. [37]. Moreover, the estimation of C_p (only C_p) was not very interesting for this study, where we focus on an open system where the heat is transferred by air that acts as the vector. Indeed, the λ and ρC_p are interesting thermal properties for a THS application.

2.3. Hydration experiments

The heat released and water adsorption quantities (measured by the microbalance) of the BAC and its composites were measured using a Sensys TG-DSC (thermogravimetry coupled to differential scanning calorimetry) device and a Wetsys flow humidity generator, both from

Setaram. The samples (10 mg) were dehydrated at 150 °C before hydration by increasing the temperature from 30 to 150 °C at 5 °C/min under a flow of dry air (30 mL/min), followed by a 3-hour isotherm at 150 °C for complete dehydration. The relative humidity (RH) was increased to 60 % (a pressure of 2.55 kPa) once the temperature was reduced to 30 °C and the DSC signal had attained a stable baseline. These conditions were selected to be as close to a real-life residential application as possible: 150 °C is the working temperature that can be reached using a flat-plate solar heat collectors [38,39] and 30 °C is close to the indoor air temperature during the discharging phase [40]. To completely rehydrate the material, the hydration procedure was set for 8 h; total rehydration was attained when the DSC signal returned to the baseline. The samples' hydration heat (J/g_{sample}) was deduced from the surface's integration beneath the DSC signal during hydration. To accurately calculate the hydration heat, the hydration step was initiated only after stabilization of the DSC and TGA signals. Blank experiments in the same condition of analysis were performed with empty crucibles. Then, the heat flow signal of the blank experiment was subtracted from that of the experiment in the presence of the sample. The hydration heat (J/g_{sample}) was finally obtained by integrating the surface of the obtained heat flow curve after the blank subtraction (please see Fig. 1S, Supplementary information). The Sensys Evo equipment was calibrated in the factory (Setaram) by the "Joule effect method" and the corresponding calibration curve was supplied with the sensor. These conditions are quite similar to those that would be found in a building: 150 °C is a temperature that may be easily obtained with flat-plate solar heat collectors [38,39], while 30 °C is close to the temperature of the inside air during the discharging phase [40].

3. Results and discussion

3.1. Thermal and structural properties of the composite materials

The apparent thermal conductivity of the porous support at room temperature (hydraulic and thermal balance) was measured by using a hot wire probe. At 20 °C the apparent thermal conductivity is $\lambda = 0.14 \text{ Wm}^{-1} \text{ K}^{-1}$ with a maximal relative error of 3.4 % (8 tests).

The thermal conductivity and the heat capacity were also investigated by using a hot disk apparatus. A previous study [41] showed that measurements of heat capacity, thermal diffusivity, and thermal conductivity were not satisfactory. Indeed, this technique actually measured the thermal effusivity of the material. The thermal effusivity is $E = 316 \text{ JK}^{-1} \text{ m}^{-2} \text{ s}^{-0.5}$ with a maximal relative error inferior to 10 % (12 experiments). Starting from these previous results (E and λ), the heat capacity can be calculated ($\rho C_p = \frac{E^2}{\lambda} = 0.71 \text{ MJm}^{-3} \text{ K}^{-1}$) and assuming an apparent density (600 kgm^{-3} , manufacturer data), the specific heat capacity is $C_p = 1190 \text{ Jkg}^{-1} \text{ K}^{-1}$.

The addition of hydrated salt should improve the thermal properties of the material since the thermal conductivity and specific heat capacity of hepta-hydrated salt are $0.45 \text{ Wm}^{-1} \text{ K}^{-1}$ and $1600 \text{ Jkg}^{-1} \text{ K}^{-1}$, respectively.

The thermal properties of these composite materials are better than those of classical adsorptive materials. For example, the thermophysical properties of dry zeolite 13X at 25 °C (widely used for thermochemical heat storage applications) are $0.075 \text{ Wm}^{-1} \text{ K}^{-1}$ and $900 \text{ Jkg}^{-1} \text{ K}^{-1}$ for thermal conductivity and specific heat capacity, respectively.

Table 1 summarizes the chemical composition acquired using the WDXRF method as well as the textural characteristics (S_{BET} , S_{ext} , S_m , V_p , V_m , and V_{meso}). Different concentrations of $\text{MgSO}_4 \cdot 7\text{H}_2\text{O}$ solution resulted in varying amounts of MgSO_4 anhydrous deposited in the BAC structure. As the MgSO_4 loading increases, the S_{BET} and V_p values of the BAC and related composites show a slight decrease. The size of some pore entrances can be hindered by the presence of MgSO_4 particles after impregnation, resulting in the pore being inaccessible to N_2 molecules. This explains why the apparent S_{BET} of the BAC ($1295 \text{ m}^2 \cdot \text{g}^{-1}$) was

reduced by 13.6 % when 7.6 % of MgSO_4 was added. In addition, as compared to pure BAC, the V_p of the composite 7.6- MgSO_4/BAC ($0.48 \text{ cm}^3 \cdot \text{g}^{-1}$) was decreased just by 12.7 %. MgSO_4 deposition, on the other hand, has no effect on the form of the supports' N_2 -adsorption isotherms (Fig. 2a).

BAC supports and prepared composites display type Ib isotherms (Fig. 2a) according to Rouquerol et al. [42]. A vertical adsorption line at very low relative pressure (0.01 p/p°) is followed by a convex curve and a plateau toward $\text{p/p}^\circ = 1$. Microporous (pore size $< 2 \text{ nm}$) materials are indicated by high adsorption at very low p/p° . The micropores are narrower when the line is sharper. The PSD of the composites and pure BAC shown in Fig. 2b has been obtained by applying the DFT method with the NLDFT model.

All the samples, including the BAC and the composites, show the same distribution of pores (only the V_p decreases), with three peaks located at 0.8, 1.2, and 1.7 nm. This distribution validates that the BAC and its composites are highly microporous materials. This was also demonstrated by the microporous surface (S_m) ratio, which accounts for approximately 85 % of the apparent S_{BET} after impregnation. With the maintenance of the PSD of the composites, the pore sizes are clearly not affected. Thus, the decrease of V_p is due to the fact that certain pores were completely blocked by aggregates of salt particles.

To fully understand the microporous structure, CO_2 adsorption at 0 °C was performed on all samples (Fig. 2c) to investigate the ultra-micropores ($< 1 \text{ nm}$).

Fig. 2d shows the PSD of these samples using the CO_2 -DFT calculations, with two main peaks located at 0.58 nm and 0.84 nm. With the presence of the MgSO_4 particles, the specific surface as well as the porous volume of the impregnated samples decreased slightly compared to the BAC (see Table 2). Furthermore, the PSD CO_2 adsorption is the same for all samples (Fig. 2d), which led to the conclusion that there is no influence on the pore sizes. As the porous volume decreases slightly, certain pores are also completely blocked by the salt aggregates, which reduces the dispersion of the salt as well as the $\text{MgSO}_4/\text{H}_2\text{O}$ interaction surfaces. As a result, the overall performance of these materials can be significantly impacted in terms of the thermal energy released.

To further investigate the surface structure and the morphology, a series of characterizations (SEM, EDX, and XRD) were conducted on the three composites and on the commercial BAC.

SEM and EDX mapping of pure BAC supports and BAC-based composites were used to gain information about the morphology and homogeneity of MgSO_4 deposition on the surface (Fig. 3). In all samples, a smooth surface with a high carbon content is seen. These composites had a homogeneous surface with no macro MgSO_4 crystallites. The EDX mapping study also verifies the uniformity of MgSO_4 deposition on all composites. This finding is corroborated by XRD diffractograms, which show that no peak corresponding to moderately large MgSO_4 crystallites was identified in any of the BAC-based composites.

The XRD patterns of pristine BAC and related composites (Fig. 4) presented two broad diffraction peaks at 24° and 43°, corresponding to two planes (002) and (100), which are reflections of the graphitic plane and the disordered graphitic plane, respectively [43,44]. There were no reflections detected associated with MgSO_4 in the BAC- MgSO_4 series of composites. This is an indication of the presence of an amorphous phase of partially hydrated MgSO_4 [22,39] formed during the deposition step or to the presence of very small salt crystallites with dimensions below the XRD spectrometer detection level. This latter result leads to the absence of well-defined peaks related to MgSO_4 on the XRD patterns.

3.2. TG-DSC analysis for hydration behaviors

A TG-DSC device was used to measure the hydration heat released and water sorption capacities of the BAC support and its composites under controlled temperature and pressure. The heat produced upon hydration (Fig. 5a) and the water adsorption capacity (designated as " w_e " in Eq. (1)) (Fig. 5b) were calculated from the variation of the heat

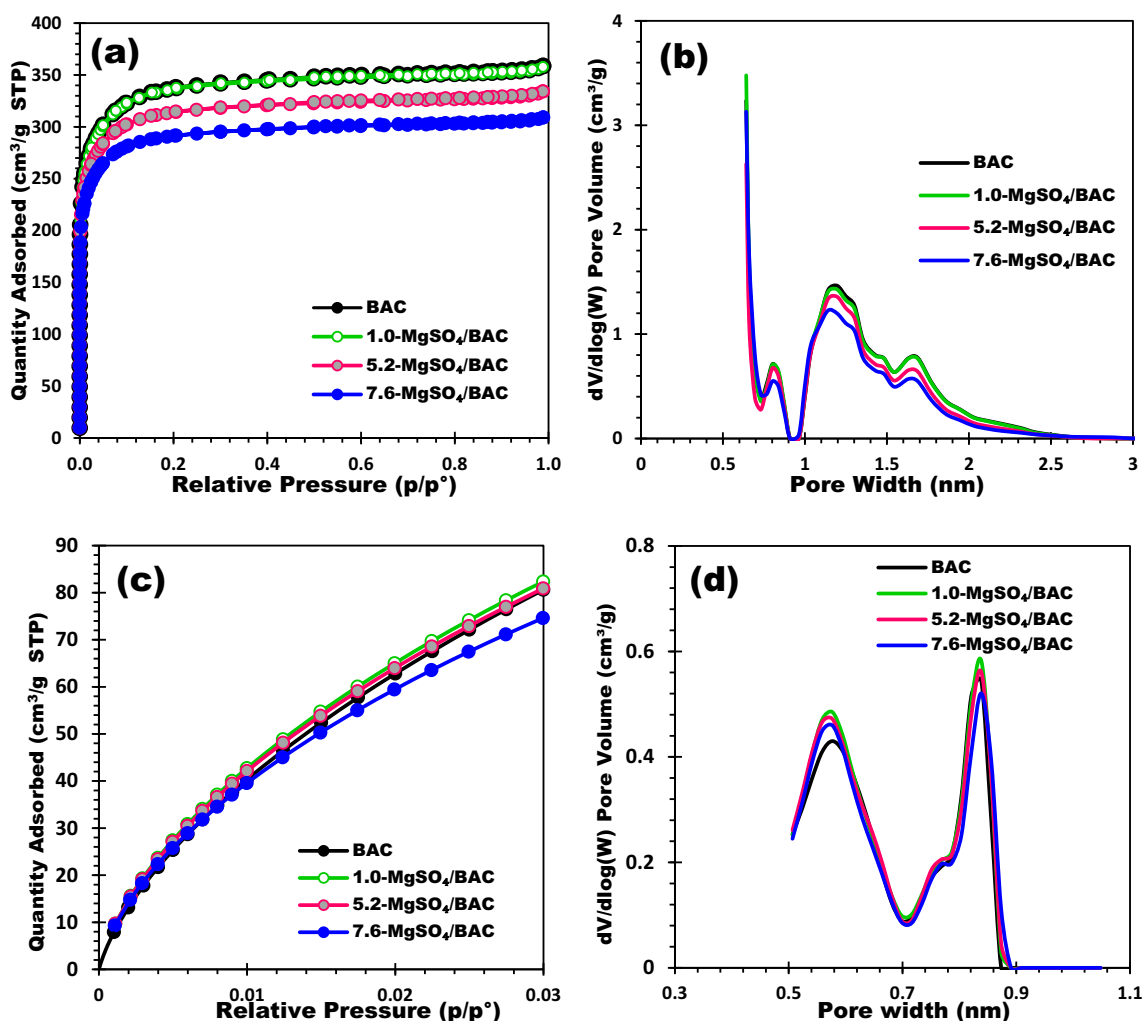


Fig. 2. (a) N₂ adsorption-desorption isotherms, (b) PSD (N₂) of BAC and its composites with MgSO₄, (c) CO₂ adsorption isotherms, (d) PSD (CO₂) of BAC and its composites with MgSO₄.

Table 2

Physicochemical characteristics of BAC support and MgSO₄/BAC composites obtained from CO₂ (0 °C) adsorption isotherm data.

Sample	MgSO ₄ content (wt%)	S _{BET} (m ² ·g ⁻¹) ^a	V _p (cm ³ ·g ⁻¹) ^b
BAC	–	653	0.14
1.0-MgSO ₄ /BAC	1.0	646	0.14
5.2-MgSO ₄ /BAC	5.2	619	0.14
7.6-MgSO ₄ /BAC	7.6	562	0.13

^a Calculated using the BET equation in the range 0.009–0.03 p/p^o (cross-sectional area of 0.170 nm²).

^b Determined from the amount of CO₂ adsorbed at p/p^o = 0.03.

flow and the mass of the sample as a function of time. Heat production and water uptake increased as salt concentration increased in three manufactured composites. Indeed, when more salt was deposited on the porous structure, the contact surface between salt particles and water vapor expanded greatly. Therefore, more exothermic reactions took place, leading to a more larger thermal energy density.

$$w_e = \frac{m_h - m_d}{m_d} \quad (1)$$

where w_e is the water adsorption capacity (g_{H₂O}/g_{sample} or g/g in short), m_h (g) and m_d (g) correspond respectively to the final mass of the hydrated sample and the dehydrated sample. However, these values

doubled their respective calculated ones, which are shown in Table 3.

The calculated values are made from the contributions of the MgSO₄ salt and the porous BAC support based on their respective contents in the composites. Although the BAC support (BAC/H₂O interaction) contributed a certain amount to the overall heat storage density, it did not have a significant impact.

The contribution from the exothermic reaction MgSO₄/H₂O is the most important since it is the main energy source of the system. There was another source of thermal energy, which comes from the condensation of water molecules on another layer of water molecules (first layer in contact with MgSO₄ particles) or from the formation of a saturated solution of MgSO₄ resulting from overhydration [45].

In general, overhydration takes place whenever the RH during the adsorption is greater than the DRH of the salt. In this paper, the operating conditions are 30 °C and 60 % RH, while the DRH of MgSO₄ is about 90 %. However, the deliquescence RH of salts confined in porous matrix can be usually dramatically reduced [46]. It is the case for the samples presented in Fig. 5, for which the water uptake exceeds 7 mol of H₂O per mol of MgSO₄, confirming the formation of a saturated solution in the pores. As stated in the review by Gordeeva and Aristov [46], the salt is the principal component responsible for the sorption process in a composite, but the contribution of the host matrix is still quite important. To begin with, the matrix is the component that prevents the salt particles from agglomerating. The matrix facilitates the diffusion of water molecules to the salt particles and the transmission of the heat that

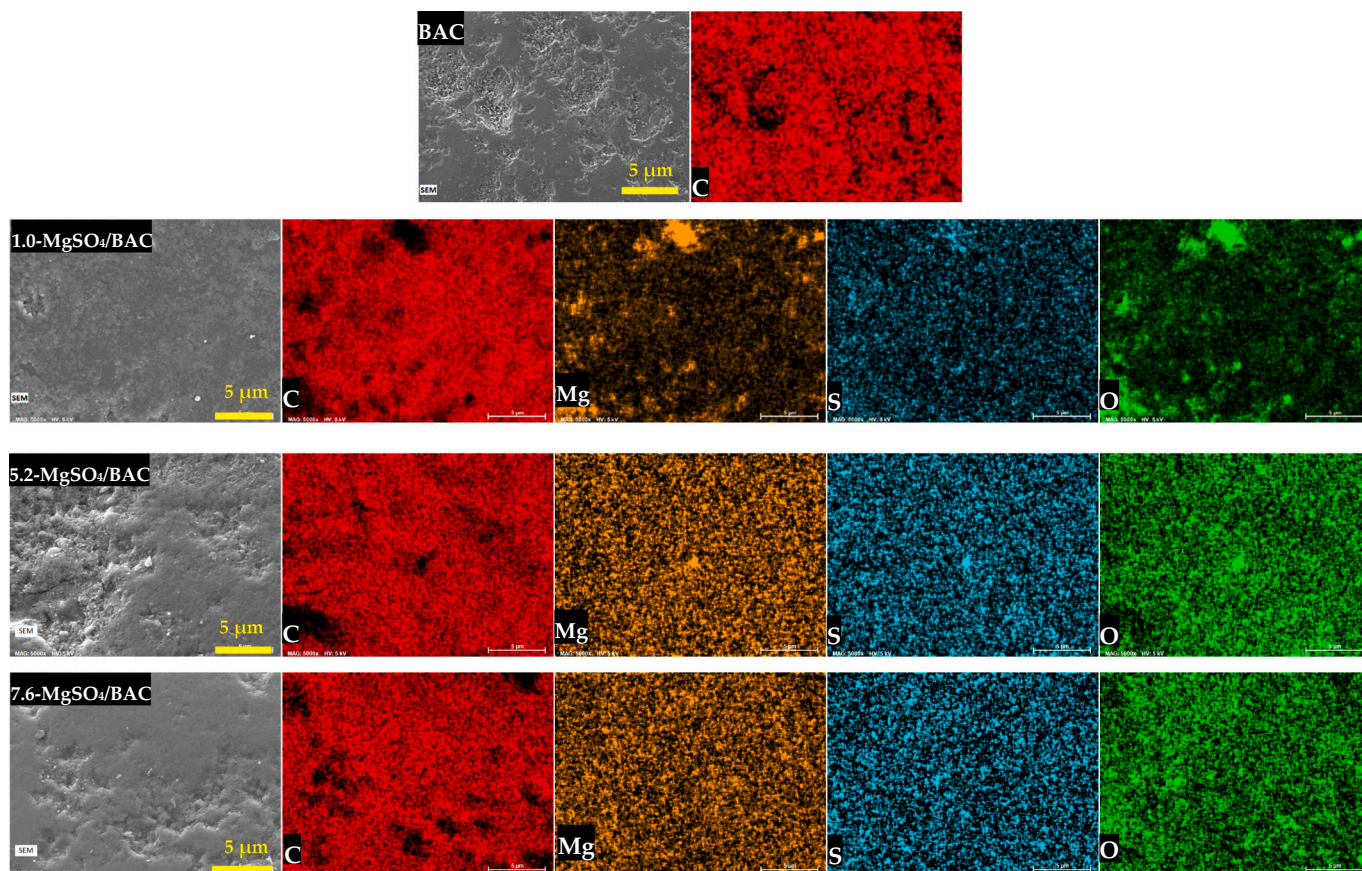


Fig. 3. SEM images of BAC original and its composites with MgSO₄.

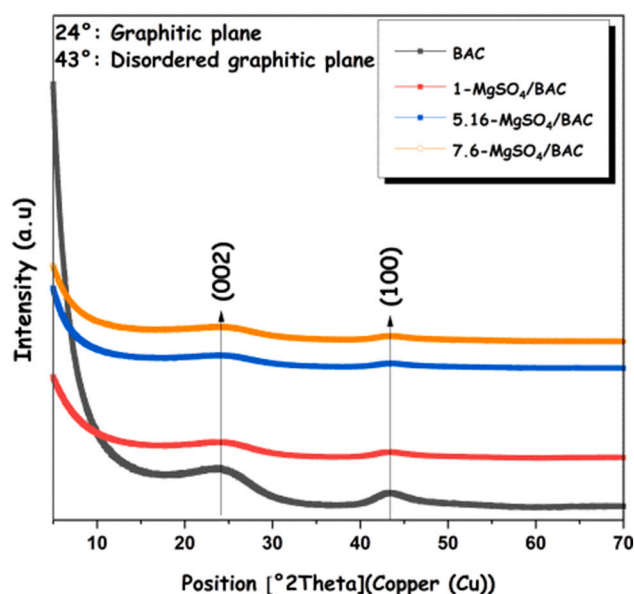


Fig. 4. XRD patterns of BAC and its composites.

is either produced or consumed during the reaction. Both mechanisms contribute to increase the rate of sorption and desorption [47–50]. In addition, the matrix plays a significant role in the sorption equilibrium between the salt and the sorbates: the equilibrium is significantly shifted toward adsorption due to the confinement of the salt inside the matrix pores [51].

To support this interpretation, Ponomarenko et al. [52] observed a

dramatic change in the salt sorption properties in CaCl₂/SBA-15 composites. The dispersed salt forms a dihydrate CaCl₂·2H₂O at a relative pressure of water vapor 2.5–4 times lower than in the case of bulk salt. It was shown that the water sorption equilibrium of CaCl₂ confined into the pores of a meso-structured silicate, SBA-15, with a variable pore size appeared to depend on the SBA pore diameter (8.1 and 11.8 nm) [52]. The sorption isotherms presented two segments with a steep increase during water uptake, corresponding to the formation of CaCl₂·2H₂O and the transformation of this hydrate to an aqueous solution of CaCl₂. Interestingly, the pressure at which CaCl₂·2H₂O hydration occurs is lower in smaller pores, namely 1.0–1.1 and 1.2–1.3 kPa at 50 °C. The decrease in the hydration pressure is caused by the fact that particles of the confined salt are smaller in narrow pores and, hence, sorb water easier due to the improved water molecule transfer.

Accordingly, the energies obtained experimentally for the studied composites are higher than those calculated, probably due to the condensation of water molecules in the pore structure of BAC and the improved mass transfer. Table 4 compares the performance of the 7.6-MgSO₄/BAC composite to other composite storage materials reported in the literature, which show a better performance of this composite over certain reported materials.

BAC alone, the measurements of heat released and water adsorption show that the heat released per gram of water is close to the latent heat of water ($L_v \approx 2300 \text{ J/g}_{\text{water}}$).

The theoretical heat released by impregnated materials is estimated by adding the heat of salt hydration (from 1 to 6 water molecules), i.e. $\Delta H_{\text{exp}} = 3200 \text{ J/g}_{\text{water}}$ and latent heat of water according to the equation below:

$$Q = S\% \cdot (6 - 1) \cdot \frac{18}{120.4} \cdot \Delta H_{\text{exp}} + L_v \cdot \left(W_{\text{exp}} - S\% \cdot (6 - 1) \cdot \frac{18}{120.4} \right)$$

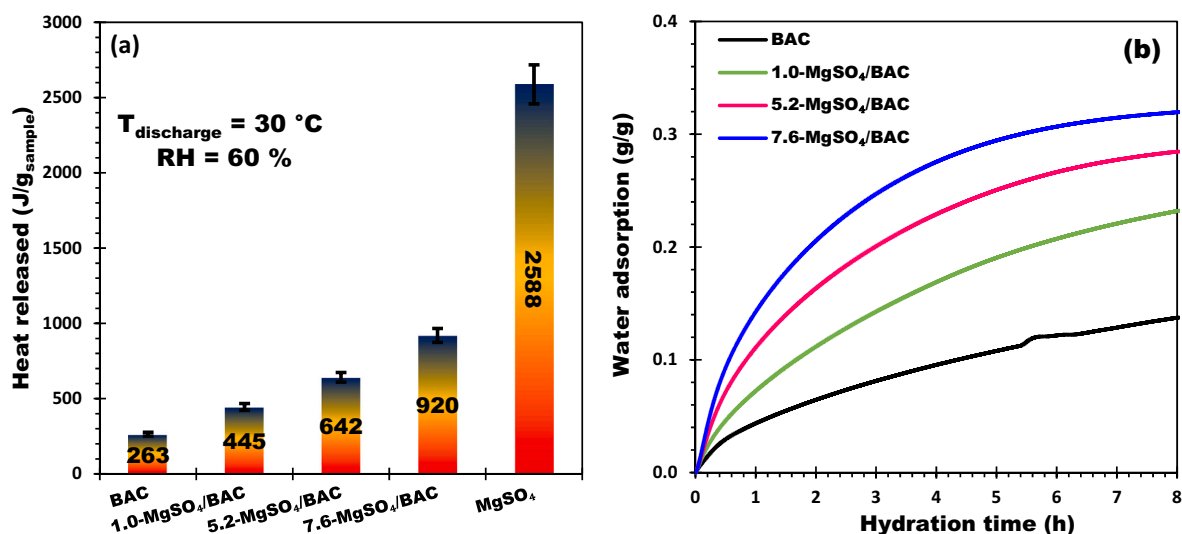


Fig. 5. (a) Hydration behavior of MgSO_4 and BAC composites at $30\text{ }^\circ\text{C}$ and 60 \% RH (b) Water adsorption curves of BAC support and composites ($T_{\text{discharge}} = 30\text{ }^\circ\text{C}$; $\text{RH} = 60\text{ \%}$; 8 h of hydration).

Table 3

Experimental results and calculated values of MgSO_4 , BAC and its composites.

Sample	Heat released Q_{exp} (J/ g_{sample})	Heat released calculated Q (J/ g_{sample}) ^b	VSD_b^c (GJ/ m^3)	VSD_g^d (GJ/ m^3)	Water adsorption W_{exp} (g/g)	Water adsorption calculated (g/g) ^b
MgSO_4^a	2588	–	2.41	6.88	0.809	–
BAC	263	–	0.16	0.34	0.138	–
1.0- MgSO_4 / BAC	445	540	0.27	0.58	0.232	0.151
5.2- MgSO_4 / BAC	642	688	0.40	0.88	0.284	0.179
7.6- MgSO_4 / BAC	920	902	0.58	1.29	0.370	0.194

^a Determined experimentally by TG-DSC/Wetsys.

^b Calculated by addition of the heat contribution of MgSO_4 salt and BAC support in each sample.

^c Volumetric Storage Density calculated by using density of composite bed (b).

^d Volumetric Storage Density calculated by using density of composite grain (g).

Table 4

Comparison of 7.6- MgSO_4 /BAC with other sulfate-based composites in the literature.

Composite materials	Operating conditions	Energy storage density (J/g)	Reference	Year
7.6- MgSO_4 /BAC	$T_{\text{hyd}} = 30\text{ }^\circ\text{C}$; $\text{RH} = 60\text{ \%}$	920	This work	2022
20- MgSO_4 /HAP	$T_{\text{hyd}} = 30\text{ }^\circ\text{C}$; $\text{RH} = 60\text{ \%}$	464	[53]	2022
30- MgSO_4 /Diatomite (D30)	$T_{\text{hyd}} = 25\text{ }^\circ\text{C}$; $\text{RH} = 80\text{ \%}$	460 773	[54]	2021
60- MgSO_4 /Diatomite (D60)				
50- MgSO_4 /Expanded graphite (EG50)	$T_{\text{hyd}} = 25\text{ }^\circ\text{C}$; $\text{RH} = 85\text{ \%}$	496.4	[55]	2021
MgSO_4 /13x with % MgSO_4 up to 20 %	$T_{\text{hyd}} = 25\text{ }^\circ\text{C}$; $\text{RH} = 60\text{ \%}$	510–575	[35]	2019
MgSO_4 /zeolite (laboratory pilot)	$T_{\text{hyd}} = 25\text{ }^\circ\text{C}$; $\text{RH} = 85\text{ \%}$	401	[8]	2018
MgSO_4 /zeolite Modernite	$T_{\text{hyd}} = 22\text{ }^\circ\text{C}$; $\text{RH} = 50\text{ \%}$	507	[39]	2013
MgSO_4 /zeolites H-Y	$T_{\text{hyd}} = 20\text{ }^\circ\text{C}$; $\text{RH} = 55\text{ \%}$	867	[56]	2013
MgSO_4 /zeolites Na-Y		1090		

3.3. Hydration kinetic modeling

According to Fig. 5b, BAC supports and composites adsorb water at different rates. Visually, water sorption occurs quickly at the beginning for all samples, then becomes sluggish over the hydration time. It is observed that after the first hour, the BAC adsorption capacity is already at two-thirds of the equilibrium level, while the impregnated composites adsorb around half of the maximum capacity. After that, the kinetics of all samples decreased substantially. While the kinetic curve of the BAC support reached equilibrium after 6 h of hydration, the prepared composites approached their respective equilibrium states at the 7th hour of hydration. The amount of salt deposited appears to have the most impact on hydration behavior. As salt concentration increases, water vapor diffusion becomes less favorable, and more time is required for the hydration reaction to take place.

In order to investigate the kinetics of water adsorption onto BAC composites more deeply, different kinetic models: pseudo first order, intraparticle diffusion, diffusion into homogeneous material (Crank's diffusion model), diffusion through a surrounding salt layer, and Elovich have been applied (Table 5). The fitting results are then reported in Fig. 6.

The PFO model is often used in the literature for studying the adsorption kinetics of water in heat storage materials. This model used for the liquid phase assumes a sorption kinetic proportional to the difference in concentration at the surface. The limiting step of this model is

Table 5
Non-linear kinetic adsorption models.

Kinetic model	Equation	Description of parameters	Ref.
Pseudo First Order (PFO)	$w_t = w_e [1 - \exp(-K_1 t)]$	w_t is the water uptake at time t ($g_{water}/g_{composite}$), w_e : the water uptake at equilibrium ($g_{water}/g_{composite}$), t is the hydration time (h), K_1 is the rate constant of the PFO model (s^{-1}) and k_{id} is the rate constant of the IPD model ($g_{composite}/g_{water} \cdot s^{-0.5}$)	[57–61]
Intraparticle diffusion (IPD)	$w_t = k_{id} \sqrt{t} + C$	D_t is the apparent diffusion coefficient (m^2/s), R the particle radius	
Crank's diffusion	$w_t = w_e \left(1 - \sum_{n=1}^{\infty} \frac{6}{n^2 \pi^2} e^{-\frac{n^2 \pi^2 D t}{R^2}} \right)$		
Layer diffusion	$w_t = w_e \left(1 - \sum_{k=0}^{\infty} \frac{8}{(2k+1)^2 \pi^2} e^{-\frac{(2k+1)^2 \pi^2 D t}{e^2}} \right)$	e is the layer thickness (m) calculated according to salt mass balance	
Elovich	$w_t = E_0 + E_1 \ln(t)$	E_0, E_1 are Elovich equation parameters	

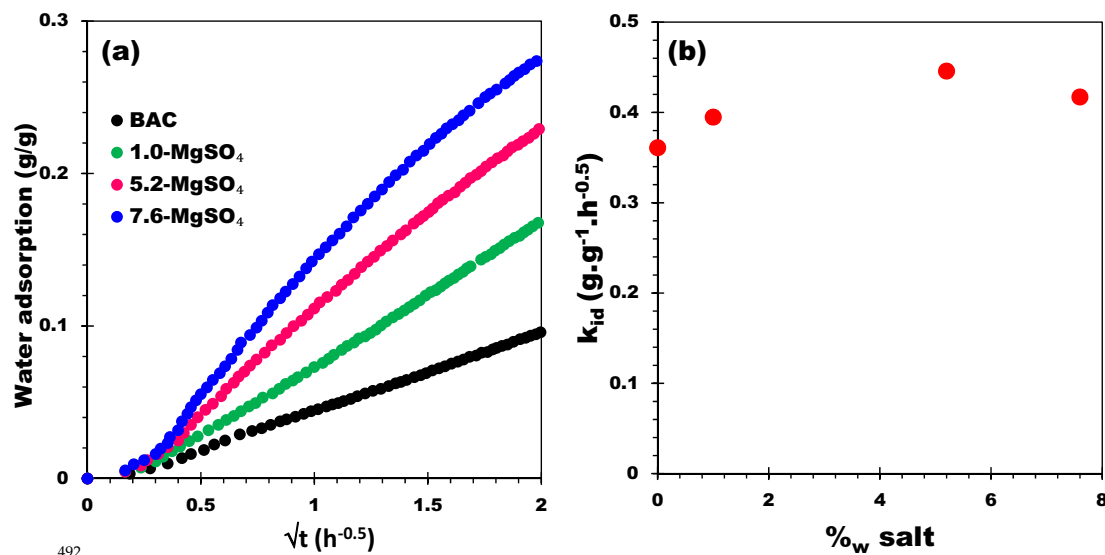


Fig. 6. (a) Application of intraparticle diffusion model on the adsorption kinetics of BAC and composites at different salt contents. (b) The rate constant of the IPD model versus salt content.

physisorption. The intraparticle diffusion model assumes that diffusion is the rate-limiting step in the particle's water sorption. The Crank's model assumes that the water diffuses as homogeneous, porous, spherical particles. The fourth assumes that the impregnated salt forms a layer around the BAC. The thickness of this layer is calculated respecting salt mass balance, and the mass transfer in this layer is assumed to be diffusive. The last one (Elovich model) is a logarithmic rate law for describing chemisorption in porous solids. It does not consider mechanisms that are limited by gaseous diffusion, such as Knudsen diffusion.

The first observation is that the PFO and the Elovich models don't accurately describe the experimental kinetics, especially at the beginning of hydration. The form of these two equations doesn't allow them to properly fit the experimental data. In the same way, the two diffusive models (Crank and salt layer) are not a good numerical approximation of the experimental results. First, the model coming from the differential equation of diffusive mass transfer doesn't describe diffusive mechanisms in a microporous material. For the diffusive model through a salt layer, the uncertainty of the layer thickness estimation (calculated by respecting salt mass balance) is the major issue for obtaining a good numerical approximation.

Unlike the other models, the intraparticle model proposed by Weber and Morris allows good fitting of the experimental data, as shown in Fig. 6a. It has been widely applied for the study of adsorption kinetics in different porous materials (micro, meso, and macro). When the rate kinetic constant is divided by the water uptake at equilibrium (Fig. 6b), it becomes quasi-independent of the salt concentration and increases

with the amount of impregnated salt. This means that the adsorption mechanisms are the same and have the same strengths (Fig. 6b), no matter how much salt is used.

3.4. Cyclability and stability of composite 7.6-MgSO₄/BAC

The 7.6-MgSO₄/BAC composite was subjected to five consecutive cycles of hydrating and dehydrating at temperatures of 150 °C (dehydration) and 30 °C (hydration) at a relative humidity of 60 % as part of the stability study. The heat released after each cycle was obtained and compared to the previous ones in order to check if the material was still stable. Fig. 8 shows that just a minor fluctuation (about 10 %) in thermal energy density was found between each cycle, confirming the composite's good stability. Fig. 9 shows the EDX images after 1 cycle and after 10 cycles of 7.6-MgSO₄/BAC. No aggregates of salt particles were observed in any images, confirming the cyclability of the prepared composite (7.6-MgSO₄/BAC).

4. Conclusions

In this work, we investigate the composite of MgSO₄ salt impregnated inside beads of activated carbon. It was shown that the composites can be easily prepared by impregnating the salt solutions in the beads with activated carbon. The composites were investigated by a series of physico-chemical methods (XRD, apparent S_{BET} , and SEM). With an energy storage density of 920 J/g ($T_{adsorption} = 30$ °C, $T_{desorption} =$

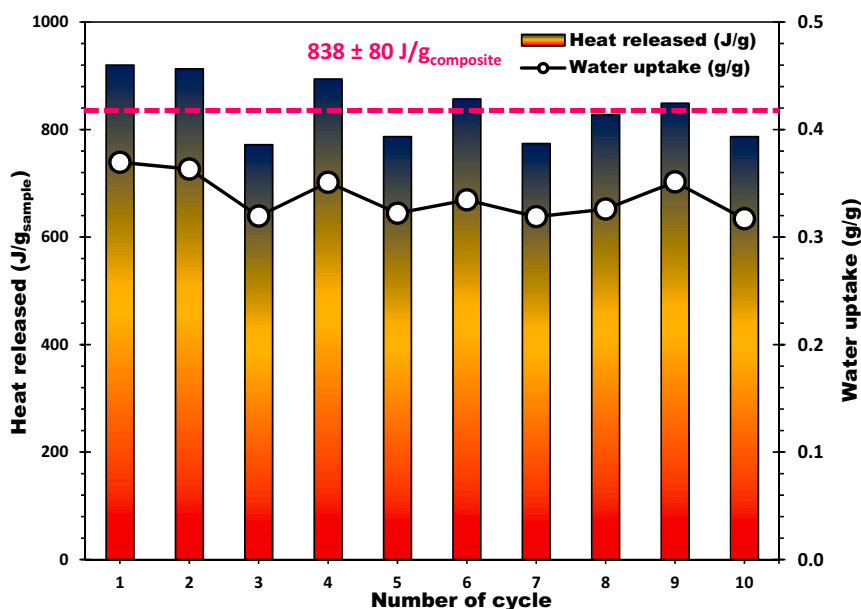


Fig. 8. Evaluation of 7.6-MgSO₄/BAC composite stability for 10 cycles.

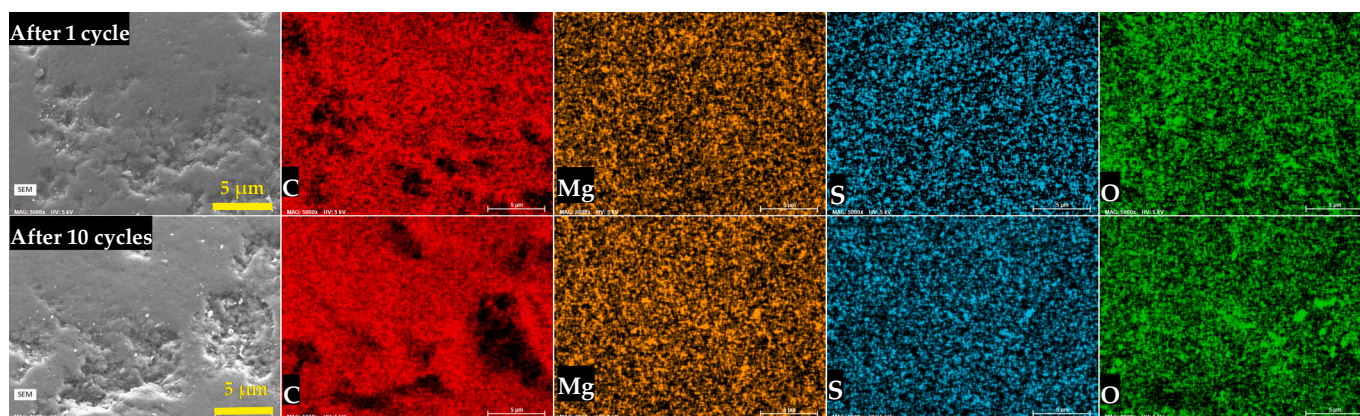


Fig. 9. SEM and EDX images of 7.6-MgSO₄/BAC after 1 cycle and after 10 cycles.

150 °C, and RH = 60 %), the 7.6-MgSO₄/BAC composite outperforms the other prepared composites. The salt's high dispersion improves composite materials' storage capacity. When choosing a storage material for thermochemical heat storage systems, high heat and water storage capacities aren't the only considerations. The system's utility also necessitates fast water sorption kinetics. The good fitting of the kinetic experimental data with the IPD model equation has been successfully performed, allowing us to determine the kinetic rate of water diffusion in BAC particles. The repeated stability of MgSO₄-BAC is evaluated, revealing that 7.6-MgSO₄/BAC composite performance is relatively constant after 10 cycles.

Further study can be focused on the energy storage density improvement, cyclic adsorption and desorption performances, and the corresponding kinetic models of the prepared composites. Also, it is a good idea to look into how the composites behave thermochemically in an experiment-sized reactor.

The BAC composites are very promising heat storage materials, also considering the shape of the final materials that can facilitate the filling of the reactor and improve the fluid-dynamics of the system. The transfer of the water molecules presents in the carrier gas (humid air) onto the overall material is then homogeneous. Hotspots can also be avoided by using BAC due to its relatively high thermal conductivity

(when compared to other mineral supports such as zeolites, alumina, MOFs, silica gels, the aluminophosphate AIPO and SAPO). On the one hand, by avoiding the local enhancement of the temperature, the material is preserved by thermal degradation in the long term. On the other hand, by keeping the local temperature constant, the hydration process is performed under controlled conditions, and the local water adsorption equilibrium is optimized by avoiding desorption phenomena during the hydration step due to the eventual temperature increase.

Nomenclature

TES	thermal energy storage
TCHS	thermochemical heat storage
BAC	bead activated carbon
DRH	deliquescence relative humidity;
XRD	X-Ray Diffraction
WDXRF	wavelength-dispersive X-Ray Fluorescence
SEM	Scanning Electron Microscope
EDX	Energy Dispersive X-ray
BET	Brunauer, Emmett and Teller
PSD	pore size distribution
DFT	Density Functional Theory

TG thermogravimetry
 DSC Differential Scanning Calorimetry
 RH relative humidity

Supplementary data to this article can be found online at <https://doi.org/10.1016/j.est.2022.106452>.

ORCID iD authorship contribution statement

Minh Hoang Nguyen: Data curation, Writing - Original draft preparation, validation, investigation, Visualization. **Mohamed Zbair:** Data curation, Writing - Original draft preparation, validation, investigation, Writing - Review & Editing, Visualization. **Patrick Dutournié:** methodology, validation, formal analysis, Writing - Review & Editing, supervision. **Simona Bennici:** Conceptualization, validation, Writing - Review & Editing, supervision, project administration, funding acquisition.

Declaration of competing interest

No conflict of interest.

Data availability

Data will be made available on request.

Acknowledgments

The authors would like to thank the Carnot Institutes MICA (France) for supporting a part of this study within the STOCKENER; Region Grand Est (France) for providing funding for the acquisition of the TG-DSC equipment, in the frame of STOCKFATAL project, and financing a part of the PhD-grant of Mr. Minh Hoang Nguyen.

All physicochemical characterizations were performed on the IS2M technical platforms. The authors are very grateful to L. Michelin (XRF) and L. Josien (SEM + EDX) for their contribution.

Funding

- Region Grand Est for providing funding for the acquisition of the TG-DSC equipment within the “STOCKFATAL” project and for the contribution to Mr. Minh Hoang Nguyen's thesis grant.
- Carnot MICA and Region Grand Est for funding part of this study in the frame of the STOCKENER project.
- IS2M for the postdoctoral grant of M. Zbair in the frame of the “Projets Structurants” call.

Institutional review board statement

Not applicable.

Informed consent statement

Not applicable.

References

- [1] Statistical Review of World Energy | Energy economics | Home, (n.d.).
- [2] C. Zou, Q. Zhao, G. Zhang, B. Xiong, Energy revolution: from a fossil energy era to a new energy era, *Nat. Gas Ind. B* 3 (2016), <https://doi.org/10.1016/j.ngib.2016.02.001>.
- [3] M.P. Vandenberg, J.M. Gilligan, *Beyond Politics: The Private Governance Response to Climate Change*, Cambridge University Press, 2017, <https://doi.org/10.1017/9781316848555>.
- [4] K.S. Babu, E.A. Kumar, Thermodynamic analysis of compressor operated resorption thermochemical energy storage system for heat storage, combined cooling and heat upgradation, *J. Energy Storage* 50 (2022), 104659, <https://doi.org/10.1016/j.est.2022.104659>.
- [5] E. Borri, G. Zsembinszki, L.F. Cabeza, Recent developments of thermal energy storage applications in the built environment: a bibliometric analysis and systematic review, *Appl. Therm. Eng.* 189 (2021), <https://doi.org/10.1016/j.applthermaleng.2021.116666>.
- [6] T. Yang, W. Liu, G.J. Kramer, Q. Sun, Seasonal thermal energy storage: a techno-economic literature review, *Renew. Sust. Energy Rev.* 139 (2021), <https://doi.org/10.1016/j.rser.2021.110732>.
- [7] G. Airo' Farulla, M. Cellura, F. Guarino, M. Ferraro, A review of thermochemical energy storage systems for power grid support, *Appl. Sci.* 10 (2020) 3142, <https://doi.org/10.3390/app10093142>.
- [8] C. Xu, Z. Yu, Y. Xie, Y. Ren, F. Ye, X. Ju, Study of the hydration behavior of zeolite-MgSO₄ composites for long-term heat storage, *Appl. Therm. Eng.* 129 (2018) 250–259, <https://doi.org/10.1016/j.applthermaleng.2017.10.031>.
- [9] S. Hongois, F. Kuznik, P. Stevens, J.-J. Roux, Development and characterisation of a new MgSO₄-zeolite composite for long-term thermal energy storage, *Sol. Energy Mater. Sol. Cells* 95 (2011) 1831–1837, <https://doi.org/10.1016/j.solmat.2011.01.050>.
- [10] I. Sarbu, C. Sebarchievici, A comprehensive review of thermal energy storage, *Sustainability*. 10 (2018) 191, <https://doi.org/10.3390/su10010191>.
- [11] W. Li, M. Zeng, Q. Wang, Development and performance investigation of MgSO₄/SrCl₂ composite salt hydrate for mid-low temperature thermochemical heat storage, *Sol. Energy Mater. Sol. Cells* 210 (2020), 110509, <https://doi.org/10.1016/j.solmat.2020.110509>.
- [12] K.E. N'Tsoukpoe, H. Liu, N. Le Pierrès, L. Luo, A review on long-term sorption solar energy storage, *Renew. Sust. Energy Rev.* 13 (2009) 2385–2396, <https://doi.org/10.1016/j.rser.2009.05.008>.
- [13] G.T. Whiting, D. Grondin, D. Stosic, S. Bennici, A. Auroux, Zeolite-MgCl₂ composites as potential long-term heat storage materials: influence of zeolite properties on heats of water sorption, *Sol. Energy Mater. Sol. Cells* 128 (2014) 289–295, <https://doi.org/10.1016/j.solmat.2014.05.016>.
- [14] H. Wu, F. Salles, J. Zajac, A critical review of solid materials for low-temperature thermochemical storage of solar energy based on solid-vapour adsorption in view of space heating uses, *Molecules* 24 (2019) 945, <https://doi.org/10.3390/molecules24050945>.
- [15] P. Tatsidjoudoung, N. Le Pierrès, L. Luo, A review of potential materials for thermal energy storage in building applications, *Renew. Sust. Energy Rev.* 18 (2013) 327–349, <https://doi.org/10.1016/j.rser.2012.10.025>.
- [16] L.G. Gordeeva, Y.D. Tu, Q. Pan, M.L. Palash, B.B. Saha, Y.I. Aristov, R.Z. Wang, Metal-organic frameworks for energy conversion and water harvesting: a bridge between thermal engineering and material science, *Nano Energy* 84 (2021), 105946, <https://doi.org/10.1016/j.nanoen.2021.105946>.
- [17] S. Bennici, P. Dutournié, J. Cathalan, M. Zbair, M.H. Nguyen, E. Scullier, C. Vault, Heat storage: hydration investigation of MgSO₄/active carbon composites, from material development to domestic applications scenarios, *Renew. Sust. Energy Rev.* 158 (2022), 112197, <https://doi.org/10.1016/j.rser.2022.112197>.
- [18] J. Xu, T. Li, T. Yan, J. Chao, R. Wang, Dehydration kinetics and thermodynamics of magnesium chloride hexahydrate for thermal energy storage, *Sol. Energy Mater. Sol. Cells* 219 (2021), 110819, <https://doi.org/10.1016/j.solmat.2020.110819>.
- [19] K.E. N'Tsoukpoe, T. Schmidt, H.U. Rammelberg, B.A. Watts, W.K.L. Ruck, A systematic multi-step screening of numerous salt hydrates for low temperature thermochemical energy storage, *Appl. Energy* 124 (2014) 1–16, <https://doi.org/10.1016/j.apenergy.2014.02.053>.
- [20] Q. Zhao, J. Lin, H. Huang, Z. Xie, Y. Xiao, Enhancement of heat and mass transfer of potassium carbonate-based thermochemical materials for thermal energy storage, *J. Energy Storage*. 50 (2022), 104259, <https://doi.org/10.1016/j.est.2022.104259>.
- [21] L.C. Söğütöglu, P.A.J. Donkers, H.R. Fischer, H.P. Huinink, O.C.G. Adan, In-depth investigation of thermochemical performance in a heat battery: cyclic analysis of K₂CO₃, MgCl₂ and Na₂S, *Appl. Energy* 215 (2018) 159–173, <https://doi.org/10.1016/j.apenergy.2018.01.083>.
- [22] V.M. van Essen, H.A. Zondag, J.C. Gores, L.P.J. Bleijendaal, M. Bakker, R. Schuitema, W.G.J. van Helden, Z. He, C.C.M. Rindt, Characterization of MgSO₄ hydrate for thermochemical seasonal heat storage, *J. Sol. Energy Eng.* 131 (2009), <https://doi.org/10.1115/1.4000275>.
- [23] A. Mehrabadi, M. Farid, New salt hydrate composite for low-grade thermal energy storage, *Energy* 164 (2018) 194–203, <https://doi.org/10.1016/j.energy.2018.08.192>.
- [24] E.A. Levitskij, Y.I. Aristov, M.M. Tokarev, V.N. Parmon, Chemical heat accumulators: a new approach to accumulating low potential heat, *Sol. Energy Mater. Sol. Cells* 44 (1996) 219–235, [https://doi.org/10.1016/0927-0248\(96\)00010-4](https://doi.org/10.1016/0927-0248(96)00010-4).
- [25] T. Yan, T. Li, J. Xu, J. Chao, R. Wang, Y.I. Aristov, L.G. Gordeeva, P. Dutta, S. S. Murthy, Ultrahigh-energy-density sorption thermal battery enabled by graphene aerogel-based composite sorbents for thermal energy harvesting from air, *ACS Energy Lett.* 6 (2021) 1795–1802, <https://doi.org/10.1021/acsenenergylett.1c00284>.
- [26] A. Permyakova, S. Wang, E. Courbon, F. Nouar, N. Heymans, P. D'Ans, N. Barrier, P. Billemont, G. De Weirld, N. Steunou, M. Frère, C. Serre, Design of salt-metal organic framework composites for seasonal heat storage applications, *J. Mater. Chem. A* 5 (2017) 12889–12898, <https://doi.org/10.1039/C7TA03069J>.
- [27] L.G. Gordeeva, Y.I. Aristov, Composites ‘salt inside porous matrix’ for adsorption heat transformation: a current state-of-the-art and new trends, *Int. J. Low-Carbon Technol.* 7 (2012) 288–302, <https://doi.org/10.1093/ijlct/cts050>.
- [28] J. Xu, T. Li, J. Chao, S. Wu, T. Yan, W. Li, B. Cao, R. Wang, Efficient solar-driven water harvesting from arid air with metal-organic frameworks modified by hygroscopic salt, *Angew. Chemie Int. Ed.* 59 (2020) 5202–5210, <https://doi.org/10.1002/anie.201915170>.

- [29] P.A. Kallenberger, K. Posern, K. Linnow, F.J. Brieler, M. Steiger, M. Fröba, Alginate-derived Salt/Polymer composites for thermochemical heat storage, *Adv. Sustain. Syst.* 2 (2018) 1700160, <https://doi.org/10.1002/advs.201700160>.
- [30] P. D'Ans, E. Courbon, A. Permyakova, F. Nouar, C. Simonnet-Jégat, F. Bourdreux, L. Malet, C. Serre, M. Frère, N. Steunou, A new strontium bromide MOF composite with improved performance for solar energy storage application, *J. Energy Storage* 25 (2019), 100881, <https://doi.org/10.1016/j.est.2019.100881>.
- [31] A. Shkatulov, R. Joosten, H. Fischer, H. Huinink, Core-Shell encapsulation of salt hydrates into mesoporous silica shells for thermochemical energy storage, *ACS Appl. Energy Mater.* 3 (2020) 6860–6869, <https://doi.org/10.1021/acsaem.0c00971>.
- [32] L. Calabrese, V. Brancato, V. Palomba, A. Frazzica, L.F. Cabeza, Magnesium sulphate-silicone foam composites for thermochemical energy storage: assessment of dehydration behaviour and mechanical stability, *Sol. Energy Mater. Sol. Cells* 200 (2019), 109992, <https://doi.org/10.1016/j.solmat.2019.109992>.
- [33] K. Posern, C. Kaps, Calorimetric studies of thermochemical heat storage materials based on mixtures of MgSO₄ and MgCl₂, *Thermochim. Acta* 502 (2010) 73–76, <https://doi.org/10.1016/j.tca.2010.02.009>.
- [34] A. Jabbari-Hichri, S. Bennici, A. Auroux, CaCl₂-containing composites as thermochemical heat storage materials, *Sol. Energy Mater. Sol. Cells* 172 (2017) 177–185, <https://doi.org/10.1016/j.solmat.2017.07.037>.
- [35] Q. Wang, Y. Xie, B. Ding, G. Yu, F. Ye, C. Xu, Structure and hydration state characterizations of MgSO₄-zeolite 13x composite materials for long-term thermochemical heat storage, *Sol. Energy Mater. Sol. Cells* 200 (2019), 110047, <https://doi.org/10.1016/j.solmat.2019.110047>.
- [36] T. Yan, C.Y. Wang, D. Li, Performance analysis of a solid-gas thermochemical composite sorption system for thermal energy storage and energy upgrade, *Appl. Therm. Eng.* 150 (2019) 512–521, <https://doi.org/10.1016/j.applthermaleng.2019.01.004>.
- [37] E. Scuille, P. Dutournié, M. Zbair, S. Bennici, Thermo-physical properties measurements of hygroscopic and reactive material (zeolite 13X) for open adsorptive heat storage operation, *J. Therm. Anal. Calorim.* 147 (2022) 12409–12416, <https://doi.org/10.1007/s10973-022-11439-9>.
- [38] P.A.J. Donkers, L.C. Söğütoglu, H.P. Huinink, H.R. Fischer, O.C.G. Adan, A review of salt hydrates for seasonal heat storage in domestic applications, *Appl. Energy* 199 (2017) 45–68, <https://doi.org/10.1016/j.apenergy.2017.04.080>.
- [39] G. Whiting, D. Grondin, S. Bennici, A. Auroux, Heats of water sorption studies on zeolite–MgSO₄ composites as potential thermochemical heat storage materials, *Sol. Energy Mater. Sol. Cells* 112 (2013) 112–119, <https://doi.org/10.1016/j.solmat.2013.01.020>.
- [40] S. Bennici, T. Polimann, M. Ondarts, E. Gonze, C. Vulot, N. Le Pierrès, Long-term impact of air pollutants on thermochemical heat storage materials, *Renew. Sustain. Energy Rev.* 117 (2020), 109473, <https://doi.org/10.1016/j.rser.2019.109473>.
- [41] S. Elliot, D. Patrick, Z. Mohamed, B. Simona, Thermo-physical properties measurements of hygroscopic and reactive material (zeolite 13X) for open adsorptive heat storage operation, *J. Therm. Anal. Calorim.* (2022), <https://doi.org/10.1007/s10973-022-11439-9>.
- [42] F. Rouquerol, J. Rouquerol, K. Sing, Assessment of mesoporosity, in: *Adsorption by Powders Porous Solids*, Elsevier, 1999, pp. 191–217, <https://doi.org/10.1016/B978-012598920-6/50008-7>.
- [43] M. Zbair, K. Ainassaari, A. Drif, S. Ojala, M. Bottlinger, M. Pirlä, R.L. Keiski, M. Bensitel, R. Brahma, Toward new benchmark adsorbents: preparation and characterization of activated carbon from argan nut shell for bisphenol A removal, *Environ. Sci. Pollut. Res.* (2018), <https://doi.org/10.1007/s11356-017-0634-6>.
- [44] M. Zbair, K. Ainassaari, Z. El Assal, S. Ojala, N. El Ouahedy, R.L. Keiski, M. Bensitel, R. Brahma, Steam activation of waste biomass: highly microporous carbon, optimization of bisphenol a, and diuron adsorption by response surface methodology, *Environ. Sci. Pollut. Res.* 25 (2018) 35657–35671, <https://doi.org/10.1007/s11356-018-3455-3>.
- [45] K. Posern, K. Linnow, M. Niermann, C. Kaps, M. Steiger, Thermochemical investigation of the water uptake behavior of MgSO₄ hydrates in host materials with different pore size, *Thermochim. Acta* 611 (2015) 1–9, <https://doi.org/10.1016/j.tca.2015.04.031>.
- [46] L.G. Gordeeva, Y.I. Aristov, Composites 'salt inside porous matrix' for adsorption heat transformation: a current state-of-the-art and new trends, *Int. J. Low-Carbon Technol.* 7 (2012) 288–302, <https://doi.org/10.1093/ijlct/cts050>.
- [47] Y. Hirata, K. Fujioka, S. Fujiki, Preparation of fine particles of calcium chloride with expanded graphite for enhancement of the driving reaction for chemical heat pumps, *J. Chem. Eng. Jpn.* 36 (2003) 827–832, <https://doi.org/10.1252/jcej.36.827>.
- [48] Y. Alyousef, A.A. Antukh, A.P. Tsitovich, L.L. Vasiliev, Three adsorbents solar cooler with composite sorbent bed and heat pipe thermal control, *Appl. Therm. Eng.* 38 (2012) 124–130, <https://doi.org/10.1016/j.applthermaleng.2011.12.031>.
- [49] K. Fujioka, K. Hatanaka, Y. Hirata, Composite reactants of calcium chloride combined with functional carbon materials for chemical heat pumps, *Appl. Therm. Eng.* 28 (2008) 304–310, <https://doi.org/10.1016/j.applthermaleng.2006.02.032>.
- [50] Z. Aidoun, M. Terman, Salt impregnated carbon fibres as the reactive medium in a chemical heat pump: the NH₃-CoCl₂ system, *Appl. Therm. Eng.* 22 (2002) 1163–1173, [https://doi.org/10.1016/S1359-4311\(02\)00037-6](https://doi.org/10.1016/S1359-4311(02)00037-6).
- [51] I.A. Simonova, A. Freni, G. Restuccia, Y.I. Aristov, Water sorption on composite "silica modified by calcium nitrate", *Microporous Mesoporous Mater.* 122 (2009) 223–228, <https://doi.org/10.1016/j.micromeso.2009.02.034>.
- [52] I. Glaznev, I. Ponomarenko, S. Kirik, Y. Aristov, Composites CaCl₂/SBA-15 for adsorptive transformation of low temperature heat: pore size effect, *Int. J. Refrig.* 34 (2011) 1244–1250, <https://doi.org/10.1016/j.ijrefrig.2011.02.007>.
- [53] M.H. Nguyen, M. Zbair, P. Dutournié, A. Gervasini, C. Vulot, S. Bennici, Toward new low-temperature thermochemical heat storage materials: investigation of hydration/dehydration behaviors of MgSO₄/hydroxyapatite composite, *Sol. Energy Mater. Sol. Cells* 240 (2022), 111696, <https://doi.org/10.1016/j.solmat.2022.111696>.
- [54] Y. Zhang, Q. Miao, X. Jia, Y. Jin, Z. Li, L. Tan, Y. Ding, Diatomite-based magnesium sulfate composites for thermochemical energy storage: preparation and performance investigation, *Sol. Energy* 224 (2021) 907–915, <https://doi.org/10.1016/j.solener.2021.05.054>.
- [55] Q. Miao, Y. Zhang, X. Jia, L. Tan, Y. Ding, MgSO₄-expanded graphite composites for mass and heat transfer enhancement of thermochemical energy storage, *Sol. Energy* 220 (2021) 432–439, <https://doi.org/10.1016/j.solener.2021.03.008>.
- [56] D. Mahon, G. Claudio, P.C. Eames, An experimental investigation to assess the potential of using MgSO₄ impregnation and Mg²⁺ ion exchange to enhance the performance of 13X molecular sieves for interseasonal domestic thermochemical energy storage, *Energy Convers. Manag.* 150 (2017) 870–877, <https://doi.org/10.1016/j.enconman.2017.03.080>.
- [57] S. Langergen, B.K. Svenska, Zur theorie der sogenannten adsorption geloester stoffe, *Vetensk. Handl.* 24 (1898) 1–39.
- [58] G. McKay, Pseudo-second order model for sorption processes, *Proc Biochem.* 34 (1999) 451.
- [59] H.N. Tran, S.J. You, A. Hosseini-Bandegharai, H.P. Chao, Mistakes and inconsistencies regarding adsorption of contaminants from aqueous solutions: a critical review, *Water Res.* 120 (2017) 88–116, <https://doi.org/10.1016/j.watres.2017.04.014>.
- [60] F.-C. Wu, R.-L. Tseng, R.-S. Juang, Initial behavior of intraparticle diffusion model used in the description of adsorption kinetics, *Chem. Eng. J.* 153 (2009) 1–8, <https://doi.org/10.1016/j.cej.2009.04.042>.
- [61] I.S. McLintock, The elovich equation in chemisorption kinetics, *Nature* 216 (1967) 1204–1205, <https://doi.org/10.1038/2161204a0>.

Thermochemical sorption heat storage: Investigate the heat released from activated carbon beads used as porous host matrix for MgSO₄ salt

Minh Hoang Nguyen^{1,2}, Mohamed Zbair^{1,2}, Patrick Dutournié^{1,2}, and Simona Bennici^{1,2*}

¹ Institut de Science des Matériaux de Mulhouse (IS2M), Université de Haute-Alsace, CNRS,
IS2M UMR 7361,

F-68100 Mulhouse, France; minh-hoang.nguyen@uha.fr; mohamed.zbair@uha.fr;
patrick.dutournie@uha.fr; simona.bennici@uha.fr

² Université de Strasbourg, France

* Correspondance: simona.bennici@uha.fr; Tel.: +33 (0)3 89336729

Supplementary Information

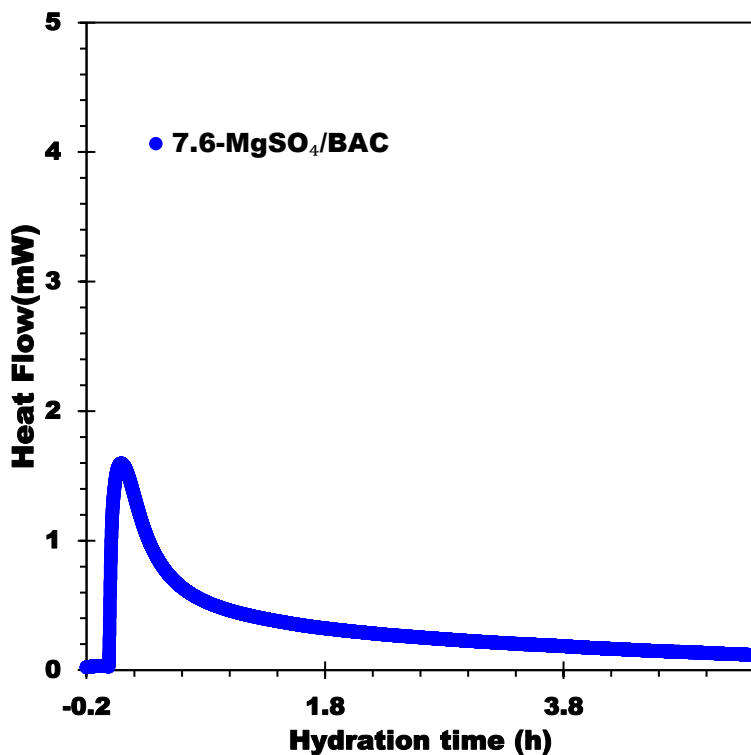
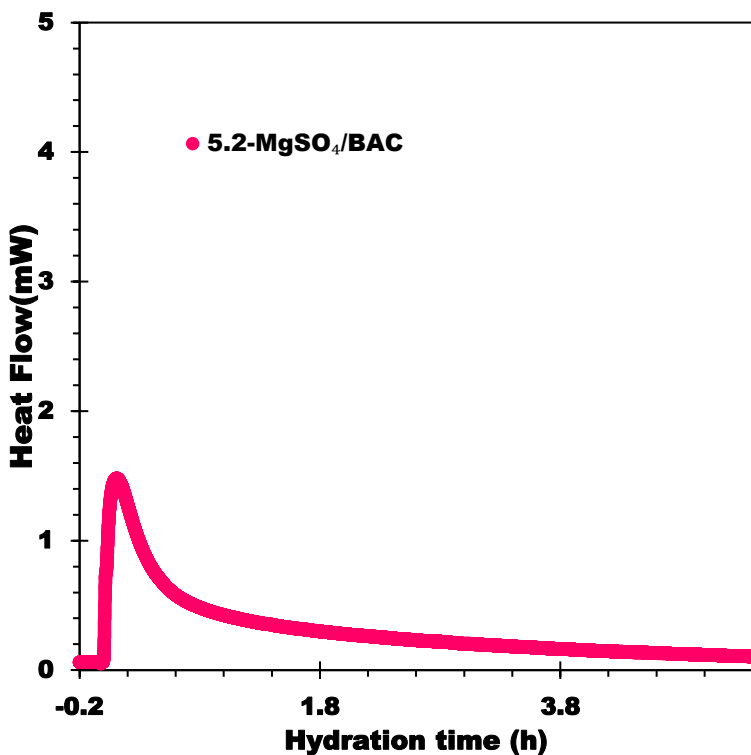
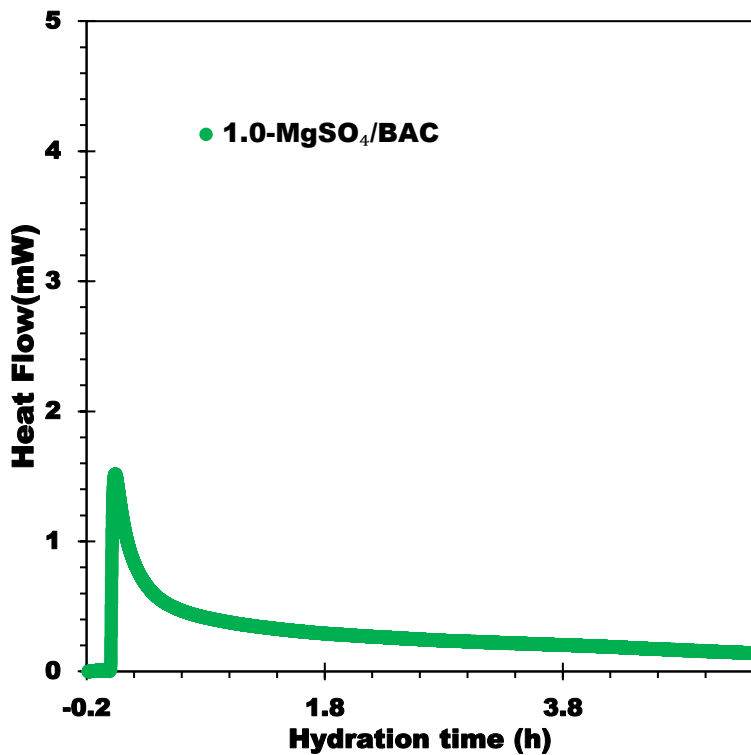
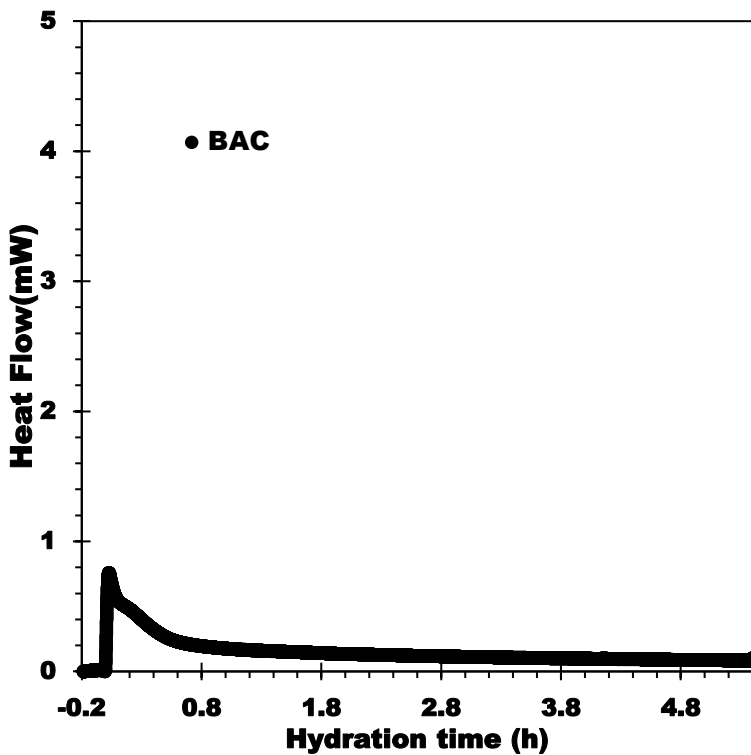


Figure 1S. DSC spectra of hydration for all samples (after subtraction of the blank analysis performed in the same conditions).

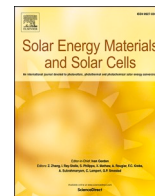
Chapter IV

Toward new low-temperature thermochemical heat storage materials: Investigation of hydration/dehydration behaviors of MgSO₄/Hydroxyapatite composite

Solar Energy Materials and Solar Cells 240, 111696 (2022)

Résumé

Dans le cadre d'une collaboration avec l'université de Milan, nous avons testé, pour la première fois, de l'hydroxyapatite comme support pour la conception d'un matériau de stockage de la chaleur. Deux composites à base de MgSO_4 ont été préparés par imprégnation par voie humide avec 5 % et 20 % en masse de sel. L'analyse des isothermes d'adsorption d'azote montre que les composites préparés avec l'hydroxyapatite sont des matériaux mésoporeux avec des surfaces spécifiques de l'ordre de $100 \text{ m}^2/\text{g}$. La distribution de taille des pores se situe principalement dans le domaine mésoporeux (entre 2 et 50 nm) et à cela, de petits macropores (50 – 100 nm) ce qui pourrait faciliter l'inclusion du sel dans la porosité du support. Les cartographies EDX obtenues pour les échantillons juste préparés et après 20 cycles d'hydratation/déshydratation montrent que le sel est et reste bien dispersé dans la matrice. Les résultats de sorption d'eau montrent un meilleur transfert pour les composites comparé au sel hydraté seul et au support (hydroxyapatite non imprégnée). Cette propriété est directement liée à la puissance qui peut être obtenue dans un système de stockage employant ces composites. Une bonne stabilité du composite contenant 20 % en masse de sel a été prouvée en effectuant 20 cycles de sorption : la capacité de stockage et la capacité d'adsorption d'eau se sont montrées stables. La densité d'énergie moyenne du composite a été mesurée à 472 J/g de composite.



Toward new low-temperature thermochemical heat storage materials: Investigation of hydration/dehydration behaviors of MgSO₄/Hydroxyapatite composite

Minh Hoang Nguyen^{a,b}, Mohamed Zbair^{a,b}, Patrick Dutournié^{a,b}, Antonella Gervasini^c, Cyril Vaultot^{a,b}, Simona Bennici^{a,b,*}

^a Université de Haute-alsace, CNRS, IS2M UMR 7361, F-68100, Mulhouse, France

^b Université de Strasbourg, France

^c Dipartimento di Chimica, Università degli Studi di Milano, via Camillo Golgi, 19, 20133, Milano, Italy

ARTICLE INFO

Keywords:

Thermochemical storage of solar heat
Magnesium sulfate
Hydroxyapatite
Water sorption
Adsorption kinetics

ABSTRACT

A new two-component (composite) water sorbent MgSO₄/Hydroxyapatite has been developed for sorption-based solar heat storage. The matrix of the composite is a hydroxyapatite (HAP) material with ordered structure, high surface area of 111.3 m²/g and mesopore dimensions centered at 45 nm. The composites, prepared by wet-impregnation of HAP with MgSO₄, have lower specific surface area and similar mesopore dimensions as the matrix. The maximum water sorption capacity of HAP is 0.039 g/g, while the composite (20-MgSO₄/HAP) possesses 3.7 times higher maximum water sorption capacity due to the presence of the salt in the matrix. The HAP composite containing 20% MgSO₄ achieved the highest heat of hydration 464 J/g. A long-term cycling (dehydration at 150 and hydration at 30 °C at a relative humidity of 60%) confirms a comparatively good stability of the composite.

1. Introduction

Solar energy is considered a viable alternative to conventional energy sources, and its potential applications in residential and industrial surroundings have been extensively studied [1,2]. Though, the imbalance between energy supply and demand makes it difficult to put into practice. Thermal energy storage (TES) is an evolving technology and an effective way to achieve long-term solar energy use [3,4]. Latent heat storage, sensible heat storage, and thermochemical heat storage (TCHS) are three types of system using TES technologies. While latent and sensible heat storage have been extensively studied in recent decades [5,6], there have been few studies on TCHS, which is highly competitive and have been attracting growing interests due to higher energy storage density and negligible heat loss over long storage periods [7,8]. Based on the reversible sorption reaction, heat is stored following the endothermic reaction (charging) and this energy can be retrieved later on from the exothermic reaction (discharging) for many practical applications in particular in the building sector. In these application the most common configuration is based on the sorption phenomena of a sorbate

(often water) on a sorbent (generally a solid material).

The solid thermochemical storage material has to be chosen carefully to ensure a good working system. Basically, it must possess certain properties such as high energy density, high affinity for the sorbate (water in most cases), a high mass and heat transfer with a charging temperature as low as possible to fit in residential applications [9,10]. In addition, the material needs to be eco-friendly, non-toxic and inexpensive. With these criteria, salt hydrates appear to be a promising storage materials [11]. SrBr₂, MgCl₂, and MgSO₄ hydrates are among the best potential salt hydrates, with MgSO₄ hydrate having the highest theoretical heat storage density of 2.8 GJ/m³ and a low charging temperature (<150 °C), which is suitable for building applications with solar collectors, being the most cost-effective [12,13], and, most importantly, having a dehydration temperature that matches well with the thermal solar collectors. Furthermore, to broaden the applications panel, the salt's relative humidity of deliquescence (RHD) is a crucial metric to consider. The RHD is the relative humidity limit at which the salt will dissolve in the adsorbed water in proportion to temperature, resulting in absorption into the material. Excessive water absorption permits more

* Corresponding author. Université de Haute-alsace, CNRS, IS2M UMR 7361, F-68100, Mulhouse, France.

E-mail addresses: minh-hoang.nguyen@uha.fr (M.H. Nguyen), mohamed.zbair@uha.fr (M. Zbair), patrick.dutournie@uha.fr (P. Dutournié), antonella.gervasini@unimi.it (A. Gervasini), cyril.vaultot@uha.fr (C. Vaultot), simona.bennici@uha.fr (S. Bennici).

<https://doi.org/10.1016/j.solmat.2022.111696>

Received 30 June 2021; Received in revised form 27 February 2022; Accepted 5 March 2022

Available online 12 March 2022

0927-0248/© 2022 Elsevier B.V. All rights reserved.

water to be absorbed, increasing the amount of heat generated by the process. The production of saline solution, on the other hand, might produce corrosion issues [14]. The deliquescence process of $\text{MgSO}_4 \cdot n\text{H}_2\text{O}$, for example, will not occur below 80% relative humidity (RH) at temperatures ranging from 10 to 80 °C since it is thermodynamically stable at this temperature and humidity range [15,16]. The major drawbacks of this system are the overhydration, the formation of aggregates occurring during rehydration, the kinetic hindrance limiting the mass and heat transfer, and the poor cyclability [15]. Consequently, the system's full potential could not be reached and, as a result of these constraints, the energy storage capacity was low. One way to take advantage of the MgSO_4 's great potential is to make composites by dispersing the salt in a porous matrix to avoid swelling and aggregates formation, which represent one of the main materials' drawbacks. To overcome these issues, efforts have been focused on the development of high-performance composite materials using porous matrix and salt hydrates [11,17].

The composite sorbents are also known as "composite salt in porous matrix" (CSPM), a term used by Yuri Aristov et al. [18]. However, if composite sorbents are subjected to a wet environment for an extended period of time and the collected water is insufficient to be held inside the pores, they are at risk of solution leakage. As a result, developing a porous matrix with an ultrahigh pore volume to load a high content of salts and store a big amount of collected water is extremely important in order to avoid the risk of liquid leakage.

For that reason, several sorbent materials as a matrix for hydrated salts, such as silica gel [19,20], activated alumina [21], zeolite [22,23], MOFs [24], vermiculite [25], and expanded graphite [26,27], has received considerable attention. However, in order to be an appropriate material for TES applications, the matrix must fulfill a number of criteria, including cheap cost, a low regeneration temperature, a high storage density, and good mass and heat transfers that enable long-term storage with high efficiency and an easier recovery of the heat by different means (air vector, solid/liquid, solid/air heat exchangers).

Despite the fact that a variety of innovative composite sorbents for heat storage have been developed [24,28–32], there is still a significant gap between the materials and their practical applications. As supporting matrices, for example, different zeolites, which are aluminosilicate minerals having microporous structures for moisture adsorption, are commonly used. Wang et al. [22] performed the solution impregnation approach to create the MgSO_4 @zeolite-13x composite thermochemical sorbent. They indicated that the sorbent contained 8% by weight MgSO_4 performed better at a high RH of 80%, with no salt crystals visible on the surface. However, the low ESD of about 600 J/g and cyclability need to be further improved. MgSO_4 @zeolite has been proven to be financially viable for home interseasonal energy storage, however it may not entirely fulfill a household's heating requirement [30]. The adsorption capacity of MgSO_4 @zeolite sorbent, on the other hand, would considerably decrease if the hydration temperature is above 50 °C [4], implying that the maximum discharge temperature in the application would not exceed 50 °C. Zhang et al. [33] produced a range of form-stable cylindrical structures using zeolite-13X as a matrix. The sample with the optimal mass ratio (zeolite-13X: CaCl_2 : MgSO_4 = 10: 54: 36) exhibited a gravimetric-ESD of 1410 J/g at a dehydration temperature of 250 °C, and the value reduced by 20% after 20 dehydration-hydration cycles. Although zeolites are common and inexpensive matrices, inherent defects such as a high charging temperature (>200 °C) and a low thermal conductivity.

Aristov et al. [18] studied different composites by embedding hygroscopic salts (e.g., CaCl_2 and LiBr) in mesoporous and microporous silica gels. The salts were distributed rather than bulk, which helps to reduce swelling and agglomeration and to speed up mass and heat transmission. The pore structure and chemical content of the host matrix materials have a significant impact on the heat storage capacity of salt/porous matrix composites [34], therefore choosing the right host porous material is crucial. By impregnating CaCl_2 into SBA-15 pores,

Ponomarenko et al. [35] produced a composite material that could adsorb 0.47 g/g. Courbon et al. [36] presented an improved synthesis process for silica gel and CaCl_2 composites. The energy storage density was 300 Wh/kg, and the cycle loading uptake was 0.4 g/g. Whiting et al. [37] investigated the use of zeolite as a porous matrix to increase MgSO_4 heat storage. When impregnated with MgSO_4 , the zeolite Na-Y with the largest surface area ($780 \text{ m}^2\text{g}^{-1}$) and total pore volume ($0.32 \text{ cm}^3\text{g}^{-1}$) produced the highest heat of hydration (1090 J/g). The water sorption process on expanded vermiculite/ CaCl_2 composites was researched by Aristov and coworkers [38], who claimed that impregnation of CaCl_2 into expanded vermiculite can increase the water sorption capacity even at low water vapor pressure. However, expanded vermiculite's surface area is low ($9 \text{ m}^2\text{g}^{-1}$), making it unsuitable for salt loading and mass transfer. Although these porous materials can increase the heat storage capacity of organic salts, they have low pore size and it is hard to modulate their structures and properties.

Shi et al. [24] made-up CaCl_2 -based metal-organic frameworks (MOFs) composites with a high storage energy of 1274 J/g with moderate stability via 17 continuous adsorption/desorption cycles. Palomba and coworkers encapsulate LiCl into silica gel to improve the dynamic behavior of a long-term adsorption heat storage with a maximum useful heat of 450 J/g [39]. Calabrese [40] designed a silicone foam/ MgSO_4 composite and shown that this material improved mechanical stability and cycle performance considerably.

It is obvious from the above literature study that there are still improvements to be made in TES materials for heat storage. Certainly, the studies on composites appear to be too diverse. However, various flaws, such as vermiculite's low heat conductivity, zeolite's high desorption temperature, and MOFs' poorer thermo-mechanical characteristics, must be addressed.

The type of porosity (micro/meso) is a significant element in composite design, according to these studies. The salt may plug the pores if they are too tiny, preventing water molecules from diffusing and lowering energy storage capacity. Other materials, such as mesoporous activated carbon or silica-gels, have also been shown to be excellent supports. Salt may be incorporated through their large pores, increasing their energy storage capacity while preventing pore obstruction [41,42]. Aside from the high surface area and the existence of mesoporosity, strong thermal conductivity is a significant consideration in selecting the best support. This parameter is critical for the heat transport phenomena to be optimized.

A porous host matrix with a large pore size structure (mesoporous) is needed to improve the composite material's water uptake. In this study, in addition to the commonly used porous materials (zeolites, silica gel, and so on), a new host matrix is used: hydroxyapatite (HAP), a calcium phosphate apatite with a developed mesoporous structure [43].

HAP - $\text{Ca}_{10}(\text{PO}_4)_6(\text{OH})_2$, is a well-known biomaterial of the calcium phosphate family with high biocompatibility. Recently, Hu et al. [44] discovered that a HAP nanowire membrane could be used as a separator, especially for high-temperature Li-ion battery applications. Because of its low cost, superior compatibility with surrounding materials, and higher adsorption ability, nanoscale HAP is regarded as one of the most significant biomaterial adsorbents. HAP can be used also as an adsorbent to absorb heavy metal ions like Pb^{2+} , Cu^{2+} , and Cd^{2+} , which are attributed to the ion Ca^{2+} in solution through metal cations [45]. HAP is also regarded as one of the most promising adsorption materials for absorbing different organic and inorganic pollutants [46]. Amedlous et al. [47] have been used natural mesoporous hydroxyapatite as support for copper loading as eco-friendly Fenton-like catalyst to effectively remove organic dyes. Furthermore, Wang et al. [48] determined that HAP has a thermal conductivity of 0.15–0.20 W/m K, indicating that it has a high heat transfer capacity. As a consequence, employing HAP as a porous matrix for hygroscopic salts is valuable, as it will allow to better understand water sorption and heat transport in composite materials.

For all the above-mentioned reasons and to the best of our knowledge, this is the first work which reports the use of HAP as adsorbent in

Table 1Physicochemical characteristics of HAP support and MgSO₄/HAP composites.

Sample	MgSO ₄ content (wt%)	S _{BET} (m ² ·g ⁻¹) ^a	S _{ext} (m ² ·g ⁻¹) ^b	S _m (m ² ·g ⁻¹) ^b	V _p (cm ³ ·g ⁻¹) ^c	V _{meso} (cm ³ ·g ⁻¹) ^b
HAP	–	111.3	99.6	11.7	0.664	0.659
5-MgSO ₄ /HAP	4.11	93.9	83.3	10.6	0.499	0.494
20-MgSO ₄ /HAP	17.27	63.1	63.1	0	0.358	0.358

^a Calculated using the BET equation at p/p° between 0.01 and 0.40.^b Determined using the t-plot method with thickness range 3.5–5 Å.^c Determined from the amount of N₂ adsorbed at p/p° = 0.99.

TCHS application. Incorporation of MgSO₄ in HAP matrix may increase the total charge storage capacity and potentially overcome its limitations. In addition, the HAP shows a low density and mesoporous structure, which is very conducive to its application in TCHS system [49]. The OH- group in HAP can form hydrogen bonds with water which inhibits the leakage of the salt [48]. In this study, composites designed by impregnation of MgSO₄ on a HAP support were prepared, characterized, and their performance assessed. In addition to the heat of hydration released, the experimental kinetic data were examined. The goal was to produce composite materials with high energy density storage with a fast reaction kinetics.

2. Materials and methods

2.1. Composite materials preparation

2.1.1. Hydroxyapatite (HAP) preparation

Hydroxyapatite synthesis was carried by using pure reagent-grade salt precursors, namely, calcium nitrate tetra hydrate, Ca(NO₃)₂·4H₂O (>99.0% from Merck ACS); and ammonium dihydrogen phosphate, (NH₄)H₂PO₄ (>98.0% from Sigma-Aldrich).

Stoichiometric hydroxyapatite was synthesized by the conventional co-precipitation method by fixing the Ca/P molar ratio of the reagents in solution at 1.67, operating by the procedure reported in Campisi work [50]. For the preparation of ca. 4 g of stoichiometric hydroxyapatite, 250 mL of an aqueous solution containing 0.167 mol of Ca(NO₃)₂·4H₂O was added to 250 mL of a 0.1 mol of (NH₄)H₂PO₄ solution placed in a 4-neck round flask and maintained under stirring at 80 °C. During the synthesis, the pH value was maintained at value of 10 by an appropriate addition of a 28–30% NH₄OH solution (from Sigma-Aldrich). The formed precipitate was slowly filtered, washed with hot water, and dried first at 50 °C under vacuum and then at 120 °C for 8 h. The grain size of HAP obtained is in the range of 0.5–1 mm with a density of 3.16 g/cm³.

2.1.2. Composite materials (MgSO₄/HAP) preparation

Incipient Wetness Impregnation (IWI) method [51] was used for embedding MgSO₄ (MgSO₄·7H₂O 99.9% from Sigma-Aldrich) inside HAP adsorbent. This traditional method consists of only filling the pores of the HAP with an aqueous solution of MgSO₄. To do this, the HAP support was firstly oven-dried at 150 °C to remove any trace of water from the pores. An aqueous solution of MgSO₄ was then applied on the dried support (room temperature and pressure) until it starts to get wet. The impregnated materials were then dried at 150 °C for 12 h. Accordingly, two composites were prepared by IWI and then labelled as x-MgSO₄/HAP (1st column in Table 1) with x is the theoretical content of MgSO₄ in the composites. The first composite contains 5 wt% of MgSO₄ and the second one contain 20 wt% of MgSO₄ which is the maximum amount that can be integrated inside HAP. The experimental salt content was determined by means of X-Ray Fluorescence. The density of HAP is 3.16 g/cm³ and the density of anhydrous MgSO₄ is 2.66 g/cm³. With the law of mixture, the density of the composites would be 3.07 g/cm³ for the 20-MgSO₄/HAP and 3.14 g/cm³ for the 5-MgSO₄/HAP.



Fig. 1. A Sensys TG-DSC apparatus equipped with a microbalance and connected to a humidity regulator Wetsys by a thermal transfer line (from Setaram).

2.2. Physicochemical characterizations methods

X-Ray Diffraction (XRD) analyses were performed on the compacted powder of the samples on a diffractometer PANalytical MPD X'Pert Pro, equipped with a Pixel real-time multiple strip detector, operating with an angular aperture of 3.347° 2θ in 3°–80° 2θ range, and using CuKα radiation with 0.15418 nm wavelength. Diffractograms were recorded at 22 °C with a step size of 0.013° 2θ and a scan time of 220 s per step.

A wavelength dispersion X-Ray Fluorescence (WDXRF) spectrometer (from PANalytical, Zetium) was used to perform the XRF measurements on pellets made of 0.2 g of the sample.

High-resolution micrographics were acquired by a Scanning Electron Microscope (SEM) from JEOL, JSM-7900F model. The semi-quantitative chemical analysis and atomic composition mapping of the sample was performed by means of Energy Dispersive X-ray (EDX).

N₂ adsorption/desorption isotherms of support and composites at –196 °C were acquired in a ASAP 2420 device from Micrometrics (Micromeritics, Norcross, GA, USA). The samples were previously degassed at 150 °C for 12 h and then, again at 150 °C for 2 h directly in the calorimetric cell before analysis. The specific surface area was calculated applying the Brunauer, Emmett and Teller (BET) equation (S_{BET}) (0.01 < p/p° < 0.40). The mesoporous volumes (V_m), external surface (ext) and microporous surface (S_m) were determined by applying the t-plot method (thickness range: 0.35–0.50). Finally, the pore size distribution (PSD) was determined using Barrett, Joyner and Halenda (BJH) method applied on the desorption branch of the isotherms.

2.3. Hydration/dehydration experiments

A Sensys TG-DSC (Thermogravimetry coupled to differential scanning calorimetry) apparatus, equipped with a Wetsys flow humidity generator both from Setaram (Fig. 1) were used to measure the heat released and the water adsorption amounts (measured by the microbalance) of the HAP and its composites. Prior to the hydration process, the samples (~10 mg) were dehydrated at 150 °C by increasing the

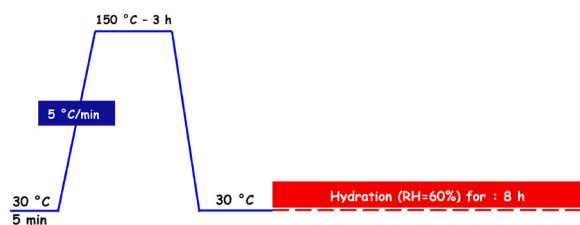


Fig. 2a. Thermal cycle used for the TG-DSC/WETSYS analyses.

temperature from 30 to 150 °C at 5 °C/min under a flow of dry air (30 mL/min) with a subsequent isotherm of 3 h at 150 °C to ensure a complete dehydration. Then, each sample was cooled down to 30 °C and, once having attained a stable thermal (DSC signal) baseline, the relative humidity (RH) of the air flow was increased to 60% (equivalent to a water vapor partial pressure of 2.55 kPa). The hydration process was set for 8 h in order to completely rehydrate the material – the complete rehydration was reached when the DSC signal returned to the baseline. Fig. 2a depicts the temperature profile used for all the calorimetric experiments. These conditions were selected to be as close to a real-life residential application as possible: 150 °C is the average working temperature that can be reached using a flat-plate solar heat collectors [37, 52] and 30 °C is close to the indoor air temperature during the discharging phase [53]. To accurately calculate the dehydration/hydration heat, the dehydration/hydration process for each sample was performed after stabilizing the DSC and TGA signals. Blank experiments with empty crucibles in the same conditions were also performed. The signals (DSC

and TGA) of the blank experiment were then subtracted from the sample experiment. The dehydration/hydration heat (J/g_{sample}) were finally obtained by integrating the surface of the subtracted curves (see Fig. 2b as an example).

3. Results and discussion

3.1. Structural properties of the composite materials

Table 1 summarizes the chemical composition obtained using the WDXRF method as well as the textural parameters (S_{BET} , S_{ext} , S_{m} , V_{p} , and V_{meso} , where S_{ext} is the external surface and V_{meso} is the mesoporous volume). With increasing MgSO_4 loading, the S_{BET} and V_{p} (total pore volume) values of the HAP and related composites show a significant decrease. This might be explained by the pore blocking by MgSO_4 and then a decrease in the pore accessibility by the N_2 molecules. Actually, the initial V_{p} ($0.664 \text{ cm}^3/\text{g}$) diminished by 25% ($0.499 \text{ cm}^3/\text{g}$) after the impregnation of 4.11% MgSO_4 , and it shrank to only $0.358 \text{ cm}^3/\text{g}$ after HAP was incorporated by 17.27% MgSO_4 . HAP s and prepared composites display type IV isotherm according to Ref. [54]. We can observe that the deposition of MgSO_4 do not impact the isotherm shape even if by increasing the quantity of impregnated salt, the adsorbed volumes decrease. (Fig. 3a). The adsorption curves appear slightly convex at a very low p/p° (insert in Fig. 3a), representing a minor part of microporosity in the different materials (Type I isotherm). A type IV isotherm is particularly identified by capillary condensation/evaporation at high relative pressures (from 0.8–1.0 p/p°) interpreted by a hysteresis loop. In the present cases, the adsorption and desorption branches appear

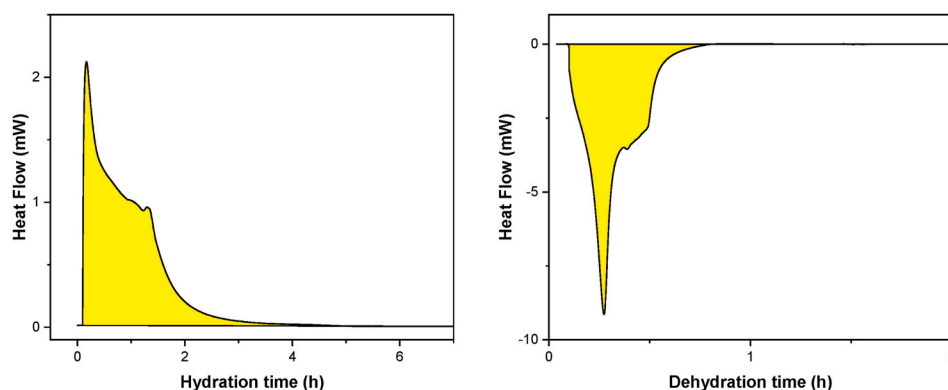


Fig. 2b. Example of DSC peaks for hydration and dehydration (after subtraction of the blank analysis performed in the same conditions) for the 20- MgSO_4/HAP sample. The (yellow area) represents the heat. (For interpretation of the references to colour in this figure legend, the reader is referred to the Web version of this article.)

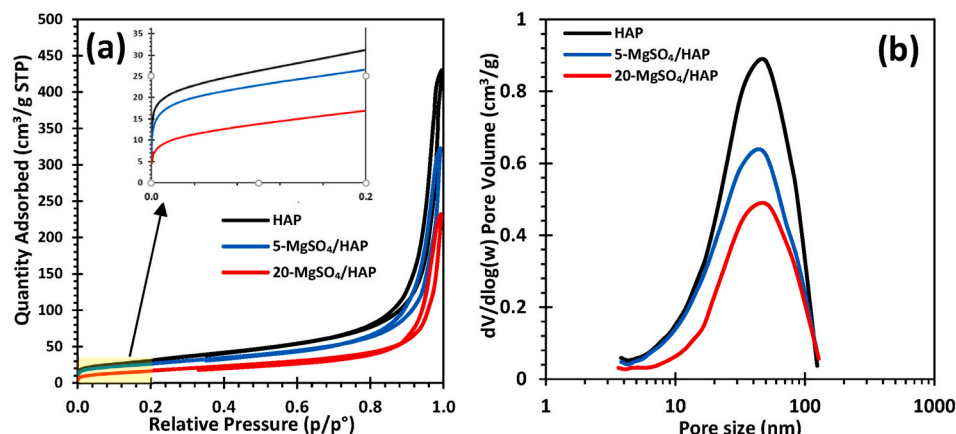


Fig. 3. (a) N_2 adsorption-desorption isotherms and (b) pore size distribution of HAP and its composites with MgSO_4 .

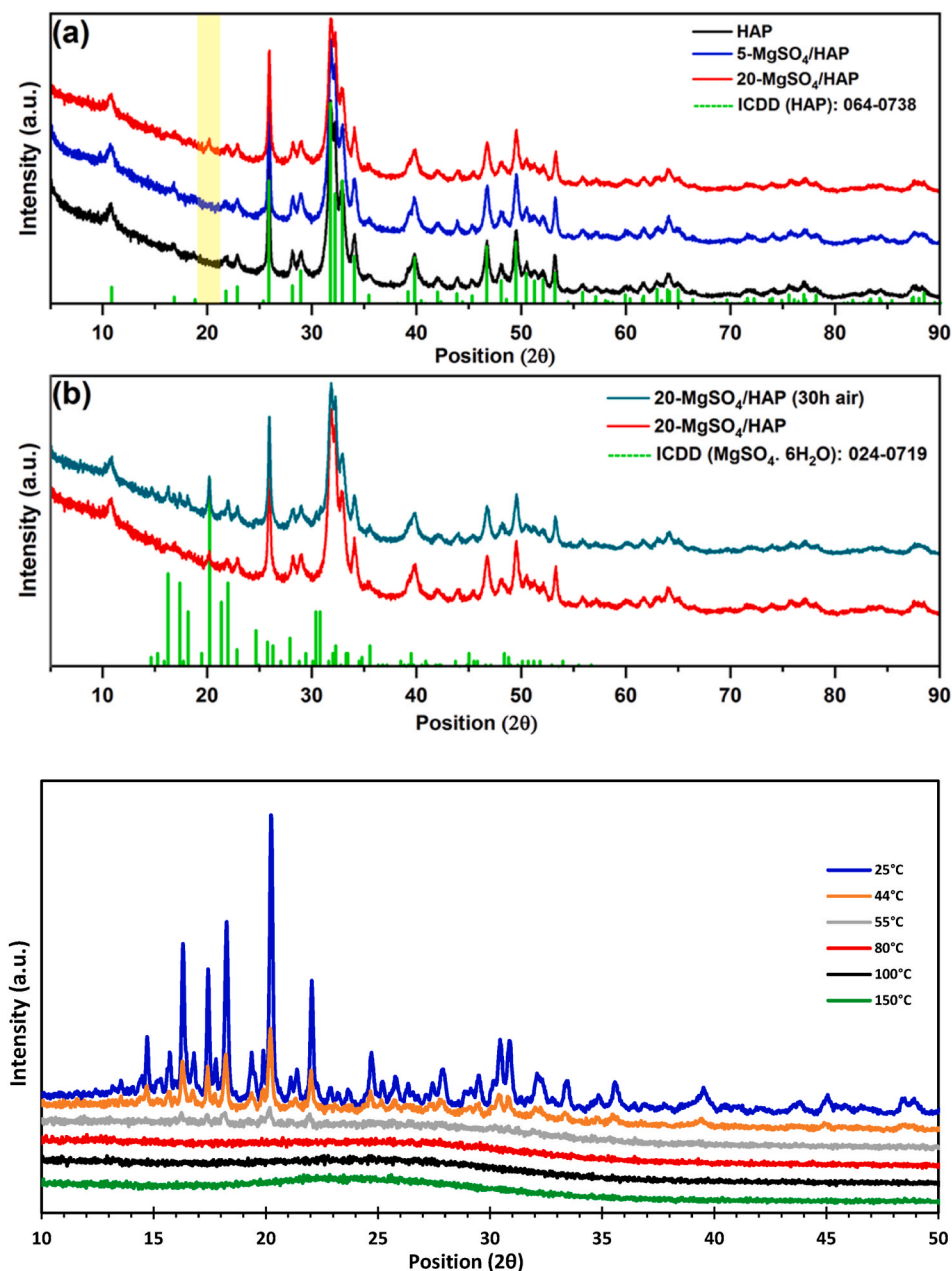


Fig. 4. a) XRD patterns of HAP and its composites, b) Identification of $\text{MgSO}_4 \cdot 6\text{H}_2\text{O}$ formation after 30 h at ambient air exposition, c) In-situ XRD patterns of $\text{MgSO}_4 \cdot 7\text{H}_2\text{O}$ during its dehydration from 25 to 150 °C.

relatively parallel, and the phenomena seems to finish at about $p/p^\circ = 0.8$. This behavior is relatively typical of type H1 hysteresis [55]. The type IV isotherm with a type H1 hysteresis and the p/p° range of the hysteresis highlight the presence of mesopores (eventually macropores) with a large distribution in the porous structure of the composite. The pore size distribution (PSD) of the composites and pure HAP shown in Fig. 3b has been obtained by applying the BJH method to the desorption branches of N_2 adsorption/desorption isotherms [56]. The composites maintain the same unimodal, but large (between 10 and 200 nm), distribution as the HAP (only the pore volume is diminished) with peaks centered at around 45 nm. This distribution confirms the predominance of the large mesopores and macropores in the composites porous structures. Since the PSD of the composites is maintained, the size of the pore entrance is not affected. This result suggests the filling and complete blocking of several pores by aggregates of salt particles; no narrowing of the pores due to the deposition of salt can be deduced.

The crystallinity and phase identification of the prepared samples were determined using XRD. The XRD patterns of all samples (Fig. 4a) revealed a pure HAP phase ($\text{Ca}_{10}(\text{PO}_4)_6(\text{OH})_2$), with all reflections identical to the reference database (ICDD 00-064-0738). Nonetheless, an unidentified peak at around 20° 2 θ was observed on the XRD pattern of 20- MgSO_4/HAP (Fig. 4a). To verify the source of such peak, the sample was exposed to ambient air for 30 h. Further hydration occurred, and then the intensity of this peak increased alongside the appearance of additional peaks between 17 and 20° 2 θ (Fig. 4b). These peaks have been identified using database of X'Pert HighScore Plus software and they were assigned to $\text{MgSO}_4 \cdot 6\text{H}_2\text{O}$ (ICDD 00-024-0719) (Fig. 4b). On the other hand, no additional MgSO_4 reflections were observed in the XRD patterns, suggesting that an amorphous $\text{MgSO}_4 \cdot y\text{H}_2\text{O}$ phase ($y < 6$) could be present in the sample [57]. In fact, the amorphicity of the $\text{MgSO}_4 \cdot y\text{H}_2\text{O}$ phase was confirmed after analyzing the diffractograms of MgSO_4 during the dehydration process up to 150 °C (Fig. 4c). At first, at

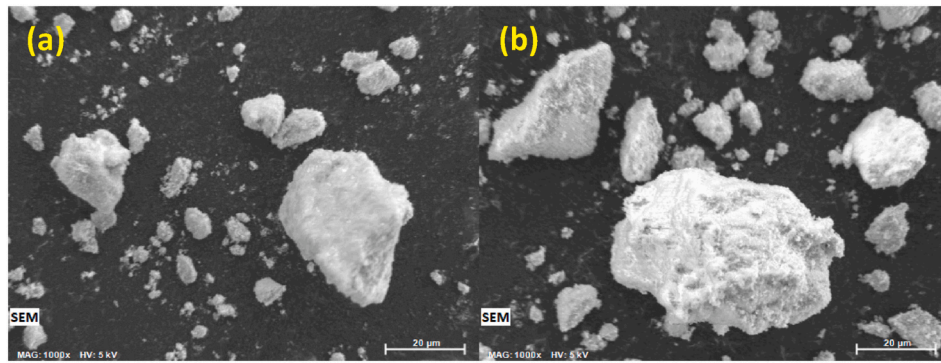


Fig. 5. SEM images of a) 5-MgSO₄/HAP and b) 20-MgSO₄/HAP.

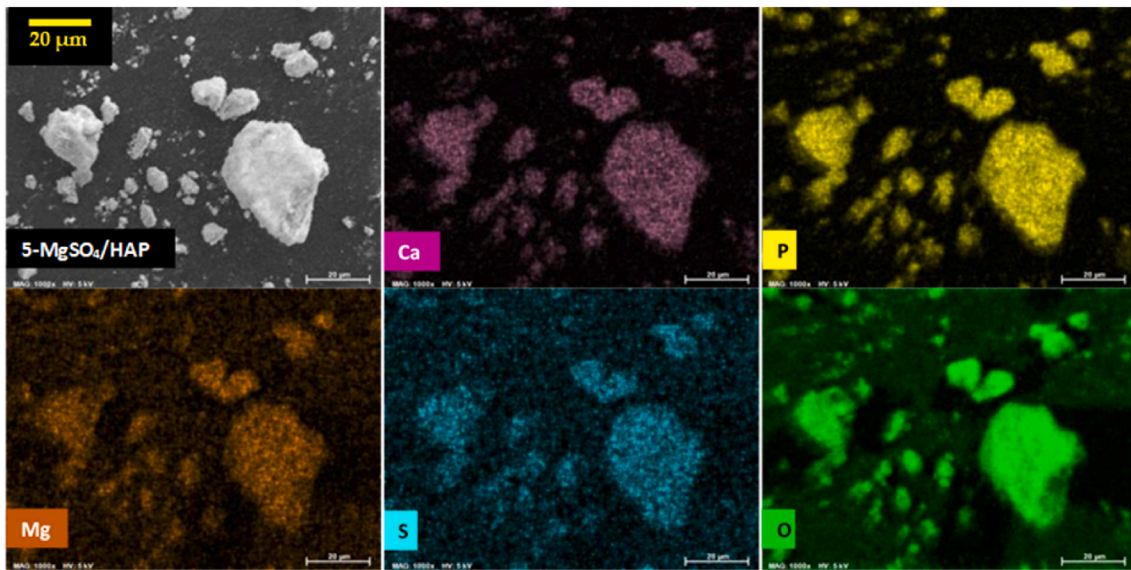


Fig. 6. EDX mapping for 5-MgSO₄/HAP.

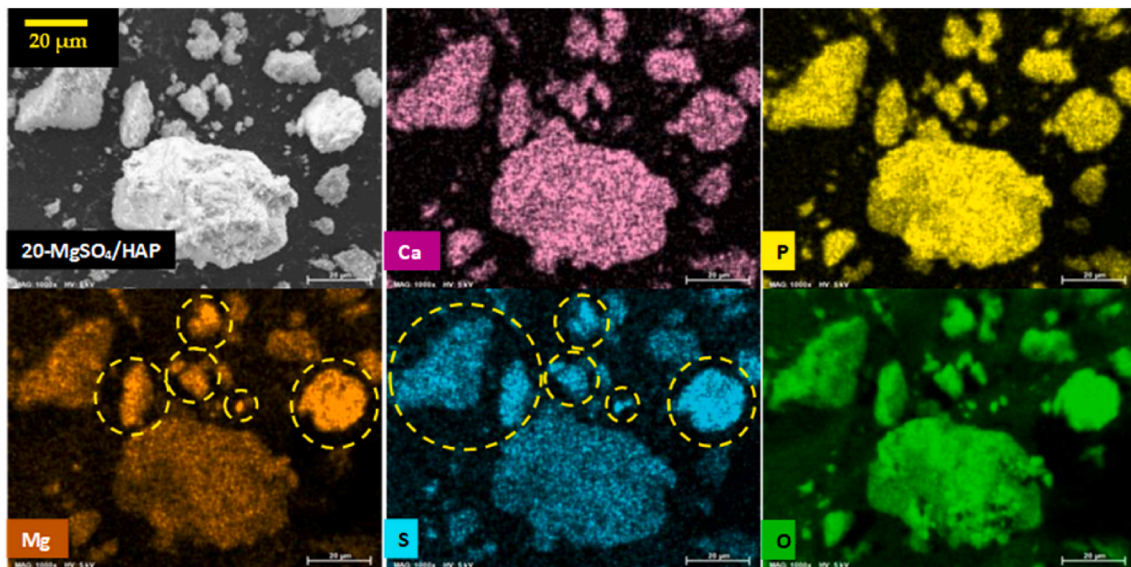


Fig. 7. EDX mapping for 20-MgSO₄/HAP.

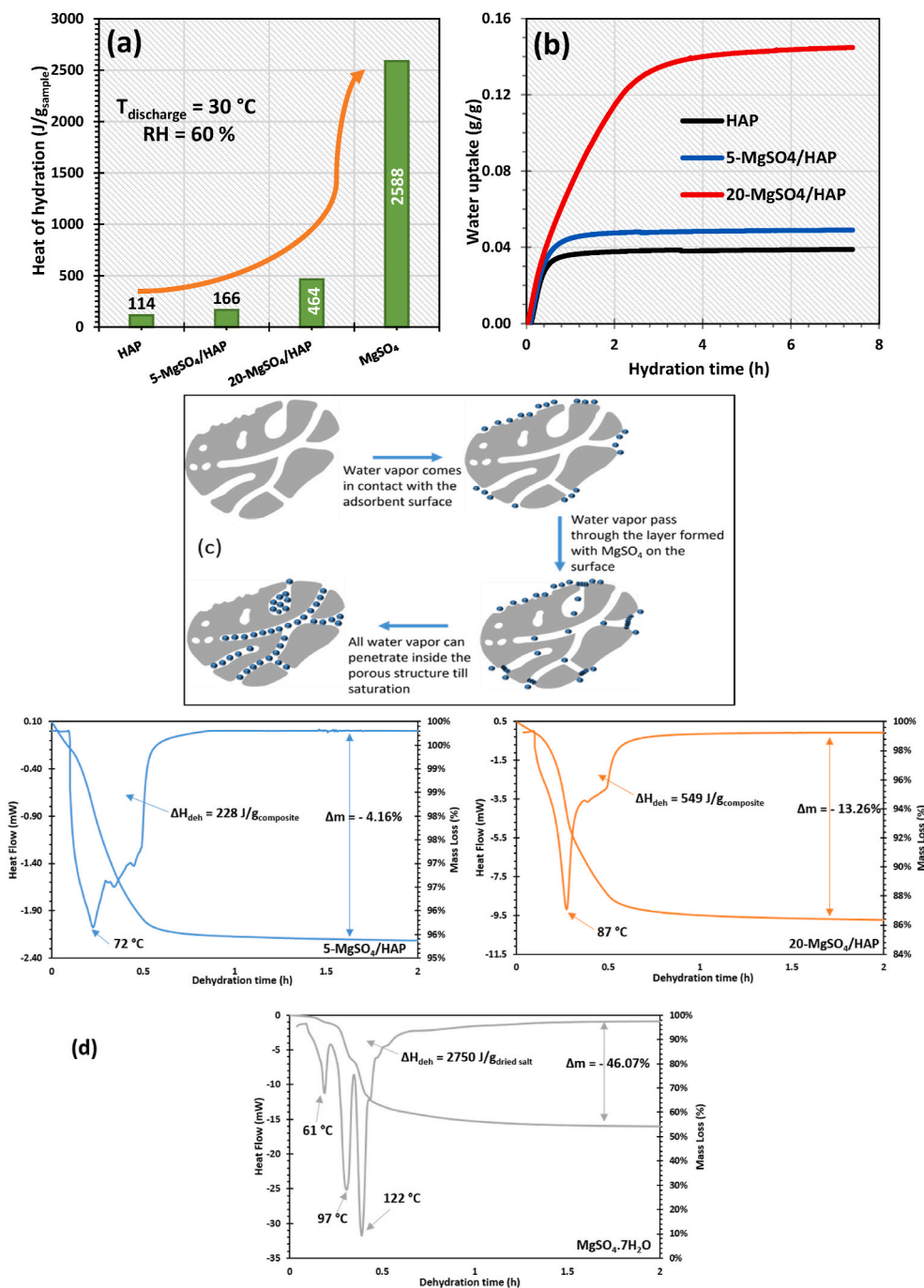


Fig. 8. a) Hydration behavior of MgSO₄ and HAP composites at 30 °C and 60%RH b) Water uptake curves of HAP support and composites ($T_{\text{discharge}} = 30\text{ }^{\circ}\text{C}$; $\text{RH} = 60\%$; 24 h of hydration c) Water adsorption mechanism on the storage material and d) Dehydration behaviour of MgSO₄ and HAP composites from 30 to 150 °C under dried air.

25 °C the sample showed high crystallinity. Then the degree of crystallinity gradually decreased increasing the temperature at 44 °C and 55 °C. Finally, the diffractogram shows no crystallinity between 80 and 150 °C. Furthermore, the dehydration was incomplete at this point, leading to the fact that there are amorphous hydrated phases present. This could be related to the blocking of the pores which hinders the initial dehydration (after impregnation) of the hydrated salt confined in the porous structure [37]. Another suggestion is that the MgSO₄ crystallites could be smaller than the detection limit of the XRD spectrometer and so, no well-defined peaks are observed on the XRD patterns.

In order to investigate the morphology and the salt deposition homogeneity, SEM analyses were performed. Based on Fig. 5 (a and b),

different particle sizes with different morphologies have been observed for the both HAP composites. For more insight, the EDX mapping (Fig. 6) have been performed in order to have an idea about the possible distribution of the salt on the HAP surface. As seen in Fig. 6, the elements Mg and S were homogeneously distributed on the surface of the 5-MgSO₄/HAP. However, for the 20-MgSO₄/HAP sample (Fig. 7), the distribution of Mg and S elements on the surface was still homogenous on most of the HAP grains, some particles (highlighted by yellow dotted circles) presented a higher concentration of Mg and S, which relates to higher loading of MgSO₄ indicating the formation of salt aggregates on the surface of HAP. The presence of aggregates could potentially block the pore network, thus reducing the reaction surface between water

Table 2
Experimental results and calculated values of MgSO₄, HAP and its composites.

Sample	Heat released (J/g _{sample})	Heat released calculated (J/g _{sample}) ^b	Water adsorption (g/g)	Water adsorption calculated (g/g) ^b
MgSO ₄ ^a	2588	–	0.809	–
HAP	114	–	0.039	–
5-MgSO ₄ /HAP	166	216	0.049	0.071
20-MgSO ₄ /HAP	464	541	0.155	0.172

^a Determined experimentally by TG-DSC/Wetsys.

^b Calculated by addition of the heat contribution of MgSO₄ salt and HAP support in each sample.

Table 3
Performance comparison of 20-MgSO₄/HAP and other sulfate-supported composites.

Material components	Operating conditions	Energy storage density (J/g)	Reference	Year
20-MgSO ₄ /HAP	T _{hyd} = 30 °C; RH = 60%	464	This paper	
30-MgSO ₄ /Diatomite (D30)	T _{hyd} = 25 °C; RH = 80%	460 773	[60]	2021
60-MgSO ₄ /Diatomite (D60)				
50-MgSO ₄ /Expanded graphite (EG50)	T _{hyd} = 25 °C; RH = 85%	496.4	[61]	2021
MgSO ₄ /13x with % MgSO ₄ up to 20%	T _{hyd} = 25 °C; RH = 60%	510–575	[22]	2019
MgSO ₄ /zeolite (laboratory pilot)	T _{hyd} = 25 °C; RH = 85%	401	[4]	2018
MgSO ₄ /zeolite Modernite	T _{hyd} = 22 °C; RH = 50%	507	[62]	2013

vapor and salt.

3.2. TG-DSC analysis for hydration behaviors

The hydration heat released and water sorption capacities of the HAP support and its composites were measured respectively by TG-DSC under controlled RH, regulated by a Wetsys apparatus. From the variation of the heat flow and the mass of the sample as a function of time, the heat released upon hydration (Fig. 8a) and the water adsorption capacity (defined as “w_e” in Equation (1)) (Fig. 8b) were deduced. The amount of heat produced and water uptake in both prepared composites increased as the salt concentration in the composites increased. This is probably due to the fact that, the more salt was dispersed onto the porous structure, the more active sites were generated for the exothermic reaction between salt particles and water vapor. The hydration behavior of MgSO₄ was also experimented with the same temperature profile.

$$w_e = \frac{m_h - m_d}{m_d} \tag{1}$$

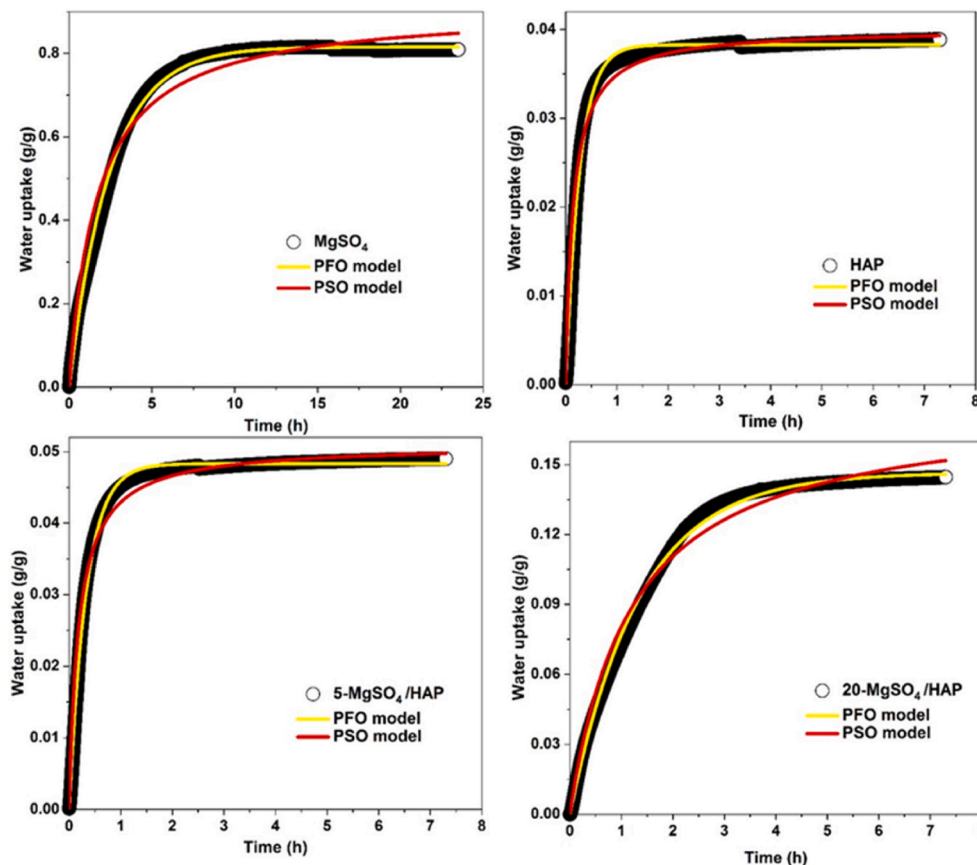


Fig. 9. Adsorption kinetics fitting results of MgSO₄, HAP support and two composites with 5% and 20% salt content. (Hydration temperature: 30 °C; RH: 60%; sample mass: ~10 mg; MgSO₄ density: 2.66 g/cm³; HAP density: 3.16 g/cm³; 20-MgSO₄/HAP density: 3.07 g/cm³; 5-MgSO₄/HAP density: 3.14 g/cm³).

Table 4
Non-linear kinetic adsorption models.

Kinetic model	Equation	Description of parameters	Ref.
Pseudo First Order (PFO)	$w_t = w_e [1 - \exp(-K_1 t)]$	w_t is the water uptake at time t (g/g), w_e : the water uptake at equilibrium (g/g), t is the hydration time (h), K_1 and K_2 are respectively the rate constant of the PFO and PSO models (s^{-1}).	[63–65]
Pseudo Second Order (PSO)	$w_t = \frac{w_e^2 K_2 t}{1 + w_e K_2 t}$	w_t is the water uptake at time t (g/g), w_e : the water uptake at equilibrium (g/g), t is the hydration time (h), K_1 and K_2 are respectively the rate constant of the PFO and PSO models (s^{-1}).	[63–65]
Elovich	$w_t = \frac{1}{\beta} \ln(\alpha\beta) + \frac{1}{\beta} \ln(t)$	α is the initial adsorption rate (mg/g min), and β is the extent of the surface coverage and activation energy of the process	[65,66]
Vermeulen	$w_t = w_e \sqrt{1 - \exp\left(-\frac{4\pi^2 D_v t}{d_p^2}\right)}$	D_v is the diffusion coefficient; d_p is the particle radius	[67,68]
Unipore	$K_v = \frac{4\pi^2 D_v}{d_p^2}$ $w_t = w_e \times 6 \left(\frac{D_e \times t}{\pi}\right)^{0.5}$	D_e is the diffusion coefficient	[69]

where w_e is the water adsorption capacity (g_{H_2O}/g_{sample} or g/g in short), m_h (g) and m_d (g) correspond respectively to the final mass of the hydrated sample and the dehydrated sample. For $MgSO_4$, the water uptake is expressed as g_{H_2O}/g of dehydrated salt and for the composite is expressed as g_{H_2O}/g of dehydrated composite.

However, these values are lower than their respective calculated ones which are shown in Table 2. The calculated values are performed by simple addition of the contribution of the $MgSO_4$ salt and of the HAP support based on their respective content in the composites. This can be explained with the presence of the partially amorphous hydrated phases of $MgSO_4 \cdot yH_2O$ (absence of crystalline phase in the XRD patterns) [57, 58]. The storage density of these partially hydrated are lower compared to the anhydrous $MgSO_4$, therefore the heat released of the composite is less significant. Moreover, the bare HAP presents a very low hydration heat that did not contribute greatly to the enhancement of heat storage density. Besides that, because of the pore blocking, there could be a certain amount of salt that cannot be reached by the water vapor (Fig. 8c). Thus, the hydration energy released as well as the water uptake did not meet expectations. The performance of 20- $MgSO_4$ /HAP was also compared with other sulfate-support composites previously reported in literatures. Table 3 shows that the 20- $MgSO_4$ /HAP has good energy storage density and has a potential to be a candidate for medium and low temperature applications.

Fig. 8d shows the dehydration behavior of $MgSO_4$ and HAP composites. The $MgSO_4 \cdot 7H_2O$ decomposed at around 61 °C and produced an unstable phase that eventually decomposed to form $MgSO_4 \cdot H_2O$ with a mass loss of 46% and a dehydration enthalpy of 2.75 kJ/g_{dried salt}. The difference in the behavior of the composites can be explained by the good dispersion of the salt into the HAP pore structure. The decrease in dehydration temperature can also be due to the change in their crystallinity after impregnation into the HAP su [59]. This result confirmed that the use of HAP can be beneficial for certain applications.

3.3. Hydration kinetic modeling

Fig. 9 shows the water uptake curves for the HAP support and two prepared composites. Similarly, they all display an initial short and fast water sorption rate during the first 30 min of hydration. However, after the initial fast adsorption, the kinetic curve of the 5- $MgSO_4$ /HAP composite is similar to the curve of the support HAP which quickly reached

Table 5
The kinetic parameters obtained by different adsorption kinetic models.

	$MgSO_4$	HAP	5- $MgSO_4$ /HAP	20- $MgSO_4$ /HAP
Pseudo-First-Order (PFO)				
W_e (g/g)	0.815	0.038	0.048	0.146
K_1 ($10^{-4} s^{-1}$)	1.133	10.24	8.347	2.069
R^2	0.996	0.988	0.993	0.997
Pseudo-Second-Order (PSO)				
W_e (g/g)	0.909	0.040	0.051	0.176
K_2 ($10^{-4} s^{-1}$)	1.794	462.5	288.1	13.16
R^2	0.957	0.953	0.962	0.977

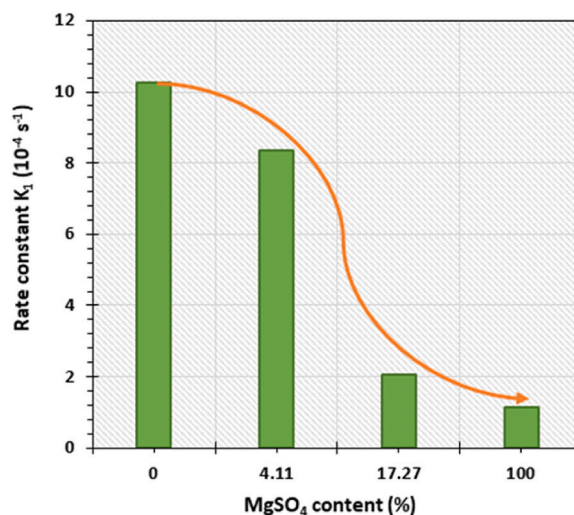


Fig. 10. Influence of the salt content on the kinetic rate constants.

the water sorption equilibrium only after 2 h of hydration. While for the 20- $MgSO_4$ /HAP composite, after the initial fast adsorption, the kinetic curve slowed down significantly and then barely reached the equilibrium after over 7 h of hydration. This behavior is shown to be strongly impacted by the amount of salt deposited. When more salt was deposited, water vapor diffusion could become problematic as it takes more time for water vapor to reach entirely salt particles.

To investigate the kinetics of water uptake, several kinetic models were tested (Table 4). Among all of these kinetic equation models, six kinetic models showed a poor fitting based on the correlation coefficient R^2 : Elovich model (0.70–0.94), Vermeulen model (0.95–0.97) and Unipore model (0.17–0.78). With the exception of the pseudo-first order (PFO) and pseudo-second order (PSO), which are two well-known kinetic models [63–65]. The fitting results are reported in Fig. 9 and the obtained kinetic parameters are listed in Table 5.

It can be seen from Fig. 9 that the PFO model described better the adsorption processes of all samples than the PSO model (with R^2 coefficients of around 0.99). From the kinetic rate constant K_1 obtained from the PFO model, the hydration kinetics can be classified as following order (from fastest to slowest): HAP > 5- $MgSO_4$ /HAP > 20- $MgSO_4$ /HAP > $MgSO_4$. The $MgSO_4$ presents a slow kinetic compared to others materials (Fig. 9). The salt required 15 h to attain a stable hydration state, which is twice the rate of the 20- $MgSO_4$ /HAP composite. This well-known slow hydration kinetic of the $MgSO_4$ was already investigated. According to Linnow et al. [15], when exposed to humid air, a thin layer of hydrated salt forms quickly on the support surface, restricting water vapor diffusion and thereby slowing the reaction rate. The HAP rt presents a fastest kinetic which is probably due to the fast physical adsorption process during hydration. The impregnation of $MgSO_4$ has then a significant impact on this speed. In the case of the 5- $MgSO_4$ /HAP composite, the kinetic was slightly impacted when the salt was integrated in the HAP porous structure. However, when the surface coverage

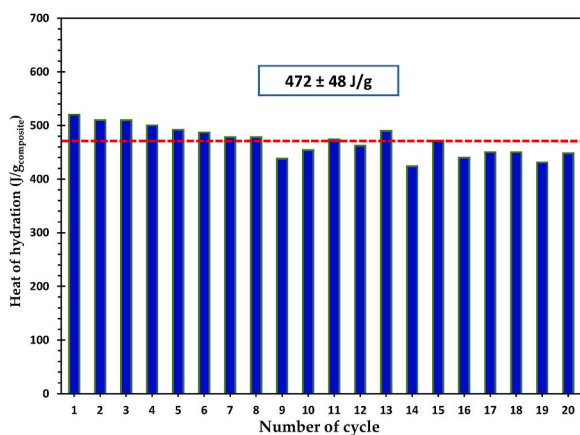


Fig. 11. Evaluation of 20-MgSO₄/HAP composite stability for 20 cycles of hydration/dehydration.

of the salt was extended, as in the case of the 20-MgSO₄/HAP composite, the hydration kinetic significantly slows down (rate constant K₁ 4 times lower) (Fig. 10). As aforementioned, these behaviors are related to the difficulty of water vapor to diffuse inside the material pore network, in

particular composites with higher salt content. Another result is that the slow kinetic of MgSO₄ was greatly improved as it was dispersed in the porous matrix HAP (the kinetic rate constant of the composites are higher than MgSO₄). This latter could have a remarkable value in residential applications, because it will reduce considerably the hydration time and thus improve the operating flexibility of the overall storage system.

3.4. Cyclability and stability

To evaluate the cyclability and stability of the 20-MgSO₄/HAP composite, the sample has been exposed to a short-cycle hydration/dehydration treatment consisting of 20 cycles between temperatures of 150 °C (Dehydration) and 30 °C (Hydration, at a relative humidity of 60%). In the following step, the heat released for each cycle has been determined as a first benchmark. As it can be seen in Fig. 11, there is only a small fluctuations of heat released between each cycle, which confirms the good stability with an average ESD of 472 J/g.

Fig. 12 shows the TGA signals during hydration and dehydration of 5 different cycles in the cyclability test (1st, 5th, 10th, 17th, 20th). During the hydration reactions, a degradation in water uptake during the first 10 cycles is noted, from 0.188 g/g in the first hydration but down to 0.157 g/g after the 10th hydration. From this point onwards, the water

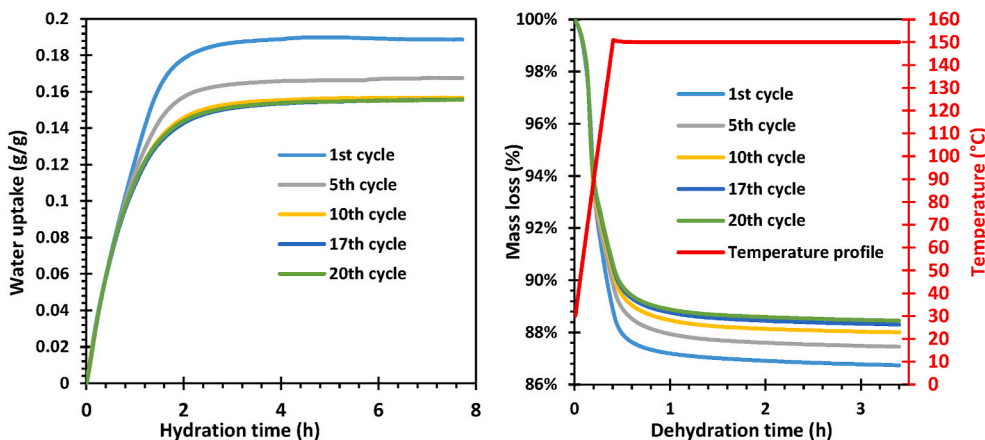


Fig. 12. TGA curves of 5 different cycles during the cyclability experiment (1st, 5th, 10th, 17th, 20th).

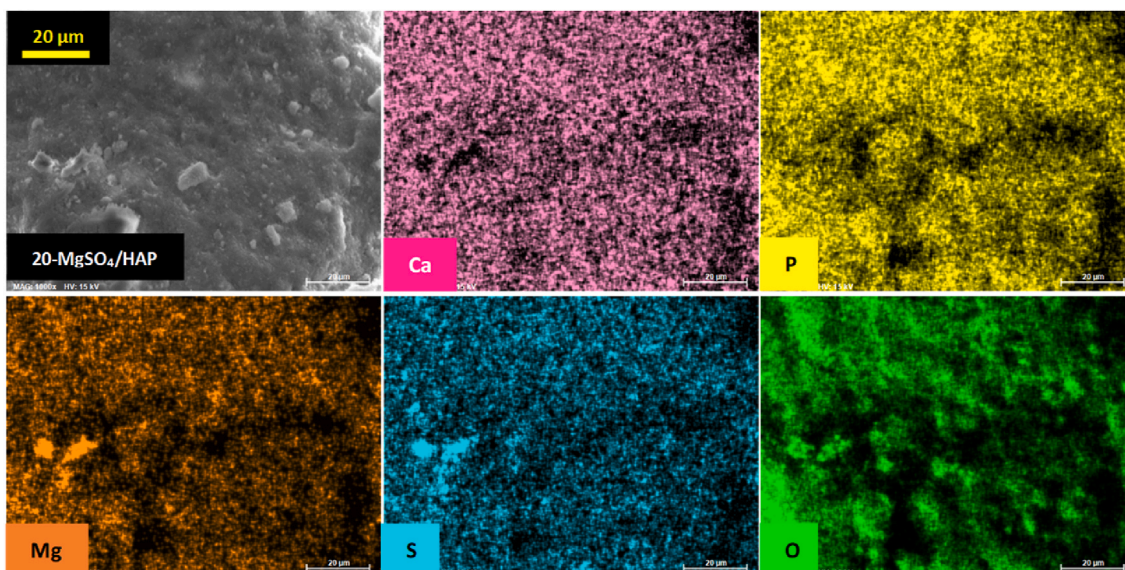


Fig. 13. EDX mapping for 20-MgSO₄/HAP after 20 cycles.

adsorption capacity is stabilized at 0.157 g/g (83.5% compared to 0.188 g/g) until the 20th hydration. The hydration kinetic rate is also reported to be stable at around $1.2 \cdot 10^{-4} \text{ s}^{-1}$ during the cycling experiment.

In terms of dehydration reactions, a loss of 13.26% in mass is recorded in the first dehydration. Over cycling, the dehydration becomes less and less effective, but not significantly since during the last dehydration, a loss of 11.55% (about 87.1% compared to 13.26%) in mass is reported.

The SEM and EDX mapping (Fig. 13) of sample after 20 cycles have been done to verify if there are any changes in term of salts distribution, agglomeration and so on. The results showed that there is no significance difference before and after cycling experiment, which confirm also the morphological stability of the composites. Consequently, these composites can be a base for the development of potential material for TCHS application based on HAP. A research regarding the development of new composites on other HAP types with the objective to enhance the water uptake and increase the amount of deposited salt in order to improve the thermal storage capacity is ongoing.

4. Conclusions

Wide pore hydroxyapatite composite materials impregnated with different amounts of MgSO_4 , as prospective thermochemical seasonal heat storage materials, have been studied using the TG-DSC apparatus. Despite the fact that magnesium sulfate was unable to fully exploit its sorption capacities, a composite containing 20% MgSO_4 produced the maximum heat (464 J/g) as compared to HAP impregnated with 5% MgSO_4 (166 J/g). The excellent dispersion of MgSO_4 increases the storing capability of composite materials. High heat and water storage capabilities are not the only factors to consider when selecting a storage material in thermochemical heat storage systems. A rapid water sorption kinetics is also necessary for the system's usability. Good fitting of the kinetic experimental data with the model equation has been successfully performed, allowing us to determine the rate controlling adsorption mechanism, which is an important factor in thermochemical heat storage system design. The repeated stability of MgSO_4 -HAP is evaluated, revealing that this two-component sorbent is relatively well constant after 20 dehydration/hydration cycles. In perspective, these promising results open the way to the optimization of a new thermochemical heat storage composite materials' family based on HAP. New HAP compositions and morphology can be then studied in order to improve the salt dispersion and the water mass transfer.

Funding

- Region Grand Est for providing funding for the acquisition of the TG-DSC equipment within the "STOCKFATAL" project and for the contribution to Mr. Minh Hoang Nguyen's thesis grant.

- Carnot MICA for funding part of this study in the frame of the STOCKENER project.

- IS2M for the postdoctoral grant of M. Zbair in the frame of the "Projets Structurants" call.

Institutional review board statement

Not applicable.

Informed consent statement

Not applicable.

Data availability statement

Not applicable.

CRedit authorship contribution statement

Minh Hoang Nguyen: Investigation, Writing – original draft, Visualization, Formal analysis, Data curation. **Mohamed Zbair:** Visualization, Data curation, Writing – original draft, Writing – review & editing. **Patrick Dutournié:** Writing – review & editing, Supervision, Methodology. **Antonella Gervasini:** Investigation, Writing – original draft. **Cyril Vaultot:** Investigation. **Simona Bennici:** Project administration, Validation, Methodology, Resources, Supervision, Conceptualization, Funding acquisition.

Declaration of competing interest

The authors declare that they have no known competing financial interests or personal relationships that could have appeared to influence the work reported in this paper.

Acknowledgments

The authors would like to thank the Carnot Institute MICA (France) for supporting a part of this study within the STOCKENER; Region Grand Est (France) for providing funding for the acquisition of the TG-DSC equipment, in the frame of STOCKFATAL project, and financing a part of the PhD-grant of Mr. Minh Hoang Nguyen.

All physicochemical characterizations were performed on the IS2M technical platforms. The authors are very grateful to L. Michelin (XRF) and L. Josien (SEM + EDX) for their contribution.

Nomenclature

TES	thermal energy system
TCHS	thermochemical heat storage
HAP	hydroxyapatite;
IWI	Incipient Wetness Impregnation
XRD	X-ray Diffraction
WDXRF	wavelength-dispersive X-Ray Fluorescence
SEM	Scanning Electron Microscope
EDX	Energy Dispersive X-ray
BET	Brunauer, Emmett and Teller
PSD	pore size distribution
BJH	Barrett, Joyner and Halenda
TG	thermogravimetry
DSC	Differential Scanning Calorimetry
RH	relative humidity
PFO	pseudo-first order
PSO	pseudo-second order

References

- [1] F.J. Barba, M. Gavahian, I. Es, Z. Zhu, F. Chemat, J.M. Lorenzo, A. Mousavi Khaneghah, Solar radiation as a prospective energy source for green and economic processes in the food industry: from waste biomass valorization to dehydration, cooking, and baking, *J. Clean. Prod.* 220 (2019) 1121–1130, <https://doi.org/10.1016/j.jclepro.2019.02.175>.
- [2] A.V. da Rosa, J.C. Ordóñez, Storage of energy, in: *Fundam. Renew. Energy Process*, Elsevier, 2022, pp. 855–896, <https://doi.org/10.1016/B978-0-12-816036-7.00031-2>.
- [3] G. Airò Farulla, M. Cellura, F. Guarino, M. Ferraro, A review of thermochemical energy storage systems for power grid support, *Appl. Sci.* 10 (2020) 3142, <https://doi.org/10.3390/app10093142>.
- [4] C. Xu, Z. Yu, Y. Xie, Y. Ren, F. Ye, X. Ju, Study of the hydration behavior of zeolite- MgSO_4 composites for long-term heat storage, *Appl. Therm. Eng.* 129 (2018) 250–259, <https://doi.org/10.1016/j.applthermaleng.2017.10.031>.
- [5] A comprehensive review of thermal energy storage, *Sustainability* 10 (2018) 191, <https://doi.org/10.3390/su10010191>.
- [6] W. Li, M. Zeng, Q. Wang, Development and performance investigation of $\text{MgSO}_4/\text{SrCl}_2$ composite salt hydrate for mid-low temperature thermochemical heat storage, *Sol. Energy Mater. Sol. Cells* 210 (2020) 110509, <https://doi.org/10.1016/j.solmat.2020.110509>.
- [7] G.T. Whiting, D. Grondin, D. Stosic, S. Bennici, A. Auroux, Zeolite- MgCl_2 composites as potential long-term heat storage materials: influence of zeolite

- properties on heats of water sorption, *Sol. Energy Mater. Sol. Cells* 128 (2014) 289–295, <https://doi.org/10.1016/j.solmat.2014.05.016>.
- [8] H. Wu, F. Salles, J. Zajac, A critical review of solid materials for low-temperature thermochemical storage of solar energy based on solid-vapour adsorption in view of space heating uses, *Molecules* 24 (2019) 945, <https://doi.org/10.3390/molecules24050945>.
- [9] P. Tatsidjodoung, N. Le Pierrès, L. Luo, A review of potential materials for thermal energy storage in building applications, *Renew. Sustain. Energy Rev.* 18 (2013) 327–349, <https://doi.org/10.1016/j.rser.2012.10.025>.
- [10] L.G. Gordeeva, Y.D. Tu, Q. Pan, M.L. Palash, B.B. Saha, Y.I. Aristov, R.Z. Wang, Metal-organic frameworks for energy conversion and water harvesting: a bridge between thermal engineering and material science, *Nano Energy* 84 (2021) 105946, <https://doi.org/10.1016/j.nanoen.2021.105946>.
- [11] M. Zhair, S. Bennici, Survey summary on salts hydrates and composites used in thermochemical sorption heat storage: a review, *Energies* 14 (2021) 3105, <https://doi.org/10.3390/en14113105>.
- [12] S.Z. Xu, Lemington, R.Z. Wang, L.W. Wang, J. Zhu, A zeolite 13X/magnesium sulfate–water sorption thermal energy storage device for domestic heating, *Energy Convers. Manag.* 171 (2018) 98–109, <https://doi.org/10.1016/j.enconman.2018.05.077>.
- [13] K.E. N'Tsoukpoe, T. Schmidt, H.U. Rammelberg, B.A. Watts, W.K.L. Ruck, A systematic multi-step screening of numerous salt hydrates for low temperature thermochemical energy storage, *Appl. Energy* 124 (2014) 1–16, <https://doi.org/10.1016/j.apenergy.2014.02.053>.
- [14] H. Ait Ousaleh, S. Sair, S. Mansouri, Y. Abboud, A. Faik, A. El Bouari, New hybrid graphene/inorganic salt composites for thermochemical energy storage: synthesis, cyclability investigation and heat exchanger metal corrosion protection performance, *Sol. Energy Mater. Sol. Cells* 215 (2020) 110601, <https://doi.org/10.1016/j.solmat.2020.110601>.
- [15] K. Linnow, M. Niermann, D. Bonatz, K. Posern, M. Steiger, Experimental studies of the mechanism and kinetics of hydration reactions, *Energy Proc.* 48 (2014) 394–404, <https://doi.org/10.1016/j.egypro.2014.02.046>.
- [16] K.-D. Grevel, J. Majzlan, A. Benisek, E. Dachs, M. Steiger, A.D. Fortes, B. Marler, Experimentally determined standard thermodynamic properties of synthetic MgSO₄·4H₂O (starkeyite) and MgSO₄·3H₂O: a revised internally consistent thermodynamic data set for magnesium sulfate hydrates, *Astrobiology* 12 (2012) 1042–1054, <https://doi.org/10.1089/ast.2012.0823>.
- [17] T. Yan, T. Li, J. Xu, J. Chao, R. Wang, Y.I. Aristov, L.G. Gordeeva, P. Dutta, S. S. Murthy, Ultrahigh-energy-density sorption thermal battery enabled by graphene aerogel-based composite sorbents for thermal energy harvesting from air, *ACS Energy Lett.* 6 (2021) 1795–1802, <https://doi.org/10.1021/acsenerylett.1c00284>.
- [18] Y. Aristov, G. Restuccia, G. Cacciola, V. Parmon, A family of new working materials for solid sorption air conditioning systems, *Appl. Therm. Eng.* 22 (2002) 191–204, [https://doi.org/10.1016/S1359-4311\(01\)00072-2](https://doi.org/10.1016/S1359-4311(01)00072-2).
- [19] L. Silvester, Q. Touloumet, A. Kamaruddin, F. Chassagneux, G. Postole, A. Auroux, L. Bois, Influence of silica functionalization on water sorption and thermochemical heat storage of mesoporous SBA-15/CaCl₂ composites, *ACS Appl. Energy Mater.* 4 (2021) 5944–5956, <https://doi.org/10.1021/acsaem.1c00786>.
- [20] E. Courbon, P. D'Ans, A. Permyakova, O. Skrylnyk, N. Steunou, M. Degrez, M. Frère, A new composite sorbent based on SrBr₂ and silica gel for solar energy storage application with high energy storage density and stability, *Appl. Energy* 190 (2017) 1184–1194, <https://doi.org/10.1016/j.apenergy.2017.01.041>.
- [21] B. Ding, C. Xu, Z. Liao, F. Ye, Study on long-term thermochemical thermal storage performance based on SrBr₂-expanded vermiculite composite materials, *J. Energy Storage* 42 (2021) 103081, <https://doi.org/10.1016/j.est.2021.103081>.
- [22] Q. Wang, Y. Xie, B. Ding, G. Yu, F. Ye, C. Xu, Structure and hydration state characterizations of MgSO₄-zeolite 13x composite materials for long-term thermochemical heat storage, *Sol. Energy Mater. Sol. Cells* 200 (2019) 110047, <https://doi.org/10.1016/j.solmat.2019.110047>.
- [23] J.X. Xu, T.X. Li, J.W. Chao, T.S. Yan, R.Z. Wang, High energy-density multi-form thermochemical energy storage based on multi-step sorption processes, *Energy* 185 (2019) 1131–1142, <https://doi.org/10.1016/j.energy.2019.07.076>.
- [24] W. Shi, Y. Zhu, C. Shen, J. Shi, G. Xu, X. Xiao, R. Cao, Water sorption properties of functionalized MIL-101(Cr)-X (X=–NH₂, –SO₃H, –CH₃, –F) based composites as thermochemical heat storage materials, *Microporous Mesoporous Mater.* 285 (2019) 129–136, <https://doi.org/10.1016/j.micromeso.2019.05.003>.
- [25] A.I. Shkatulov, J. Houben, H. Fischer, H.P. Huinink, Stabilization of K₂CO₃ in vermiculite for thermochemical energy storage, *Renew. Energy* 150 (2020) 990–1000, <https://doi.org/10.1016/j.renene.2019.11.119>.
- [26] H. Ait Ousaleh, S. Sair, A. Zaki, A. Younes, A. Faik, A. El Bouari, Advanced experimental investigation of double hydrated salts and their composite for improved cycling stability and metal compatibility for long-term heat storage technologies, *Renew. Energy* 162 (2020) 447–457, <https://doi.org/10.1016/j.renene.2020.08.085>.
- [27] W. Li, J.J. Klemeš, Q. Wang, M. Zeng, Development and characteristics analysis of salt-hydrate based composite sorbent for low-grade thermochemical energy storage, *Renew. Energy* 157 (2020) 920–940, <https://doi.org/10.1016/j.renene.2020.05.062>.
- [28] T.S. Yan, T.X. Li, J.X. Xu, R.Z. Wang, Water sorption properties, diffusion and kinetics of zeolite NaX modified by ion-exchange and salt impregnation, *Int. J. Heat Mass Tran.* 139 (2019) 990–999, <https://doi.org/10.1016/j.ijheatmasstransfer.2019.05.080>.
- [29] P. D'Ans, E. Courbon, A. Permyakova, F. Nouar, C. Simonnet-Jégat, F. Bourdreux, L. Malet, C. Serre, M. Frère, N. Steunou, A new strontium bromide MOF composite with improved performance for solar energy storage application, *J. Energy Storage* 25 (2019) 100881, <https://doi.org/10.1016/j.est.2019.100881>.
- [30] D. Mahon, P. Henshall, G. Claudio, P.C. Eames, Feasibility study of MgSO₄ + zeolite based composite thermochemical energy stores charged by vacuum flat plate solar thermal collectors for seasonal thermal energy storage, *Renew. Energy* 145 (2020) 1799–1807, <https://doi.org/10.1016/j.renene.2019.05.135>.
- [31] W. Li, J.J. Klemeš, Q. Wang, M. Zeng, Salt hydrate-based gas-solid thermochemical energy storage: current progress, challenges, and perspectives, *Renew. Sustain. Energy Rev.* 154 (2022) 111846, <https://doi.org/10.1016/j.rser.2021.111846>.
- [32] J. Lin, Q. Zhao, H. Huang, H. Mao, Y. Liu, Y. Xiao, Applications of low-temperature thermochemical energy storage systems for salt hydrates based on material classification: a review, *Sol. Energy* 214 (2021) 149–178, <https://doi.org/10.1016/j.solener.2020.11.055>.
- [33] Z. Xueling, W. Feifei, Z. Qi, L. Xudong, W. Yanling, Z. Yeqiang, C. Chuanxiao, J. Tingxiang, Heat storage performance analysis of ZMS-Porous media/CaCl₂/MgSO₄ composite thermochemical heat storage materials, *Sol. Energy Mater. Sol. Cells* 230 (2021) 111246, <https://doi.org/10.1016/j.solmat.2021.111246>.
- [34] J. Jänchen, H. Stach, Adsorption properties of porous materials for solar thermal energy storage and heat pump applications, *Energy Proc.* 30 (2012) 289–293, <https://doi.org/10.1016/j.egypro.2012.11.034>.
- [35] I.V. Ponomarenko, I.S. Glaznev, A.V. Gubar, Y.I. Aristov, S.D. Kirik, Synthesis and water sorption properties of a new composite “CaCl₂ confined into SBA-15 pores, Microporous Mesoporous Mater. 129 (2010) 243–250, <https://doi.org/10.1016/j.micromeso.2009.09.023>.
- [36] E. Courbon, P. D'Ans, A. Permyakova, O. Skrylnyk, N. Steunou, M. Degrez, M. Frère, Further improvement of the synthesis of silica gel and CaCl₂ composites: enhancement of energy storage density and stability over cycles for solar heat storage coupled with space heating applications, *Sol. Energy* 157 (2017) 532–541, <https://doi.org/10.1016/j.solener.2017.08.034>.
- [37] G. Whiting, D. Grondin, S. Bennici, A. Auroux, Heats of water sorption studies on zeolite–MgSO₄ composites as potential thermochemical heat storage materials, *Sol. Energy Mater. Sol. Cells* 112 (2013) 112–119, <https://doi.org/10.1016/j.solmat.2013.01.020>.
- [38] L.G. Gordeeva, Y.I. Aristov, Composites ‘salt inside porous matrix’ for adsorption heat transformation: a current state-of-the-art and new trends, *Int. J. Low Carbon Technol.* 7 (2012) 288–302, <https://doi.org/10.1093/ijlct/cts050>.
- [39] V. Palomba, A. Sapienza, Y. Aristov, Dynamics and useful heat of the discharge stage of adsorptive cycles for long term thermal storage, *Appl. Energy* 248 (2019) 299–309, <https://doi.org/10.1016/j.apenergy.2019.04.134>.
- [40] L. Calabrese, V. Brancato, V. Palomba, A. Frazzica, L.F. Cabeza, Magnesium sulphate-silicone foam composites for thermochemical energy storage: assessment of dehydration behaviour and mechanical stability, *Sol. Energy Mater. Sol. Cells* 200 (2019) 109992, <https://doi.org/10.1016/j.solmat.2019.109992>.
- [41] A. Jabbari-Hichri, S. Bennici, A. Auroux, CaCl₂-containing composites as thermochemical heat storage materials, *Sol. Energy Mater. Sol. Cells* 172 (2017) 177–185, <https://doi.org/10.1016/j.solmat.2017.07.037>.
- [42] L.G. Gordeeva, Y.I. Aristov, Composites ‘salt inside porous matrix’ for adsorption heat transformation: a current state-of-the-art and new trends, *Int. J. Low Carbon Technol.* 7 (2012) 288–302, <https://doi.org/10.1093/ijlct/cts050>.
- [43] J.A. Lett, M. Sundareswari, K. Ravichandran, M.B. Latha, S. Sagadevan, M.R. Bin Johan, Tailoring the morphological features of sol-gel synthesized mesoporous hydroxyapatite using fatty acids as an organic modifier, *RSC Adv.* 9 (2019) 6228–6240, <https://doi.org/10.1039/C9RA00051H>.
- [44] H. Li, D. Wu, J. Wu, L.-Y. Dong, Y.-J. Zhu, X. Hu, Flexible, high-wettability and fire-resistant separators based on hydroxyapatite nanowires for advanced lithium-ion batteries, *Adv. Mater.* 29 (2017) 1703548, <https://doi.org/10.1002/adma.201703548>.
- [45] N.A. Medellin-Castillo, R. Leyva-Ramos, E. Padilla-Ortega, R.O. Perez, J.V. Flores-Cano, M.S. Berber-Mendoza, Adsorption capacity of bone char for removing fluoride from water solution. Role of hydroxyapatite content, adsorption mechanism and competing anions, *J. Ind. Eng. Chem.* 20 (2014) 4014–4021, <https://doi.org/10.1016/j.jiec.2013.12.105>.
- [46] M. Ibrahim, M. Labaki, J.-M. Giraudon, J.-F. Lamonier, Hydroxyapatite, a multifunctional material for air, water and soil pollution control: a review, *J. Hazard Mater.* 383 (2020) 121139, <https://doi.org/10.1016/j.jhazmat.2019.121139>.
- [47] A. Amedlous, O. Amadine, Y. Essamlali, H. Maati, N. Semlal, M. Zahouily, Copper loaded hydroxyapatite nanoparticles as eco-friendly fenton-like catalyst to effectively remove organic dyes, *J. Environ. Chem. Eng.* 9 (2021) 105501, <https://doi.org/10.1016/j.jece.2021.105501>.
- [48] Y. Wang, D. Liang, F. Liu, W. Zhang, X. Di, C. Wang, A polyethylene glycol/hydroxyapatite composite phase change material for thermal energy storage, *Appl. Therm. Eng.* 113 (2017) 1475–1482, <https://doi.org/10.1016/j.applthermaleng.2016.11.159>.
- [49] Y. Wu, C. Wang, J. Li, Y. Li, Porous hydroxyapatite foams: excellent carrier of hydrated salt with adjustable pores for thermal energy storage, *Ind. Eng. Chem. Res.* 60 (2021) 1259–1265, <https://doi.org/10.1021/acs.iecr.0c05480>.
- [50] S. Campisi, C. Castellano, A. Gervasini, Tailoring the structural and morphological properties of hydroxyapatite materials to enhance the capture efficiency towards copper(II) and lead(II) ions, *New J. Chem.* 42 (2018) 4520–4530, <https://doi.org/10.1039/C8NJ00468D>.
- [51] P. Munnik, P.E. de Jongh, K.P. de Jong, Recent developments in the synthesis of supported catalysts, *Chem. Rev.* 115 (2015) 6687–6718, <https://doi.org/10.1021/cr500486u>.

- [52] P.A.J. Donkers, L.C. Sögütoglu, H.P. Huinink, H.R. Fischer, O.C.G. Adan, A review of salt hydrates for seasonal heat storage in domestic applications, *Appl. Energy* 199 (2017) 45–68, <https://doi.org/10.1016/j.apenergy.2017.04.080>.
- [53] S. Bennici, T. Polimann, M. Ondarts, E. Gonze, C. Vaulot, N. Le Pierrès, Long-term impact of air pollutants on thermochemical heat storage materials, *Renew. Sustain. Energy Rev.* 117 (2020) 109473, <https://doi.org/10.1016/j.rser.2019.109473>.
- [54] F. Rouquerol, J. Rouquerol, K. Sing, Assessment of mesoporosity, in: *Adsorpt. By Powders Porous Solids*, Elsevier, 1999, pp. 191–217, <https://doi.org/10.1016/B978-012598920-6/50008-7>.
- [55] M. Thommes, K. Kaneko, A.V. Neimark, J.P. Olivier, F. Rodriguez-Reinoso, J. Rouquerol, K.S.W. Sing, Physisorption of gases, with special reference to the evaluation of surface area and pore size distribution (IUPAC Technical Report), *Pure Appl. Chem.* 87 (2015) 1051–1069, <https://doi.org/10.1515/pac-2014-1117>.
- [56] I.C. Medeiros-Costa, C. Laroche, J. Pérez-Pellitero, B. Coasne, Characterization of hierarchical zeolites: combining adsorption/intrusion, electron microscopy, diffraction and spectroscopic techniques, *Microporous Mesoporous Mater.* 287 (2019) 167–176, <https://doi.org/10.1016/j.micromeso.2019.05.057>.
- [57] V.M. van Essen, H.A. Zondag, J.C. Gores, L.P.J. Bleijendaal, M. Bakker, R. Schuitema, W.G.J. van Helden, Z. He, C.C.M. Rindt, Characterization of MgSO₄ hydrate for thermochemical seasonal heat storage, *J. Sol. Energy Eng.* 131 (2009), <https://doi.org/10.1115/1.4000275>.
- [58] D.T. Vaniman, D.L. Bish, S.J. Chipera, C.I. Fialips, J. William Carey, W.C. Feldman, Magnesium sulphate salts and the history of water on Mars, *Nature* 431 (2004) 663–665, <https://doi.org/10.1038/nature02973>.
- [59] H. Zhou, D. Zhang, Effect of graphene oxide aerogel on dehydration temperature of graphene oxide aerogel stabilized MgCl₂·6H₂O composites, *Sol. Energy* 184 (2019) 202–208, <https://doi.org/10.1016/j.solener.2019.03.076>.
- [60] Y. Zhang, Q. Miao, X. Jia, Y. Jin, Z. Li, L. Tan, Y. Ding, Diatomite-based magnesium sulfate composites for thermochemical energy storage: preparation and performance investigation, *Sol. Energy* 224 (2021) 907–915, <https://doi.org/10.1016/j.solener.2021.05.054>.
- [61] Q. Miao, Y. Zhang, X. Jia, L. Tan, Y. Ding, MgSO₄-expanded graphite composites for mass and heat transfer enhancement of thermochemical energy storage, *Sol. Energy* 220 (2021) 432–439, <https://doi.org/10.1016/j.solener.2021.03.008>.
- [62] G. Whiting, D. Grondin, S. Bennici, A. Auroux, Heats of water sorption studies on zeolite-MgSO₄ composites as potential thermochemical heat storage materials, *Sol. Energy Mater. Sol. Cells* (2013), <https://doi.org/10.1016/j.solmat.2013.01.020>.
- [63] S. Langergen, B.K. Svenska, Zur theorie der sogenannten adsorption gelöster stoffe, *Vetensk. Handl.* 24 (1898) 1–39.
- [64] G. McKay, Pseudo-second order model for sorption processes, *Process Biochem.* 34 (1999) 451.
- [65] H.N. Tran, S.J. You, A. Hosseini-Bandegharaei, H.P. Chao, Mistakes and inconsistencies regarding adsorption of contaminants from aqueous solutions: a critical review, *Water Res.* 120 (2017) 88–116, <https://doi.org/10.1016/j.watres.2017.04.014>.
- [66] I.S. Mclintock, The Elovich equation in chemisorption kinetics, *Nature* 216 (1967) 1204–1205, <https://doi.org/10.1038/2161204a0>.
- [67] M. Balsamo, F. Montagnaro, Fractal-like vermeulen kinetic equation for the description of diffusion-controlled adsorption dynamics, *J. Phys. Chem. C* 119 (2015) 8781–8785, <https://doi.org/10.1021/acs.jpcc.5b01783>.
- [68] T. Vermeulen, Theory for irreversible and constant-pattern solid diffusion, *Ind. Eng. Chem.* 45 (1953) 1664–1670, <https://doi.org/10.1021/ie50524a025>.
- [69] A. Davarpanah, B. Mirshekari, Experimental investigation and mathematical modeling of gas diffusivity by carbon dioxide and methane kinetic adsorption, *Ind. Eng. Chem. Res.* 58 (2019) 12392–12400, <https://doi.org/10.1021/acs.iecr.9b01920>.

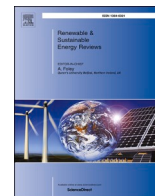
Chapter V

Heat storage: Hydration investigation of MgSO₄/active carbon composites, from material development to domestic applications scenarios

Renewable and Sustainable Energy Reviews 158, 112197 (2022)

Résumé

Le but de ce chapitre est de préparer une série de composites en utilisant un support carboné et mésoporeux : il s'agit d'un granulé de carbone activé commercial (L27W de Norit N.V, Pays Bas). La série de composites a été préparée avec des teneurs en sel variant entre 5 et 50 % en masse. Les observations par microscopie MEB montrent que le sel est déposé de façon très homogène sur la surface du carbone activé, même pour des teneurs en sel élevées (i.e. jusqu'à 40 % en masse). A partir de 50 % en masse de sel déposé, la dispersion est moins homogène et la présence d'agrégats de sel a été mise en évidence. La surface spécifique diminue progressivement en augmentant la quantité de sel déposée, mais la distribution poreuse reste inchangée. Ce comportement suggère que le sel est rentré dans les pores en diminuant l'espace disponible à l'adsorption des molécules d'azote. Le composite avec une teneur en sel de 30 % en masse a donné les meilleurs résultats en termes de capacité de stockage (1.3 kJ/g de composite, pour une capacité d'adsorption d'eau de plus de 50 % en masse). Une bonne cyclabilité a également été démontrée pendant 8 cycles de sorption/désorption. Les propriétés améliorées des composites préparés à partir du carbone activé commercial rendent possible une application pratique. Pour cela, des scénarios ont été définis à partir de données expérimentales prometteuses, pour l'utilisation de ce composite dans des applications de chauffage domestique d'une habitation et de production d'eau chaude sanitaire.



Heat storage: Hydration investigation of MgSO₄/active carbon composites, from material development to domestic applications scenarios

Simona Bennici^{a,b,*}, Patrick Dutournié^{a,b}, Jérémy Cathalan^{a,b}, Mohamed Zbair^{a,b},
Minh Hoang Nguyen^{a,b}, Elliot Scuiller^{a,b}, Cyril Vaultot^{a,b}

^a Université de Haute-alsace, CNRS, IS2M UMR 7361, 68100, Mulhouse, France

^b Université de Strasbourg, France

ARTICLE INFO

Keywords:

Thermochemical storage
Solar energy
Magnesium sulfate
Activated carbon
Salts hydrates

ABSTRACT

The scarcity of durable and low-cost sorbent materials remains a significant technological barrier to long-term heat storage. In the present work, composite materials based on activated carbon supports and magnesium sulfate hydrates (labelled MgSO₄/AC) were developed in order to increase the energy density and improve mass and heat transport phenomena. The results of composite characterization revealed uniform dispersion of magnesium sulfate in composites produced via incipient wetness impregnation. The hydration enthalpy increased as the MgSO₄ content on AC increased, reaching a plateau for MgSO₄ content of more than 30%wt (30-MgSO₄/AC and 40-MgSO₄/AC samples). The hydration experiment performed on the 30-MgSO₄/AC sample at RH = 60% verified the relation between the salt hydration level and the hydration enthalpy. Higher water partial pressure enhanced water molecule transport and improved salt hydration. The hydration enthalpy of 30-MgSO₄/AC showed an increase from 859 J/g_{dry} material at RH = 30% to 1324 J/g_{dry} material at RH = 60%. After 8 cycles of hydration/dehydration, the 30-MgSO₄/AC sample was practically stable. Furthermore, the 30-MgSO₄/AC composite was modeled in two distinct scenarios for house heating and sanitary hot water generation. Finally, the experimentally obtained calorimetric data were used to implement a numerical model. Two different scenarios were considered, the first for heating a house and the second for producing hot sanitary water. Both scenarios show the possibility of using the MgSO₄/AC composite in a multifunction thermochemical heat storage system.

1. Introduction

Fuel consumption will almost certainly double by 2050, owing to continuous increases in global technology progress [1]. The average use of energy, especially fossil fuels, has increased dramatically as countries are becoming more industrialized and people's standards of living have increased [2,3]. While uncontrolled utilization depletes fossil fuel reserves, it also causes environmental issues such as pollution, greenhouse gas emissions (mainly CO₂), and global warming. Kelvin et al. [4] reported that the anthropogenic emission of CO₂ has been the major source of CO₂ emissions into the atmosphere, with fossil fuel combustion engines (392 Mt) and coal-fired power plants (279 Mt) as the major

contributors.

Global CO₂ emissions have been increasing on average in recent years, with CO₂ emissions 1.9% higher in 2019 than in 2018 [4,5]. According to Janssens-Maenhout et al. [6], total global greenhouse gas (GHG) emissions (excluding land-use change) increased by 2% in 2018, equivalent to 51.8 Gt of CO₂ with an annual growth rate of 1.3%. Global greenhouse gas emissions in 2018 amounted to 55.6 Gt CO₂ including those for land-use change. This increase occurred as global economic growth in 2018 increased to an average annual rate of 3.5%, the highest since 2012 [7].

Current emissions of greenhouse gases that exclude those from land-use change today are approximately 57% higher than in 1990 and 43%

Abbreviations: TES, thermal energy system; AC, activated carbon; RH, relative humidity; IWI, Incipient Wetness Impregnation; XRD, X-ray Diffraction; XRF, X-Ray Fluorescence; SEM, Scanning Electron Microscope; EDX, Energy Dispersive X-ray; TGA, Thermogravimetric Analyses; DSC, Differential Scanning Calorimetry; BET, Brunauer, Emmett and Teller; DFT, Density Functional Theory; S.A., Surface Area; V_p, pore volume; V_{micro}, micropore volume; ΔH, enthalpy; C_p, specific heat; α, thermal diffusivity; λ, thermal conductivity; ρ, mass volume.

* Corresponding author. Université de Haute-alsace, CNRS, IS2M UMR 7361, 68100, Mulhouse, France.

E-mail address: simona.bennici@uha.fr (S. Bennici).

<https://doi.org/10.1016/j.rser.2022.112197>

Received 23 May 2020; Received in revised form 25 November 2021; Accepted 23 January 2022

Available online 29 January 2022

1364-0321/© 2022 Elsevier Ltd. All rights reserved.

in 2000. CO₂ levels are now alarming and indicate the need to take immediate action to prevent serious repercussions from climate change [8]. While, during the Paris Climate Conference (COP21), 195 countries decided to prevent a global temperature upsurge of less than 2 °C, it is now fairly common knowledge that CO₂ emissions are predicted to increase by over 40% in 2040 compared with those of 2010, all due to the increase in energy demand. Hence, finding a renewable and clean fuel source is thus one of the most cost-effective options [2,9].

One of the Paris Agreement's goals is to completely switch away from fossil fuels and toward renewable energy sources. However, the world's renewable energy potential has yet to be completely realized; only 23% of these energy sources have been used [10]. This opens up a lot of opportunities for strengthening and innovating clean energy policies. According to the U.S. Energy Information Administration's Annual Energy Outlook (AEO) report, renewable energy sources such as solar, wind, and geothermal will account for 20% of total energy generation by the end of 2020. The main issue with solar and wind energy is their intermittent nature and inability to provide electricity 24 h a day. As a result, renewable energy storage technologies (REST) that enable a stable energy supply chain are critical.

Thermal heat storage systems for residential applications are currently the focus of much research in order to extend the use of renewable energy resources [11–13]. They help in overcoming the mismatch between the heat source's availability (solar heat, waste heat) and the building's heat requirements [14–16]. The most promising choice among thermal energy storage technologies is thermochemical heat storage, which has the highest energy storage densities and hence the best compactness of the storage system [17]. Due to a lack of available space, this criterion is critical for a residential house [18–20].

The development of new materials and their subsequent application depends on a fundamental understanding of their molecular structure, relating the structure to material properties and performance [21–26].

One of the main challenges is to develop new thermochemical materials with high energy storage densities [27,28]. The material used for storage is critical. To optimize its performance, its sorption characteristics must precisely match the system's cycle working conditions [29]. Many attempts are being made to produce novel energy storage materials with particular features such as high energy storage density, good multi-cycle stability, non-toxicity, and cost-effectiveness [30,31]. Thermochemical heat storage uses a reversible sorption process. Hygroscopic inorganic salts, sorbents, or composite materials can all be used as storage materials. Silica gels [32,33], (AIPOs and SAPOs) [34], activated carbon [35], Metal Organic Frameworks (MOF) materials [36–38], and zeolites [39–41] are the most often used sorbents. Composite materials (hygroscopic salt integrated into the pores of a host matrix) provide interesting characteristics for thermal energy storage applications, with a behavior that falls between inorganic salts and porous host materials. The best feature of these materials is that the matrix reduces the issues associated with salts deliquescence, such as agglomeration, free-flowing, and corrosion [42–44], which can occur when employing pure salts. In composite materials, heat and mass transfers are also improved [45].

A number of salt/matrix combinations have been investigated in the literature. As porous host matrix, sorbents such as zeolites [40,41,46], silica gels [47–49], activated carbons [50], MOF [36,51,52], carbon nanotubes [53], or vermiculite [54] have been investigated. MgSO₄ [41, 55], CaCl₂ [56–58], LiBr [50,53,59], and LiCl [60,61] are the most commonly examined inorganic salts.

For example, zeolites are porous materials with a high water affinity, allowing water molecules to be adsorbed on their large internal and external surfaces. Despite having a high energy storage capacity (for 13X zeolite, equivalent to 131 kWh/m³ [62]), zeolites have a poor thermal conductivity (for 13X zeolite: $\lambda = 0.15$ W/(m K)) [63], which may be an issue in some applications (i.e. closed systems requiring heat exchangers). As demonstrated by A. Frazzica [44], most zeolites have a charging temperature (dehydration temperature) greater than 150 °C,

which might limit their usage in the presence of low temperature heat sources. However, some hygroscopic salts have greater nominal energy storage capacity than zeolites (for example, SrCl₂, 667 kWh/m³; CaCl₂, 583 kWh/m³; MgSO₄, 583 kWh/m³; MgCl₂, 555 kWh/m³; and Al₂(SO₄)₃, 444 kWh/m³ [64]). Unfortunately, heat and mass transfer issues are frequently observed in these materials. Their poor thermal conductivity and the formation of crusts upon hydration often enable the water molecules diffusion into the solid [65,66].

To fully use the great potential of salt hydrates, mass and heat transfer must be enhanced. An option is then to prepare composite materials, where the salt hydrates are deposited on a porous support. A suitable thermochemical heat storage composite must be capable of being cycled multiple times (many consecutive hydration/dehydration cycles).

The possibility to maintain the heat storage density upon cycling is linked to the possibility to completely rehydrate the salt. It must then be well dispersed and anchored to the support, without the formation of crusts and/or structural changes [67]. The deposition technique is therefore critical to avoid salt aggregation and the obstruction of the support's pores [64]. In certain cases, the salts were deposited on zeolites, which had previously been studied [68]. These investigations revealed that the type of porosity (micro/meso) is an important parameter in composite design. If the pores are too small, the salt might block their entrance, preventing water molecules from diffusing and limiting energy storage capacity. Other materials, such as mesoporous activated carbon or silica-gels, have been demonstrated to be extremely promising supports. The salt may be introduced into their wide pores, enhancing their energy storage capacity and avoiding pore blockage [45,69]. Besides the high surface area and the presence of mesoporosity, another important criterion in the choice of the most suitable support is good thermal conductivity. This parameter is crucial for the optimization of the heat transport phenomena. The thermal conductivity of various potential supports is depicted in Fig. 1. Fig. 1 depicts the thermal conductivity of several potential supports [70,71]. The conductivity measurements showed that activated carbon has a higher conductivity than the other sorbents, reaching 0.75 W/(m·K). It is worth noticing that the highest values reported in Fig. 1 represent the intrinsic thermal conductivity of the various materials, and that the thermal conductivity of shaped materials (pellets, spheres, etc.), generally used in real applications, is much lower due to the presence of air between the particles. In any case, selecting a material with a relatively high intrinsic thermal conductivity will reasonably permit to improving that of the final heat storage material once shaped.

Moreover, the use of activated carbon (AC) in a sorption heat storage offers considerable potential in many respects. On the one hand, the production of AC from fossil coal or biomass is potentially more cost-effective than for the previously predominant material classes like silica gel and zeolite due to the simple production steps. Material costs are significantly more relevant in seasonal heat storage applications than in heat pump applications, especially with a limited number of loading and unloading cycles throughout the system's projected service life. Furthermore, ACs have large porosities and internal surface areas, and their hydrophilicity may be adjusted by the choice of starting material and pyrolysis conditions. Furthermore, chemical modifications are possible because of AC's versatile internal surface.

To select the best salt for the TES system, the salt must be inexpensive, safe for human health and the environment, thermally stable in the temperature range where it will be used, and, of course, have a high heat storage density (comparison in Table 1). To expand the applications panel, the relative humidity of deliquescence (RHD) of the salt is an important parameter to consider. The RHD is the humidity limit at which the salt will dissolve in the adsorbed water in relation to temperature, the phenomenon of absorption into the material then occurring. Exceeding this limit allows more water to be absorbed and thus increases the amount of heat provided by the reaction. However, the formation of saline solution can cause corrosion problems and can

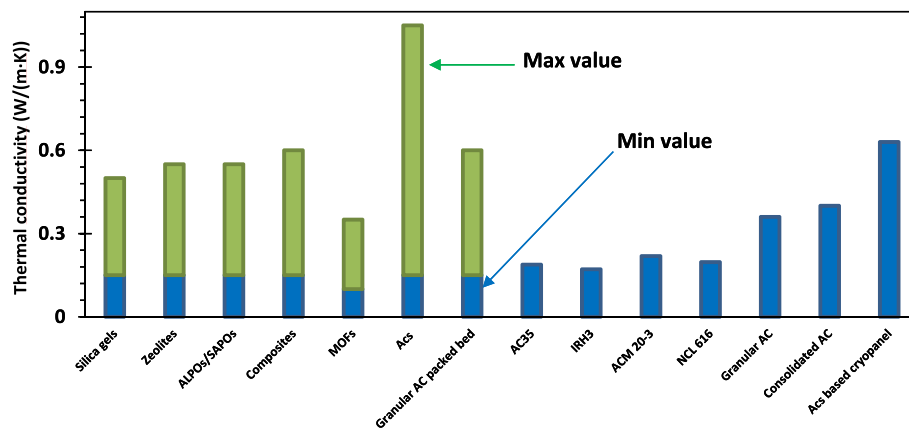


Fig. 1. Intrinsic thermal conductivity of different materials [70–76].

Table 1

Heat storage density of different composites and salt hydrates at different operating conditions.

Matrixes	Salts	Salt (wt.%)	Preparation method	Experimental Conditions	Storage density	Ref.
Vermiculite	CaCl ₂	24	Wet impregnation	25–150 °C	364.3 J/g	[77]
Vermiculite	MgSO ₄	24	Wet impregnation	25–150 °C	406.5 J/g	[77]
Vermiculite	Ca(NO ₃) ₂	24	Wet impregnation	25–150 °C	215.6 J/g	[77]
Vermiculite	Li(NO ₃) ₂	24	Wet impregnation	25–150 °C	286.9 J/g	[77]
Vermiculite	LiBr	24	Wet impregnation	25–150 °C	268.9 J/g	[77]
Activated carbon	CaCl ₂	24	Wet impregnation	25–150 °C	305.1 J/g	[77]
Silica gel	CaCl ₂	24	Wet impregnation	25–150 °C	123.3 J/g	[77]
Zeolite 13X	CaCl ₂	24	Wet impregnation	25–150 °C	168.1 J/g	[77]
Expanded clay or NZ pumice	SrCl ₂	30	Wet impregnation	128 °C, RH = 71%	2.4 GJ/m ³	[64]
–	CaCl ₂	–	Wet impregnation	146 °C, RH = 30%	2.1 GJ/m ³	[64]
–	MgSO ₄	–	Wet impregnation	150 °C, RH = 90%	2.1 GJ/m ³	[64]
–	MgCl ₂	–	Wet impregnation	230 °C, RH = 33%	2.0 GJ/m ³	[64]
–	Al ₂ (SO ₄) ₃	–	Wet impregnation	300 °C	1.6 GJ/m ³	[64]
–	MgSO ₄ /ZnSO ₄ : 9/1	–	Wet impregnation	120 °C	1422 J/g	[78]
Zeolite 13X	MgSO ₄	15	Wet impregnation	150 °C 4 h + 300 °C 2 h, RH = 80%	632 J/g	[79]
–	CrCl ₂	–	–	68 °C, 20 mbar	2.11 GJ/m ³	[80]
–	LiCl	–	–	72 °C, 20 mbar	2.08 GJ/m ³	[80]
–	LiBr	–	–	110 °C, 20 mbar	2.01 GJ/m ³	[80]
–	FeCl ₂	–	–	59 °C, 20 mbar	1.93 GJ/m ³	[80]
–	CuCl ₂	–	–	59 °C, 20 mbar	1.74 GJ/m ³	[80]
–	CaCl ₂	–	–	111 °C, 20 mbar	1.54 GJ/m ³	[80]
–	Mg(NO ₃) ₂	–	–	68 °C, 20 mbar	1.53 GJ/m ³	[80]
–	LiNO ₂	–	–	102 °C, 20 mbar	1.51 GJ/m ³	[80]
–	K ₂ CO ₃	–	–	65 °C, 20 mbar	1.3 GJ/m ³	[80]
–	MgCl ₂	–	–	104 °C, 20 mbar	1.93 GJ/m ³	[80]

degrade the porous matrix containing the salt [81]. As an example, for temperatures between 10 and 80 °C, the deliquescence process of MgSO₄·nH₂O will not occur below 80% relative humidity (RH) because its thermodynamically stable at this range of temperature and humidity [82,83]. A good affinity between the impregnated salt and the support is needed to delay the melting and the formation of agglomerates. In previous studies [64,77–80], salt hydrates were tested under different conditions in order to obtain information on the dehydration temperature range, the optimal relative humidity value for hydration, and to compare the heat storage density values. MgSO₄ and CaCl₂ are the two most investigated salts [79]. These two salts have been the subject of considerable research [44,66,84–87]. These salts are highly relevant in heat storage systems since they present the highest energy density (2.8 GJ/m³ for MgSO₄ and 2.1 GJ/m³ for MgCl₂) and a low charging temperature (<150 °C), which is suitable for building applications with solar collectors.

For all the above-mentioned reasons, novel composite materials obtained by depositing MgSO₄ on an AC support were developed, thoroughly characterized, and tested in order to achieve materials with good salt dispersion over the support surface. The goal was to produce materials that were stable throughout the cycles (to maintain a good

energy storage capacity), and had a relatively higher thermal conductivity when compared to usual heat storage materials. Finally, the experimental data obtained by performing hydration/dehydration cycles and physico-chemical characterizations has been implemented in a numerical model. Following that, several scenarios involving the usage of such material in building applications were simulated.

2. Experimental

2.1. Material preparation

The carbon material chosen as support was an activated carbon (AC) L27W from Norit N-V (Amersfoort, Netherlands), chemically activated by phosphoric acid for enhancing the mesoporosity. First, the AC was rinsed and filtrated several times on a Buchner funnel with abundant water to eliminate the residual phosphoric acid, until the pH of the filtrated water was constant (pH = 5.8). Then, the powder was dried in a stove at 100 °C for 12 h until complete dehydration. Successively, MgSO₄·7H₂O, from Sigma-Aldrich was deposited at different loading (from 5 to 50 wt% of MgSO₄) on the AC support by Incipient Wetness Impregnation (IWI). The obtained composites were dried during 12 h at

100 °C and labelled as reported in Table 2.

2.2. Characterization of the samples

X-Ray Diffraction (XRD) analyses were performed on the compacted powder of the samples on a diffractometer X'Celerator, equipped with a real-time multiple strip detector. The XRD phenomenon is based on constructive interference between monochromatic X-rays and crystalline samples. X-rays were generated by a cathode ray tube, filtered to get monochromatic rays, assembled to concentrate and then directed towards the sample [88–90], operating with an angular aperture of $2.12^\circ 2\theta$ in the 3° to $50^\circ 2\theta$ range, and CuK α radiation with a wavelength of 0.15406 nm. Diffractograms were recorded at room temperature with a step size of $0.017^\circ 2\theta$ and a scan time of 4 s per step.

A wavelength dispersion X-Ray Fluorescence (XRF) spectrometer (from PANalytical, Zetium) was used to perform the XRF measurements on pellets made of 0.1 g of the sample and 0.2 g of binder (boric acid, H₃BO₃) powder.

High-resolution micrographies were acquired by a Scanning Electron Microscope (SEM) from Philips, XL30 model to observe the morphology of AC [88] and composites and to determine the elemental analysis of activated carbon and the distribution of deposited salt. Prior to analysis, the samples were coated with carbon in order to create a thin conductive layer to improve the quality of the images. The semi-quantitative chemical analysis and atomic composition mapping of the sample were performed by means of Energy Dispersive X-ray (EDX).

The thermal conductivity ($\lambda = 90 \pm 8 \text{ mWm}^{-1}\text{K}^{-1}$) and the heat capacity ($\rho C_p = 307 \pm 26 \text{ kJ m}^{-3} \text{ K}^{-1}$) of the samples were determined starting from the values of thermal diffusivity ($\alpha = 2.9 \pm 0.4 \cdot 10^{-7} \text{ m}^2 \text{ s}^{-1}$) and thermal effusivity ($E = 166 \pm 8 \text{ Wm}^{-2}\text{K}^{-1} \text{ s}^{0.5}$) obtained by a Hot Disk TPS 500 analyzer. The sample pellets were placed in a covered sample holder where the Kapton sensor was horizontally placed between two layers of the material. The experiments were conducted at 20 °C for 160 s at a heating power of 100 W. Each measurement was repeated at least 5 times.

Nitrogen adsorption/desorption isotherms at -198°C were acquired in an ASAP 2420 device from Micrometrics. The samples were previously degassed at room temperature overnight, and then at 120 °C for 12 h before analysis [88]. The specific surface area was calculated by applying the Brunauer, Emmett, and Teller (BET) equation, and the porous volume was determined by Density Functional Theory (DFT) calculations.

2.3. Hydration/dehydration cycling and heat storage density determination

A Sensys Evo TG-DSC (Thermogravimetry coupled to differential scanning calorimetry) apparatus, equipped with a Wetsys flow humidity generator (from Setaram) was used to measure the heat and the water adsorption/desorption capacities of the composites and verify the cycling (see Fig. 2).

The procedure was divided into three steps (Fig. 3). First, the

composite was totally dehydrated at 300 °C by raising the temperature from 30 to 300 °C with a ramp of 10 °C/min under a flow of dry air (30 mL/min), followed by a 30-min isotherm at 300 °C. Then, the sample was cooled down at 30 °C and, once the temperature stabilized at 30 °C, the relative humidity of the air flow was increased to the desired value (RH = 30 or 60%). The hydration step was prolonged for 20 h in order to completely rehydrate the material. Finally, the sample was heated-up to 300 °C at 5 °C/min. After the 30-min of isothermal step, the sample was cooled to 30 °C and cycled a certain number of times.

Fig. 3 schematically summarizes the dehydration/hydration/dehydration cycle. For the composite containing 30 wt% of MgSO₄, similar experiments were carried out by performing several successive cycles (with 7 h hydration steps) with a pre-treatment performed at 150 °C, in order to study its stability over cycling.

2.4. Simulation of domestic application scenarios

The system operation was simulated using two scenarios, depending on the implementation of the MgSO₄/AC composites. The first concerned using the system for winter heating, while the second concerned producing residential hot water in the summer. For this purpose, the simulations have been performed on the basis of a 100 m² passive house, which requires an air exchange of 250 m³/h (double flow mechanical ventilation system). The entire or a part of this flowrate (Q_{inlet}) was used in the model for heat generation. The indoor air was assumed to be at $T_0 = 20^\circ \text{C}$, RH = 70% (i.e. $X_w(z=0) = X_0 = 10.2 \text{ g/kg}_{\text{d.a.}}$) in winter, and at $T_0 = 25^\circ \text{C}$, RH = 70% (i.e. $X_w(z=0) = X_0 = 13.9 \text{ g/kg}_{\text{d.a.}}$) in summer. To supply sufficient heat for winter heating, a cylindrical reactor (1 m in length and 0.94 m in radius) containing 1000 kg of composite was modeled. The cylindrical geometry of the reactor was chosen to simplify the filling of the adsorbent material and maintain consistency with a real application [91]. The fluid was assumed to be perfectly mixed at the reactor's inlet. The airflow was assumed to be laminar and one-dimensional.

A set of equations composed of 5 partial differential equations (eqs (1)–(5), detailed in section 3.4) and 3 algebraic equations (air density, air density derivative, and reaction heat) were used to model the system. The differential equations have been spatially discretized by using the finite difference method in order to get an algebraic system of 8 equations, which were solved for each time interval (explicit Euler method). Thus, the system was directly solved. The program was written in Fortran-90.

3. Results and discussion

3.1. Composition, thermal conductivity, structure, and morphology of the composites

Six composites with a MgSO₄ content in the 4–43 wt% interval were prepared by incipient wetness impregnation. The elemental composition was determined by XRF in order to verify if the magnesium sulfate content corresponded to the theoretical. Moreover, the phosphor residue

Table 2
Samples composition, surface area and porosity.

Sample	Composition (wt.%)						S.A. (m ² /g)	V _p (cm ³ /g)	V _{micro} (cm ³ /g)
	Theoretical			Measured by XRF					
	C	MgSO ₄	P	C	MgSO ₄	P			
AC	100	0	0	98.92	0.16	0.92	1643	1.019	0.588
5-MgSO ₄ /AC	95	5	0	91.36	4.11	4.53	1411	0.805	0.511
10-MgSO ₄ /AC	90	10	0	84.31	10.91	4.78	1219	0.721	0.449
20-MgSO ₄ /AC	80	20	0	75.49	20.34	4.17	829	0.466	0.323
30-MgSO ₄ /AC	70	30	0	70.69	26.00	3.31	732	0.369	0.266
40-MgSO ₄ /AC	60	40	0	61.52	35.36	3.12	562	0.254	0.205
50-MgSO ₄ /AC	50	50	0	54.27	43.09	2.64	342	0.208	0.162

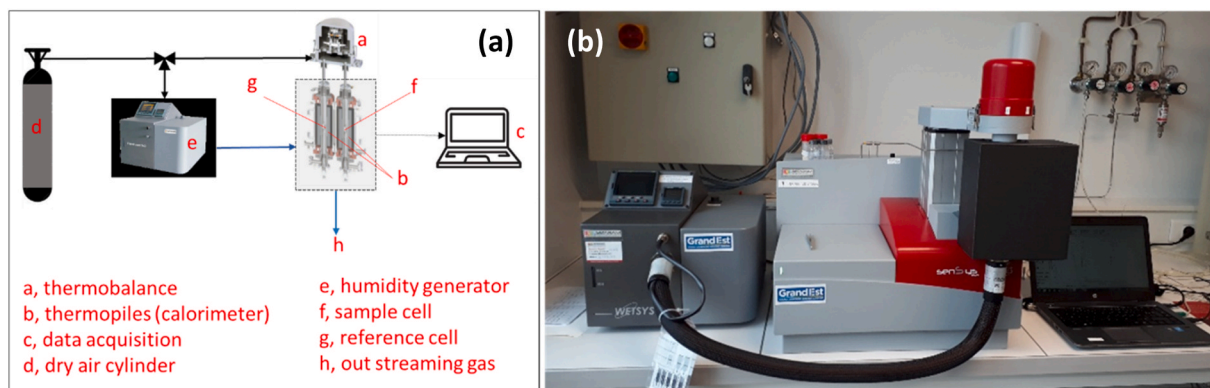


Fig. 2. Schema (a) and photo (b) of the TG-DSC-WETSYS set-up.

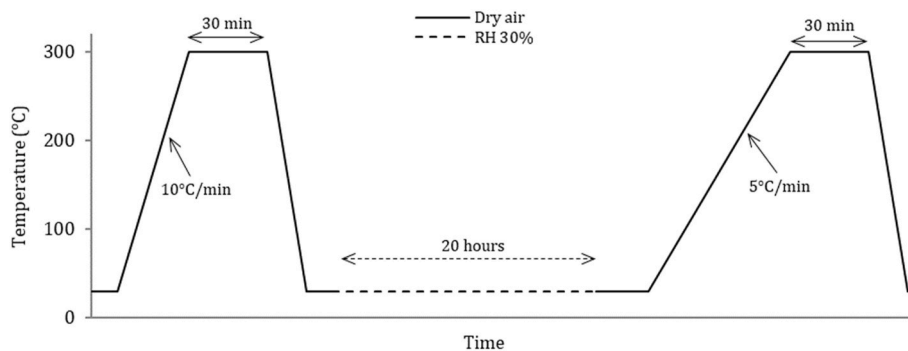


Fig. 3. Thermal cycle used for the TG-DSC-WETSYS analyses (Time not at scale).

of the parent AC was also measured (Table 2).

The experimental values are in agreement with the theoretical values for composites with low MgSO_4 content. Otherwise, when the theoretical salt content value was higher, the measured MgSO_4 concentration value was lower than expected. These results might be related to matrix inaccuracy in the XRF calibration curve. Indeed, the XRF calibration was based on conventional carbon materials and might deviate in the case of a high concentration of salt (starting from the sample containing 30 wt% of MgSO_4).

A second possible explanation is the presence of residues of phosphoric acid that have not been completely eliminated by the washing prior to deposition. Indeed, XRF analysis carried out on the samples shows P-contents of between 2.6 wt% and 4.8 wt%.

The thermal conductivity (λ) was estimated starting from the measure of the thermal diffusivity determined by hot-disk ($\lambda = \alpha \cdot \rho \cdot C_p$, where α is the thermal diffusivity, ρ the bulk density, and C_p the specific heat, respectively). The measured thermal conductivity for bare active carbon was $0.26 \text{ W}/(\text{m}\cdot\text{K})$ (for a measured $\alpha = 2.20 \cdot 10^{-7} \text{ m}^2/\text{s}$), $0.53 \text{ W}/(\text{m}\cdot\text{K})$ for magnesium sulfate heptahydrate salt (for a measured $\alpha = 1.60 \cdot 10^{-7} \text{ m}^2/\text{s}$), and to $0.43 \text{ W}/(\text{m}\cdot\text{K})$ for 30- MgSO_4/AC composite (for a measured $\alpha = 2.21 \cdot 10^{-7} \text{ m}^2/\text{s}$). The C_p values considered in the calculation of λ were of $1300 \text{ J}/(\text{kg}\cdot\text{K})$ for the AC [92] and $1556 \text{ J}/(\text{kg}\cdot\text{K})$ for the salt [93]. The bulk density (ρ) has been experimentally determined by weighing a known volume of the materials; it was found to be, respectively, equal to $895 \text{ kg}/\text{m}^3$ for the AC and $1878 \text{ kg}/\text{m}^3$ for $\text{MgSO}_4 \cdot 7\text{H}_2\text{O}$. The results obtained for the salt are comparable to those reported in the literature (and confirm the reliability of the used methodology [94]). The composite presented a relatively high thermal conductivity when compared to other composites reported in the literature (see Fig. 1). This value is particularly high because it is measured on the shaped sample (cylindrical pellets), and represents the true value of the heat storage materials that will be potentially charged in a real storage system.

All composites and the bare support have been observed by SEM. The homogeneity of the salt deposition was verified for the various composites. The eventual presence of a crust of salt on the surface was also investigated, as previously observed on composites prepared on different porous supports [41].

Observing the micrographies reported in Fig. 4, no large crystallites can be seen on the composite containing 30 wt% of magnesium sulfate (Fig. 4b); no substantial differences can be observed when compared to with the SEM micrographies of the parent activated carbon (Fig. 4a). The salt deposition is uniform, and no macroscopic aggregates are visible on the composite surface or in the macropores' entrance.

A mapping of the elements present in the samples was performed by EDX; the results for the samples containing 40 and 50 wt% of MgSO_4 are shown in Fig. 5. The uniformity of the impregnation of the salt on the carbon support can be confirmed for the 40- MgSO_4/AC composite (Fig. 5a). In the four cartographies, each analyzed element (C, S, O, and Mg) is dispersed in uniform layers. Otherwise, for 50- MgSO_4/AC (Fig. 5b), zones rich in Mg, S, and O (light colors) can be differentiated from the carbon support (dark zones) due to the presence of crystallites of MgSO_4 segregated on the support. The presence of such aggregates can cause different problems, for example, the blocking of the AC pores and the formation of salt crusts. Therefore, both phenomena contribute to the decrease of the mass transfer performance of the material (i.e. water molecules diffusion during the hydration/dehydration process).

The SEM + EDX analyses were confirmed by the XRD analysis of the samples (Fig. 6). The XRD pattern of AC showed an amorphous structure with two broad peaks at 17° and 23° , which are characteristic of amorphous carbon. No peaks related to crystallized magnesium sulfate are visible on the samples containing up to 30 wt% of MgSO_4 . For the 40- MgSO_4/AC sample, crystallization begins, and two small peaks assigned to MgSO_4 can be observed at 21 and 29° . The salt present in the 50- MgSO_4/AC sample is highly crystallized, as already observed by the presence of aggregates visualized by SEM analysis. The pattern of the 50-

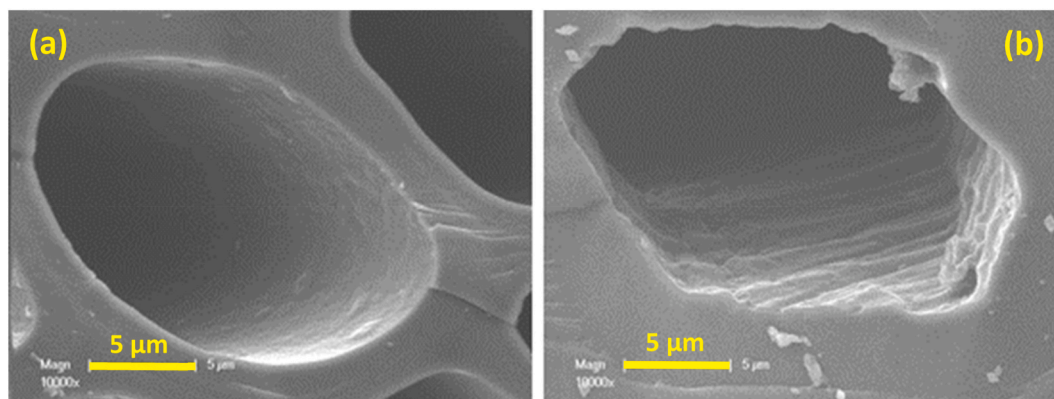


Fig. 4. (a) SEM picture of the activated carbon and (b) SEM picture of the activated carbon impregnated with 30% of MgSO_4 (30- MgSO_4/AC).

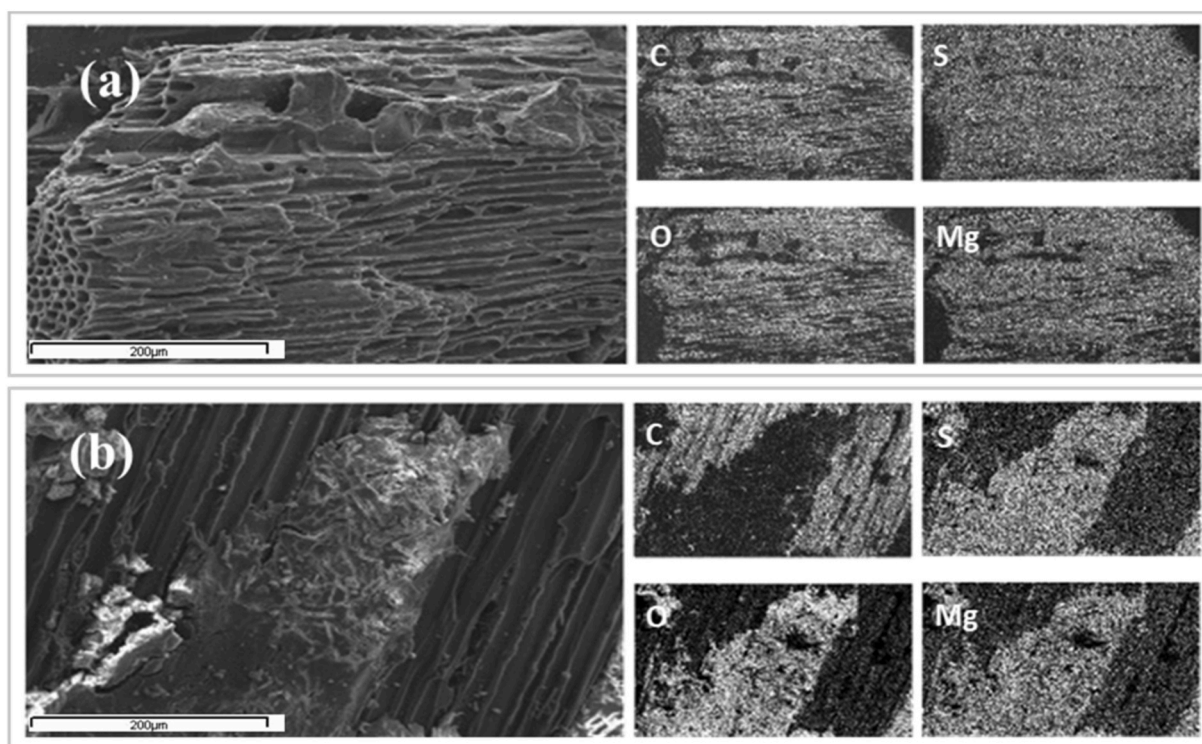


Fig. 5. (a): SEM picture (left) of 40- MgSO_4/AC composite and its EDX mapping pictures in right hand (C, S, O, and Mg content); (b): SEM picture (left) of 50- MgSO_4/AC composite and its EDX mapping pictures in right hand (C, S, O, and Mg content).

MgSO_4/AC sample mainly corresponds to that of $\text{MgSO}_4 \cdot 2\text{H}_2\text{O}$, reported in Fig. 5 for comparison.

In order to investigate the impact of the salt deposition on the porosity of the various composites, N_2 -adsorption at -198°C was performed (Fig. 7).

Information on the microstructure of the samples can be deduced by analyzing the shape of the curves and the hysteresis of the nitrogen physisorption isotherms, by referring to the IUPAC classification [95]. For the low magnesium sulfate-containing samples, the hysteresis is quite pronounced, but, even if less visible, its shape does not vary for all the samples. The isotherm shape is of type I (Fig. 7), typical of microporous samples (like activated carbons and molecular sieves) characterized by a relatively small external surface, for which the limiting nitrogen uptake is driven by the micropores' accessibility. In addition, isotherms presented an H4 type hysteresis loop.

Fig. 8 shows the pore distribution of the samples. All composites

maintain the distribution as the parent active carbon after the addition of MgSO_4 .

The samples are mostly micro- and mesoporous (pore diameters of $<20 \text{ \AA}$ and from 20 to 500 \AA , respectively). A smaller fraction of macropores (pore diameters $>500 \text{ \AA}$) is also observed. The porous volume decreases by increasing the quantity of salt deposited. Indeed, magnesium sulfate prevalently blocks access to micropores and mesopores. For instance, bare activated carbon, for example had a microporous volume of $0.145 \text{ cm}^3/(\text{g} \cdot \text{Å})$, while the 50- MgSO_4/AC sample had a pore volume of only $0.052 \text{ cm}^3/(\text{g} \cdot \text{Å})$, which was 3 times lower (see Table 2). Macropores are definitely less affected by salt deposition.

Fig. 9 shows the inverse correlation between the pore volume and the surface area as a function of the magnesium sulfate content. The two curves follow almost the same decreasing trend; the lower surface area is related to the blockage of the pores and to the impossibility of the nitrogen molecule to adsorb on the internal surface. The decrease in

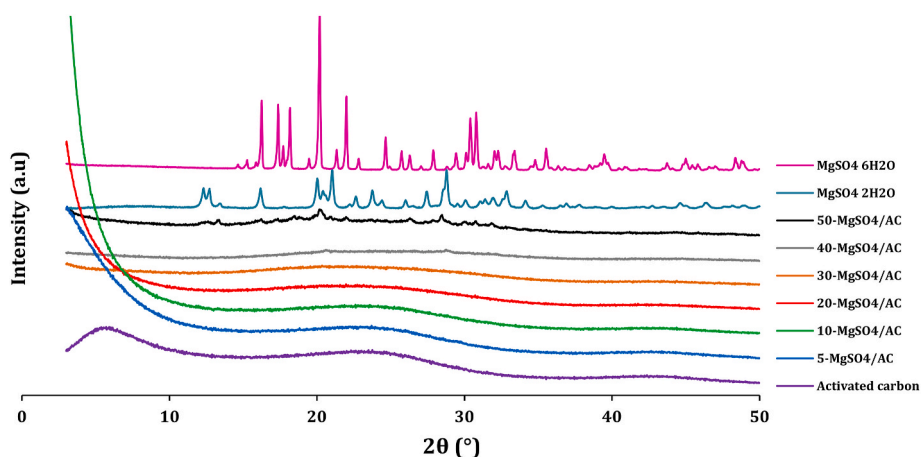


Fig. 6. XRD diffractogram of activated carbon, MgSO_4 salts, and all prepared composite samples dried at 150°C for 3 h.

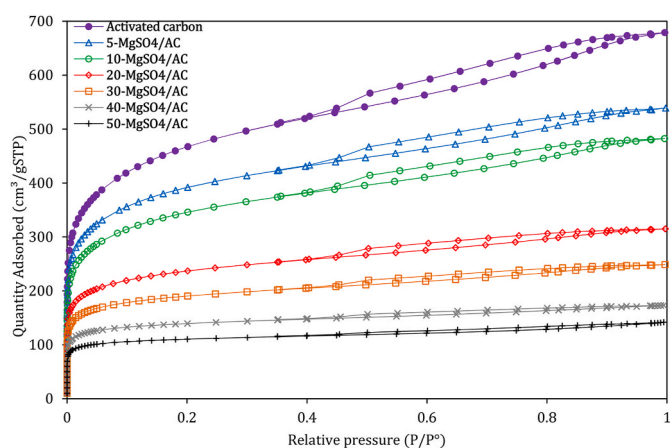


Fig. 7. N_2 adsorption-desorption isotherms of activated carbon and all prepared composites.

surface area can also diminish the surface available for water adsorption during the hydration/dehydration processes and diminish the heat storage capacity of the material. A compromise between the amount of salt deposited and the maintain of the specific surface area and porosity is then crucial for the design of these composites. This point has been then further investigated by measuring the water sorption and heat storage capacities, as reported in the next section.

3.2. Heat and water sorption capacity

The heat and water sorption capacities of the various composites were measured in the TG-DSC-Wetsys coupling described in Section 2.2. The calorimetric hydration peaks (here reported as an example for the 30- MgSO_4/AC sample) obtained during water uptake under air flow with a relative humidity (RH) of 30 and 60% are respectively reported in Figs. 10 and 11. The integration of the surface of the peak represents the heat released (in $\text{kJ}/\text{kg}^{-1}_{\text{dry material}}$), lately reported on the left Y-axes of Fig. 12, for comparing all composites after hydration at 30% RH (and 60% RH for 30- MgSO_4/AC only). The hydration heat values have an uncertainty of approximately $\pm 15 \text{ kJ}/\text{kg}^{-1}_{\text{dry material}}$.

The integration of the sections of the calorimetric curve at different times of adsorption permits the determination of the interaction energy between the water molecules and the sorbent (i.e. the composite). These values (expressed in $\text{kJ}/\text{mol}_{\text{H}_2\text{O}}$) are reported on the right Y-axes of Figs. 10–12. The water molecules adsorbed on the composite surface with decreasing energy with the progress of the sample hydration: the related points present a decreasing behavior. The energy of water molecule adsorption on the composites at different coverage extents (corresponding to different time intervals), and represented by the diamond-shaped symbols, varies from 65 (for the first fraction of water molecules adsorbed) to 20 $\text{kJ}/\text{mol}_{\text{H}_2\text{O}}$ (for the water molecules just physisorbed on the composite). These values are the average over the intervals considered; the first water molecules react with the salt with a high enthalpy of adsorption. For this reason, the total enthalpy of hydration expressed in $\text{kJ}/\text{mol}_{\text{H}_2\text{O}}$ calculated over the entire hydration

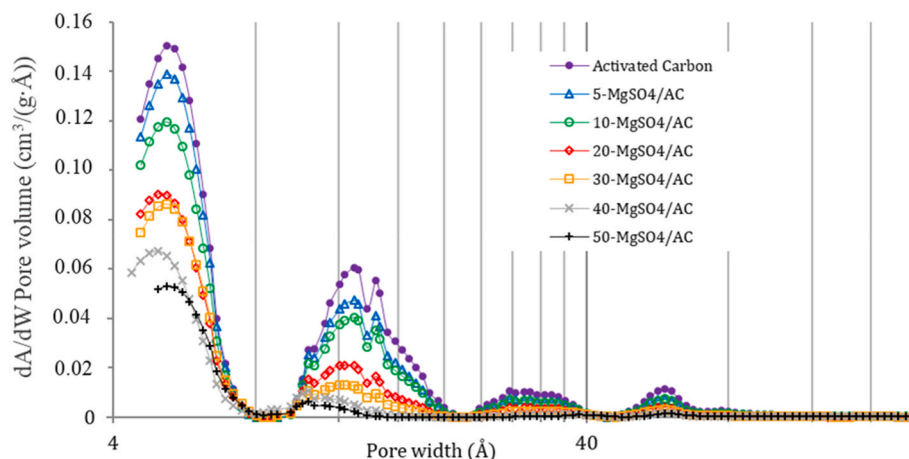


Fig. 8. Pore volume distribution vs. pore width of activated carbon and all prepared composites.

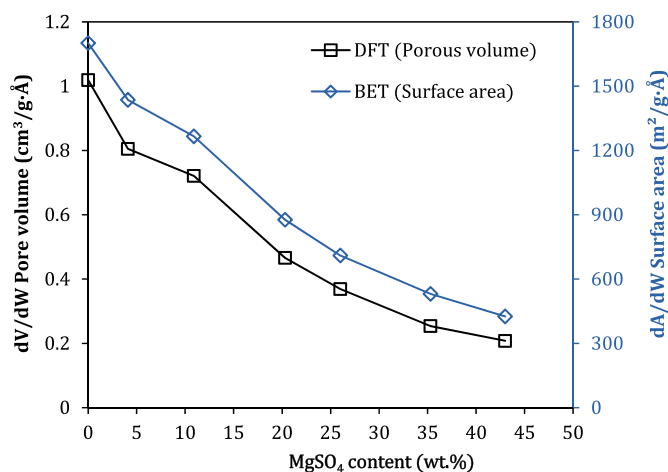


Fig. 9. Effect of MgSO_4 content deposited into activated carbon on total pore volume and surface area of each studied sample.

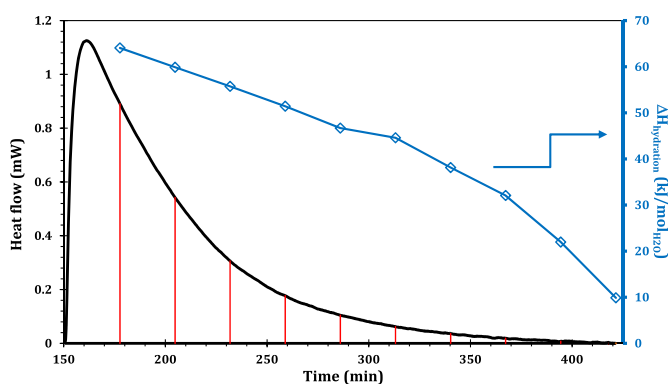


Fig. 10. Hydration enthalpy integration at regular times intervals for the 30- MgSO_4/AC sample (Dehydration at $300\text{ }^\circ\text{C}$ at $5\text{ }^\circ\text{C}/\text{min}$; hydration at $30\text{ }^\circ\text{C}$; RH = 30%; time: 20 h).

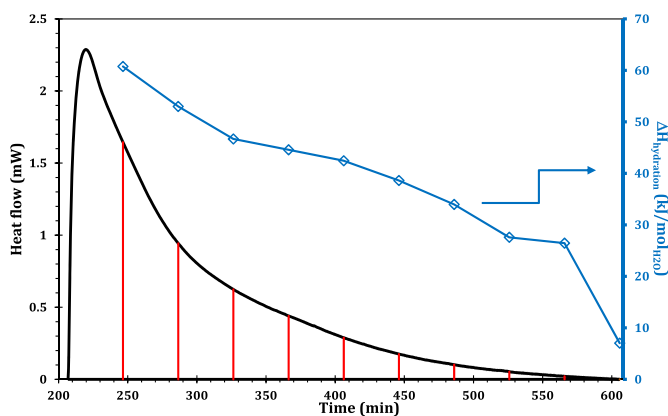


Fig. 11. Hydration enthalpy integration at regular times intervals for the 30- MgSO_4/AC sample (Dehydration at $300\text{ }^\circ\text{C}$ at $5\text{ }^\circ\text{C}/\text{min}$; hydration at $30\text{ }^\circ\text{C}$; RH = 60%; time: 20 h).

process is higher for the composites containing the smallest amount of MgSO_4 (Fig. 12). These composites (5- MgSO_4/AC and 10- MgSO_4/AC) present on their surface thin layers of salt (as previously observed by SEM and XRD analysis) that can be easily and completely be hydrated, therefore exploiting the intrinsic heat storage capacity of the salt (high hydration enthalpy).

Grevel et al. [83] measured and enlightened the existence of a linear

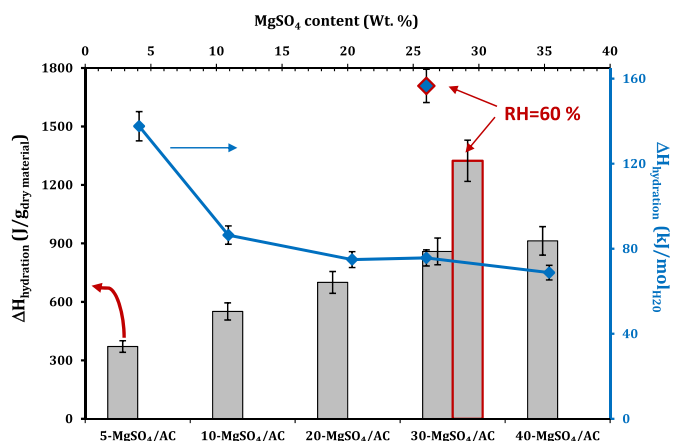


Fig. 12. Hydration enthalpy (J/g) per gram of prepared composites and mole of water adsorbed ($\text{kJ}/\text{mol}_{\text{H}_2\text{O}}$) for a full hydration (RH = 30% and RH = 60% for 30- MgSO_4/AC sample).

correlation between the number of water molecules adsorbed and the enthalpy of formation of magnesium sulfate hydrates. Therefore, the higher the degree of hydration of the salt, the greater the energy released. Unfortunately, the impregnation of magnesium sulfate on the AC decreases the pore volume and the surface of the composites, thus decreasing the salt fraction involved in the hydration process (salt trapped in the pores and inaccessible by water molecules, or salt forming thick layers towards which the diffusion of water is restricted). A compromise needs then to be found between the highest quantity of salt that can be deposited on the AC support and the highest heat storage density that can be obtained through the hydration process.

If the heat release during magnesium sulfate hydration is linearly proportional to its hydration level, as claimed by Grevel et al. [83], it is possible to estimate the necessary amount of magnesium sulfate to deposit in order to optimize the hydration level. Indeed, when the ratio between the quantity of water sorbed per mass unit of composite ($m_{\text{H}_2\text{O}}/m_{\text{dry material}}$) and the quantity of magnesium sulfate present on the composite (MgSO_4 quantity, wt.%) is below the dotted linear trend curve represented in Fig. 13, the optimal quantity of salt to deposit is overtaken. The experimental points in Fig. 13 have been obtained by measuring, using thermogravimetric analysis, the mass difference between the dehydrated and the fully hydrated material. In order to take

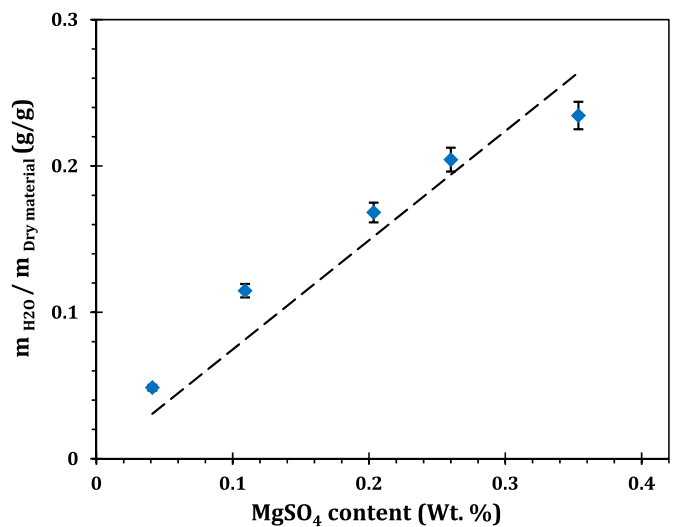


Fig. 13. Effect of MgSO_4 salt content on water sorption on the prepared composites (Dehydration at $300\text{ }^\circ\text{C}$ at $5\text{ }^\circ\text{C}/\text{min}$; hydration at $30\text{ }^\circ\text{C}$; RH = 30%; time: 20 h).

into account the quantity of water adsorbed exclusively by MgSO_4 , the measured values were corrected by subtracting the quantity of water adsorbed by the AC support ($0.097 \text{ g}_{\text{H}_2\text{O}}/\text{g}_{\text{dry AC}}$).

The MgSO_4 optimal quantity limit is then located between 26 and 35 wt% of magnesium sulfate. This result is confirmed by the heat storage density ($\Delta H_{\text{hydration}}$) measured on the samples and reported in Fig. 12. The hydration enthalpy increases with the quantity of MgSO_4 to reach a plateau for a MgSO_4 content above 30%wt (30- MgSO_4/AC and 40- MgSO_4/AC samples). The 30- MgSO_4/AC is also the sample presenting a good salt dispersion with the highest MgSO_4 content of the series of composites, as previously shown by XRD and SEM + EDX analysis.

The correlation between the salt hydration level and the hydration enthalpy is also confirmed by the hydration experiment performed on the 30- MgSO_4/AC sample at $\text{RH} = 60\%$. At higher water partial pressure, the water molecule diffusion is improved, and the salt hydration is ameliorated, as previously observed for $\text{MgSO}_4/\text{zeolite}$ composites [79] and potassium carbonate salt hydrate [96]. The water sorption increased from 0.28 to $0.52 \text{ g}_{\text{H}_2\text{O}}/\text{g}_{\text{dry material}}$. The hydration enthalpy of $859 \text{ J}/\text{g}_{\text{dry material}}$ measured at $\text{RH} = 30\%$ increases to $1324 \text{ J}/\text{g}_{\text{dry material}}$ at $\text{RH} = 60\%$. Such values are very promising when compared to those obtained for well-performing storage materials reported in the literature [68,69,79].

3.3. Hydration/dehydration cycles

In order to evaluate the stability of the composites after several hydration/dehydration cycles, several consecutive experiments have been performed on the 30- MgSO_4/AC sample, alternating dehydration steps at 150°C and short hydration steps of 4 h' duration at $\text{RH} = 30\%$. The measures of hydration enthalpies are reported in Fig. 14. For the first 8 cycles, no decreasing trend was detected in the heat storage capacity of the material.

Moreover, with the aim to verifying if any modification of the salt deposit on the AC surface took place, SEM observations were performed after cycling (Fig. 15).

The magnesium sulfate salt reorganizes on the AC surface during the successive hydration/dehydration steps. The very well dispersed salt film, present on the fresh composite (Fig. 4), forms, after 8 cycles, salt filaments homogeneously dispersed on the surface (Fig. 15). Despite this structural change, the hydration enthalpy remains unchanged. This modification of the structure does not evidently affect the water diffusion, and the salt hydration remains efficient. On the AC support, the crystallization and the formation of a thick salt crust are absent or, in

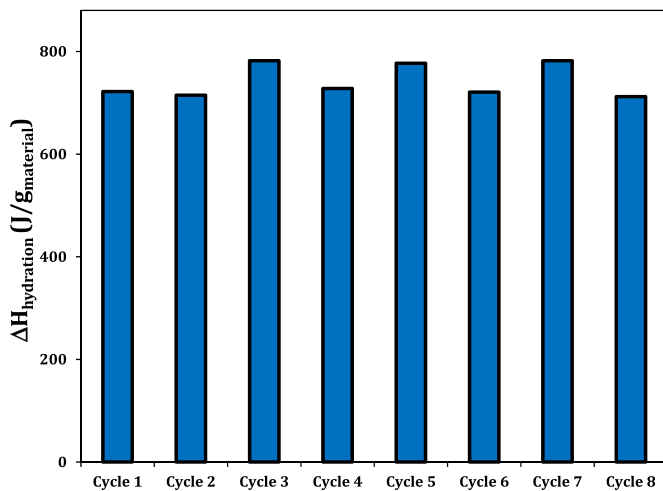


Fig. 14. Heat of hydration and mass changes to study stability over cycles for 30- MgSO_4/AC sample (Dehydration at 150°C at $5^\circ\text{C}/\text{min}$; hydration at 30°C ; $\text{RH} = 30\%$; time: 20 h).

any case, not pronounced enough to decrease the diffusion of water molecules.

3.4. Operation scenarios of a thermochemical heat storage system for domestic use

The aim of the following numerical study is to develop a numerical tool able to simulate different operating scenarios. The heat storage and release were simulated for ambient and domestic water heating in a passive house. The 30- MgSO_4/AC composite was the storage material selected for simulating the system.

In order to provide a simple, flexible, and effective simulation tool, the selected geometry for the storage reactor was cylindrical. An asymmetric 1D unsteady model was then developed; it included mass, momentum, and energy balances in the material and in the fluid (air). In the model, the fluid (moist air from controlled ventilation) enters the reactor, passes through the material, and transports the heat to the exit of the reactor. The air acts, at the same time as a water and heat carrier.

The modelling program simulates the thermal behavior of a tubular reactor operating under laminar flow. The fluid (moist air) is assumed to be perfectly mixed at the reactor inlet. The flow field in the reactor is described by the unsteady mass, energy, and water concentration balances [97]. The equations used in the model are presented as follows.

The continuity equation is:

$$\left(\frac{\partial \rho_a}{\partial T_a}\right) \left(\frac{\partial T_a}{\partial t}\right) + \frac{d(\rho_a u)}{dz} = 0 \quad (1)$$

where ρ_a , T_a are respectively the air density and temperature, u the air velocity in the reactor, t the time, and z the reactor axis coordinate.

The energy balance in the material is expressed by the following equation:

$$\left[\rho_m C p_m \frac{\partial T_m}{\partial t} - \lambda_m \frac{\partial^2 T_m}{\partial z^2}\right] S dz = \Delta_r H(m_w) \frac{\partial m_w}{\partial t} + h S (T_a - T_m) \quad (2)$$

where ρ_m , $C p_m$, λ_m , T_m are the density, the specific heat, the thermal conductivity, and the temperature of the material, respectively. S is the reactor section, m_w is the mass of water in the material, h is the heat exchange coefficient between air and the material and $\Delta_r H(m_w)$ is the reaction heat.

A linear law was applied to take into account the kinetics of adsorption in the material. The amount of adsorbed water during dt in the volume $S dz$ is:

$$\frac{\partial m_w}{\partial t} = X_w \frac{m_w(\infty) - m_w(t, z)}{m_w(\infty)} \rho_a u S \quad (3)$$

where X_w is the water content in the material and $m_w(\infty)$ the mass of water adsorbed in the material at equilibrium.

The energy balance in air is expressed as:

$$\left[\rho_a C p_a \left(\frac{\partial T_a}{\partial t} + u \frac{\partial T_a}{\partial z}\right) - \lambda_a \frac{\partial^2 T_a}{\partial z^2}\right] S dz = -h S (T_a - T_m) \quad (4)$$

where $C p_a$ and λ_a are the specific heat and the thermal conductivity of air, respectively.

And the water mass balance in the air as:

$$\rho_a S dz \frac{\partial X_w}{\partial t} = -\frac{\partial m_w}{\partial t} \quad (5)$$

The heat released from the storage material during hydration was deduced from the experimental results obtained by differential scanning calorimetry coupled to thermogravimetry (thermal flux and mass vs. time). For this purpose, $\Delta_r H(m_w)$ was calculated by numerical integration for various amounts of adsorbed water. Fig. 16 shows the heat released from the material during hydration with air at 30°C (at 30% RH), as a function of the mass fraction of water in the material.

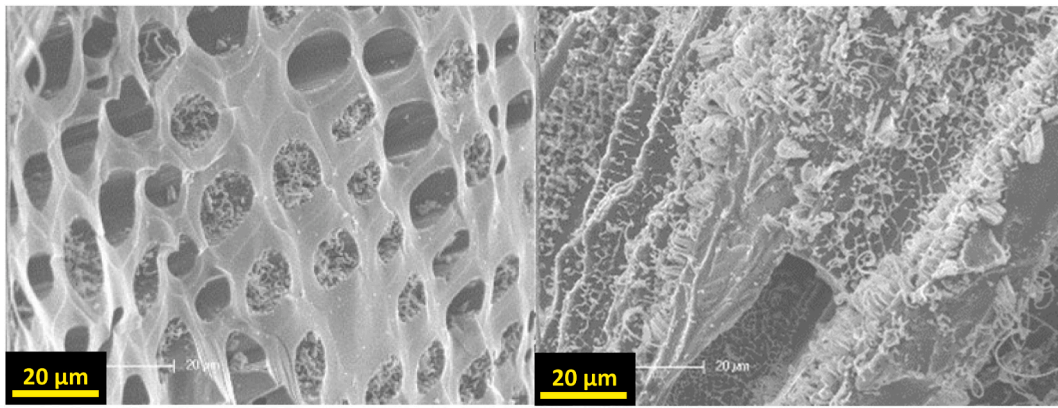


Fig. 15. Salt crystallization after the first cycle on 30-MgSO₄/AC. (Dehydration at 300 °C at 5 °C/min; hydration at 30°C; RH = 30%; time: 20 h).

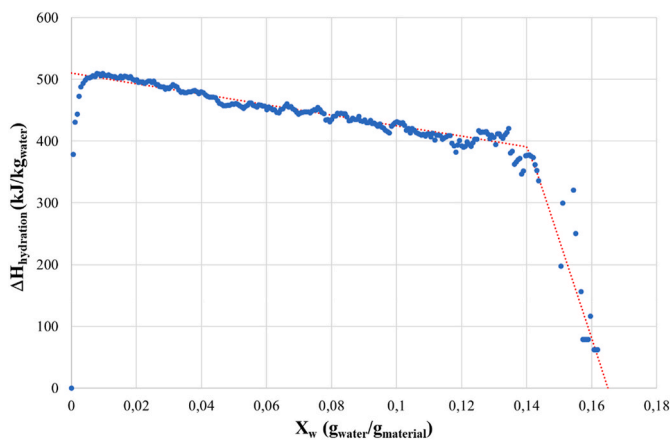


Fig. 16. Heat release during water adsorption versus mass fraction of water sorbed. Test performed at T = 30 °C and 30% RH.

Then, a linear approximation was performed to obtain:

$$\frac{m_w}{\rho_m S dz} \leq 0.14 \Delta_r H = f(m_w) = 510 - 850 \frac{m_w}{\rho_m S dz} \text{ (kJ/kg of sorbed water).}$$

$$0.14 < \frac{m_w}{\rho_m S dz} \leq 0.165 \Delta_r H = f(m_w) = 2640 - 16,000 \frac{m_w}{\rho_m S dz} \text{ (kJ/kg of sorbed water).}$$

The boundary conditions were: $T_a(z = 0) = T_0$, $T_m(z, t = 0) = T_0$, $u(t,$

$$z = 0) = \frac{Q_{inlet}}{\rho_a S}, X_w(z = 0, t) = X_0$$

Fig. 17 is a schematic representation of the two studied scenarios. The first scenario (Fig. 17a) is based on the use of the storage system for heating the house (during winter for example). The second (Fig. 17b) is oriented on the use of the storage system for supplying a complement of energy for producing hot sanitary water. This scenario corresponds to the periods in which the demand for central heating is absent or low. In the first case, the storage unit is an additional system intended to provide energy for special situations (severe weather conditions). The second is the use of the stored energy for heating domestic water during short periods in which the solar irradiation is limited (mostly in summer).

For the two simulations, the material is supposed to be firstly completely dehydrated by the hot and dry air by means of solar heaters.

For the first scenario (heating), the reactor permits production of 361 kWh of thermal energy with an air temperature of 65.6 °C at the reactor outlet. If the inlet air is maximized, the system can deliver a heat power of about 3.6 kW for more than 4 days. This value is in agreement with the required heat input for such type building (passive house, ~15 kWh/(m²·year)) [98].

The heat demand management is linearly controlled by the fraction of indoor air directly send into the reactor ($0 < Q_{inlet} < 250 \text{ m}^3/\text{h}$, being $250 \text{ m}^3/\text{h}$ the maximum flow of the recirculating system).

In the second scenario, the heat storage system is used to supply a complement of energy to warm-up the sanitary water, when the energy

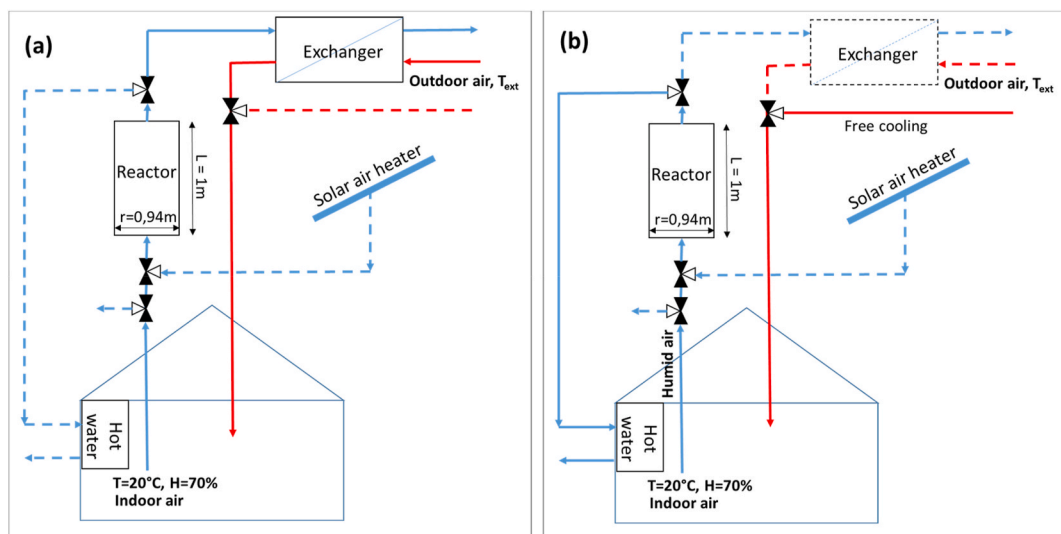


Fig. 17. Schemes of the two studied scenarios. House heating (a) and sanitary hot water production (b).

given by the solar heater is not sufficient (i.g. cloudy days). For this purpose, the entire flow of air entering/exiting from the reactor ($Q_{inlet} = 250 \text{ m}^3/\text{h}$) is sent to the “hot water” system (see Fig. 17 b). The heating power is approximately 3.5 kW, which is sufficient to warm-up for 14 times 300 L of water from 15 to approximately 60 °C in less than 8 h (assuming an effective efficiency of 60%), with no need to recharge the system [99].

4. Conclusion

Heat storage by sorption has been investigated in this study by several MgSO_4/AC composites. The results of composite characterization revealed a homogeneous dispersion of magnesium sulfate in composites prepared by incipient wetness impregnation. The hydration enthalpy showed an increase by increasing the MgSO_4 content on AC to reach a plateau for a MgSO_4 content above 30%wt (30- MgSO_4/AC and 40- MgSO_4/AC samples). The correlation between the salt hydration level and the hydration enthalpy was also confirmed by the hydration experiment performed on the 30- MgSO_4/AC sample at $\text{RH} = 60\%$. At higher water partial pressure, the water molecule diffusion was improved, and the salt hydration was ameliorated.

The hydration enthalpy of 30- MgSO_4/AC at $\text{RH} = 30\%$ was increased from 859 J/g_{dry material} to 1324 J/g_{dry material} at $\text{RH} = 60\%$. The stability of 30- MgSO_4/AC sample was found to be nearly stable after 8 cycles of hydration/dehydration. Moreover, two different scenarios for heating a house and for the production of sanitary hot water were simulated for the 30- MgSO_4/AC composite. In addition to the need to test the stability of the material under a higher number of hydration/dehydration cycles, in both scenarios, the possibility to implement the synthesized material in a domestic heat storage system was confirmed. New research is ongoing related to the effect of binary salt impregnation and the effect of different methods of composites preparation on heat storage performance.

Credit author statement

Simona Bennici: Conceptualization, Methodology, Resources, Writing - Original Draft, Writing - Review & Editing, Supervision, Project administration, Funding acquisition, Validation. **Patrick Dutournié:** Methodology, Software, Writing - Review & Editing, Supervision, Validation, Formal Analysis, Data Curation. **Jérémy Cathalan:** Writing - Original Draft, Investigation. **Mohamed Zbair:** Validation, Writing - Review & Editing, Visualization. **Minh Hoang Nguyen:** Investigation. **Elliot Scullier:** Investigation. **Cyril Vaultot:** Investigation.

Funding

Région Grand Est for providing funding for the acquisition of the TG-DSC equipment within the “STOCKFATAL project and for the contribution to Mr. Minh Hoang Nguyen’s thesis grant.

Carnot MICA for funding part of this study in the frame of the STOCKENER project.

Declaration of competing interest

The authors declare that they have no known competing financial interests or personal relationships that could have appeared to influence the work reported in this paper.

Acknowledgements

The authors would like to thank the Carnot Institutes MICA(France) for supporting a part of this study within the STOCKENER; Region Grand Est (France) for providing funding for the acquisition of the TG-DSC equipment, in the frame of STOCKFATAL project, and financing a part

of the PhD-grant of Mr Minh Hoang Nguyen.

All physico-chemical characterizations were performed on the IS2M technical platforms. The authors are very grateful to L. Michelin (XRF) and L. Josien (SEM + EDX) for their contribution.

References

- [1] Adeniyi AG, Otoikhian KS, Ighalo JO. Steam reforming of biomass pyrolysis oil: a review. *Int J Chem React Eng* 2019;17. <https://doi.org/10.1515/ijcre-2018-0328>.
- [2] Hosseini S, Moradi GR, Bahrami K. Acidic functionalized nanobohemite: an active catalyst for methyl ester production. *Int J Chem React Eng* 2019;17. <https://doi.org/10.1515/ijcre-2018-0283>.
- [3] Roschat W, Siritanon T, Kaewpuang T, Yoosuk B, Promarak V. Economical and green biodiesel production process using river snail shells-derived heterogeneous catalyst and co-solvent method. *Bioresour Technol* 2016;209:343–50. <https://doi.org/10.1016/j.biortech.2016.03.038>.
- [4] Yoro KO, Daramola MO. CO₂ emission sources, greenhouse gases, and the global warming effect. *Adv. Carbon Capture, Elsevier* 2020:3–28. <https://doi.org/10.1016/B978-0-12-819657-1.00001-3>.
- [5] Fasihi M, Efimova O, Breyer C. Techno-economic assessment of CO₂ direct air capture plants. *J Clean Prod* 2019;224:957–80. <https://doi.org/10.1016/j.jclepro.2019.03.086>.
- [6] Janssens-Maenhout G, Crippa M, Guizzardi D, Muntean M, Schaaf E, Dentener F, et al. EDGAR v4.3.2 Global Atlas of the three major greenhouse gas emissions for the period 1970–2012. *Earth Syst Sci Data* 2019;11:959–1002. <https://doi.org/10.5194/essd-11-959-2019>.
- [7] Wang C, Li X, Min Q, Wang W, Sardans J, Zeng C, et al. Responses of greenhouse-gas emissions to land-use change from rice to jasmine production in subtropical China. *Atmos Environ* 2019;201:391–401. <https://doi.org/10.1016/j.atmosenv.2018.12.032>.
- [8] Pettinari C, Tombesi A. Metal–organic frameworks for carbon dioxide capture. *MRS Energy Sustain* 2020;7:35. <https://doi.org/10.1557/mre.2020.30>.
- [9] Sandesh S, Kristachar PKR, Manjunathan P, Halgeri AB, Shanbhag GV. Synthesis of biodiesel and acetins by transesterification reactions using novel CaSn(OH)₆ heterogeneous base catalyst. *Appl Catal Gen* 2016;523:1–11. <https://doi.org/10.1016/j.apcata.2016.05.006>.
- [10] Peng X, Root TW, Maravelias CT. Storing solar energy with chemistry: the role of thermochemical storage in concentrating solar power. *Green Chem* 2017;19:2427–38. <https://doi.org/10.1039/C7GC00023E>.
- [11] Li G. Organic Rankine cycle performance evaluation and thermoeconomic assessment with various applications part I: energy and exergy performance evaluation. *Renew Sustain Energy Rev* 2016;53:477–99. <https://doi.org/10.1016/j.rser.2015.08.066>.
- [12] Li G, Zheng X. Thermal energy storage system integration forms for a sustainable future. *Renew Sustain Energy Rev* 2016;62:736–57. <https://doi.org/10.1016/j.rser.2016.04.076>.
- [13] Li G. Energy and exergy performance assessments for latent heat thermal energy storage systems. *Renew Sustain Energy Rev* 2015;51:926–54. <https://doi.org/10.1016/j.rser.2015.06.052>.
- [14] Li G, Hwang Y, Radermacher R, Chun H-H. Review of cold storage materials for subzero applications. *Energy* 2013;51:1–17. <https://doi.org/10.1016/j.energy.2012.12.002>.
- [15] Li G, Hwang Y, Radermacher R. Review of cold storage materials for air conditioning application. *Int J Refrig* 2012;35:2053–77. <https://doi.org/10.1016/j.ijrefrig.2012.06.003>.
- [16] Li G, Hwang Y. Energy storage systems for buildings. *Handb. Integr. Sustain. Build. Equip. Syst. Vol. I Energy Syst.*, ASME Press 2017:347–420. https://doi.org/10.1115/1.861271_ch8.
- [17] Chen X, Jin X, Zhang Z, Song D, Ling X, Wang Y, et al. Experimental investigation of CaCO₃/CaO in a spiral coil reactor for thermochemical energy storage. *Chem Eng J* 2022;428:131971. <https://doi.org/10.1016/j.cej.2021.131971>.
- [18] Aydin D, Casey SP, Riffat S. The latest advancements on thermochemical heat storage systems. *Renew Sustain Energy Rev* 2015;41:356–67. <https://doi.org/10.1016/j.rser.2014.08.054>.
- [19] Cabeza LF, Solé A, Barreneche C. Review on sorption materials and technologies for heat pumps and thermal energy storage. *Renew Energy* 2017;110:3–39. <https://doi.org/10.1016/j.renene.2016.09.059>.
- [20] N'Tsoukpoe KE, Liu H, Le Pierrès N, Luo L. A review on long-term sorption solar energy storage. *Renew Sustain Energy Rev* 2009;13:2385–96. <https://doi.org/10.1016/j.rser.2009.05.008>.
- [21] Kausar A, Sher F, Hazafa A, Javed A, Sillanpää M, Iqbal M. Biocomposite of sodium-alginate with acidified clay for wastewater treatment: kinetic, equilibrium and thermodynamic studies. *Int J Biol Macromol* 2020;161:1272–85. <https://doi.org/10.1016/j.ijbiomac.2020.05.266>.
- [22] Rashid T, Iqbal D, Hazafa A, Hussain S, Sher F, Sher F. Formulation of zeolite supported nano-metallic catalyst and applications in textile effluent treatment. *J Environ Chem Eng* 2020;8:104023. <https://doi.org/10.1016/j.jece.2020.104023>.
- [23] Sehar S, Sher F, Zhang S, Khalid U, Sulejmanović J, Lima EC. Thermodynamic and kinetic study of synthesised graphene oxide-CuO nanocomposites: a way forward to fuel additive and photocatalytic potentials. *J Mol Liq* 2020;313:113494. <https://doi.org/10.1016/j.molliq.2020.113494>.
- [24] Rasheed T, Shafi S, Bilal M, Hussain T, Sher F, Rizwan K. Surfactants-based remediation as an effective approach for removal of environmental pollutants—a

- review. *J Mol Liq* 2020;318:113960. <https://doi.org/10.1016/j.molliq.2020.113960>.
- [25] Rasheed T, Ahmad N, Nawaz S, Sher F. Photocatalytic and adsorptive remediation of hazardous environmental pollutants by hybrid nanocomposites. *Case Stud Chem Environ Eng* 2020;2:100037. <https://doi.org/10.1016/j.csee.2020.100037>.
- [26] Rasheed T, Hassan AA, Kausar F, Sher F, Bilal M, Iqbal HMN. Carbon nanotubes assisted analytical detection – sensing/delivery cues for environmental and biomedical monitoring. *TrAC Trends Anal Chem (Reference Ed)* 2020;132:116066. <https://doi.org/10.1016/j.trac.2020.116066>.
- [27] Li G, Qian S, Lee H, Hwang Y, Radermacher R. Experimental investigation of energy and exergy performance of short term adsorption heat storage for residential application. *Energy* 2014;65:675–91. <https://doi.org/10.1016/j.energy.2013.12.017>.
- [28] Li G, Hwang Y, Radermacher R. Experimental investigation on energy and exergy performance of adsorption cold storage for space cooling application. *Int J Refrig* 2014;44:23–35. <https://doi.org/10.1016/j.ijrefrig.2014.05.013>.
- [29] Tatsidjoudoung P, Le Pierrès N, Luo L. A review of potential materials for thermal energy storage in building applications. *Renew Sustain Energy Rev* 2013;18:327–49. <https://doi.org/10.1016/j.rser.2012.10.025>.
- [30] Dicaire D, Tezel FH. Regeneration and efficiency characterization of hybrid adsorbent for thermal energy storage of excess and solar heat. *Renew Energy* 2011;36:986–92. <https://doi.org/10.1016/j.renene.2010.08.031>.
- [31] Yan T, Wang RZ, Li TX, Wang LW, Fred IT. A review of promising candidate reactions for chemical heat storage. *Renew Sustain Energy Rev* 2015;43:13–31. <https://doi.org/10.1016/j.rser.2014.11.015>.
- [32] Deshmukh H, Maiya MP, Srinivasa Murthy S. Study of sorption based energy storage system with silica gel for heating application. *Appl Therm Eng* 2017;111:1640–6. <https://doi.org/10.1016/j.applthermaleng.2016.07.069>.
- [33] Lim K, Che J, Lee J. Experimental study on adsorption characteristics of a water and silica-gel based thermal energy storage (TES) system. *Appl Therm Eng* 2017;110:80–8. <https://doi.org/10.1016/j.applthermaleng.2016.08.098>.
- [34] Henninger SK, Ernst S-J, Gordeeva L, Bendix P, Fröhlich D, Grekova AD, et al. New materials for adsorption heat transformation and storage. *Renew Energy* 2017;110:59–68. <https://doi.org/10.1016/j.renene.2016.08.041>.
- [35] Rustam L, Jeremias F, Henninger SK, Wolff T, Munz GM. Tuning of adsorbent properties – oxidative hydrophilization of activated carbon monoliths for heat storage applications. *Energy Build* 2019;196:206–13. <https://doi.org/10.1016/j.enbuild.2019.05.024>.
- [36] Permyakova A, Skrylnyk O, Courbon E, Affram M, Wang S, Lee U-H, et al. Synthesis optimization, shaping, and heat reallocation evaluation of the hydrophilic metal-organic framework MIL-160(Al). *ChemSusChem* 2017;10:1419–26. <https://doi.org/10.1002/cssc.201700164>.
- [37] Elsayed A, Elsayed E, Al-Dadah R, Mahmoud S, Elshaer A, Kaialy W. Thermal energy storage using metal-organic framework materials. *Appl Energy* 2017;186:509–19. <https://doi.org/10.1016/j.apenergy.2016.03.113>.
- [38] Bon V. Metal-organic frameworks for energy-related applications. *Curr Opin Green Sustain Chem* 2017;4:44–9. <https://doi.org/10.1016/j.cogsc.2017.02.005>.
- [39] Köll R, van Helden W, Engel G, Wagner W, Dang B, Jänchen J, et al. An experimental investigation of a realistic-scale seasonal solar adsorption storage system for buildings. *Sol Energy* 2017;155:388–97. <https://doi.org/10.1016/j.solener.2017.06.043>.
- [40] Whiting GT, Grondin D, Stosic D, Bennici S, Auroux A. Zeolite–MgCl₂ composites as potential long-term heat storage materials: influence of zeolite properties on heats of water sorption. *Sol Energy Mater Sol Cells* 2014;128:289–95. <https://doi.org/10.1016/j.solmat.2014.05.016>.
- [41] Whiting G, Grondin D, Bennici S, Auroux A. Heats of water sorption studies on zeolite–MgSO₄ composites as potential thermochemical heat storage materials. *Sol Energy Mater Sol Cells* 2013;112:112–9. <https://doi.org/10.1016/j.solmat.2013.01.020>.
- [42] D'Ans P, Courbon E, Frère M, Descy G, Segato T, Degrez M. Severe corrosion of steel and copper by strontium bromide in thermochemical heat storage reactors. *Corrosion Sci* 2018;138:275–83. <https://doi.org/10.1016/j.corsci.2018.04.020>.
- [43] Solé A, Miró L, Barreneche C, Martorell I, Cabeza LF. Corrosion of metals and salt hydrates used for thermochemical energy storage. *Renew Energy* 2015;75:519–23. <https://doi.org/10.1016/j.renene.2014.09.059>.
- [44] Zhair M, Bennici S. Survey summary on salts hydrates and composites used in thermochemical sorption heat storage: a review. *Energies* 2021;14:3105. <https://doi.org/10.3390/en14113105>.
- [45] Gordeeva LG, Aristov YI. Composites 'salt inside porous matrix' for adsorption heat transformation: a current state-of-the-art and new trends. *Int J Low Carbon Technol* 2012;7:288–302. <https://doi.org/10.1093/ijlct/cts050>.
- [46] Yan TS, Li TX, Xu JX, Wang RZ. Water sorption properties, diffusion and kinetics of zeolite NaX modified by ion-exchange and salt impregnation. *Int J Heat Mass Tran* 2019;139:990–9. <https://doi.org/10.1016/j.ijheatmasstransfer.2019.05.080>.
- [47] Aristov YI, Kovalevskaya YA, Tokarev MM, Paukov IE. Low temperature heat capacity of the system “silica gel–calcium chloride–water. *J Therm Anal Calorim* 2011;103:773–8. <https://doi.org/10.1007/s10973-010-0981-8>.
- [48] Tokarev M, Gordeeva L, Romannikov V, Glaznev I, Aristov Y. New composite sorbent CaCl₂ in mesopores for sorption cooling/heating. *Int J Therm Sci* 2002;41:470–4. [https://doi.org/10.1016/S1290-0729\(02\)01339-X](https://doi.org/10.1016/S1290-0729(02)01339-X).
- [49] Courbon E, D'Ans P, Permyakova A, Skrylnyk O, Steunou N, Degrez M, et al. A new composite sorbent based on SrBr₂ and silica gel for solar energy storage application with high energy storage density and stability. *Appl Energy* 2017;190:1184–94. <https://doi.org/10.1016/j.apenergy.2017.01.041>.
- [50] Gordeeva L, Restuccia G, Freni A, Aristov Y. Water sorption on composites “LiBr in a porous carbon. *Fuel Process Technol* 2002;79:225–31. [https://doi.org/10.1016/S0378-3820\(02\)00186-8](https://doi.org/10.1016/S0378-3820(02)00186-8).
- [51] Shi W, Zhu Y, Shen C, Shi J, Xu G, Xiao X, et al. Water sorption properties of functionalized MIL-101(Cr)-X (X=–NH₂, –SO₃H, H, –CH₃, –F) based composites as thermochemical heat storage materials. *Microporous Mesoporous Mater* 2019;285:129–36. <https://doi.org/10.1016/j.micromeso.2019.05.003>.
- [52] D'Ans P, Courbon E, Permyakova A, Nouar F, Simonnet-Jégat C, Bourdreux F, et al. A new strontium bromide MOF composite with improved performance for solar energy storage application. *J Energy Storage* 2019;25:100881. <https://doi.org/10.1016/j.est.2019.100881>.
- [53] Grekova A, Gordeeva L, Aristov Y. Composite sorbents “Li/Ca halogenides inside multi-wall carbon nano-tubes” for thermal energy storage. *Sol Energy Mater Sol Cells* 2016;155:176–83. <https://doi.org/10.1016/j.solmat.2016.06.006>.
- [54] Aristov YI, Restuccia G, Tokarev MM, Buerger HD, Freni A. Selective water sorbents for multiple applications. 11. CaCl₂ confined to expanded vermiculite. *React Kinet Catal Lett* 2000;71:377–84. <https://doi.org/10.1023/A:1010351815698>.
- [55] Mahon D, Henshall P, Claudio G, Eames PC. Feasibility study of MgSO₄ + zeolite based composite thermochemical energy stores charged by vacuum flat plate solar thermal collectors for seasonal thermal energy storage. *Renew Energy* 2020;145:1799–807. <https://doi.org/10.1016/j.renene.2019.05.135>.
- [56] Aristov YI, Tokarev MM, Cacciola G, Restuccia G. Selective water sorbents for multiple applications, 1. CaCl₂ confined in mesopores of silica gel: sorption properties. *React Kinet Catal Lett* 1996;59:325–33. <https://doi.org/10.1007/BF02068130>.
- [57] Courbon E, D'Ans P, Permyakova A, Skrylnyk O, Steunou N, Degrez M, et al. Further improvement of the synthesis of silica gel and CaCl₂ composites: enhancement of energy storage density and stability over cycles for solar heat storage coupled with space heating applications. *Sol Energy* 2017;157:532–41. <https://doi.org/10.1016/j.solener.2017.08.034>.
- [58] Gaeni M, Rouws AL, Salari JWO, Zondag HA, Rindt CCM. Characterization of microencapsulated and impregnated porous host materials based on calcium chloride for thermochemical energy storage. *Appl Energy* 2018;212:1165–77. <https://doi.org/10.1016/j.apenergy.2017.12.131>.
- [59] Gordeeva LG, Restuccia G, Cacciola G, Aristov YI. Selective water sorbents for multiple applications, 5. LiBr confined in mesopores of silica gel: sorption properties. *React Kinet Catal Lett* 1998;63:81–8. <https://doi.org/10.1007/BF02475434>.
- [60] Gordeeva LG, Aristov YI. Composite sorbent of methanol “LiCl in mesoporous silica gel” for adsorption cooling: dynamic optimization. *Energy* 2011;36:1273–9. <https://doi.org/10.1016/j.energy.2010.11.016>.
- [61] Brancato V, Gordeeva LG, Grekova AD, Sapienza A, Vasta S, Frazzica A, et al. Water adsorption equilibrium and dynamics of LiCl/MWCNT/PVA composite for adsorptive heat storage. *Sol Energy Mater Sol Cells* 2019;193:133–40. <https://doi.org/10.1016/j.solmat.2019.01.001>.
- [62] Hongois S, Kuznik F, Stevens P, Roux J-J. Development and characterisation of a new MgSO₄–zeolite composite for long-term thermal energy storage. *Sol Energy Mater Sol Cells* 2011;95:1831–7. <https://doi.org/10.1016/j.solmat.2011.01.050>.
- [63] Narayanan S, Li X, Yang S, McKay I, Kim H, Wang EN. Design and optimization of high performance adsorption-based thermal battery. In: *Heat transf. Energy syst. Thermophys. Prop. Theory fundam. Res. Heat transf.*, vol. 1. American Society of Mechanical Engineers; 2013. <https://doi.org/10.1115/HT2013-17472>.
- [64] Mehrabadi A, Farid M. New salt hydrate composite for low-grade thermal energy storage. *Energy* 2018;164:194–203. <https://doi.org/10.1016/j.energy.2018.08.192>.
- [65] Bouché M, Richter M, Linder M. Heat transformation based on CaCl₂/H₂O – Part B: open operation principle. *Appl Therm Eng* 2016;102:641–7. <https://doi.org/10.1016/j.applthermaleng.2016.03.102>.
- [66] de Jong A-J, Trausel F, Finck C, van Vliet L, Cuypers R. Thermochemical heat storage – system design issues. *Energy Proc* 2014;48:309–19. <https://doi.org/10.1016/j.egypro.2014.02.036>.
- [67] Donkers PAJ, Pel L, Adan OCG. Experimental studies for the cyclability of salt hydrates for thermochemical heat storage. *J Energy Storage* 2016;5:25–32. <https://doi.org/10.1016/j.est.2015.11.005>.
- [68] Whiting GT, Grondin D, Stosic D, Bennici S, Auroux A. Zeolite–MgCl₂ composites as potential long-term heat storage materials: influence of zeolite properties on heats of water sorption. *Sol Energy Mater Sol Cells* 2014;128:289–95. <https://doi.org/10.1016/j.solmat.2014.05.016>.
- [69] Jabbari-Hichri A, Bennici S, Auroux A. CaCl₂-containing composites as thermochemical heat storage materials. *Sol Energy Mater Sol Cells* 2017;172:177–85. <https://doi.org/10.1016/j.solmat.2017.07.037>.
- [70] Frazzica A, Cabeza LF. Recent advancements in materials and systems for thermal energy storage. Cham: Springer International Publishing; 2019. <https://doi.org/10.1007/978-3-319-96640-3>.
- [71] Hermosilla-Lara G. Stockage de l'hydrogène par adsorption sur charbon actif : étude des effets thermiques lors de la charge dynamique d'un réservoir à lit fixe adsorbant. Université Joseph-Fourier - Grenoble I; 2007.
- [72] Oskouei MK, Tamainot-Telto Z. Effect of packing density on thermal properties of granular activated carbon packed bed by using of inverse heat conduction method. *10th Int. Conf. Heat Transf. Fluid Mech. Thermodyn.* 2014:944–8.
- [73] Jin Z, Tian B, Wang L, Wang R. Comparison on thermal conductivity and permeability of granular and consolidated activated carbon for refrigeration. *Chin J Chem Eng* 2013;21:676–82. [https://doi.org/10.1016/S1004-9541\(13\)60525-X](https://doi.org/10.1016/S1004-9541(13)60525-X).

- [74] Verma R, Nagendra HN, Kasthuriengan S, Shivaprakash NC, Behera U. Thermal conductivity studies on activated carbon based cryopanel. *IOP Conf Ser Mater Sci Eng* 2019;502:12197. <https://doi.org/10.1088/1757-899X/502/1/012197>.
- [75] Menard D, Py X, Mazet N. Activated carbon monolith of high thermal conductivity for adsorption processes improvement. *Chem Eng Process Process Intensif* 2005;44:1029–38. <https://doi.org/10.1016/j.cep.2005.02.002>.
- [76] Kuwagaki H, Meguro T, Tatami J, Komeya K, Tamura K. An improvement of thermal conduction of activated carbon by adding graphite. *J Mater Sci* 2003;38:3279–84. <https://doi.org/10.1023/A:1025138005230>.
- [77] Casey SP, Elvins J, Riffat S, Robinson A. Salt impregnated desiccant matrices for 'open' thermochemical energy storage—selection, synthesis and characterisation of candidate materials. *Energy Build* 2014;84:412–25. <https://doi.org/10.1016/j.enbuild.2014.08.028>.
- [78] Rehman AU, Khan M, Maosheng Z. Hydration behavior of MgSO₄–ZnSO₄ composites for long-term thermochemical heat storage application. *J Energy Storage* 2019;26:101026. <https://doi.org/10.1016/j.est.2019.101026>.
- [79] Wang Q, Xie Y, Ding B, Yu G, Ye F, Xu C. Structure and hydration state characterizations of MgSO₄-zeolite 13x composite materials for long-term thermochemical heat storage. *Sol Energy Mater Sol Cells* 2019;200:110047. <https://doi.org/10.1016/j.solmat.2019.110047>.
- [80] Donkers PAJ, Sögütoglu LC, Huinink HP, Fischer HR, Adan OCG. A review of salt hydrates for seasonal heat storage in domestic applications. *Appl Energy* 2017;199:45–68. <https://doi.org/10.1016/j.apenergy.2017.04.080>.
- [81] Ferchaud C, Zondag HA, Boer R De. Material research on salt hydrates for seasonal heat storage application in a residential environment. *Proc Int Symp Innov Mater Process Energy Syst* 2013;4–6.
- [82] Linnow K, Niermann M, Bonatz D, Posern K, Steiger M. Experimental studies of the mechanism and kinetics of hydration reactions. *Energy Proc* 2014;48:394–404. <https://doi.org/10.1016/j.egypro.2014.02.046>.
- [83] Grevel K-D, Majzlan J, Benisek A, Dachs E, Steiger M, Fortes AD, et al. Experimentally determined standard thermodynamic properties of synthetic MgSO₄·4H₂O (starkeyite) and MgSO₄·3H₂O: a revised internally consistent thermodynamic data set for magnesium sulfate hydrates. *Astrobiology* 2012;12:1042–54. <https://doi.org/10.1089/ast.2012.0823>.
- [84] Fopah Lele A, Kuznik F, Opel O, Ruck WKL. Performance analysis of a thermochemical based heat storage as an addition to cogeneration systems. *Energy Convers Manag* 2015;106:1327–44. <https://doi.org/10.1016/j.enconman.2015.10.068>.
- [85] Ferchaud CJ, Zondag HA, Rubino A, De Boer R. Seasonal sorption heat storage – research on thermochemical materials and storage performance. *Proc. Heat Power Cycle* 2012;2012:1–7.
- [86] Bertsch F, Jaehnic D, Asenbeck S, Kerskes H, Drueck H, Wagner W, et al. Comparison of the thermal performance of a solar heating system with open and closed solid sorption storage. *Energy Proc* 2014;48:280–9. <https://doi.org/10.1016/j.egypro.2014.02.033>.
- [87] Boer R de, Haije WG, Veldhuis JBJ. Smeding petten (Netherlands)] SF [ECN EE in IEEI. In: *Solid-sorption cooling with integrated thermal storage*. Netherlands: The SWEAT prototype; 2004.
- [88] Sher F, Iqbal SZ, Albazzaz S, Ali U, Mortari DA, Rashid T. Development of biomass derived highly porous fast adsorbents for post-combustion CO₂ capture. *Fuel* 2020;282:118506. <https://doi.org/10.1016/j.fuel.2020.118506>.
- [89] Jubeen F, Liaqat A, Sultan M, Zafar Iqbal S, Sajid I, Sher F. Green synthesis and biological evaluation of novel 5-fluorouracil derivatives as potent anticancer agents. *Saudi Pharmaceut J* 2019;27:1164–73. <https://doi.org/10.1016/j.jsps.2019.09.013>.
- [90] Jubeen F, Liaqat A, Amjad F, Sultan M, Iqbal SZ, Sajid I, et al. Synthesis of 5-fluorouracil cocrystals with novel organic acids as cofomers and anticancer evaluation against HCT-116 colorectal cell lines. *Cryst Growth Des* 2020;20:2406–14. <https://doi.org/10.1021/acs.cgd.9b01570>.
- [91] Kuznik F, Johannes K, Obrecht C, David D. A review on recent developments in physisorption thermal energy storage for building applications. *Renew Sustain Energy Rev* 2018;94:576–86. <https://doi.org/10.1016/j.rser.2018.06.038>.
- [92] Yao Z, You S, Ge T, Wang C-H. Biomass gasification for syngas and biochar co-production: energy application and economic evaluation. *Appl Energy* 2018;209:43–55. <https://doi.org/10.1016/j.apenergy.2017.10.077>.
- [93] Grevel K-D, Majzlan J. Internally consistent thermodynamic data for magnesium sulfate hydrates. *Geochem Cosmochim Acta* 2009;73:6805–15. <https://doi.org/10.1016/j.gca.2009.08.005>.
- [94] Kleiner F, Posern K, Osburg A. Thermal conductivity of selected salt hydrates for thermochemical solar heat storage applications measured by the light flash method. *Appl Therm Eng* 2017;113:1189–93. <https://doi.org/10.1016/j.applthermaleng.2016.11.125>.
- [95] Thommes M, Kaneko K, Neimark AV, Olivier JP, Rodriguez-Reinoso F, Rouquerol J, et al. Physisorption of gases, with special reference to the evaluation of surface area and pore size distribution (IUPAC Technical Report). *Pure Appl Chem* 2015;87:1051–69. <https://doi.org/10.1515/pac-2014-1117>.
- [96] Zuo S, Yang J, Liu J, Cai X. Significance of the carbonization of volatile pyrolytic products on the properties of activated carbons from phosphoric acid activation of lignocellulosic material. *Fuel Process Technol* 2009;90:994–1001. <https://doi.org/10.1016/j.fuproc.2009.04.003>.
- [97] Byron Bird R, Stewart WE, Lightfoot EN. *Transport phenomena*. second ed. Revised; 2007.
- [98] Wang Y, Kuckelkorn J, Zhao F-Y, Spliethoff H, Lang W. A state of art of review on interactions between energy performance and indoor environment quality in Passive House buildings. *Renew Sustain Energy Rev* 2017;72:1303–19. <https://doi.org/10.1016/j.rser.2016.10.039>.
- [99] ThemExcel. In: Production of domestic hot water; 2021. https://www.thermexcel.com/french/ressourc/dimensionnement_production_eau_chaude_sanitaire.htm.

Chapter VI

“Corn cobs” biochar as a macroporous host of salt hydrates for heat storage applications

(submitted to Biochar)

Résumé

Une série de composites à base de sulfate de magnésium a été préparée par imprégnation sur un biochar issu de la pyrolyse de rafles de maïs. Quatre composites comportant différentes teneurs en sel MgSO_4 (allant de 5 % à 20 % en masse) ont été préparés avec succès. Alors que les analyses des isothermes d'adsorption de CO_2 ont montré que le support est principalement microporeux, l'analyse de porosimétrie par intrusion de mercure montrent l'existence de la macroporosité. En analysant les cartographies EDX – (microanalyse dispersive en énergie des rayons X) des différents composites, on peut observer que pour les faibles teneurs, le sel est bien dispersé sur la totalité de la surface, externe et macroporeuse. Quelle que soit la teneur en sel, les observations (microscopie, quantité d'eau adsorbée et énergie stockée) montrent une bonne dispersion du sel à la surface et dans les macropores du matériau. En termes de performance, le composite contenant 20 % de MgSO_4 présente une capacité de stockage de 635 J/g et un niveau d'hydratation de 0,23 $\text{g}_{\text{eau}}/\text{g}_{\text{mat}}$.

‘Corn cobs’ biochar as a macroporous host of salt hydrates for heat storage applications

Minh Hoang Nguyen^{a,b}, Mohamed Zbair^{a,b}, Patrick Dutournié^{a,b}, Lionel Limousy^{a,b}, and Simona Bennici^{a,b*}

^a Institut de Science des Matériaux de Mulhouse (IS2M), Université de Haute-Alsace, CNRS, IS2M UMR 7361, F-68100 Mulhouse, France; minh-hoang.nguyen@uha.fr; mohamed.zbair@uha.fr; patrick.dutournie@uha.fr; simona.bennici@uha.fr

^b Université de Strasbourg, France

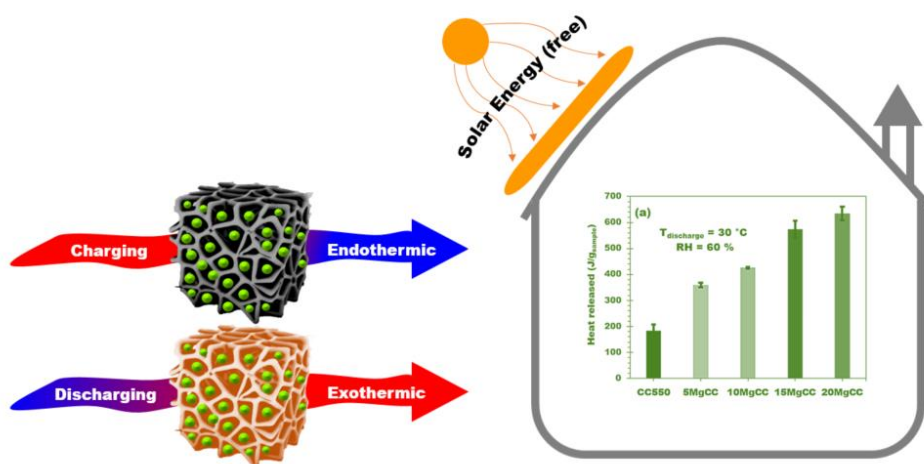
* Corresponding author, simona.bennici@uha.fr; Tel.: +33 (0)3 89336729

Abstract: Heat storage technologies are essential for increasing the use of solar energy in the household sector. Their development can be achieved by designing new storage materials; one way is to impregnate a porous matrix with hygroscopic salts. In this article, the possibility of using biochar-based composite sorbents to develop promising new heat storage materials for efficient thermal storage is explored. Biochar-based composites with defined salt loadings (5, 10, 15, and 20%) were produced by impregnating MgSO₄ into a biochar matrix derived from corn-cobs. The new materials demonstrated a high water sorption capacity of 0.24 g/g (20MgCC). After 6 successive charging-discharging cycles (dehydration/dehydration cycles), only a negligible variation of the heat released and of the water uptake was measured, confirming the absence of deactivation of 20MgCC upon cycling. The new 20MgCC composite showed an energy storage density of 635 J/g (T_{discharge} = 30 °C and RH = 60%), higher than that of the most part of the other composites containing a similar amount of hydrate salt reported in the literature. The macroporous nature of this biochar increases the available surface for salt deposition. During the hydration step, the water molecules effectively diffuse through a homogeneous layer of salt, as described by the intra-particle model applied in this work. The new efficient biochar-based composites open a low-carbon path for the production of sustainable thermal energy storage materials and applications.

Article Highlights:

- A new composites sorbents made of MgSO₄ and biochar were produced using the impregnation approach.
- The highest energy storage density achieved is 635 J/g.
- Hydration kinetics and water uptake of prepared sorbents were studied.
- Biochar with 20 wt% of MgSO₄ has a good stability over 6 discharge/charge cycles.

Graphical abstract



Keywords: Thermochemical energy storage; Solid/gas sorption; Biochar; Salt hydrate; Material characterization.

1 Introduction

Thermochemical Heat storage (TCHS) systems that are very broad implanted in the areas of solar photo/thermal utilization, building insulation, and industrial applications, are becoming increasingly important as a means to increase the energy efficiency (Cabeza et al. 2021). TCHS systems have an important industrial application value to guarantee the adaptability and stability in renewable energy implementation. TCHS systems increase the utilization efficiency as a result of their high heat storage capacity, the possibility to achieve long-lasting energy storage period, and the negligible energy loss during storage (Carrillo et al. 2019). Salt hydrate-based TCHS materials have emerged as the best candidate as storage material in a variety of TCHS systems, due to the simple reaction involved (hydration), the non-toxicity, and then absence of side reactions (Lin et al. 2021; Liu et al. 2021). Most part of TCHS operates on the principle of the reversible sorption reaction (generally water sorption), where heat is stored during desorption (charge) and released during adsorption at a later time (discharge). To convert the system into a practical residential application (space heating and domestic hot water generation), the TCHS material must be carefully selected. The selection criteria for salt hydrates (N'Tsoukpoe et al. 2014; Xu et al. 2021; Zhao et al. 2022) include a high energy density, a low charging temperature with a good mass and heat transfer (Zbair and Bennici 2021), and an improved thermal conductivity (Bennici et al. 2022). The working pair $\text{MgSO}_4\text{-H}_2\text{O}$ has been getting a lot of attention (Zbair and Bennici 2021; Bennici et al. 2022) due to the high theoretical energy density (2.8 GJ/m^3) and the high deliquescence relative humidity (DRH) of 90 %. However, overhydration, aggregate formation during rehydration, kinetic hindrance limiting mass and heat transfer, and poor cyclability (Linnow et al. 2014) are the major drawbacks of salt hydrate-based TCHS. Consequently, the potential of the system has not yet been achieved and, due to these constraints, the energy storage capacity is still too low. Attempting to make composites by dispersing the salt in a porous matrix to prevent swelling and aggregation of the salt is one way to take advantage of MgSO_4 's great potential and overcome one of the main materials' drawbacks: mass and heat transfer limitation. In order to achieve the goal of an efficient and low-temperature thermochemical heat storage, it is necessary to design and synthesize novel TCHS composites that not only present excellent storage capacity and hydration behavior, but that also assure a long hydration/dehydration cycle reliability. The goal can be reached by finding suitable support for dispersing the salt hydrate in order to minimize the thickness of the salt deposit and consequently improve the water molecule diffusion. A promising candidate is biochar.

In contrast to its widespread application in other domains such as conversion and storage of energy (Liu et al. 2019), supercapacitors as well as batteries (Saning et al. 2019; Senthil and Lee 2021), to the best of our knowledge, there is no study reporting on the application of biochar materials derived from biomass waste in the field of thermochemical heat storage by sorption.

Biomass is predominantly composed of biopolymers such as cellulose, hemicellulose, and lignin (Tursi 2019), which serve as a suitable carbon skeleton framework for the production of carbonaceous materials, as biochars. Bamboo bagasse (Gunasekaran et al. 2018), cotton rose wood (Ma et al. 2020), pinewood (Jaswal et al. 2019), and so on are some example. A diverse spectrum of biomass precursors rich in biomolecules such as carbohydrates and proteins contributes to significant scientific progress in the development of functional biomass-based carbons (Hou et al. 2017). A particularly renewable and sustainable source of biochar is woody biomass, such as agriculture's waste (Giudicianni et al. 2013; Frikha et al. 2021).

Pyrolysis is a sustainable method of converting biomass into biochar and biofuels. It consists in the thermal conversion of biomass in an oxygen-deficient atmosphere (Freddo et al. 2012; Bruckman et al. 2016). Due to its distinctive physicochemical characteristics, the biochar has a wide range of potential uses in a variety of fields, including energy production, soil conditioning, soil remediation, and catalysis (Ahmad et al. 2014; Nanda et al. 2016; Tan et al. 2017; El-Naggar et al. 2019; Zheng et al. 2023). The pyrolysis temperature is the most important parameter in terms of the properties of the resulting biochar (Fang et al. 2015; Suárez-Abelenda et al. 2017). Biochar produced at high pyrolysis temperatures ($> 600 \text{ }^\circ\text{C}$) has a high pH, a large surface area (porosity), and a high aromaticity. Lower process temperatures, on the other hand, result in higher char yield and higher amount of volatiles (that re-condense on the biochar surface) and oxygen-containing surface functions that provide higher electrical conductivity and cation-exchange capacity (Kambo and Dutta 2015; Nanda et al. 2016; Ulusal et al. 2021).

Moreover, it should be mentioned that biomass is an entirely renewable energy source because the CO_2 generated during its combustion and utilization processes is not accounted as contribution to the atmospheric CO_2 (thanks to the neutral carbon balance, due to its biogenic origin). In other words, plants utilize CO_2 , which is released into the environment as a result of other plants' decomposition processes, for growth and metabolic functions (Tkemaladze and Makhashvili 2016). Therefore, using biomass just accelerates the release of CO_2 into the atmosphere, but do not affect the global carbon balance; once released, CO_2 will be metabolized by plants to create new biomass (Kaltschmitt 2013).

Biochar derived from biomass waste has already displayed excellency in energy storage and catalysis due to its valuable advantages of low carbon footprint (Zhang et al. 2022), wide availability, and low cost (Deng et al. 2016; Chen et al. 2021). Moreover, it has to be pointed out that the annual production of biomass is around 130 billion tons worldwide (Sheldon 2014); this huge quantity assures the possibility to produce biochar in sufficient quantities for the eventual development of the TCHS sector.

Converting the biomass waste into a support for producing TCHS materials is an interesting idea: such composites can store and convert renewable energy through a sustainable technology, applying a sustainable material, and contributing to the sustainable development (Ma et al. 2021).

In this study, MgSO_4 was incorporated into a porous biochar support derived from corncobs pyrolysis. The corresponding MgSO_4 TCHS composites were synthesized, thoroughly characterized, and tested in order to achieve materials with good salt dispersion over the support surface. Also, to gain a better understanding of the effect of MgSO_4 salt, studies of the hydration and energy release behavior of the materials have been detailed.

2 Experimental

2.1 Composite materials preparation

The biochar was prepared in a pilot pyrolyzer at RAPSODEE-UMR CNRS 5302 laboratory, following the procedure detailed in (Frikha et al. 2021). In the present case, the parent biomass was constituted of corncobs collected in the Alsace region (to answer to circular economy issues) and dried at 105 °C for 24 h. They were then pyrolyzed at 550 °C under N_2 flow of 100 mL/min. The pyrolysis temperature was reached with a heating rate of 4 °C/min and maintained for 1.5 h. The biochar obtained after the pyrolysis was sieved between 2.5-4 mm and labeled CC550. The obtained biochar was used as a porous support for MgSO_4 salt hydrate.

The impregnation method was used to deposit MgSO_4 ($\text{MgSO}_4 \cdot 7\text{H}_2\text{O}$, 99.9 % from Sigma-Aldrich) onto the CC550 porous support. The method consists of intimately mixing the porous support with an aqueous solution of MgSO_4 . Previous to impregnation, the biochar was dried in an oven at 150 °C to remove any trace of water from the pores. The aqueous solution of MgSO_4 was then added over the dried support. The mixture was subjected to constant mixing for 4 h to homogenize the impregnation. The obtained powders were then dried at 60 °C for 12 h and successively at 150 °C for 12 h more. 4 composites were prepared and then labelled as $x\text{MgCC}$ (Table 1), with x is the theoretical content of MgSO_4 in the composites. The real salt content was then verified by X-ray fluorescence.

2.2 Characterizations methods

X-Ray Diffraction (XRD) analyses were performed on the compacted powder of the samples on a diffractometer PANalytical MPD X'Pert Pro, equipped with a Pixcel real-time multiple strip detector, operating with an angular aperture of $3.347^\circ 2\theta$ in 3° to $80^\circ 2\theta$ range, and using $\text{CuK}\alpha$ radiation with 0.15418 nm wavelength. Diffractograms were recorded at 22 °C with a step size of $0.013^\circ 2\theta$ and a scan time of 220 s per step.

A wavelength dispersion X-Ray Fluorescence (WDXRF) spectrometer (from PANalytical, Zetium) was used to perform the XRF measurements on pellets made of 0.1 g of the sample and 0.2 g of acid boric H_3BO_3 .

High-resolution micrographics were acquired by a Scanning Electron Microscope (SEM) from JEOL, JSM-7900F model. The semi-quantitative chemical analysis and atomic composition mapping of the sample was performed by means of Energy Dispersive X-ray (EDX).

CO_2 adsorption isotherm of the biochar at 0 °C was acquired in an ASAP 2420 device from Micromeritics (Micromeritics, Norcross, GA, USA). The sample was previously degassed at 150 °C for 12 h and then at 150 °C for 2 h directly in the measurement cell before analysis. The specific surface area was calculated applying the Brunauer, Emmett and Teller (BET) equation (S_{BET}). Finally, the pore size distribution (PSD) was determined using the CO_2 -DFT model.

Mercury porosimetry analysis on the biochar was subcontracted to FiLAB provider that performed the analysis with a Autopore IV device from Micromeritics. The sample was degassed at ambient temperature and at 50 μmHg pressure for 3 h. Mercury intrusion was performed at 22 °C with a contact angle of 130 °C and a pressure range from 0.52 to 60000 psia (0.036 to 4137 bar), covering a pore range from 350 μm to 3 nm.

2.3 Hydration experiments

A Sensys TG-DSC instrument equipped with a Wetsys flow humidity generator, both from Setaram, were used to quantify the heat delivered and the amount of water sorption of the corncob-derived biochar and the composites. The samples (15-25 mg) were firstly dehydrated at 150 °C under a flow of dry air (30 mL/min) followed by 3 h at 150 °C isotherm to perform the dehydration. The dehydration temperature was selected on the basis of the temperature that can be obtained in a real application by using a flat-plate solar heat collectors (Whiting et al. 2013; Donkers et al. 2017). After the dehydration step, the sample was cooled down to 30 °C. The sample was kept at this temperature in dry air until the DSC signal attained a stable baseline. Then the relative humidity (RH) of the air flow was increased to 60 % to begin the hydration phase. In order to reach a complete rehydration, the samples

were hydrated during 8 hours and until the DSC signal returned to the baseline. The samples' hydration heat (J/g_{sample}) was deduced from the surface's integration beneath the DSC signal during hydration.

3 Results and discussion

3.1 Textural and structural properties of the composite materials

Table 1 summarizes the chemical composition obtained by WDXRF (2nd column). The support was characterized by CO_2 manometric adsorption and the isotherms were collected at 0 °C. **Figure 1a and b** respectively display the CO_2 adsorption isotherm and the pore size distribution (PSD) of the biochar. PSD was obtained by applying the CO_2 -DFT model. The PSD clearly showed the microporous structure of the biochar and, in addition, the existence of ultramicroporosity (conventional for biomass-derived carbon materials). Three populations of pore size were detected: the first centered at 0.56 nm with a sharp and clear peak, and two others centered at 0.82 and 1.00 nm. The specific surface area S_{BET} and the pore volume V_p were then determined, and the result showed $S_{\text{BET}} = 175 \text{ m}^2/\text{g}$ and $V_p = 0.06 \text{ cm}^3/\text{g}$, due to the ultra-micro and microporosity.

Table 1 Amount of salt determined by XRF and hydration experiments results

Sample	MgSO ₄ content (wt%)	Heat released (J/g_{sample})	Water adsorption (g/g)
CC550	0.0	183	0.07
5MgCC	4.42	360	0.13
10MgCC	9.10	426	0.16
15MgCC	12.60	574	0.21
20MgCC	19.51	635	0.24

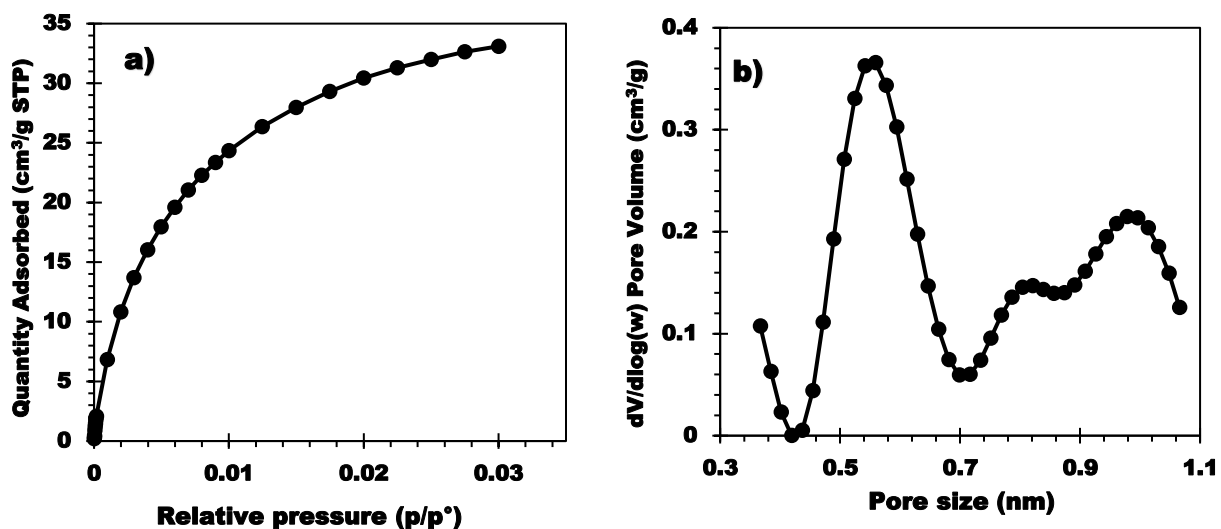


Fig. 1 (a) CO_2 adsorption isotherm and (b) Pore size distribution of CC550.

The biochar support was also characterized by mercury intrusion porosimetry to probe also the macroporosity. The estimated total pore area due to macropores was $78.4 \text{ m}^2/\text{g}$ (this surface was estimated considering perfectly cylindrical pores). **Figure 2a** shows the distribution of the macropores sizing from $300 \mu\text{m}$ to about $0.01 \mu\text{m}$; 3 main pore size ranges were identified. The first was centered at $8 \mu\text{m}$ (in the 20 to $3 \mu\text{m}$ range), the second at $0.37 \mu\text{m}$ (characterized by a band in the 0.7 to $0.18 \mu\text{m}$ range) and the third at 0.07 , with a band between 0.18 and $0.01 \mu\text{m}$. The first two pore size populations, observed on the left side of **Fig. 2a**, correspond to the inter-particle filling between the granules. This result shows that the biochar support possess a macroporosity network in addition to micropores. This can provide an accessible surface for the salt that can be homogeneously dispersed into the macropores. The possibility to charge into the support higher amount of salt allows to reach higher heat capacities. Moreover, if the salt can be efficiently dispersed on a larger accessible surface, the mass transfer is potentially ameliorated due to the thin layer of salt deposited. As a result, hydration kinetics can be improved. The other four composites were also characterized by Hg intrusion

and the results are shown in **Fig. 2b**. The pore size distribution of all 4 composites shows 2 main peaks located in the macropore range: 3 μm and 40 nm. A significant decrease in the 3 μm peak can be observed as the salt content increases. The decrease in the 3 μm peak also led to a reduction by 15 % in terms of total porosity (from 70 % to 55 %) and more than 50 % (from 1.89 to 0.81 cm^3/g) in terms of pores' volume.

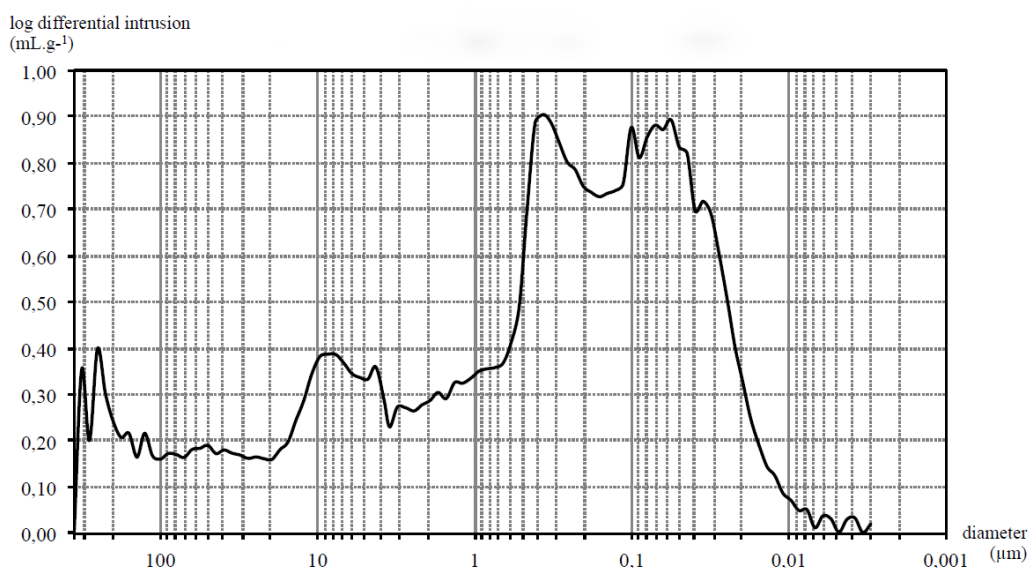


Fig. 2a Pore size distribution resulted from Hg porosimetry analysis of the biochar support.

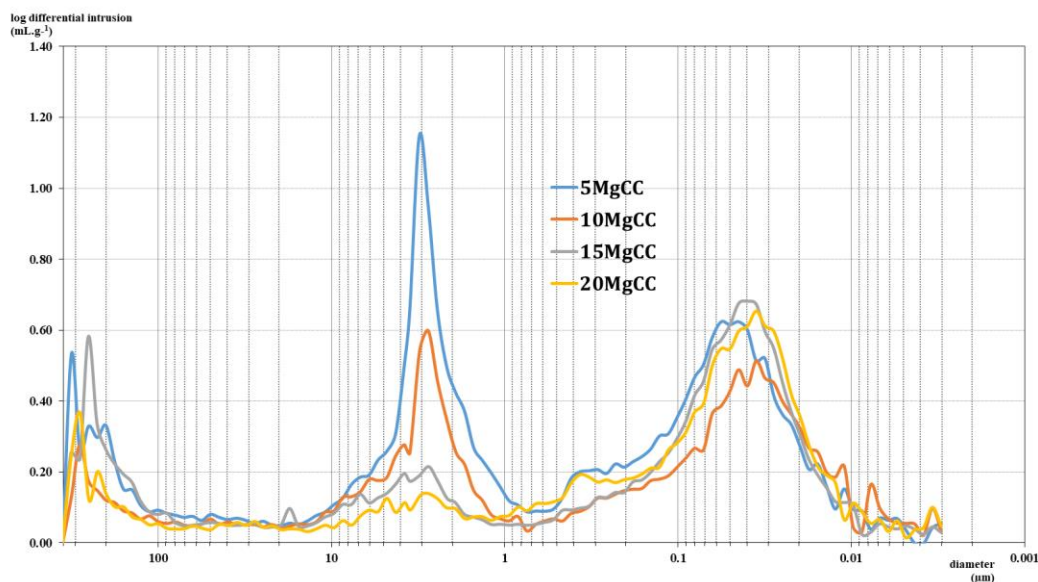


Fig. 2b Pore size distribution resulted from Hg porosimetry analysis of the 4 composites.

XRD is a powerful method to investigate the eventual presence of crystalline impurities on the biochar and to identify the salt hydrate phases. The XRD patterns of all samples (**Fig. 3**) display an amorphous graphite peak at $23^\circ 2\theta$. This peak is less visible in the most charged sample (20MgCC). Three tiny sharp peaks can be identified at 28° , 30° and $40^\circ 2\theta$ in the XRD pattern of the biochar support, which were assigned to Sylvite KCl. Prakongkep et al. (Prakongkep et al. 2015) investigated 14 biochars made from agricultural wastes like corn cobs and found that K-minerals are contained in most of them, including Sylvite KCl. However, those peaks were no anymore present in the XRD patterns of the composites. KCl was probably removed or overlapped during the MgSO_4 impregnation procedure. According to the database of X'Pert HighScore Plus software, the XRD patterns of the 15MgCC and 20MgCC samples showed sharp crystallinity diffraction peaks that were identified as $\text{MgSO}_4 \cdot 1.25\text{H}_2\text{O}$ (Ref. Code: 00-028-0631), indicating that the dehydration at 150°C was partial, as expected (van Essen et al. 2009). The intensity of the diffraction peaks indicates that more $\text{MgSO}_4 \cdot 1.25\text{H}_2\text{O}$ crystallites were found in the 20MgCC sample. This can be explained by the fact that

more salt was deposited on the surface of the biochar, resulting in clusters or thicker layers of MgSO_4 salt that are more difficult to dehydrate. It should be noted that, to our knowledge, no literature has illuminated the formation of $\text{MgSO}_4 \cdot 1.25\text{H}_2\text{O}$ (Ref. Code: 00-028-0631) on supported MgSO_4 . The confinement of the salt into the porous structure of biochar might be the reason for the stabilization of this phase.

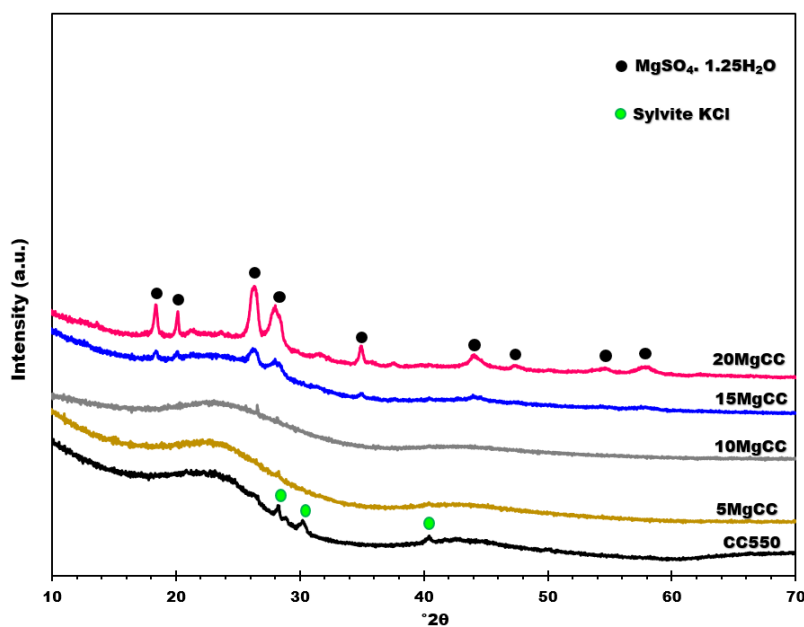


Fig. 3 XRD patterns of CC550 and its composites.

SEM analyses were performed to investigate the morphology and salt deposition homogeneity on the biochar surface. According to Fig. 4, an irregular macropore network is observed, which confirms the results of Hg porosimetry. SEM analyses were also performed for the synthesized composites, and for further information, EDX mapping was conducted to analyze the salt distribution at the biochar surface. As shown in Fig. 5, for the 5MgCC composite, the MgSO_4 salt was deposited both on the external surface as well as inside the macropores. When the salt loading content started to increase, the macropore entrance became less and less accessible, as it can be observed by the SEM picture in Fig. 5 for the different composites at increasing salt content. EDX mapping showed in each case a homogeneous deposition of the salt on the external surface. Unfortunately, it is not possible to visualize the salt inside the pores: due to the deepness the electron beams cannot probe the internal surface (see Fig. S1-S4 in Supplementary Information file).

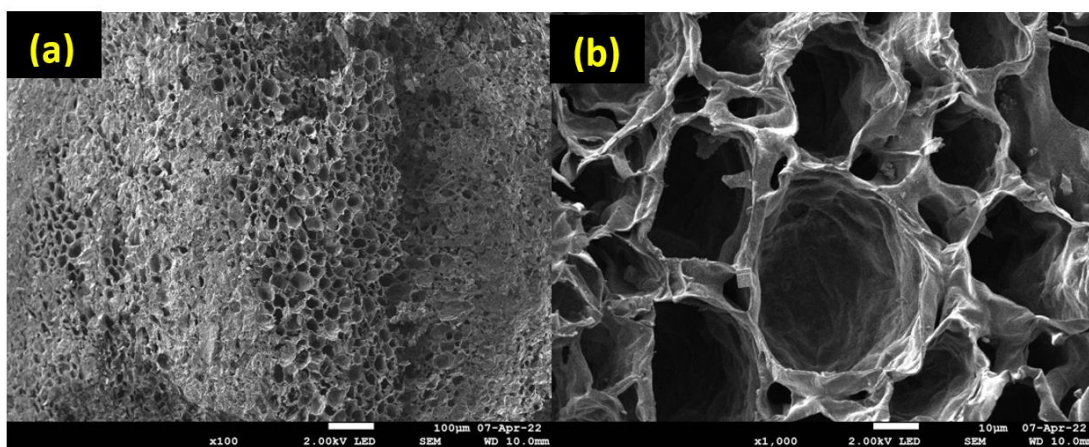


Fig. 4 SEM images of CC550.

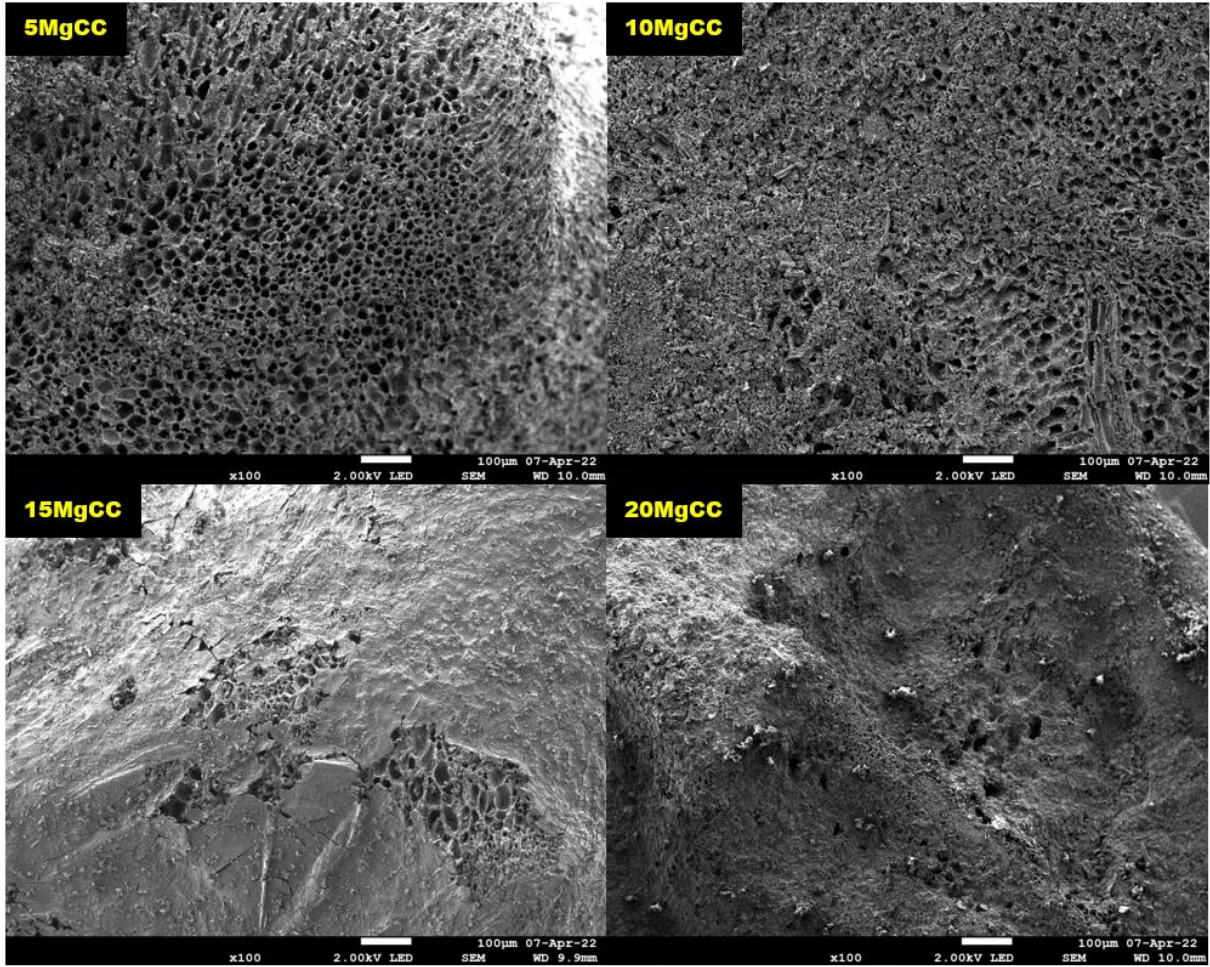


Fig. 5 SEM images of the synthesized composites at different salt content.

3.2 TG-DSC analysis for hydration behaviors

The heat of hydration (Fig. 6a) and the water adsorption capacity (designated as “ w_e ” in Equation (1)) (Fig. 6b) were calculated from the variation of the heat flow and the mass of the sample as a function of time.

$$w_e = \frac{m_h - m_d}{m_d} \quad (1)$$

where w_e is the water adsorption capacity ($\text{g}_{\text{H}_2\text{O}}/\text{g}_{\text{sample}}$ or g/g in short), m_h (g) and m_d (g) correspond respectively to the final mass of the hydrated sample and the dehydrated sample.

The biochar support CC550 adsorbed 0.07 g of water per gram of dry composite with a corresponding heat release of 183 J/g. The 5MgCC composite with 4.4 % MgSO_4 released 360 J/g of energy (water adsorption 0.126 g/g). As the salt concentration increased up to 19.5 % (20MgCC composite), the heat production and the water uptake of the composites continue to increase to over 635 J/g and 0.235 g/g in water adsorption capacity for the 20MgCC composite. By the observation of the hydration curves, it can be observed the hydration process is relatively fast and that the isotherms quickly reach a plateau respectively after 2 and 3 hours for the support and the 5MgCC composite. Differently, the beginning of the hydration process presents a lower rate (lower slope of the isotherm) for the other composites; even after 8 hours of hydration, the plateau (complete hydration) was not attained.

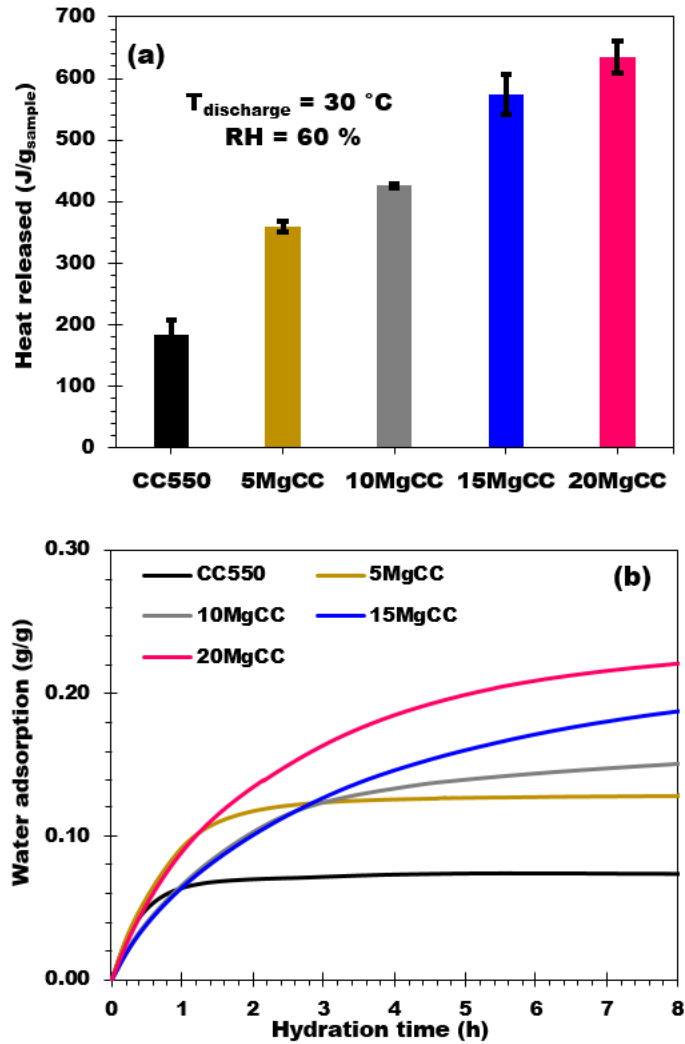


Fig. 6 (a) Hydration behavior and (b) Water adsorption curves of biochar support and synthesized composites ($T_{\text{discharge}} = 30\text{ }^{\circ}\text{C}$; RH = 60 %; 8 h of hydration)

Table 2 reports on the heat released by the biochar support and the four composites expressed as J/g_{comp} and J/g_{water} . The heat released by the biochar is close to the water condensation heat (vapor \rightarrow liquid) at $30\text{ }^{\circ}\text{C}$, which is about $2\,400\text{ }J/g_{\text{water}}$ (Ayoub et al. 2014). This means that the heat released by the biochar is related to the condensation of water vapor on the biochar surface. The heat released (in J/g_{water}) by the biochar and related composites is plotted as a function of the salt content in Fig. 7a. The curve shows an increasing trend which tends to reach a value between $2\,900$ and $3\,200\text{ }J/g_{\text{water}}$ (Grevel et al. 2012) corresponding to the hydration of the salt from monohydrate to hexahydrate and from monohydrate to heptahydrate, respectively. From this observation, one can conclude that after the hydration process, the final hydration state is between 6 and 7 molecules of water. Similar to the heat release behaviour, the water adsorption has also been plotted as a function of the salt content, showing a linear increasing trend (Fig. 7b). These results prove that all the composites adsorb water vapor in a similar manner regardless the amount of salt deposited on the biochar support (no apparent mass transfer limitation).

Table 2 Heat released during the hydration of the biochar and its composites

Sample	Heat released (J/g_{comp})	Heat released ($J/g_{\text{H}_2\text{O}}$)
CC	183	2607
5MgCC	360	2854
10MgCC	426	2940
15MgCC	574	3031
20MgCC	635	3100

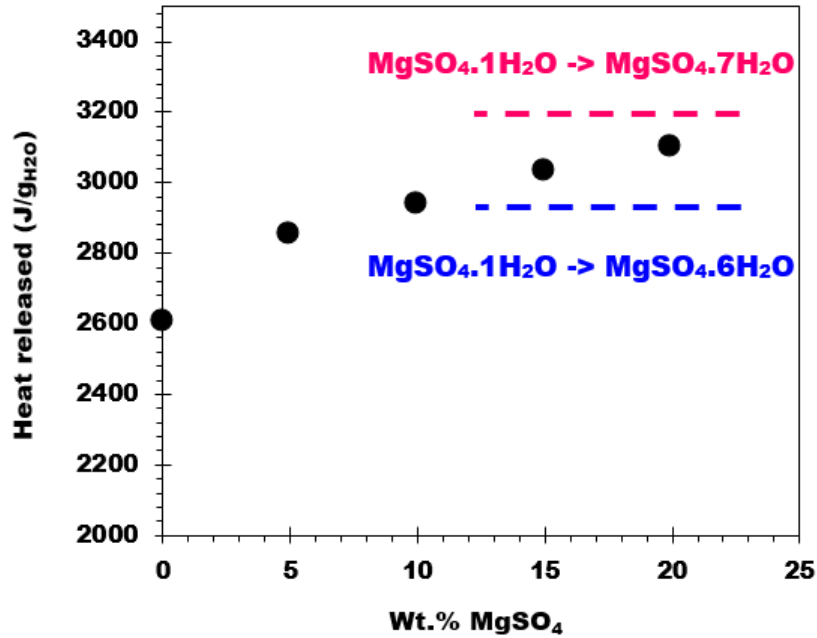


Fig. 7a Heat released (J/g water) as a function of the salt content.

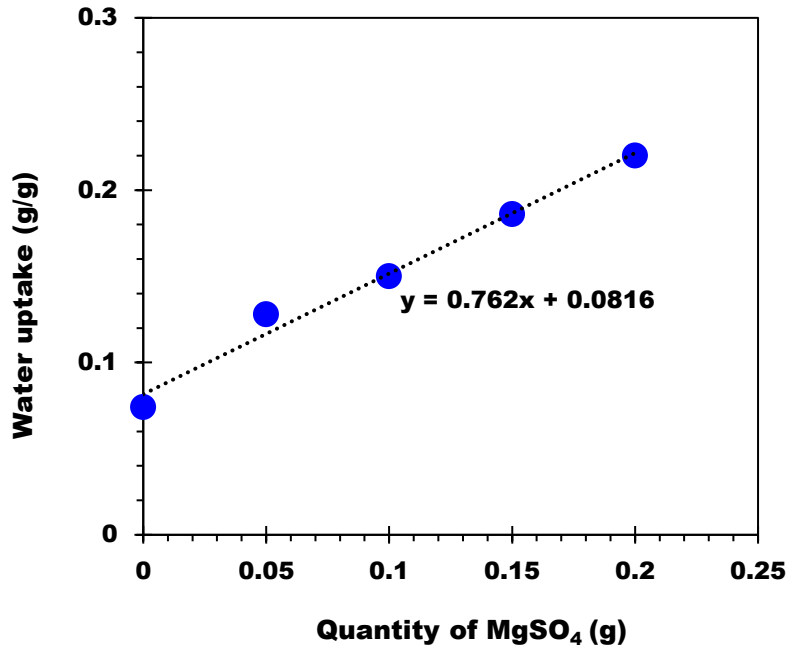


Fig. 7b Water uptake of the materials as a function of the salt content

Table 3 compares the performance of the 20MgCC sample with other composite storage materials (also impregnated with MgSO₄) reported in the literature. Supporting MgSO₄ on the corncob biochars seems to give origin to composites with a higher heat storage capacity than other composites previously reported (even when containing higher quantities of salt).

Table 3 Comparison of 20MgCC with other sulfate-based composited in the literatures.

Composite materials	Operating conditions	Energy storage density (J/g)	Reference	Year
20MgCC	T _{hyd} = 30 °C; RH = 60 %	635	This work	2022
20-MgSO ₄ /HAP	T _{hyd} = 30 °C; RH = 60 %	464	(Nguyen et al. 2022)	2022
		773		
60-MgSO ₄ /Diatomite (D60)	T _{hyd} = 25 °C; RH = 80 %		(Zhang et al. 2021)	2021
50-MgSO ₄ /Expanded graphite (EG50)	T _{hyd} = 25 °C; RH = 85 %	496.4	(Miao et al. 2021)	2021
MgSO ₄ /13x with %MgSO ₄ up to 20 %	T _{hyd} = 25 °C; RH = 60 %	510–575	(Wang et al. 2019)	2019
MgSO ₄ /zeolite Modernite	T _{hyd} = 22 °C; RH = 56 %	507	(Whiting et al. 2013)	2013

3.3 Hydration kinetic modeling

Various kinetic models are available in the literature and have been applied for the study of the kinetics of hydration of sorbernt materials (Wang and Guo 2020). Among the models, the intra-particle diffusion model (**Fig. 8a**), described by the equation here below, achieves good numerical approximations when applied to the hydration of biochar and related composites and better describes the physical phenomena involved during the water uptake.

$$q_t = k_i * t^{0.5} + C$$

with k_i intra-particle diffusion rate constant ($\text{g} \cdot \text{g}^{-1} \cdot \text{h}^{-0.5}$)
 t the hydration time (h)
 C represents the material transfer resistance (g/g)

This model assumes the diffusion of water on composites with a homogeneous dispersion of the salt. As shown in **Fig. 8b**, the amount of water adsorbed is a linear function of the square root of the hydration time for all the materials. The intra-particle diffusion rate constant of each material was then deduced and showed a similar outcome between 0.09 and 0.11, for all samples. These results validate the model assumptions and confirm that the intra-particle model provides a good description of the hydration phenomena for this type of materials.

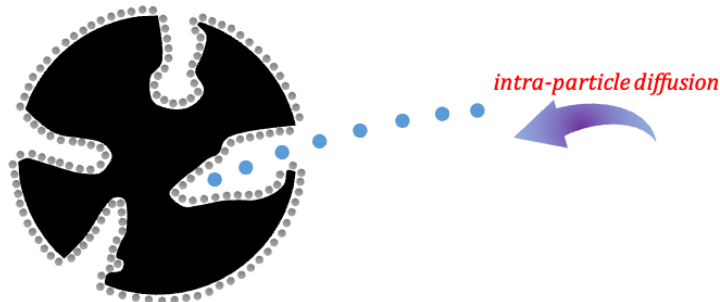


Fig. 8a Representation of the intra-particle diffusion model.

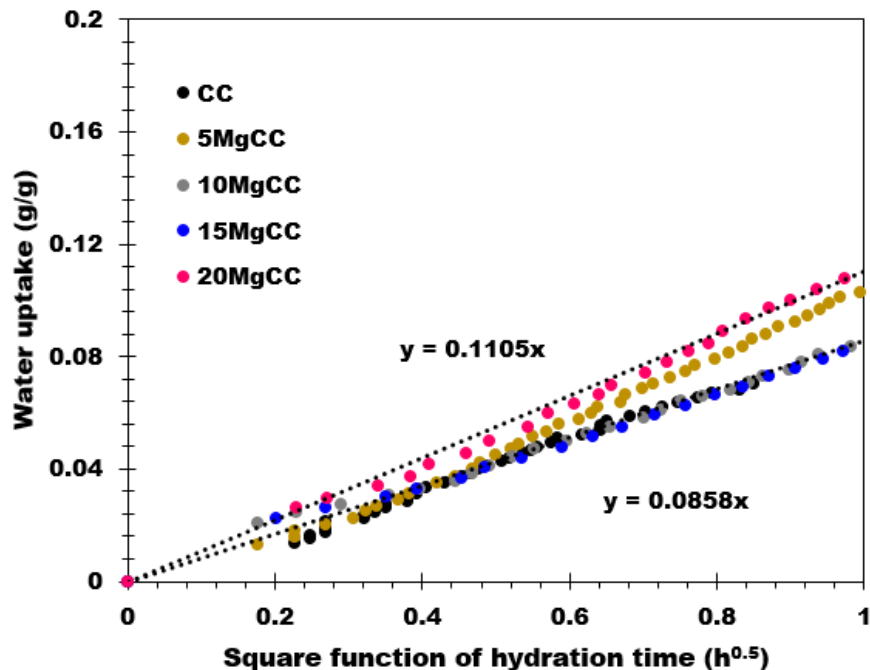


Fig. 8b Water uptake as a function of the square root of the hydration time.

3.4 Cyclability and Stability

In order to test the cyclability of the best-performing composite, the 20MgCC sample was submitted to 6 consecutive cycles of hydration (30 °C and an RH of 60%) and dehydration (150 °C). The heat released after each cycle was recorded and compared to the previous ones in order to check if the hydration behaviour was the same. **Figure 9** shows a negligible variation in the heat released and water uptake, confirming the good cyclability of the composite. **Figure 10** shows the EDX images after 6 cycles of 20MgCC. The salt remained still well dispersed on the support, confirming the stability of the synthesized 20MgCC composite.

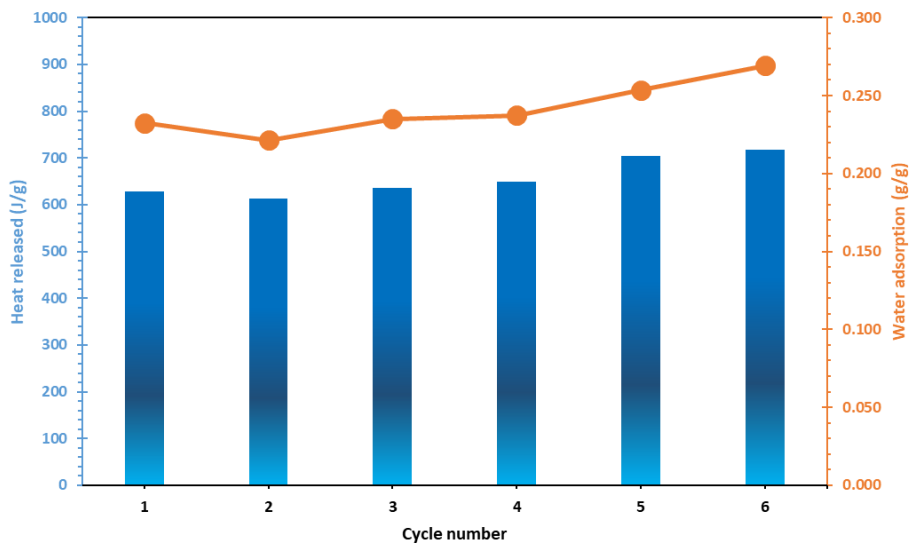


Fig. 9 Heat released of the composite 20MgCC for 6 successive cycles of dehydration/hydration.

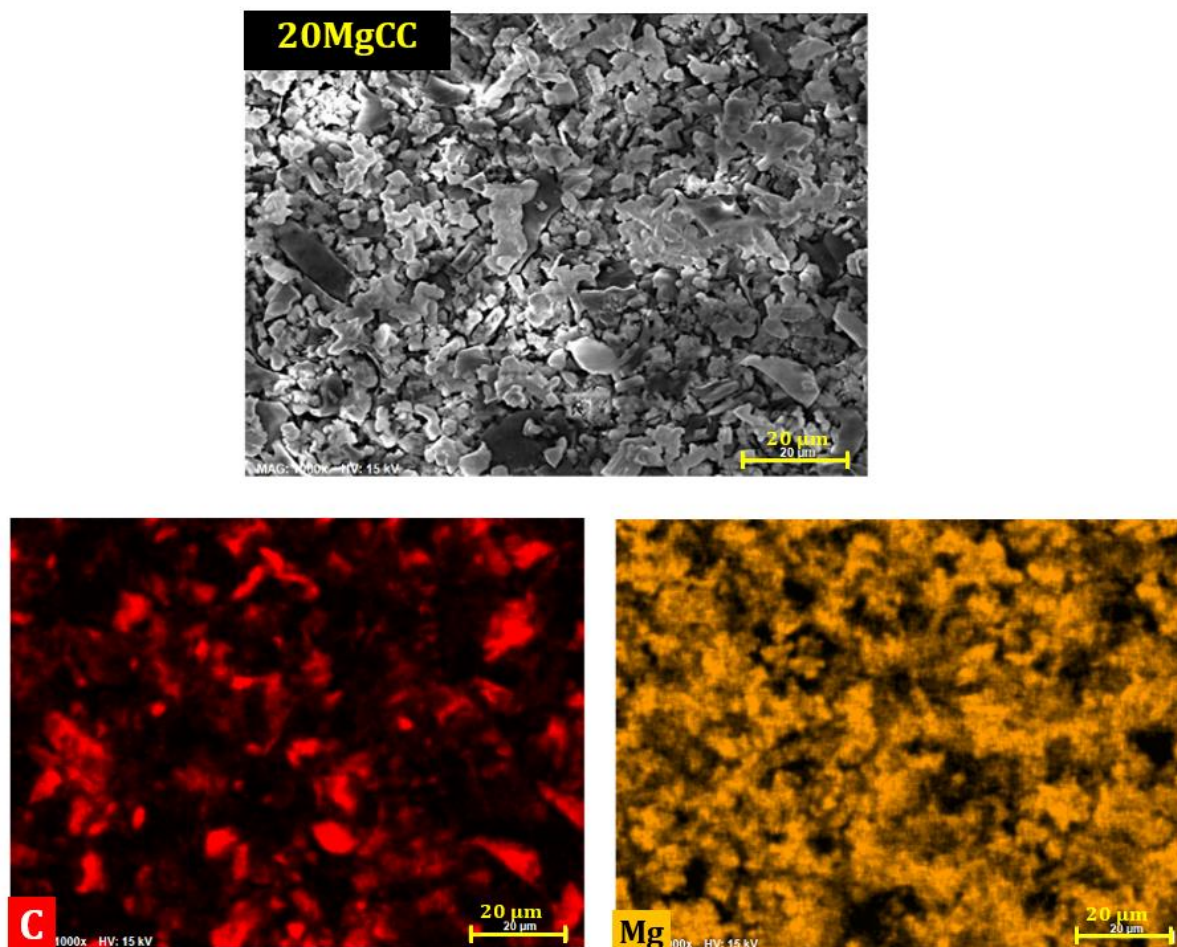


Fig. 10 SEM/EDX images of the composite 20MgCC after 6 cycles.

4 Conclusions

In this work, we synthesized a novel series of composites based on an agriculture waste (corn cob) to be applied as long-term heat storage material. The composites were synthesized by impregnating MgSO_4 onto the corn cob biochar and then characterized by a series of physico-chemical techniques (XRD, BET, SEM). The CO_2 sorption results show that the support has a small microporous surface ($175 \text{ m}^2/\text{g}$), and that present an enhanced macroporous structure. This feature can potentially allow to homogeneously deposit a larger quantity of salt. The 20MgCC composite with an energy storage density of 635 J/g ($T_{\text{ads}} = 30 \text{ }^\circ\text{C}$ and $\text{RH} = 60 \%$) was the best performant composite of the prepared series. The mechanism of the hydration of the synthesized composites results well described by the intra-particle model, where the molecule of water diffuses through a homogeneous layer of salt deposited on the surface and inside the larger pores. Moreover, the cyclability of the $\text{MgSO}_4/\text{biochar}$ composites was confirmed on the 20MgCC composite that resultant still stable after 6 hydration/dehydration cycles.

Finally, the good results obtained using biosourced materials (corn cob derived biochar) as a constituent of heat storage composites demonstrate the possibility of pushing the green management of thermal energy even further. Given the impact of material precursors on carbon footprint, the ability to apply circular economy practices to biomass supply, and overall system sustainability, it becomes critical for the long-term development of the thermochemical heat storage sector. The large availability of biomass types to produce biochars opens a new way in the research of more environmentally friendly heat storage materials.

Author's contributions

M. H. N., M. Z., S. B., contributed to Methodology, conceptualization and Writing—Original Draft Preparation; S. B., L. L., P. D., Review & Editing—Supervision, S. B., Projects conceptualization, granting and management. The published version of the manuscript has been read and approved by all authors.

Declarations

Data availability

All data generated or used during the study appear in the submitted article.

Funding

- Region Grand Est for contributing to Mr. Minh Hoang Nguyen's thesis grant and for financing the purchase of the TG-DSC equipment for the "STOCKFATAL" project.
- Carnot MICA and Region Grand Est for financing a part of this research through the STOCKENER project.
- IS2M for M. Zbair postdoctoral grant under the "Projets Structurants" call.

Acknowledgements

The authors would like to thank the Carnot Institutes MICA(France) for supporting a part of this study within the STOCKENER; Region Grand Est (France) for providing funding for the acquisition of the TG-DSC equipment, in the frame of STOCKFATAL project, and financing a part of the PhD-grant of Mr. Minh Hoang Nguyen.

The IS2M technical platforms were used for all physicochemical characterizations. The authors sincerely appreciate the assistance of L. Michelin (XRF), L. Josien (SEM+EDX), and C. Vaultot (CO₂ adsorption).

Competing interests

The authors declare that they have no known competing financial interests or personal relationships that could have appeared to influence the work reported in this paper.

References

- Ahmad M, Rajapaksha AU, Lim JE, et al (2014) Biochar as a sorbent for contaminant management in soil and water: A review. *Chemosphere* 99:19–33. <https://doi.org/10.1016/j.chemosphere.2013.10.071>
- Ayou DS, Currás MR, Salavera D, et al (2014) Performance analysis of absorption heat transformer cycles using ionic liquids based on imidazolium cation as absorbents with 2,2,2-trifluoroethanol as refrigerant. *Energy Convers Manag* 84:512–523. <https://doi.org/10.1016/j.enconman.2014.04.077>
- Bennici S, Dutournié P, Cathalan J, et al (2022) Heat storage: Hydration investigation of MgSO₄/active carbon composites, from material development to domestic applications scenarios. *Renew Sustain Energy Rev* 158:112197. <https://doi.org/10.1016/j.rser.2022.112197>
- Bruckman VJ, Varol EA, Liu J, Uzun BB (2016) *Biochar*. Cambridge University Press
- Cabeza LF, de Gracia A, Zsembinszki G, Borri E (2021) Perspectives on thermal energy storage research. *Energy* 231:120943. <https://doi.org/10.1016/j.energy.2021.120943>
- Carrillo AJ, González-Aguilar J, Romero M, Coronado JM (2019) Solar Energy on Demand: A Review on High Temperature Thermochemical Heat Storage Systems and Materials. *Chem Rev* 119:4777–4816. <https://doi.org/10.1021/acs.chemrev.8b00315>
- Chen Y, Guo X, Liu A, et al (2021) Recent progress in biomass-derived carbon materials used for secondary batteries. *Sustain Energy Fuels* 5:3017–3038. <https://doi.org/10.1039/D1SE00265A>
- Deng J, Li M, Wang Y (2016) Biomass-derived carbon: synthesis and applications in energy storage and conversion. *Green Chem* 18:4824–4854. <https://doi.org/10.1039/C6GC01172A>

- Donkers PAJ, Sögütöglü LC, Huinink HP, et al (2017) A review of salt hydrates for seasonal heat storage in domestic applications. *Appl Energy* 199:45–68. <https://doi.org/10.1016/j.apenergy.2017.04.080>
- El-Naggar A, Lee SS, Rinklebe J, et al (2019) Biochar application to low fertility soils: A review of current status, and future prospects. *Geoderma* 337:536–554. <https://doi.org/10.1016/j.geoderma.2018.09.034>
- Fang Y, Singh B, Singh BP (2015) Effect of temperature on biochar priming effects and its stability in soils. *Soil Biol Biochem* 80:136–145. <https://doi.org/10.1016/j.soilbio.2014.10.006>
- Freddo A, Cai C, Reid BJ (2012) Environmental contextualisation of potential toxic elements and polycyclic aromatic hydrocarbons in biochar. *Environ Pollut* 171:18–24. <https://doi.org/10.1016/j.envpol.2012.07.009>
- Frikha K, Limousy L, Arif MB, et al (2021) Exhausted Grape Marc Derived Biochars: Effect of Pyrolysis Temperature on the Yield and Quality of Biochar for Soil Amendment. *Sustainability* 13:11187. <https://doi.org/10.3390/su132011187>
- Giudicianni P, Cardone G, Ragucci R (2013) Cellulose, hemicellulose and lignin slow steam pyrolysis: Thermal decomposition of biomass components mixtures. *J Anal Appl Pyrolysis* 100:213–222. <https://doi.org/10.1016/j.jaap.2012.12.026>
- Grevel KD, Majzlan J, Benisek A, et al (2012) Experimentally determined standard thermodynamic properties of synthetic $\text{MgSO}_4 \cdot 4\text{H}_2\text{O}$ (Starkeyite) and $\text{MgSO}_4 \cdot 3\text{H}_2\text{O}$: A revised internally consistent thermodynamic data set for magnesium sulfate hydrates. *Astrobiology* 12:1042–1054. <https://doi.org/10.1089/ast.2012.0823>
- Gunasekaran SS, Elumalali SK, Kumaresan TK, et al (2018) Partially graphitic nanoporous activated carbon prepared from biomass for supercapacitor application. *Mater Lett* 218:165–168. <https://doi.org/10.1016/j.matlet.2018.01.172>
- Hou J, Jiang K, Tahir M, et al (2017) Tunable porous structure of carbon nanosheets derived from puffed rice for high energy density supercapacitors. *J Power Sources* 371:148–155. <https://doi.org/10.1016/j.jpowsour.2017.10.045>
- Jaswal R, Shende A, Nan W, et al (2019) Hydrothermal Liquefaction and Photocatalytic Reforming of Pinewood (*Pinus ponderosa*)-Derived Acid Hydrolysis Residue for Hydrogen and Bio-oil Production. *Energy & Fuels* 33:6454–6462. <https://doi.org/10.1021/acs.energyfuels.9b01071>
- Kaltschmitt M (2013) Renewable Energy Renewable Energy from Biomass renewable energy from Biomass , Introduction. In: *Renewable Energy Systems*. Springer New York, New York, NY, pp 1393–1396
- Kambo HS, Dutta A (2015) A comparative review of biochar and hydrochar in terms of production, physico-chemical properties and applications. *Renew Sustain Energy Rev* 45:359–378. <https://doi.org/10.1016/j.rser.2015.01.050>
- Lin J, Zhao Q, Huang H, et al (2021) Applications of low-temperature thermochemical energy storage systems for salt hydrates based on material classification: A review. *Sol Energy* 214:149–178. <https://doi.org/10.1016/j.solener.2020.11.055>
- Linnow K, Niermann M, Bonatz D, et al (2014) Experimental Studies of the Mechanism and Kinetics of Hydration Reactions. *Energy Procedia* 48:394–404. <https://doi.org/10.1016/j.egypro.2014.02.046>
- Liu H, Wang W, Zhang Y (2021) Performance gap between thermochemical energy storage systems based on salt hydrates and materials. *J Clean Prod* 313:127908. <https://doi.org/10.1016/j.jclepro.2021.127908>
- Liu W-J, Jiang H, Yu H-Q (2019) Emerging applications of biochar-based materials for energy storage and conversion. *Energy Environ Sci* 12:1751–1779. <https://doi.org/10.1039/C9EE00206E>
- Ma L-L, Hu X, Liu W-J, et al (2021) Constructing N, P-dually doped biochar materials from biomass wastes for high-performance bifunctional oxygen electrocatalysts. *Chemosphere* 278:130508. <https://doi.org/10.1016/j.chemosphere.2021.130508>

Ma Y, Yao D, Liang H, et al (2020) Ultra-thick wood biochar monoliths with hierarchically porous structure from cotton rose for electrochemical capacitor electrodes. *Electrochim Acta* 352:136452. <https://doi.org/10.1016/j.electacta.2020.136452>

Miao Q, Zhang Y, Jia X, et al (2021) MgSO₄-expanded graphite composites for mass and heat transfer enhancement of thermochemical energy storage. *Sol Energy* 220:432–439. <https://doi.org/10.1016/j.solener.2021.03.008>

N'Tsoukpoe KE, Schmidt T, Rammelberg HU, et al (2014) A systematic multi-step screening of numerous salt hydrates for low temperature thermochemical energy storage. *Appl Energy* 124:1–16. <https://doi.org/10.1016/j.apenergy.2014.02.053>

Nanda S, Dalai AK, Berruti F, Kozinski JA (2016) Biochar as an Exceptional Bioresource for Energy, Agronomy, Carbon Sequestration, Activated Carbon and Specialty Materials. *Waste and Biomass Valorization* 7:201–235. <https://doi.org/10.1007/s12649-015-9459-z>

Nguyen MH, Zbair M, Dutournié P, et al (2022) Toward new low-temperature thermochemical heat storage materials: Investigation of hydration/dehydration behaviors of MgSO₄/Hydroxyapatite composite. *Sol Energy Mater Sol Cells* 240:111696. <https://doi.org/10.1016/j.solmat.2022.111696>

Prakongkep N, Gilkes RJ, Wiriyakitnateekul W (2015) Forms and solubility of plant nutrient elements in tropical plant waste biochars. *J Plant Nutr Soil Sci* 178:732–740. <https://doi.org/10.1002/jpln.201500001>

Saning A, Herou S, Dechtrirat D, et al (2019) Green and sustainable zero-waste conversion of water hyacinth (*Eichhornia crassipes*) into superior magnetic carbon composite adsorbents and supercapacitor electrodes. *RSC Adv* 9:24248–24258. <https://doi.org/10.1039/C9RA03873F>

Senthil C, Lee CW (2021) Biomass-derived biochar materials as sustainable energy sources for electrochemical energy storage devices. *Renew Sustain Energy Rev* 137:110464. <https://doi.org/10.1016/j.rser.2020.110464>

Sheldon RA (2014) Green and sustainable manufacture of chemicals from biomass: state of the art. *Green Chem* 16:950–963. <https://doi.org/10.1039/C3GC41935E>

Suárez-Abelenda M, Kaal J, McBeath A V. (2017) Translating analytical pyrolysis fingerprints to Thermal Stability Indices (TSI) to improve biochar characterization by pyrolysis-GC-MS. *Biomass and Bioenergy* 98:306–320. <https://doi.org/10.1016/j.biombioe.2017.01.021>

Tan X, Liu S, Liu Y, et al (2017) Biochar as potential sustainable precursors for activated carbon production: Multiple applications in environmental protection and energy storage. *Bioresour Technol* 227:359–372. <https://doi.org/10.1016/j.biortech.2016.12.083>

Tkemaladze GS, Makhashvili KA (2016) Climate changes and photosynthesis. *Ann Agrar Sci* 14:119–126. <https://doi.org/10.1016/j.aasci.2016.05.012>

Tursi A (2019) A review on biomass: importance, chemistry, classification, and conversion. *Biofuel Res J* 6:962–979. <https://doi.org/10.18331/BRJ2019.6.2.3>

Ulusal A, Apaydın Varol E, Bruckman VJ, Uzun BB (2021) Opportunity for sustainable biomass valorization to produce biochar for improving soil characteristics. *Biomass Convers Biorefinery* 11:1041–1051. <https://doi.org/10.1007/s13399-020-00923-7>

van Essen VM, Zondag HA, Gores JC, et al (2009) Characterization of MgSO₄ Hydrate for Thermochemical Seasonal Heat Storage. *J Sol Energy Eng* 131:. <https://doi.org/10.1115/1.4000275>

Wang J, Guo X (2020) Adsorption kinetic models: Physical meanings, applications, and solving methods. *J Hazard Mater* 390:122156. <https://doi.org/10.1016/j.jhazmat.2020.122156>

Wang Q, Xie Y, Ding B, et al (2019) Structure and hydration state characterizations of MgSO₄-zeolite 13x composite materials for long-term thermochemical heat storage. *Sol Energy Mater Sol Cells* 200:110047. <https://doi.org/10.1016/j.solmat.2019.110047>

Whiting G, Grondin D, Bennici S, Auroux A (2013) Heats of water sorption studies on zeolite–MgSO₄ composites as potential thermochemical heat storage materials. *Sol Energy Mater Sol Cells* 112:112–119. <https://doi.org/10.1016/j.solmat.2013.01.020>

Xu J, Li T, Yan T, et al (2021) Dehydration kinetics and thermodynamics of magnesium chloride hexahydrate for thermal energy storage. *Sol Energy Mater Sol Cells* 219:110819. <https://doi.org/10.1016/j.solmat.2020.110819>

Zhair M, Bennici S (2021) Survey Summary on Salts Hydrates and Composites Used in Thermochemical Sorption Heat Storage: A Review. *Energies* 14:3105. <https://doi.org/10.3390/en14113105>

Zhang Y, He M, Wang L, et al (2022) Biochar as construction materials for achieving carbon neutrality. *Biochar* 4:59. <https://doi.org/10.1007/s42773-022-00182-x>

Zhang Y, Miao Q, Jia X, et al (2021) Diatomite-based magnesium sulfate composites for thermochemical energy storage: Preparation and performance investigation. *Sol Energy* 224:907–915. <https://doi.org/10.1016/j.solener.2021.05.054>

Zhao Q, Lin J, Huang H, et al (2022) Enhancement of heat and mass transfer of potassium carbonate-based thermochemical materials for thermal energy storage. *J Energy Storage* 50:104259. <https://doi.org/10.1016/j.est.2022.104259>

Zheng T, Ouyang S, Zhou Q (2023) Synthesis, characterization, safety design, and application of NPs@BC for contaminated soil remediation and sustainable agriculture. *Biochar* 5:5. <https://doi.org/10.1007/s42773-022-00198-3>

‘Corn cobs’ biochar as a macroporous host of salt hydrates for heat storage applications

Minh Hoang Nguyen^{a,b}, Mohamed Zbair^{a,b}, Patrick Dutournié^{a,b}, Lionel Limousy^{a,b}, and Simona Bennici^{a,b*}

^a Institut de Science des Matériaux de Mulhouse (IS2M), Université de Haute-Alsace, CNRS, IS2M UMR 7361, F-68100 Mulhouse, France; minh-hoang.nguyen@uha.fr; mohamed.zbair@uha.fr; patrick.dutournié@uha.fr; simona.bennici@uha.fr

^b Université de Strasbourg, France

* Corresponding author, simona.bennici@uha.fr; Tel.: +33 (0)3 89336729

Supplementary Information

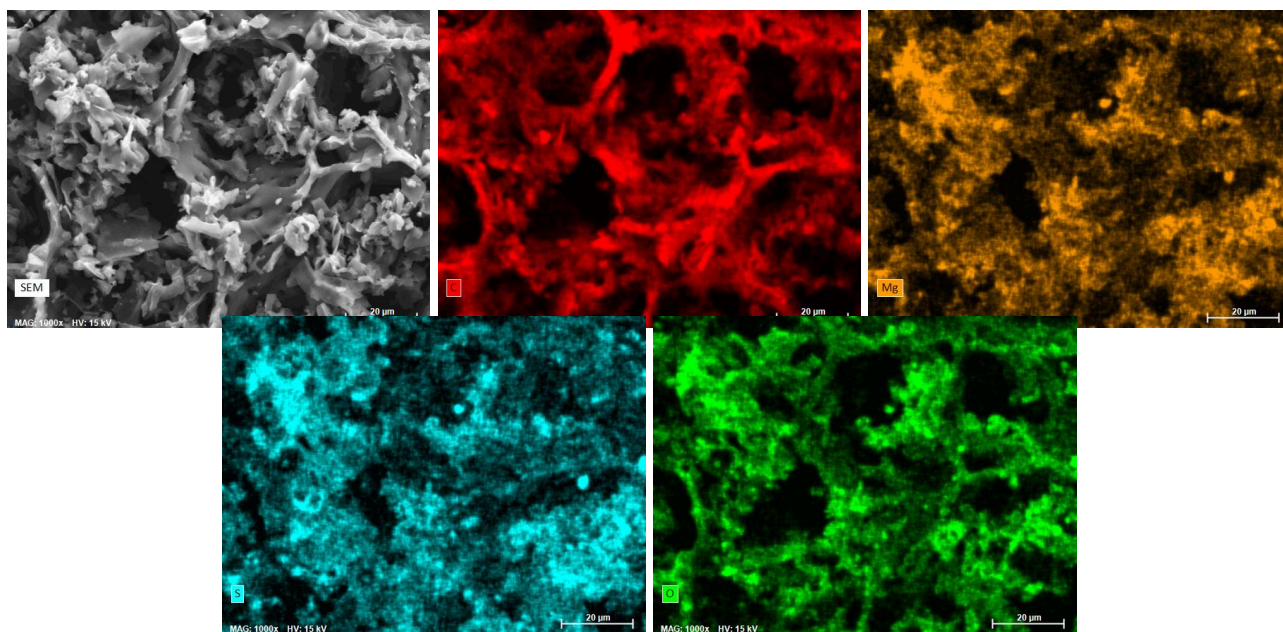


Figure S1. SEM images and EDX mappings of 5MgCC.

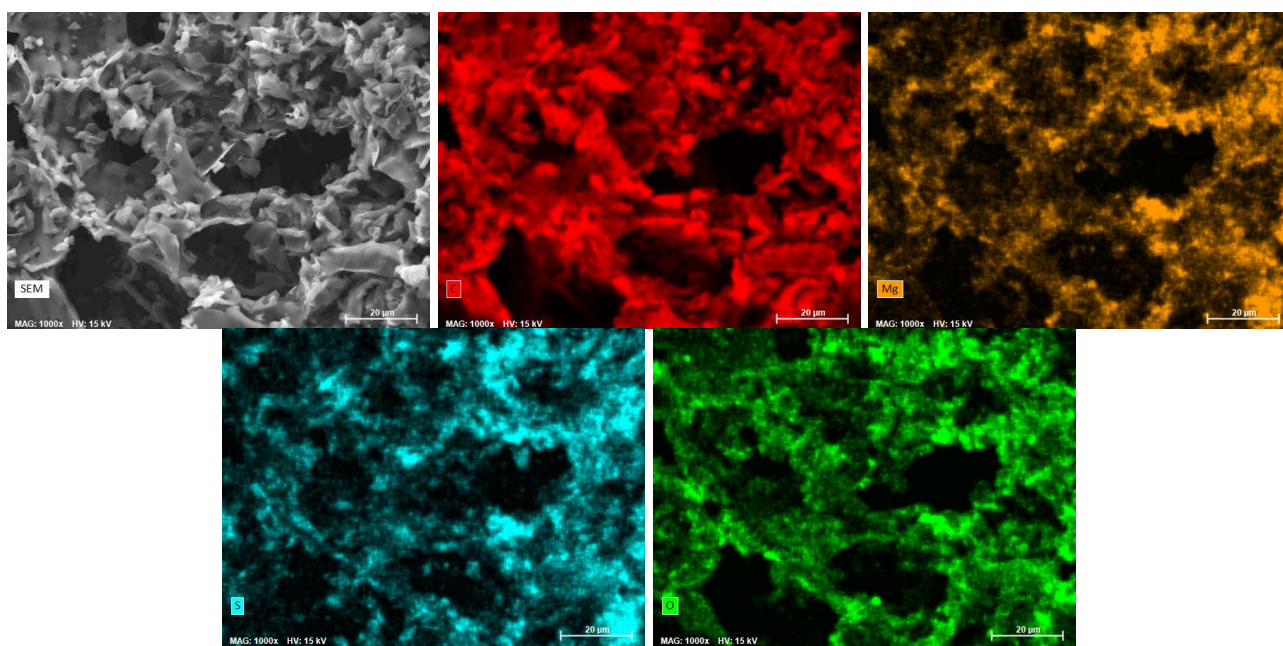


Figure S2. SEM images and EDX mappings of 10MgCC.

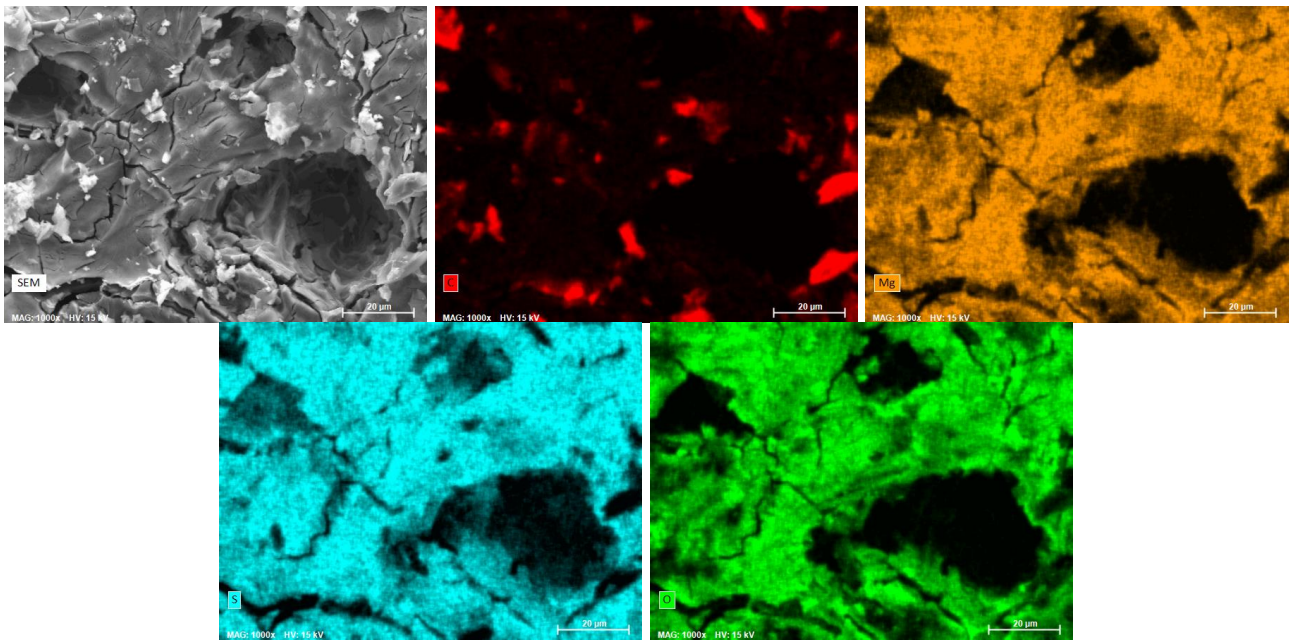


Figure S3. SEM images and EDX mappings of 15MgCC.

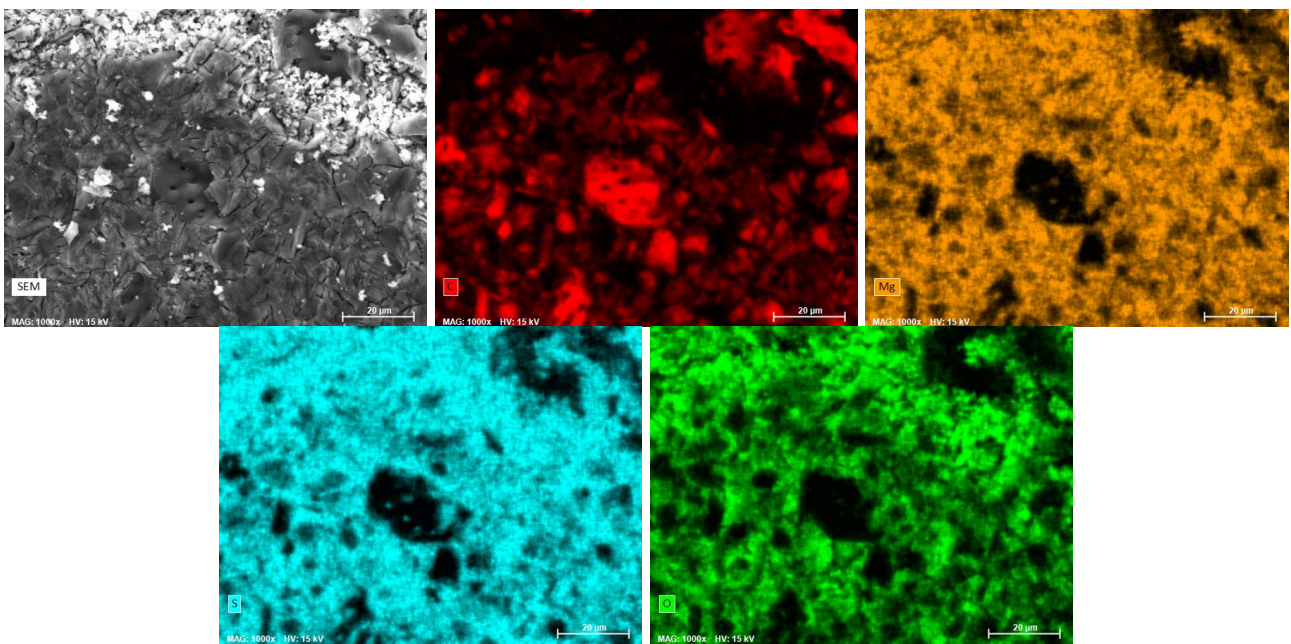


Figure S4. SEM images and EDX mappings of 20MgCC.

Chapter VII

Fast hydration kinetics and remarkable heat storage capacity of new binary salt materials for heat storage applications.

(submitted to Applied Energy)

Résumé

Des granulés de carbone activé commercial F22W ont été choisis comme support en raison de leur surface spécifique élevée, de leur plus grande conductivité thermique comparée à celle d'autres matériaux adsorbants et, bien sûr, pour leur faible coût. Deux séries de composites ont été préparés : l'une contenant classiquement du MgSO_4 (20 %, 40 % et 60 % en masse) et l'autre par imprégnation de deux sels hydratés (MgSO_4 et MgCl_2 en proportion 4 :1 et avec les mêmes concentrations totales en sels choisies pour la série contenant le MgSO_4 seul). L'analyse des isothermes d'adsorption / désorption d'azote montre que tous ces composites sont des matériaux microporeux. La surface spécifique du carbone activé F22W est de $962 \text{ m}^2/\text{g}$ et diminue à $405 \text{ m}^2/\text{g}$ pour le composite mono-sel contenant 60 % de MgSO_4 et à $188 \text{ m}^2/\text{g}$ pour le composite bi-sels contenant 60 % du mélange ($\text{MgSO}_4 + \text{MgCl}_2$). Les résultats de sorption d'eau montrent que, pour une même teneur en sel, la présence de MgCl_2 améliore les performances du composite de 24 %. Pour des conditions de réhydratation expérimentales de $30 \text{ }^\circ\text{C}$ et 60 % d'humidité relative, les molécules de MgCl_2 sont théoriquement sous forme hydratées (l'humidité relative de déliquescence à $30 \text{ }^\circ\text{C}$ est de 33 %) et pouvant potentiellement former une solution saturée. Cette solution pourrait alors servir de chemin préférentiel pour l'eau afin d'atteindre les couches inférieures de MgSO_4 (peu ou pas atteignable dans le cas du sel pur). Cet ajout d'un second sel permet d'exploiter davantage la capacité stockage du MgSO_4 et donc améliore notablement la performance des composites étudiés.

Fast hydration kinetics and remarkable heat storage capacity of new binary salt materials for heat storage applications

Mohamed Zbair^{1,2}, Minh Hoang Nguyen^{1,2}, Patrick Dutournié^{1,2}, Simona Bennici^{1,2*}

¹ Institut de Science des Matériaux de Mulhouse (IS2M), Université de Haute-Alsace, CNRS, IS2M UMR 7361, F-68100 Mulhouse, France; mohamed.zbair@uha.fr; minh-hoang.nguyen@uha.fr; patrick.dutournie@uha.fr; simona.bennici@uha.fr

² Université de Strasbourg, France

*Correspondance : simona.bennici@uha.fr; Tel.: +33 (0)3 89336729

Abstract

Applying thermochemical heat storage (THS) systems is a strategy for solving the temporal mismatch between the recovery and the supply of renewable thermal energy. Salt hydrates are good candidates as storage materials, but they present a main drawback: the maintaining of the storage heat capacity during successive cycles. New composites with improved heat storage capacity were prepared by depositing inorganic salt hydrates on a porous carbon (PC) support. A series of composites based on mono salt (MgSO_4) or binary salt ($\text{MgSO}_4\text{-MgCl}_2$) on PC were studied by thermogravimetric/differential scanning calorimetry (TG/DSC). The effect of the deposition of a mono or binary salt is discussed in terms of structural and textural characteristics, water sorption and heat release capacity. The hydration of the binary salt composites revealed a faster hydration kinetic and water adsorption capacity than those of the mono salt composites. Furthermore, in terms of water uptake, PC_60binary (0.75 g/g) surpassed PC_60MgSO₄ (0.48 g/g). The kinetic investigation revealed that the addition of MgCl₂ improves the mass transfer. Besides, the evolutionary tendency of the heat released follows the same trend as the water uptake. The heat released by PC_60MgSO₄ achieves 52 % (1356 J/g) of that obtained by pure MgSO₄. However, by impregnating PC with 60 % binary salts, the heat produced reached 70 % (1840 J/g) of the heat released by the pure mixed salt, which is an interesting outcome. All of these findings suggest that the newly developed binary salt composites present a remarkable chance to be used in long-term heat storage applications.

Keywords: Thermochemical heat storage; Water sorption; Composite; MgSO₄; MgCl₂

Highlights

- A new composite heat storage material has been synthesized by wet impregnation using porous carbon and two salts (MgSO_4 and MgCl_2).

- The physicochemical properties of prepared composite materials were studied.
- The hydration kinetics and water uptake of various samples were studied.
- The heat released that was achieved is equal to 1840 J/g.
- The binary salt impregnation on carbon enhances mass transfer, water uptake and heat release significantly.

1. Introduction

Any country's socioeconomic development is inextricably tied to its per individual energy consumption. A reasonable and prudent energy consumption is required at the present and in the future. Energy demands are rising on a daily basis as a result of technological advancements and population growth. Due to the scarcity of traditional energy supplies as well as environmental degradation, attempts have been made to find clean, renewable solutions to human energy demands and minimize carbon footprints. Scientists and engineers are currently attempting to develop new energy technologies or upgrade existing ones to make them more efficient.

Solar energy is abundant and widely used in many regions of the world, with significant yearly growth rates [1]. This source of energy may be used for a variety of purposes, including heating, fuel production, and direct power generation. Because of their easy design and installation, solar thermal utilization systems are widely employed. Solar energy's fluctuating and intermittent supply is a significant barrier to its widespread adoption [2]. Thus, thermal energy storage (TES) is a concept that has gained a great deal of attention, because of the importance of balancing heat supply and demand. In general, there are three types of TES: sensible heat storage [3,4], latent heat storage (e.g. phase change materials) [5–7], and thermochemical heat storage (THS) [8–10]. Presenting a very high heat storage density, THS is the most promising technique for low-temperature applications. Furthermore, THS method stores heat nearly without loss, which is advantageous for long-term heat storage [11]. THS is further categorized into two types: thermochemical sorption heat storage and thermochemical reaction heat storage [12]. The adsorbate uptake occurs on the adsorbent surface, which may be operated at a

medium-low temperature [13]. The latter, on the other hand, necessitates a high-temperature heat source ($> 200\text{ }^{\circ}\text{C}$) to generate strong chemical bonding of reactants [14–16]. As a result, thermochemical sorption heat storage is more in line with the goals of industrial waste heat recovery and solar energy usage at medium-low temperatures. Thermochemical sorption heat storage, being a form of THS, also has the benefit of a high heat storage density. Thermochemical sorption can be used for long-term heat storage as well as combined cold and heat storage. Consequently, thermochemical sorption heat storage technology has gotten a lot of interest in the last few years.

Energy storage material development is critical to palliate the energy shortage situation, lowering the use of non-renewable energy, and increasing the energy efficiency [17,18]. The field of energy materials known as TES materials is indeed very critical. During the conversion and consumption of heat, there is frequently a constraint due to the fact that the supply and the demand of energy do not match in time and space. The use of TES material can successfully resolve the aforementioned issue. Inorganic salt hydrates got a lot of interest because of their high heat storage density. The heat storage systems based on pure inorganic salt hydrates, on the other hand, would face issues such as overhydration, deliquescence, and formation of aggregates, resulting in limited heat storage and poor cyclability [18]. Much research has shown that adding hydrated salt into a porous matrix can improve the sorption rate. Furthermore, the porous host matrix has a large pore capacity, allowing the deposition of a considerable quantity of salt, while avoiding deliquescence [19,20]. The use of porous materials has been acclaimed for the possibility to efficiently disperse the salt, to limit the deliquescence phenomena, and to increase mass and heat transfers [21–23]. Aristov team [24] developed a class of novel materials named "hygroscopic salt inside a porous matrix with open pores." The salts are in a distributed state rather than a bulk state, which prevents swelling and agglomeration and speeds up the mass and heat transfers. The pore structure and chemical composition of the host matrix materials have considerably affect the heat storage efficiency of the resulting salt/porous matrix composites [25], implying that the host porous material selection is critical. As a result, sorbent materials such as silica gel [26], hydroxyapatite [27], zeolite [28,29], activated alumina [30], vermiculite [31], MOFs [32], and expanded graphite [33,34] have aroused a lot of interest as a matrix for hydrated salts. Despite the development of a wide range of new composite sorbents for heat storage [16,35–38], there is still a substantial gap between the materials' *design* and their potential implementation.

For instance, many studies have been conducted to investigate the hydration behavior of MgSO_4 -zeolite composites for long-term heat storage [39,40]. It was discovered that the quantity of water sorbed and the heat released during the hydration process are affected by the humidity, the hydration temperature, and the charging temperature [39]. The quantity of sorbed water and the hydration rate of the composites increase significantly as the relative humidity (RH) increases. The hydration extent of MgSO_4 -zeolite composites

decreases when the air temperature rises over 50 °C [40]. Most zeolites have a charging temperature (dehydration temperature) higher than 200 °C and low thermal conductivity, which may limit their use in the presence of low temperature heat sources [41]. Zhang and coworkers [42], synthesized a composite based on mesoporous alumina and LiCl for TES applications with a target charging temperature of 120 °C. The obtained data revealed TES densities up to 1040 J/g. Despite this promising result, only around 15 % of the salt could be loaded into the matrix; the low porosity, limited the possibility of further increasing the TES density. Shi et al. [32] studied 17 continuous adsorption/desorption cycles composites on CaCl₂-based metal-organic frameworks (MOFs); they pointed out a high heat storage (1274 J/g) accompanied to a reasonable stability. Nevertheless, the practical application of MOFs is limited by their low hydrothermal stability [43]. Aristov team [44] investigated the water sorption process on expanded vermiculite/CaCl₂ composites, claiming that impregnation of CaCl₂ into expanded vermiculite may boost the water sorption capacity even at low water vapor pressure. However, the surface area of expanded vermiculite is limited (9 m²/g), making this support inappropriate for salt deposition.

The review of the foregoing literature clearly shows that more advancements need to be accomplished in heat storage materials' *development*. However, numerous shortcomings must be corrected, such as heat and mass transfer limitations and *the materials'* hydration/dehydration cycling.

According to the literature, when designing composites, porosity, both micro and meso, is an absolute requirement. If the pores are too small (ultra-micro- and micro-pores), the salt may occlude them, which prevents water vapor diffusion and reduces the capacity of storing heat. Alternative materials have been also considered, like mesoporous activated carbon [23] and silica gels [45], that have shown to be effective supports. Aside from the high surface area and well developed porosity, a good thermal conductivity is an important factor to consider in the choice of the optimal support. This parameter is crucial for optimizing the heat transfer. The thermal conductivity of activated carbon was found to be significantly higher than that of the other sorbents (silica gels, zeolites, MOFs and so on), reaching up to 0.75 W/(mK).

The idea of using activated carbon as a host matrix for heat storage is of a great interest. The active carbons can be produced easily from waste biomass and is more cost effective than MOFs, silica gel and zeolite. Active carbons are also highly porous with a high thermal stability. Their hydrophilicity can be controlled by choosing the starting material and the pyrolysis conditions. Chemical modification can be also made thanks to the active *carbons'* richly functionalized surface.

Each salt presents its own benefits and drawbacks. Two or three appropriate chemicals may be combined to make a binary/ternary salt mixture with the aim to increase the performance and the stability in heat storage applications. To achieve a good

performance, a hydrothermal stable salt with a high DRH is combined with a little amount of a highly deliquescent salt. Sulfate and chloride are the most adapted choice for making this combination. Chloride is hygroscopic and easy to overhydrate during the hydration reaction, reducing the hydration reaction's stability. Sulfate, on the other hand, present an incomplete hydration reaction and a weak reaction kinetics due to poor water vapor transfer. By combining these two kinds of salts, the dehydrated sulfate is partially dissolved in the chloride hydrated salt solution, resulting in a greater hydration state. This prevents the instability induced by excessive chloride hydration and enhances the kinetics of the sulfate hydration reaction.

To choose the appropriate salt for heat storage systems, the costs, the potential risks for human health or for the environment, the thermostability in the temperature range in which it will be used, and the value of the heat storage density should be considered.

Magnesium sulfate (MgSO_4) has been thoroughly studied and proved to be the most adapted salt hydrate for heat storage system in terms of storage temperature, high heat storage density, ease of use, cheap cost, and nontoxicity. However, due to slow reaction kinetics, the theoretical hydration heat cannot be reached, and the hydration of bulk MgSO_4 is generally incomplete [46]. Furthermore, Hongois et al. [47] found that at 55 °C, $\text{MgSO}_4 \cdot 6\text{H}_2\text{O}$ *undergoes a phase's modification* from crystal to amorphous; the water vapor transport rate is then strongly slowed down. Van Essen et al. [48] demonstrated how RH and temperature have a significant impact on the kinetics of the $\text{MgSO}_4\text{-H}_2\text{O}$ system, despite the fact that no specific kinetic model was evaluated using the acquired experimental data. In the same direction, Linnow et al. [46] noted that the formation of a layer of anhydrous MgSO_4 may give rise to $\text{MgSO}_4 \cdot \text{H}_2\text{O}$ that is difficult to hydrate, thus further decreasing the hydration kinetics. This layer prevents water molecules from reaching the unreacted material, which slows down the reaction. During their investigation of the water migration from MgSO_4 salt crystals, Donkers et al. [49] made the hypothesis that during dehydration, the creation of fissures in the salt creates a pathway for water to leave (dehydration of salt). However, the impacts on the reaction kinetics were not specifically addressed.

As a result, binary salts have been recommended as a solution to this problem. Mixtures of two or more inorganic salts present better kinetic properties than the single salts [50]. $\text{MgSO}_4\text{-Na}_2\text{SO}_4$ [51], and $\text{MgSO}_4\text{-SrCl}_2$ [52] are among the salt hydrates employed to create salt mixtures (supported or not) to produce a new composite family based on MgSO_4 . Rehman et al. compared pure MgSO_4 and ZnSO_4 to MZ_x composites (MgSO_4 : 90% and ZnSO_4 : 10%) and found that the MZ_x composite exhibited 34% and 48% higher hydration of the respective single salts [39].

Magnesium chloride (MgCl_2) [18,29] is usually used as heat storage material and is a strong hygroscopic salt, indicating easy deliquescence. The water sorption mechanism includes hydration, deliquescence, and absorption; MgCl_2 can absorb more water than in

the case of non-deliquescent salts, although the related composites are subjected to liquid leakage. To address these disadvantages, several investigations have combined MgCl_2 with other salts, such as $\text{CaCl}_2\text{-MgCl}_2$ [11], $\text{MgCl}_2\text{-KCl-NaCl}$ [53] and $\text{MgCl}_2\cdot 6\text{H}_2\text{O}$ with $\text{NH}_4\text{Al}(\text{SO}_4)_2\cdot 12\text{H}_2\text{O}$ or $\text{KAl}(\text{SO}_4)_2\cdot 12\text{H}_2\text{O}$ [54]. In order to increase salt cycle stability, Rammelberg et al. [11] mixed various salt hydrates. The results showed that under certain conditions, the cyclability, mass, and enthalpy balances of the produced salt combinations improved notably for the CaCl_2 and MgCl_2 salt hydrate mixtures. Nonetheless, further study should be conducted to find the optimal mixing ratio and better understand the synergies.

Apart from employing pure salts, the most frequent way for improving heat and mass transfer in heat storage materials is to impregnate the salts into a porous matrix. Only a few number of studies deal with mixed salt integrated into a porous matrix. For this reason, the present research is directed to the study of the physicochemical features and hydration kinetics of various composites based on mono (MgSO_4) and binary ($\text{MgSO}_4\text{-MgCl}_2$) prepared on a porous support. The porous matrix considered is a porous carbon. MgSO_4 was selected for its high heat storage density; MgCl_2 to improve the mass transfer. The goals of this paper are to create two series of composites (mono-salt and binary-salts) by impregnating the carbon material with various amounts of MgSO_4 or $\text{MgSO}_4/\text{MgCl}_2$. The quantity of heat released was directly measured for two subsequent cycles of hydration/dehydration. Furthermore, kinetic models were applied to the experimental hydration data in order to better understand the relationship between the examined composites' physicochemical features and the heat released performances.

2. Experimental

2.1. Preparation of composites

The carbon material selected as support is a porous carbon (PC) F22W. First, the PC was washed and filtrated multiple times with abundant water on a Büchner funnel until reaching a steady pH of 6.9 in the filtrate. The PC was then dried in an oven at 150 °C for 12 hours to achieve total dehydration. Then, the composites were prepared by wet-impregnation of a solution of the mono salt (MgSO_4) or of the binary salt (MgSO_4 and MgCl_2). $\text{MgSO}_4\cdot 7\text{H}_2\text{O}$, from Sigma-Aldrich, was deposited at different loadings (from 20 to 60 wt% of MgSO_4). Binary salt impregnation was done by setting the mass proportion of MgCl_2 to 20 % in all preparations (80 % MgSO_4 + 20 % MgCl_2 = 100 %) for a total amount of salt respectively of 20, 40, and 60 wt% (see **Table 1**). Then, the obtained composites were dried for 12 hours at 100 °C. **Fig. 1** summarizes schematically visualize the preparation steps.

Table 1. Description of prepared composites.

Host support	Salt hydrates	Salt content (wt%)	Labelled
Porous carbon (PC)	MgSO ₄ ·7H ₂ O	20	PC_20MgSO ₄
		40	PC_40MgSO ₄
		60	PC_60MgSO ₄
	MgSO ₄ ·7H ₂ O and MgCl ₂ ·6H ₂ O (binary)	16 wt%MgSO ₄ + 4 wt%MgCl ₂	PC_20binary
		32 wt%MgSO ₄ + 8 wt%MgCl ₂	PC_40binary
		48 wt%MgSO ₄ + 12 wt%MgCl ₂	PC_60binary

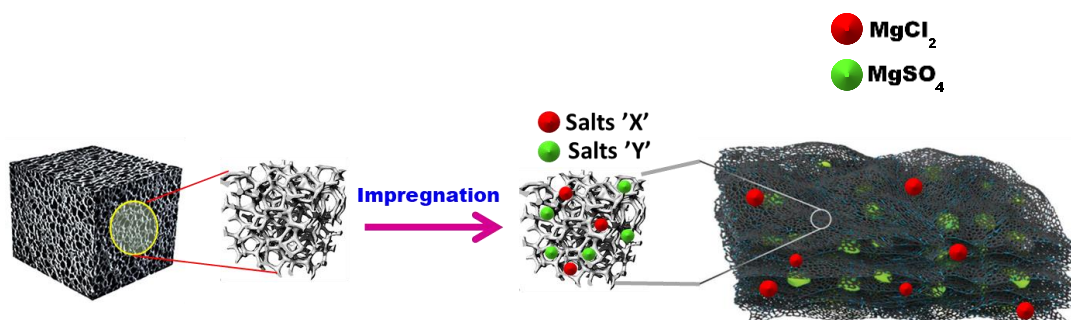


Fig. 1. Preparation of composite materials.

2.2. Physicochemical characterizations methods

X-ray Diffraction (XRD) investigations of the two series of composites' compacted powder (mono and binary) were performed on a PANalytical MPD X'Pert Pro diffractometer equipped with a Pixcel real-time multiple strip detector and operating with an angular aperture of $3.347^\circ 2\theta$ in the 3° to $80^\circ 2\theta$ range, and using CuK α radiation with a 0.15418 nm wavelength. Diffractograms were taken at 22 °C with a step size of $0.013^\circ 2\theta$ and a scan period of 220 s per step.

Using a wavelength dispersion X-ray Fluorescence (WDXRF) spectrometer (from PANalytical, Zetium), XRF experiments were carried out on pellets constituted of 0.1 g of the sample and 0.2 g of binder (boric acid, H₃BO₃) material.

A JEOL JSM-7900F Scanning Electron Microscope (SEM) was used to capture high-resolution micrographics. Energy Dispersive X-ray (EDX) was used to map the composite's atomic composition and distribution and perform a semi-quantitative chemical analysis.

Using a Micromeritics ASAP 2420 equipment, nitrogen physisorption isotherms of porous carbon and composite materials were measured at -196 °C (Micromeritics, Norcross, GA, USA). Prior to analysis, the PC and composites were degassed at 150 °C for 12 hours and then again for 2 hours in the measurement emplacement. The Brunauer, Emmett, and Teller (BET) equation (S_{BET}) ($0.01 < p/p^\circ < 0.40$) was used to calculate the specific surface area. Applying the t-plot approach, the microporous volumes (V_m) and microporous surface (S_m) were calculated (thickness range: 0.35-0.50). Finally, calculations based on density functional theory (DFT) were used to establish the pore size distribution (PSD).

2.3. Water sorption and calorimetric experiments

The heat generated by the porous carbon and its composites (as assessed by differential scanning calorimetry) and the quantities of water sorbed (as determined by the microbalance) were measured with a Sensys TG-DSC instrument associated to a Setaram humidity synthesizer (Wetsys). The samples (4 mg) were first dehydrated at 150 °C by gradually raising the temperature from 30 to 150 °C at 5 °C/min in a flow of dry air (30 mL/min), and then the temperature was kept at 150 °C during 3 h to guarantee the more extended dehydration at this temperature. After the dehydration step, the samples were cooled down at 30 °C and let under dry air until reaching a stable thermal (DSC signal) baseline. The air flow's RH was then raised to 60 % (2.55 kPa). The hydration procedure was carried on during 8 hours to fully rehydrate the material; total rehydration was achieved once the DSC signal reverted to the baseline. The hydration/dehydration conditions were chosen to be closer to those of a real home application. Flat-plate solar heat collector can provide temperature of 150 °C [55,56], while 30 °C [57] is the closest temperature to the indoor air temperature during the discharging phase at which the differential calorimeter can be stabilized. Blank experiments were carried-on in the same conditions with empty crucibles and subtracted from the sample experiment. All experiments were done in duplicate.

3. Results and discussion

3.1. Structural, textural properties of the composite materials

In order to verify the eventual crystallization of the salts deposited on the PC in the case of mono-(MgSO_4) and binary-salt (MgSO_4 and MgCl_2) composites, XRD analyses were performed. In **Fig. 2**, the XRD pattern of PC showed two broad bands. The first, in the 18-32 ° 2θ range corresponds to the (002) plan of carbon, while the second, centered between 42 and 48 ° 2θ , can be assigned to the (100) plan, both characteristic of amorphous

carbon [58]. In addition, always in **Fig. 2**, several diffraction peaks related to the presence of SiO_2 were detected at $2\theta = 20.80, 36.50, 49.45,$ and 59.68° . On all the composites containing MgSO_4 , the presence of crystallized MgSO_4 at different hydration state was found. For the sample containing 20 % of MgSO_4 , two different small peaks were visible at $18^\circ, 28^\circ,$ and 35° and 20° assigned respectively to $\text{MgSO}_4 \cdot 1.25\text{H}_2\text{O}$ (Ref. code: 00-028-0631) and $\text{MgSO}_4 \cdot 6\text{H}_2\text{O}$ (Ref. code: 00-001-0354) according to the database of X'Pert HighScore Plus software (**Fig. 2a**). In the $\text{PC}_{40}\text{MgSO}_4$ and $\text{PC}_{60}\text{MgSO}_4$ samples peaks attributed to three different hydration states of MgSO_4 ($\text{MgSO}_4 \cdot 1.25\text{H}_2\text{O}$, $\text{MgSO}_4 \cdot 4\text{H}_2\text{O}$, and $\text{MgSO}_4 \cdot 6\text{H}_2\text{O}$) were present. In the case of binary-salt composites (**Fig. 2b**), the patterns of $\text{MgSO}_4 \cdot 1.25\text{H}_2\text{O}$ and $\text{MgSO}_4 \cdot 6\text{H}_2\text{O}$ were detected. Only $\text{MgSO}_4 \cdot 4\text{H}_2\text{O}$ was not found. No peaks related to crystallized magnesium chloride were visible on all binary samples. This is probably due to the amorphous character of all or part of the MgCl_2 deposited on PC.

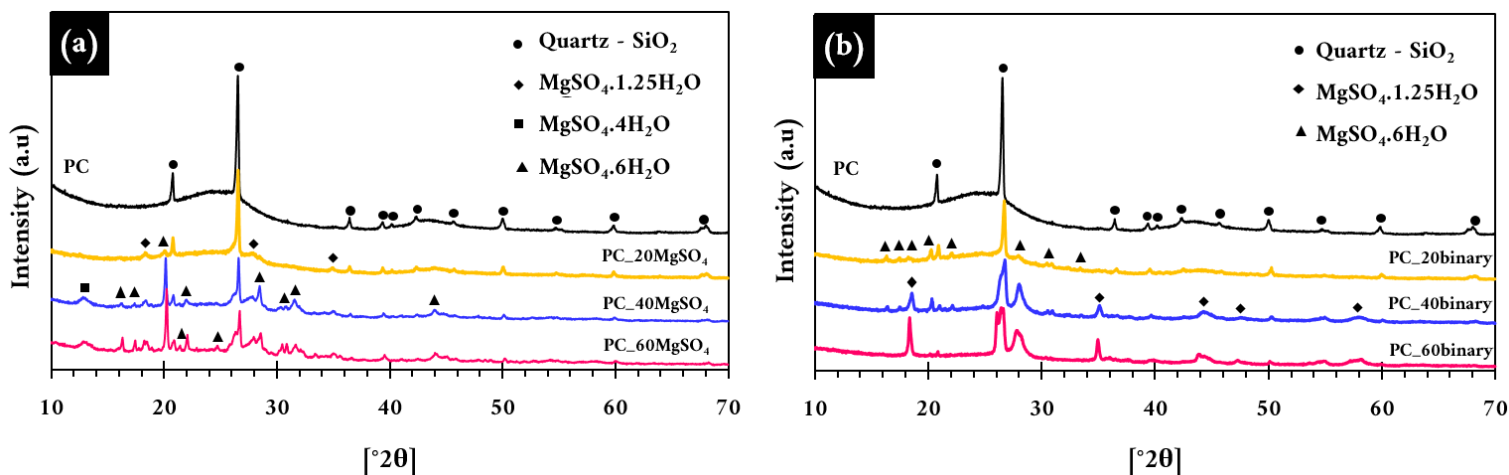


Fig. 2. a) XRD patterns of PC and its composites prepared by the impregnation of mono salt MgSO_4 , b) XRD patterns of PC and its composites prepared by the impregnation of binary salt (MgSO_4 and MgCl_2).

The exact salt content of the composites, as determined by XRF, is shown in **Table 2**. The content of each salt in the binary salt composites is as follows: $\text{PC}_{20}\text{binary}$ (15.8 wt% MgSO_4 + 2.8 wt% MgCl_2), $\text{PC}_{40}\text{binary}$ (32.5 wt% MgSO_4 + 6.07 wt% MgCl_2), and $\text{PC}_{60}\text{binary}$ (43.5 wt% MgSO_4 + 15.1 wt% MgCl_2).

Fig. 3 (a) depicts the N_2 physisorption isotherms of porous carbon (PC) and produced composites. According to the IUPAC classification [59], all composites' sorption isotherms are of type I (**Fig. 3a and 3c**), indicating the presence of a microporous network. The type I isotherm is usually associated with microporous materials with a tiny exterior surface, although some small mesopores can be found in the PC due to a little increase in N_2 adsorption at high relative pressure after filling the micropores [60]. According to the

isotherm plots of the mono-salt composites (**Fig. 3a**), the quantity of N₂ adsorbed reduces when the amount of MgSO₄ increases from 20 to 60 %, suggesting the filling or obstruction of pores by the salt. As a result, the surface specific area of PC_60MgSO₄ decreases from 962 m²/g, for the bare PC support, to 405 m²/g, for the composite. In the same way, the microporous volume was reduced by 52 % (**Table 2**). According to the isotherm plots, also for the binary-salt composites (**Fig. 3c**), increasing the quantity of binary salt (MgSO₄ + MgCl₂) from 20 to 60 %, lowered the amount of N₂ adsorbed, suggesting the filling or obstruction of pores by the salt. As a result, the surface specific area dropped down by 80 %, from 962 m²/g (PC) to 188 m²/g (PC_60 binary). The impregnation of binary salt onto PC resulted in a 76 % reduction in microporous volume (**Table 2**).

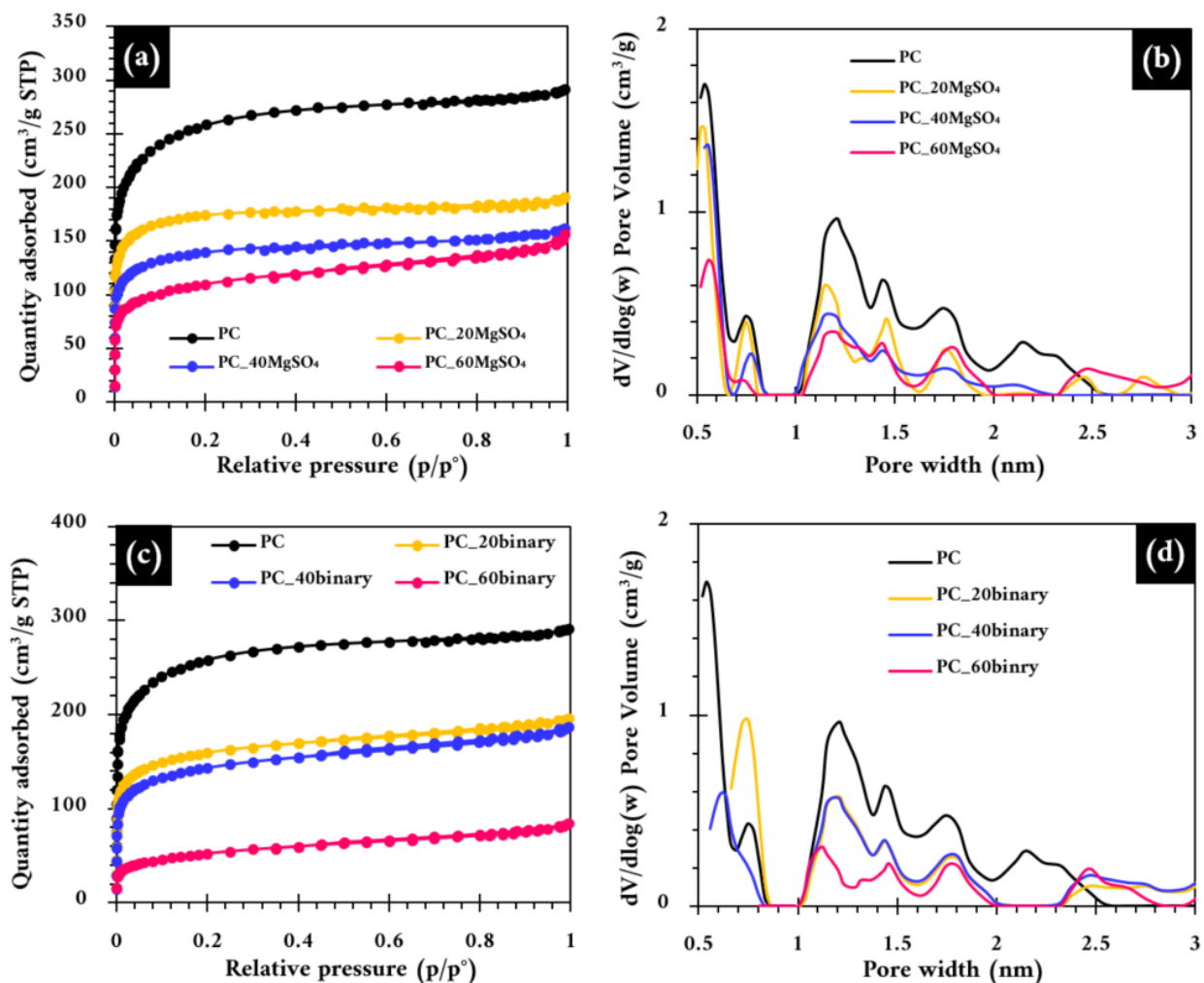


Fig. 3. a) N₂ physisorption of PC and its composites prepared by the impregnation of mono salt MgSO₄; b) Pore size distribution of PC and its composites prepared by the impregnation of mono salt MgSO₄; c) N₂ physisorption of PC and its composites prepared by the impregnation of binary salt (MgSO₄ and MgCl₂); d) Pore size distribution of PC and its composites prepared by the impregnation of binary salt (MgSO₄ and MgCl₂).

Table 2. Textural characteristics of PC and composites (mono- and binary-salts).

Sample	Salt content (wt%)	S_{BET} (m^2/g) ^a	S_{m} (m^2/g) ^b	V_{t} (cm^3/g) ^c	V_{m} (cm^3/g) ^b
PC	-	962	852	0.451	0.343
PC_20MgSO ₄	18.1	559	526	0.275	0.209
PC_40MgSO ₄	32.9	533	502	0.250	0.200
PC_60MgSO ₄	42.8	405	401	0.242	0.162
PC_20binary	18.6	600	543	0.303	0.217
PC_40binary	37.5	532	495	0.289	0.201
PC_60binary	58.6	188	188	0.131	0.082

^a Determined using the BET equation at p/p° between 0.01 and 0.40.

^b Calculated using the t -plot method with thickness range 3.5-5 Å.

^c Calculated from the amount of N₂ adsorbed at $p/p^\circ=0.99$.

Fig. 4 displays the correlation between the mono- or binary-salt content versus the pore volume (V_{t}) and the specific surface area (S_{BET}). The decreasing of the surface area is due to pore obstruction that prevents the N₂ molecule to adsorb on the interior surface; the two curves have very similar decreasing trends. The lower S_{BET} indicates the decreasing of the surface area accessible to the water molecules during the hydration process that impacts the heat storage capability. So, when preparing these composites, there the need to find a balance between the quantity of salt to be deposited and the maintaining of a relatively high surface area and porosity.

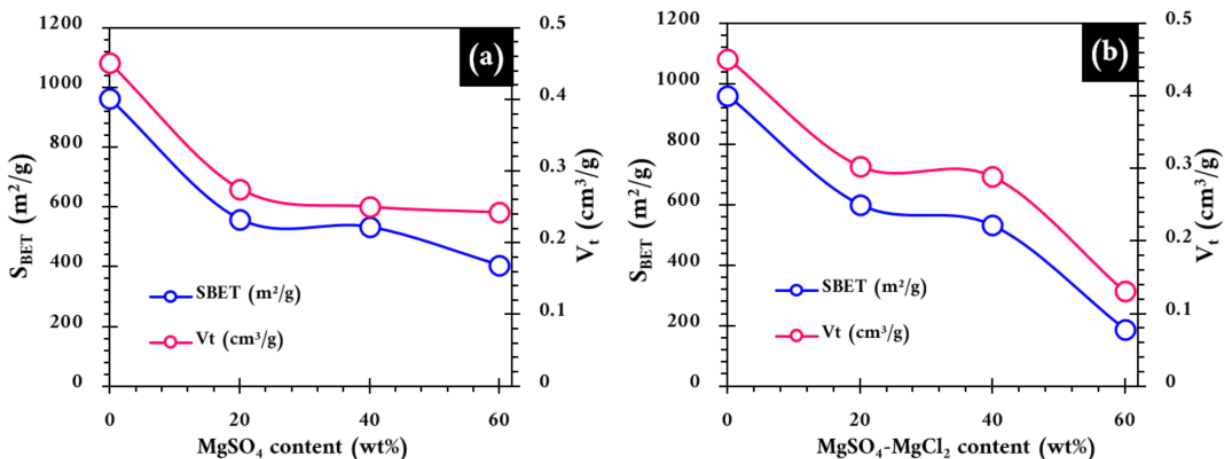


Fig. 4. Effect of MgSO₄ content (a) and MgSO₄ and MgCl₂ content (b) deposited into porous carbon on total pore volume and specific surface area of each studied sample.

SEM and EDX mapping analyses were used to study the morphology and uniformity of salt impregnation. To begin, EDX mapping of porous carbon indicated the presence of Si, as determined by XRD analysis (**Fig. 1S**) (Supplementary Information file). **Fig. 2S** shows

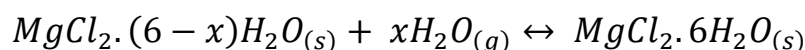
the EDX mapping images for samples containing 20, 40, and 60 %MgSO₄. For the PC 40_MgSO₄ composite, the homogeneity of the salt impregnation on the PC support can be validated. Each examined element (C, S, O, or Mg) are homogeneously distributed as shown in the cartographies (**Fig. 2S**). Nonetheless, the presence of MgSO₄-rich zones on the PC support in PC_60MgSO₄ is identified (**Fig. 2S**). The presence of such clusters may cause a variety of problems, including PC pore blockage and the formation of salt crusts. As a result, the mass transfer performance of the material might suffer as a result of these findings (i.e. slower water molecule diffusion during the hydration/dehydration process). In the case of the binary salt composites, an improved dispersion was visible also for the composites containing 60 wt% of salts.

3.2. Water sorption studies

The performance in heat storage systems is significantly influenced by the rate and capacity of water sorption in the composites. It is important to emphasize that the amount of water lost or gained during hydration, directly correlates to the variation in heat release of the sample. The boundary requirement for a good THS material is a high water sorption as a function of time and temperature. Investigating the water sorption of the material versus the rehydration time is crucial for the discovery of heat storage materials capable of providing high heat power. At a temperature of 30 °C and a RH of 60%, the hydration curves (**Fig. 5**) were examined in order to assess the hydration behavior of the prepared composites. The synthesized composites steadily adsorb the water vapor during the hydration step until reaching a plateau. All curves exhibit a conventional rehydration behavior, with the process's initial stages exhibiting the maximum water adsorption rate (a high slope value). The rate then declines until the water vapor has saturated the samples. Moreover, the salt addition shows a big impact on the global adsorption process duration, in particular concerning the time necessary to reach the water sorption equilibrium.

Fig. 5a shows that impregnating 60 % of MgSO₄ increases the water adsorption capacity from 0.10 g/g by PC to 0.48 g/g. Surprisingly, increasing the quantity of impregnated salt from 40 % (0.46 g/g) to 60 % (0.48 g/g) does not boost the water uptake for the mono-salt composites. The reason of this trend might be related to the behavior of the salt during hydration; MgSO₄ salt tends to agglomerate and can create a hard crust on the support surface, preventing the further hydration of the underneath salt layers. In the same conditions (results reported in **Fig. 5c**), the pure MgCl₂ salt showed a higher adsorption capacity (2.65 g/g) than the pure MgSO₄ (0.81 g/g), as well as improved adsorption kinetics. This does not necessarily imply that it is the best option for heat storage applications due to eventual leakage problems of MgCl₂ when RH is higher than its DRH (33 % at 30 °C for MgCl₂); overhydration and deliquescence can occur if the RH during adsorption is higher than the DRH of the salt. On the other hand, because the hydration conditions used in the present study are 30 °C and 60 % RH, being the DRH of MgSO₄

around 90 %, the possibility of deliquescence is negligible. For MgCl₂ the possibility of generating a saturated solution is high, which leads to the formation of aggregates and eventually the formation of salt crusts blocking the PC pores during the successive hydration/dehydration steps and having a negative impact on the water mass transfer. Moreover, it has been documented that at a RH higher than the DRH, MgCl₂ showed a strong propensity to decompose under hydrothermal conditions forming strong acid, for instance HCl, which can damage the equipment utilized and affect the salt hydrate's heat storage capacity [61]. To solve these limitations, binary salt impregnation is performed by limiting the quantity of MgCl₂ in all preparations by 20 % (80 %MgSO₄ + 20 %MgCl₂ = 100 %); MgCl₂ is just used as a “water pump” to facilitate the diffusion of the water molecules and facilitate the hydration of MgSO₄. According to **Fig. 5c**, the mass transfer and adsorption capacity of MgSO₄ salt hydrate are both fairly low. The MgCl₂ salt, on the other hand, present an improved water adsorption behavior, allowing the hydration reaction here to take over easily:



The absorbed water will inexorably interact with MgSO₄. During hydration, the water vapor captured by the composite would first interact with the salt particles' external surfaces before migrating into underneath salt molecules. The hydration curves of the binary-salt composites (**Fig. 5b**) demonstrated a faster hydration kinetic and water adsorption capacity than for the mono-salt samples. In addition, PC_60binary (0.75 g/g) outperformed PC_60MgSO₄ (0.48 g/g) in terms of water uptake.

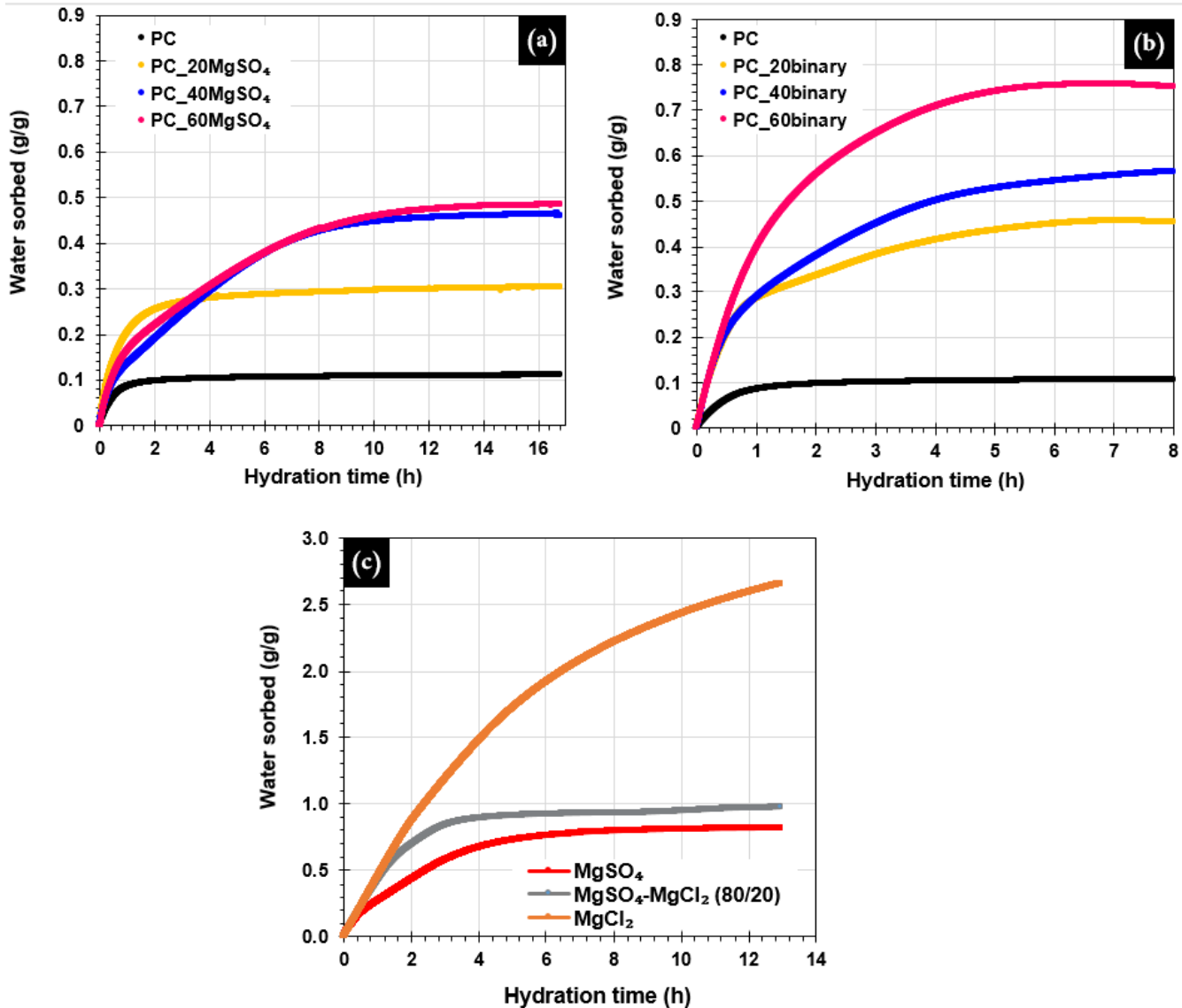


Fig. 5. Water sorption kinetic at 30°C and 60 % RH. (a): Porous carbon and mono-salt composites; (b): Binary-salt composites; (c): Pure and mixed salt.

The total (V_t) and microporous (V_m) volume values are reported in **Table 2**. The relationship between the total pore volume and the water adsorption capacity as functions of the salt content are depicted in **Fig. 6**. For the mono-salt composites (**Fig. 6a**), the V_t dramatically decreases with the salt content, until reaching a plateau for the 40 % MgSO₄ containing composite. The water uptake shows the opposite trend. In the case of binary-salt composites (**Fig. 6b**), the water uptake continuously increases even at higher salt loadings, due to the improvement of the mass transfer due to the presence of MgCl₂.

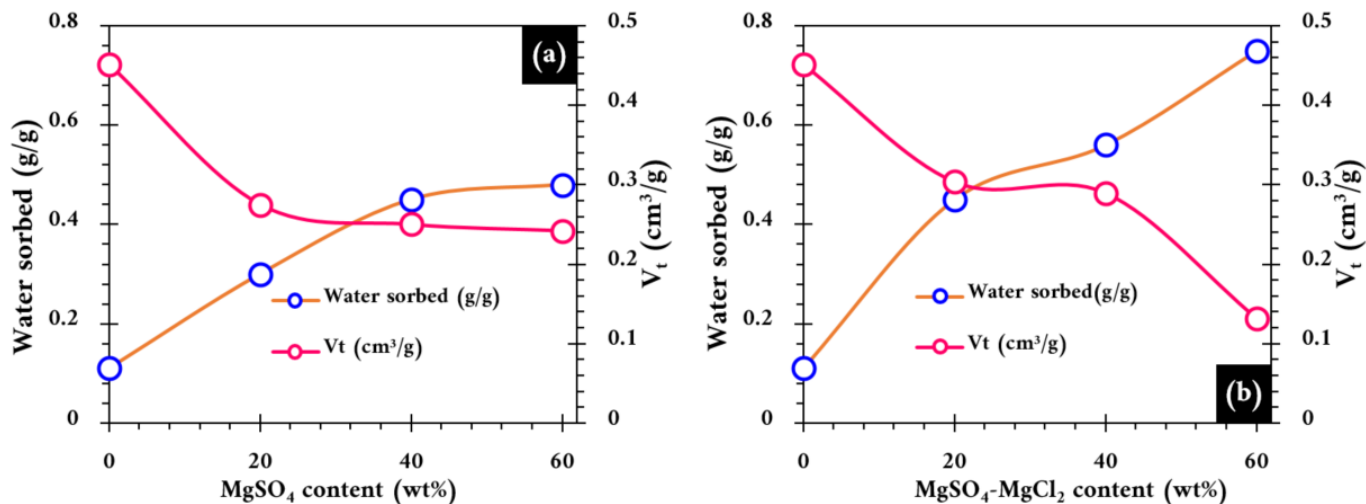


Fig. 6. Effect of salt content on water sorbed and pore volume (a): Porous carbon and mono-salt composites; (b): Binary-salt composites

3.2. Adsorption Kinetic investigation

Fig. 7 depicts the time evolution of the heat flow and the water adsorption. Since the dehydration of $\text{MgSO}_4 \cdot 7\text{H}_2\text{O}$ took place at 150°C , the initial hydration state of the salt previous to hydration corresponds to $\text{MgSO}_4 \cdot \text{H}_2\text{O}$. It has also to be underlined that, at room temperature, $\text{MgSO}_4 \cdot 7\text{H}_2\text{O}$ loses very easily a molecule of H_2O to transform into $\text{MgSO}_4 \cdot 6\text{H}_2\text{O}$. Then, it can be assumed that 1 molecule of $\text{MgSO}_4 \cdot \text{H}_2\text{O}$ can adsorb 5 molecules of H_2O , by the following reaction: $\text{MgSO}_4 \cdot \text{H}_2\text{O} + 5\text{H}_2\text{O} \rightarrow \text{MgSO}_4 \cdot 6\text{H}_2\text{O}$.

To clarify, as an example, the PC-20MgSO₄ composite contains 80 %PC and 20 %MgSO₄, so 1 g of PC-20MgSO₄ (0.8 g PC + 0.2 g MgSO₄) adsorbs maximum: $0.8 \cdot 0.1 = 0.08$ g H₂O and 0.2 g MgSO₄ adsorbs maximum: $0.2 \cdot \frac{M(\text{H}_2\text{O}) \cdot 5}{M(\text{MgSO}_4)}$, which equals 0.143 g. As a result, 1 g of PC-20MgSO₄ can absorb up to $0.08 + 0.143 = 0.223$ g of H₂O, corresponding to the orange point on the blue curve (**Fig. 7**). This point is placed at 1.54 h of hydration. However, the water uptake signal continues to rise, which is explained by water condensation on the composite surface.

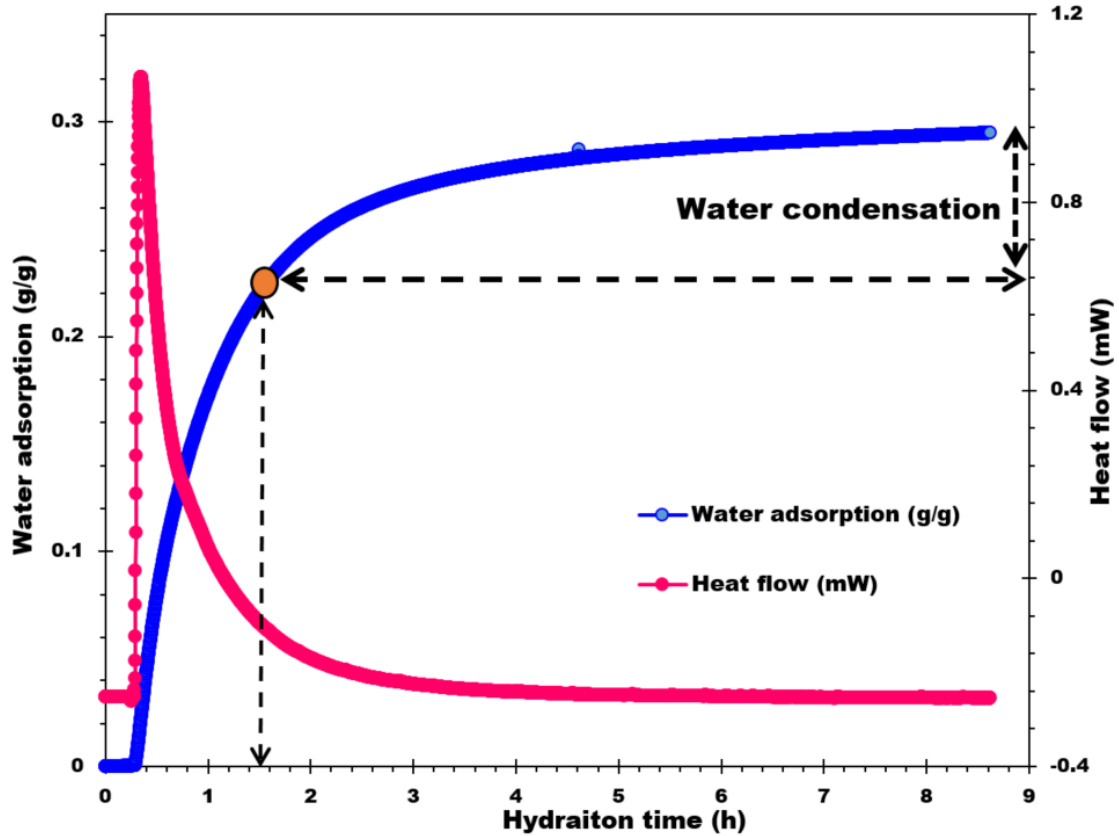


Fig. 7: Curves of the time evolution of heat flux and water adsorption

Based on the above explanations, the kinetic data of all developed composites will be studied in the 0 - 1.54 h range, then excluding the part related to condensation.

Two kinetic models based on different mass transfer assumptions were used to examine the kinetics of the water sorbed onto the various composites. In both approaches, the composite was assumed to be a spherical particle ($R = 1.5 \text{ mm}$).

The first mass transfer model (M1) assumes that diffusion takes part in a homogeneous and porous spherical particle. The salt is considered to be perfectly dispersed in the particle porosity. Water's differential mass balance is described by the following equation:

$$\frac{\partial W^*}{\partial t} = \frac{1}{r^2} \frac{\partial}{\partial r} \left(r^2 D_w \frac{\partial W^*}{\partial r} \right) \quad \text{Equation 1}$$

with $W^* = \frac{W(t) - W_\infty}{W(t=0) - W_\infty}$ the reduced moisture content, D the effective diffusion coefficient, t the time and r the radius.

This differential equation is solved with two boundary conditions ($\left. \frac{\partial W^*}{\partial r}\right|_{r=0} = 0$ and $W^*(r = R, t) = W_\infty^*$) and an initial conditions $W^*(t = 0) = W_0^* = 1$

After separation of variables, the analytical solution of this problem is:

$$W^*(r, t) = 1 - \sum_{n=1} (-1)^n \frac{2R}{n\pi r} e^{-\frac{n^2\pi^2 Dt}{R^2}} \sin\left(\frac{n\pi r}{R}\right) \quad \text{Equation 2}$$

The average water content in the particle $\bar{W}(t)$ is:

$$\bar{W}(t) = W_\infty + (W_0 - W_\infty) \sum_{n=1} \frac{6}{n^2\pi^2} e^{-\frac{n^2\pi^2 Dt}{R^2}} \quad \text{Model M1}$$

The second mass transfer model (M2) assumes that the salt is exclusively deposited on the external surface, forming a homogeneous layer (of thickness *equal to* “e”) around the particle. The mass transfer consists, in this case, in the water molecule diffusion towards the salt layer. The differential equation corresponds to eq.1, except for the boundary conditions ($r = R+e$, $W^*(R + e, t) = W_\infty^*$ and $r = R$, $\frac{\partial W^*}{\partial r}(r = R) = 0$)

Starting from these assumptions, the average water content in the salt layer is:

$$\bar{W}(t) = W_\infty + (W_0 - W_\infty) \sum_{k=0} \frac{8}{(2k + 1)^2\pi^2} e^{-\frac{(2k+1)^2\pi^2 Dt}{e^2}} \quad \text{Model M2}$$

The thickness of the salt layer is directly calculated from the deposited mass of salt. The diffusion coefficient is estimated by fitting the experimental water content with the analytical equations.

a) Kinetic investigation of mono-salt composites

The results of the fitting (numerical approximation by minimizing a quadratic criterion) are reported in **Fig. 4S** (Supplementary Information file) and the obtained diffusion coefficients are reported in **Table 3**. In the first model, the diffusion coefficient represents an effective mass transfer coefficient in the particle. If the mass transfer limitation would be only due to the diffusion into the pores, then this coefficient should be independent of the amount of salt, but in reality the diffusion coefficient varies with the increasing of the salt amount and the model M1 assumptions do not agree with the result. The second model assumes the transfer of water molecules through a homogeneous layer with a thickness

proportional to the salt ratio. In this case, the estimated diffusion coefficient is very similar for all composites, indicating that the model's assumptions (M2) and the experimental tests are in good agreement.

Table 3: Estimated diffusion coefficient for the two models

Composite	PC_20MgSO ₄	PC_40MgSO ₄	PC_60MgSO ₄
%salt	18.1 %	32.9 %	42.8 %
D (M1) (m ² /s)	6.0 E-11	1.1 E-11	5.7 E-12
D (M2) (m ² /s)	2.4 E-14	2.1 E-14	2.5 E-14

b) Kinetic investigation of binary-salt composites

In the case of the binary-salt composites, neither of the two mass transfer models provides a good fit for the kinetics of the water uptake process (**Fig. 5S**). This suggests that both mass transfer models are simply inaccurate representations of the real physical phenomena. The comparison of the experimental results with the modeling suggests that the diffusion process is facilitated (higher diffusion coefficient) when the adsorption time is longer; this behavior is due to the presence of magnesium chloride. The hydration of the first layer of salt helps the water transfer to the under-layers. The properties of the salt layer change with the degree of hydration.

3.2. Heat released investigation

The heat storage capacity of the developed composites was measured experimentally using the coupled thermogravimetric and differential thermal analyzers. This instrument allows to measure the released heat during the adsorption process. Due to their high water sorption capacity, binary- salt composites release more heat than mono-salt composites. Moreover, the evolution of the heat released shows the same trend than the water uptake. The heat released values for the PC_20binary, PC_40binary, and PC_60binary are respectively of 1156 J/g, 1684 J/g, and 1840 J/g. PC_20MgSO₄, PC_40MgSO₄, and PC_60MgSO₄ have values of 740 J/g, 1354 J/g, and 1356 J/g, respectively (**Fig. 9**). Compared to mono salt (MgSO₄) impregnated on PC, the binary-salt composites show an improvement in the heat released capacity. As a result, MgSO₄ + MgCl₂ containing composites possess higher hydration heats than MgSO₄ mono-salt composites. By impregnating PC with 60 %MgSO₄, the heat released by this composite achieves 52 % (1356 J/g) of the heat released by the pure MgSO₄ (**Fig. 9**). However, by impregnating PC with 60 % of the MgSO₄ + MgCl₂ salt mixture, the heat generated considerably increased and was equal to 70 % (1840 J/g) of the heat liberated by pure mixed salt (MgSO₄ + MgCl₂) (2639 J/g) (**Fig. 9**), which is a very interesting result.

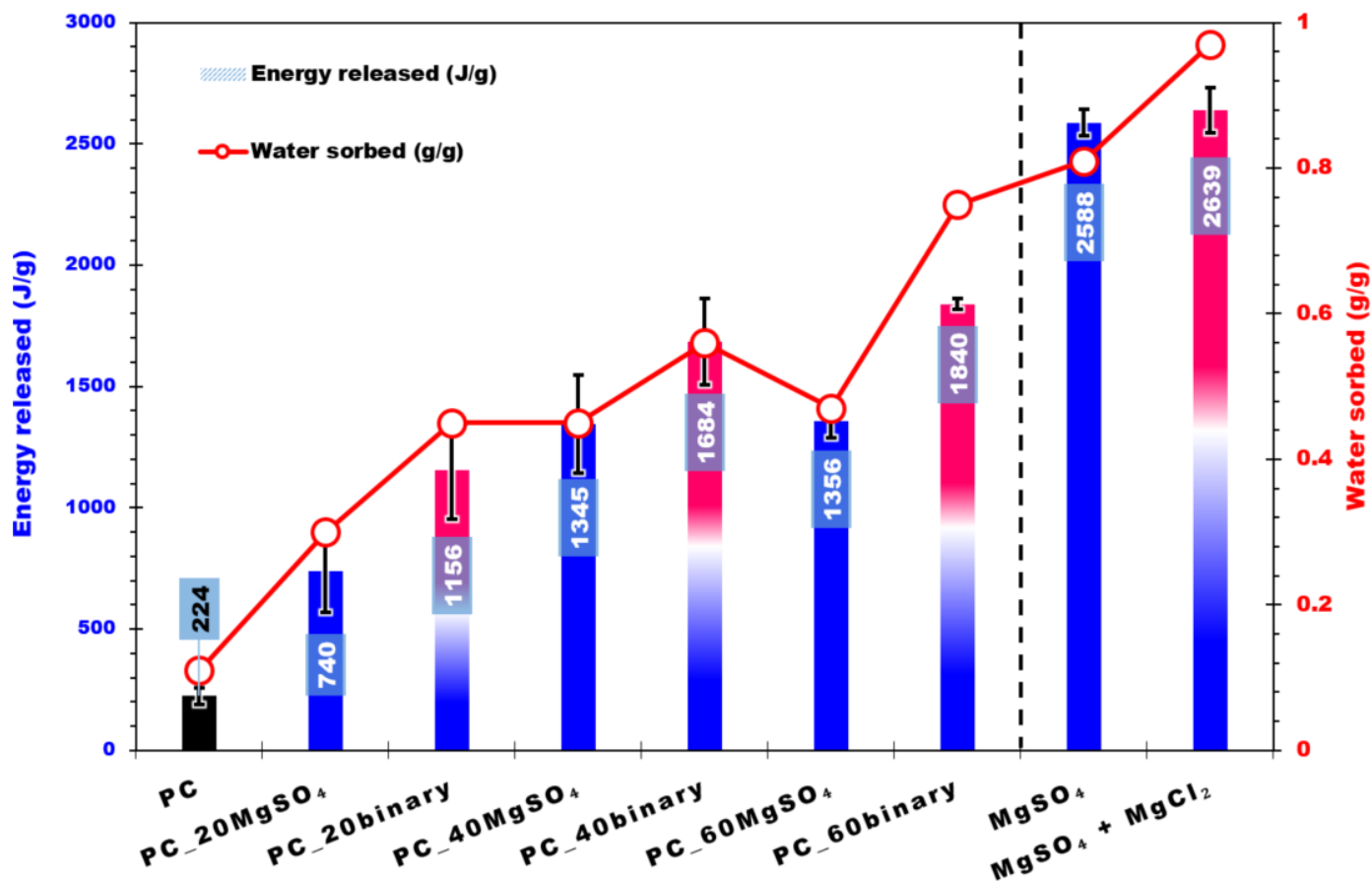


Fig. 9: Heat released from hydrated PC, composites, and salts at 30°C and 60 % RH.

For comparison, the performance of the composites developed in this research outperforms that of the majority of composites described in previously published papers (see Table 4). For example, Posern and Kaps [61] employed attapulgite as matrix material, preparing a binary salt composite, by mixing MgCl₂ with MgSO₄, for heat storage systems. They varied the mixing ratio and the adsorption/desorption temperature to measure the sorption heat under various conditions. Composite sorbents with 32.8 wt% salt content (80/20 wt% salt solutions of MgSO₄ and MgCl₂, respectively) presented a heat storage density of 1590 J/g at a hydration temperature of 30 °C and a water vapor pressure of 36 mbar. They discovered that the higher the MgCl₂ content in the composite sorbents, the greater the water absorption and the heat released. However, salt solution leakage was an identified problem. Therefore, our work successfully addressed this leakage problem and kept improving the heat released.

Table 4. Comparison of developed composites (this work) and other heat storage composites (literature).

Matrix	Salt	Salt content (wt%)	Heat storage capacity (J/g)	Adsorption temperature (°C)	Desorption temperature (°C)	Humidity Relative (%)	Ref.
Porous carbon (PC)	-	-	224	30	150	60	This work
	MgSO ₄	20	740	30	150	60	
		40	1354	30	150	60	
		60	1356	30	150	60	
	MgSO ₄ :MgCl ₂	16:4	1156	30	150	60	
		32:8	1684	30	150	60	
		48:12	1840	30	150	60	
Activated carbon	MgSO ₄	30	1324	30	300	60	[23]
Diatomite	MgSO ₄	60	773	25	120	85	[62]
Zeolite 13x	MgSO ₄	15	632	25	150	80	[28]
SBA-15	CaCl ₂	60	1711	25	150	30	[26]
MIL-101(Cr)-NH ₂	CaCl ₂	45	1205	30	120	32	[32]
MIL-101(Cr)-SO ₃ H	CaCl ₂	43	1274	30	120	32	
MIL-101(Cr)	CaCl ₂	47	1118	30	120	32	
-	MgSO ₄ :ZnSO ₄	9:1	1422	45	120	75	[39]
-	CaCl ₂ :MgSO ₄	6:4	1886	40	300	65	[63]
13X-ZMS	CaCl ₂ : MgSO ₄	10: 54: 36	1414	40	300	65	
NaY-ZMS	CaCl ₂ : MgSO ₄	20: 48: 32	1097	40	300	65	

By plotting the heat released and the total volume versus the salt content (**Fig. 6S**), a similar trend to that observed in terms of water uptake evolution (**Fig. 6a and 6b**) is shown (**Fig. 6S**). This observation confirms that the heat released is directly related to the amount of water sorbed. As shown in **Fig. 6S-b**, the heat released reaches a plateau starting from 40 % of MgSO₄ deposited. The heat released increased by adding MgCl₂ due to the improvement of the mass transfer.

4. Conclusion

This main objective of this study was to thoroughly evaluate the heat released and mass transfer of various composites obtain by impregnating mono-salt (MgSO₄) or binary-salts (MgSO₄+MgCl₂) on porous carbon (PC) for THS applications. The research focused on

the impacts of mono- and binary-salt impregnation on the structural-textural properties of the resulting composites. Their water sorption and heat release behavior were also investigated. In comparison to mono-salt composites, binary-salt composites showed a faster hydration kinetics and an improved water adsorption capacity. Furthermore, in terms of water uptake, PC_60binary (0.75 g/g) sample outperformed the PC_60MgSO₄ sample (0.48 g/g). The kinetic investigation showed that the mass transfer was improved by adding MgCl₂. Two models were applied to determine the diffusion coefficient in the different composites. The model based on the existence of a layer of salt on the external surface of the composite particle best fitted the experimental results for the composites containing MgSO₄ only. When MgCl₂ was added, the water adsorption process was modified and both the considered models did not provide a satisfactory numerical approximation of the experimental results. The salt layer seems to evolve with the adsorption extent, facilitating the water transfer when increasing the hydration of the salt layers. A new model might be developed taking in consideration the physical evidences and successive modifications of the layers.

Additionally, the heat released follows the same behavior as the water absorption. PC_60MgSO₄ produces 52 % (1356 J/g) of the heat provided by pure MgSO₄. However, it is important to note that when the PC is impregnated with 60 % binary salt (PC_60binary), the heat generated is equivalent to 70 % of the heat released by the pure mixed salt (2639 J/g). The large availability of types of carbon materials, the possibility to tailor the amount of deposited salt, as well as the option to add a second salt to create a binary-salt composites, can bring to new composites with morphologies and physical-chemical properties adapted to THS applications. Composites with high heat storage density and high heat power (improved hydration kinetics) can be then designed.

Credit author statement

Mohamed Zbair: Conceptualization, Methodology, Writing - Original Draft, Writing - Review & Editing. **Minh Hoang Nguyen:** Investigation, Visualization, Formal analysis, Data curation. **Patrick Dutournié:** Methodology, Writing-Review & Editing, Supervision, Validation, Formal Analysis, Data Curation. **Simona Bennici:** Project administration, Validation, Methodology, Writing-Review & Editing, Resources, Supervision, Conceptualization, Funding acquisition.

Funding: - Region Grand Est for providing funding for the acquisition of the TG-DSC *equipment within the "STOCKFATAL" project and for the contribution to Mr. Minh Hoang Nguyen's thesis grant.*

- Carnot MICA Institute and Region Grand Est for funding part of this study in the frame of the STOCKENER project.

- IS2M for the postdoctoral grant of M. Zbair in the frame of the “*Projets Structurants*” call.

Acknowledgments: All physicochemical characterizations were performed on the IS2M technical platforms. The authors are very grateful to L. Michelin (XRF), L. Josien (SEM+EDX), and Cyril Vaultot (N₂ adsorption) experiments for their contributions.

Declaration of Competing Interest

The authors declare that they have no known competing financial interests or personal relationships that could have appeared to influence the work reported in this paper.

References

- [1] Asgharian H, Baniasadi E. A review on modeling and simulation of solar energy storage systems based on phase change materials. *J Energy Storage* 2019;21:186–201. <https://doi.org/10.1016/j.est.2018.11.025>.
- [2] Sharma A, Chauhan R, Ali Kallioğlu M, Chinnasamy V, Singh T. A review of phase change materials (PCMs) for thermal storage in solar air heating systems. *Mater Today Proc* 2021;44:4357–63. <https://doi.org/10.1016/j.matpr.2020.10.560>.
- [3] Olivkar PR, Katekar VP, Deshmukh SS, Palatkar S V. Effect of sensible heat storage materials on the thermal performance of solar air heaters: State-of-the-art review. *Renew Sustain Energy Rev* 2022;157:112085. <https://doi.org/10.1016/j.rser.2022.112085>.
- [4] Sonar D. Renewable energy based trigeneration systems—technologies, challenges and opportunities. *Renewable-Energy-Driven Futur.*, Elsevier; 2021, p. 125–68. <https://doi.org/10.1016/B978-0-12-820539-6.00004-2>.
- [5] Sharma A, Pitchumani R, Chauhan R. Solar air heating systems with latent heat storage - A review of state-of-the-art. *J Energy Storage* 2022;48:104013. <https://doi.org/10.1016/j.est.2022.104013>.
- [6] Liu H, Wang X, Wu D. Fabrication of Graphene/TiO₂/Paraffin Composite Phase Change Materials for Enhancement of Solar Energy Efficiency in Photocatalysis and Latent Heat Storage. *ACS Sustain Chem Eng* 2017;5:4906–15. <https://doi.org/10.1021/acssuschemeng.7b00321>.
- [7] Liu Y, Zheng J, Deng Y, Wu F, Wang H. Effect of functional modification of porous medium on phase change behavior and heat storage characteristics of form-stable composite phase change materials: A critical review. *J Energy Storage* 2021;44:103637. <https://doi.org/10.1016/j.est.2021.103637>.
- [8] Kant K, Pitchumani R. Advances and opportunities in thermochemical heat storage systems for buildings applications. *Appl Energy* 2022;321:119299. <https://doi.org/10.1016/j.apenergy.2022.119299>.
- [9] Zhang T, Jin X, Owens G, Chen Z. Remediation of malachite green in wastewater by ZIF-

8@Fe/Ni nanoparticles based on adsorption and reduction. *J Colloid Interface Sci* 2021;594:398–408. <https://doi.org/10.1016/j.jcis.2021.03.065>.

- [10] Airò Farulla G, Cellura M, Guarino F, Ferraro M. A Review of Thermochemical Energy Storage Systems for Power Grid Support. *Appl Sci* 2020;10:3142. <https://doi.org/10.3390/app10093142>.
- [11] Rammelberg HU, Osterland T, Priehs B, Opel O, Ruck WKL. Thermochemical heat storage materials – Performance of mixed salt hydrates. *Sol Energy* 2016;136:571–89. <https://doi.org/10.1016/j.solener.2016.07.016>.
- [12] Yan T, Wang RZ, Li TX, Wang LW, Fred IT. A review of promising candidate reactions for chemical heat storage. *Renew Sustain Energy Rev* 2015;43:13–31. <https://doi.org/10.1016/j.rser.2014.11.015>.
- [13] Palomba V, Frazzica A. Comparative analysis of thermal energy storage technologies through the definition of suitable key performance indicators. *Energy Build* 2019;185:88–102. <https://doi.org/10.1016/j.enbuild.2018.12.019>.
- [14] An GL, Wang LW, Gao J. Two-stage cascading desorption cycle for sorption thermal energy storage. *Energy* 2019;174:1091–9. <https://doi.org/10.1016/j.energy.2019.03.069>.
- [15] Yan T, Kuai ZH, Wu SF. Experimental investigation on a MnCl₂–SrCl₂/NH₃ thermochemical resorption heat storage system. *Renew Energy* 2020;147:874–83. <https://doi.org/10.1016/j.renene.2019.09.033>.
- [16] Yan TS, Li TX, Xu JX, Wang RZ. Water sorption properties, diffusion and kinetics of zeolite NaX modified by ion-exchange and salt impregnation. *Int J Heat Mass Transf* 2019;139:990–9. <https://doi.org/10.1016/j.ijheatmasstransfer.2019.05.080>.
- [17] Kang Y, Li L, Li B. Recent progress on discovery and properties prediction of energy materials: Simple machine learning meets complex quantum chemistry. *J Energy Chem* 2021;54:72–88. <https://doi.org/10.1016/j.jechem.2020.05.044>.
- [18] Zbair M, Bennici S. Survey Summary on Salts Hydrates and Composites Used in Thermochemical Sorption Heat Storage: A Review. *Energies* 2021;14:3105. <https://doi.org/10.3390/en14113105>.
- [19] Aristov YI, Restuccia G, Tokarev MM, Buerger HD, Freni A. Selective water sorbents for multiple applications. 11. CaCl₂ confined to expanded vermiculite. *React Kinet Catal Lett* 2000. <https://doi.org/10.1023/A:1010351815698>.
- [20] Zhang Y, Miao Q, Jia X, Jin Y, Li Z, Tan L, et al. Diatomite-based magnesium sulfate composites for thermochemical energy storage: Preparation and performance investigation. *Sol ENERGY* 2021;224:907–15. <https://doi.org/10.1016/j.solener.2021.05.054>.
- [21] Gaeini M, Rouws AL, Salari JWO, Zondag HA, Rindt CCM. Characterization of microencapsulated and impregnated porous host materials based on calcium chloride for thermochemical energy storage. *Appl Energy* 2018;212:1165–77. <https://doi.org/10.1016/j.apenergy.2017.12.131>.
- [22] El Tabbal G, Dangla P, Vandamme M, Bottoni M, Granet S. Modelling the drying shrinkage of porous materials by considering both capillary and adsorption effects. *J Mech Phys Solids* 2020;142:104016. <https://doi.org/10.1016/j.jmps.2020.104016>.

- [23] Bennici S, Dutournié P, Cathalan J, Zbair M, Nguyen MH, Scullier E, et al. Heat storage: Hydration investigation of MgSO₄/active carbon composites, from material development to domestic applications scenarios. *Renew Sustain Energy Rev* 2022;158:112197. <https://doi.org/10.1016/j.rser.2022.112197>.
- [24] Aristov Y., Restuccia G, Cacciola G, Parmon V. A family of new working materials for solid sorption air conditioning systems. *Appl Therm Eng* 2002;22:191–204. [https://doi.org/10.1016/S1359-4311\(01\)00072-2](https://doi.org/10.1016/S1359-4311(01)00072-2).
- [25] Jänchen J, Stach H. Adsorption properties of porous materials for solar thermal energy storage and heat pump applications. *Energy Procedia* 2012;30:289–93. <https://doi.org/10.1016/j.egypro.2012.11.034>.
- [26] Silvester L, Touloumet Q, Kamaruddin A, Chassagneux F, Postole G, Auroux A, et al. Influence of Silica Functionalization on Water Sorption and Thermochemical Heat Storage of Mesoporous SBA-15/CaCl₂ Composites. *ACS Appl Energy Mater* 2021;4:5944–56. <https://doi.org/10.1021/acsaem.1c00786>.
- [27] Nguyen MH, Zbair M, Dutournié P, Gervasini A, Vaultot C, Bennici S. Toward new low-temperature thermochemical heat storage materials: Investigation of hydration/dehydration behaviors of MgSO₄/Hydroxyapatite composite. *Sol Energy Mater Sol Cells* 2022;240:111696. <https://doi.org/10.1016/j.solmat.2022.111696>.
- [28] Wang Q, Xie Y, Ding B, Yu G, Ye F, Xu C. Structure and hydration state characterizations of MgSO₄-zeolite 13x composite materials for long-term thermochemical heat storage. *Sol Energy Mater Sol Cells* 2019;200:110047. <https://doi.org/10.1016/j.solmat.2019.110047>.
- [29] Xu JX, Li TX, Chao JW, Yan TS, Wang RZ. High energy-density multi-form thermochemical energy storage based on multi-step sorption processes. *Energy* 2019;185:1131–42. <https://doi.org/10.1016/j.energy.2019.07.076>.
- [30] Ding B, Xu C, Liao Z, Ye F. Study on long-term thermochemical thermal storage performance based on SrBr₂-expanded vermiculite composite materials. *J Energy Storage* 2021;42:103081. <https://doi.org/10.1016/j.est.2021.103081>.
- [31] Shkatulov AI, Houben J, Fischer H, Huinink HP. Stabilization of K₂CO₃ in vermiculite for thermochemical energy storage. *Renew Energy* 2020;150:990–1000. <https://doi.org/10.1016/j.renene.2019.11.119>.
- [32] Shi W, Zhu Y, Shen C, Shi J, Xu G, Xiao X, et al. Water sorption properties of functionalized MIL-101(Cr)-X (X=–NH₂, –SO₃H, H, –CH₃, –F) based composites as thermochemical heat storage materials. *Microporous Mesoporous Mater* 2019;285:129–36. <https://doi.org/10.1016/j.micromeso.2019.05.003>.
- [33] Ait Ousaleh H, Sair S, Zaki A, Younes A, Faik A, El Bouari A. Advanced experimental investigation of double hydrated salts and their composite for improved cycling stability and metal compatibility for long-term heat storage technologies. *Renew Energy* 2020;162:447–57. <https://doi.org/10.1016/j.renene.2020.08.085>.
- [34] Li W, Klemeš JJ, Wang Q, Zeng M. *Development and characteristics analysis of salt-hydrate based composite sorbent for low-grade thermochemical energy storage*. *Renew Energy* 2020;157:920–40. <https://doi.org/10.1016/j.renene.2020.05.062>.
- [35] D'Ans P, Courbon E, Permyakova A, Nouar F, Simonnet-Jégat C, Bourdreux F, et al. A

new strontium bromide MOF composite with improved performance for solar energy storage application. *J Energy Storage* 2019;25:100881. <https://doi.org/10.1016/j.est.2019.100881>.

- [36] Mahon D, Henshall P, Claudio G, Eames PC. Feasibility study of MgSO₄ + zeolite based composite thermochemical energy stores charged by vacuum flat plate solar thermal collectors for seasonal thermal energy storage. *Renew Energy* 2020;145:1799–807. <https://doi.org/10.1016/j.renene.2019.05.135>.
- [37] Li W, Klemeš JJ, Wang Q, Zeng M. Salt hydrate–based gas-solid thermochemical energy storage: Current progress, challenges, and perspectives. *Renew Sustain Energy Rev* 2022;154:111846. <https://doi.org/10.1016/j.rser.2021.111846>.
- [38] Lin J, Zhao Q, Huang H, Mao H, Liu Y, Xiao Y. Applications of low-temperature thermochemical energy storage systems for salt hydrates based on material classification: A review. *Sol Energy* 2021;214:149–78. <https://doi.org/10.1016/j.solener.2020.11.055>.
- [39] Rehman AU, Khan M, Maosheng Z. Hydration behavior of MgSO₄–ZnSO₄ composites for long-term thermochemical heat storage application. *J Energy Storage* 2019;26:101026. <https://doi.org/10.1016/j.est.2019.101026>.
- [40] Xu C, Yu Z, Xie Y, Ren Y, Ye F, Ju X. Study of the hydration behavior of zeolite-MgSO₄ composites for long-term heat storage. *Appl Therm Eng* 2018;129:250–9. <https://doi.org/10.1016/j.applthermaleng.2017.10.031>.
- [41] Narayanan S, Li X, Yang S, McKay I, Kim H, Wang EN. Design and Optimization of High Performance Adsorption-Based Thermal Battery. Vol. 1 Heat Transf. Energy Syst. Thermophys. Prop. Theory Fundam. Res. Heat Transf., American Society of Mechanical Engineers; 2013. <https://doi.org/10.1115/HT2013-17472>.
- [42] Zhang YN, Wang RZ, Li TX. Thermochemical characterizations of high-stable activated alumina/LiCl composites with multistage sorption process for thermal storage. *Energy* 2018;156:240–9. <https://doi.org/10.1016/j.energy.2018.05.047>.
- [43] Furukawa H, Gándara F, Zhang Y-B, Jiang J, Queen WL, Hudson MR, et al. Water Adsorption in Porous Metal–Organic Frameworks and Related Materials. *J Am Chem Soc* 2014;136:4369–81. <https://doi.org/10.1021/ja500330a>.
- [44] Gordeeva LG, Aristov YI. Composites ‘salt inside porous matrix’ for adsorption heat transformation: a current state-of-the-art and new trends. *Int J Low-Carbon Technol* 2012;7:288–302. <https://doi.org/10.1093/ijlct/cts050>.
- [45] Zheng X, Ge TS, Wang RZ, Hu LM. Performance study of composite silica gels with different pore sizes and different impregnating hygroscopic salts. *Chem Eng Sci* 2014;120:1–9. <https://doi.org/10.1016/j.ces.2014.08.047>.
- [46] Linnow K, Niermann M, Bonatz D, Posern K, Steiger M. Experimental Studies of the Mechanism and Kinetics of Hydration Reactions. *Energy Procedia* 2014;48:394–404. <https://doi.org/10.1016/j.egypro.2014.02.046>.
- [47] Hongois S, Kuznik F, Stevens P, Roux J-J. Development and characterisation of a new MgSO₄–zeolite composite for long-term thermal energy storage. *Sol Energy Mater Sol Cells* 2011;95:1831–7. <https://doi.org/10.1016/j.solmat.2011.01.050>.
- [48] van Essen VM, Zondag HA, Gores JC, Bleijendaal LPJ, Bakker M, Schuitema R, et al. Characterization of MgSO₄ Hydrate for Thermochemical Seasonal Heat Storage. *J Sol*

Energy Eng 2009;131. <https://doi.org/10.1115/1.4000275>.

- [49] Donkers PAJ, Beckert S, Pel L, Stallmach F, Steiger M, Adan OCG. Water Transport in $\text{MgSO}_4 \cdot 7\text{H}_2\text{O}$ During Dehydration in View of Thermal Storage. *J Phys Chem C* 2015;119:28711–20. <https://doi.org/10.1021/acs.jpcc.5b08730>.
- [50] Kim Y, Kim N, Kim TS, Park GJ, Kwon Y, Yu HK. $\text{Mg}(\text{OH})_2$ nano-sheet decorated MgO micro-beams by electron beam irradiation for thermochemical heat storage. *Ceram Int* 2019;45:18908–13. <https://doi.org/10.1016/j.ceramint.2019.06.126>.
- [51] Gutierrez A, Ushak S, Mamani V, Vargas P, Barreneche C, Cabeza LF, et al. Characterization of wastes based on inorganic double salt hydrates as potential thermal energy storage materials. *Sol Energy Mater Sol Cells* 2017;170:149–59. <https://doi.org/10.1016/j.solmat.2017.05.036>.
- [52] Li W, Zeng M, Wang Q. Development and performance investigation of $\text{MgSO}_4/\text{SrCl}_2$ composite salt hydrate for mid-low temperature thermochemical heat storage. *Sol Energy Mater Sol Cells* 2020;210:110509. <https://doi.org/10.1016/j.solmat.2020.110509>.
- [53] Villada C, Ding W, Bonk A, Bauer T. Simulation-Assisted Determination of the Minimum Melting Temperature Composition of $\text{MgCl}_2\text{--KCl--NaCl}$ Salt Mixture for Next-Generation Molten Salt Thermal Energy Storage. *Front Energy Res* 2022;10. <https://doi.org/10.3389/fenrg.2022.809663>.
- [54] Sun W, Zhou Y, Feng J, Fang X, Ling Z, Zhang Z. Compounding $\text{MgCl}_2 \cdot 6\text{H}_2\text{O}$ with $\text{NH}_4\text{Al}(\text{SO}_4)_2 \cdot 12\text{H}_2\text{O}$ or $\text{KAl}(\text{SO}_4)_2 \cdot 12\text{H}_2\text{O}$ to Obtain Binary Hydrated Salts as High-Performance Phase Change Materials. *Molecules* 2019;24:363. <https://doi.org/10.3390/molecules24020363>.
- [55] Donkers PAJ, Sögütöglü LC, Huinink HP, Fischer HR, Adan OCG. A review of salt hydrates for seasonal heat storage in domestic applications. *Appl Energy* 2017;199:45–68. <https://doi.org/10.1016/j.apenergy.2017.04.080>.
- [56] Whiting G, Grondin D, Bennici S, Auroux A. Heats of water sorption studies on zeolite– MgSO_4 composites as potential thermochemical heat storage materials. *Sol Energy Mater Sol Cells* 2013;112:112–9. <https://doi.org/10.1016/j.solmat.2013.01.020>.
- [57] Bennici S, Polimann T, Ondarts M, Gonze E, Vaultot C, Le Pierrès N. Long-term impact of air pollutants on thermochemical heat storage materials. *Renew Sustain Energy Rev* 2020;117:109473. <https://doi.org/10.1016/j.rser.2019.109473>.
- [58] Baccile N, Weber J, Falco C, Titirici M-M. Characterization of Hydrothermal Carbonization Materials. In: TITIRICI M-M, editor. *Sustain. Carbon Mater. from Hydrothermal Process.*, Oxford, UK: John Wiley & Sons, Ltd; 2013, p. 151–211. <https://doi.org/10.1002/9781118622179.ch6>.
- [59] Thommes M, Kaneko K, Neimark A V., Olivier JP, Rodriguez-Reinoso F, Rouquerol J, et al. Physisorption of gases, with special reference to the evaluation of surface area and pore size distribution (IUPAC Technical Report). *Pure Appl Chem* 2015;87:1051–69. <https://doi.org/10.1515/pac-2014-1117>.
- [60] Elmouwahidi A, Bailón-García E, Pérez-Cadenas AF, Maldonado-Hódar FJ, Carrasco-Marín F. Activated carbons from KOH and H_3PO_4 -activation of olive residues and its application as supercapacitor electrodes. *Electrochim Acta* 2017;229:219–28. <https://doi.org/10.1016/j.electacta.2017.01.152>.

- [61] Posern K, Kaps C. Calorimetric studies of thermochemical heat storage materials based on mixtures of MgSO₄ and MgCl₂. *Thermochim Acta* 2010;502:73–6. <https://doi.org/10.1016/j.tca.2010.02.009>.
- [62] Zhang Y, Miao Q, Jia X, Jin Y, Li Z, Tan L, et al. Diatomite-based magnesium sulfate composites for thermochemical energy storage: Preparation and performance investigation. *Sol Energy* 2021;224:907–15. <https://doi.org/10.1016/j.solener.2021.05.054>.
- [63] Xueling Z, Feifei W, Qi Z, Xudong L, Yanling W, Yejiang Z, et al. Heat storage performance analysis of ZMS-Porous media/CaCl₂/MgSO₄ composite thermochemical heat storage materials. *Sol Energy Mater Sol Cells* 2021;230:111246. <https://doi.org/10.1016/j.solmat.2021.111246>.

Fast hydration kinetics and remarkable heat storage capacity of new binary salt materials for heat storage applications

Mohamed Zbair^{1,2}, Minh Hoang Nguyen^{1,2}, Patrick Dutournié^{1,2}, Simona Bennici^{1,2*}

¹ Institut de Science des Matériaux de Mulhouse (IS2M), Université de Haute-Alsace, CNRS, IS2M UMR 7361, F-68100 Mulhouse, France; mohamed.zbair@uha.fr; minh-hoang.nguyen@uha.fr; patrick.dutournié@uha.fr; simona.bennici@uha.fr

² Université de Strasbourg, France

*Correspondance : simona.bennici@uha.fr; Tel.: +33 (0)3 89336729

Supplementary Information

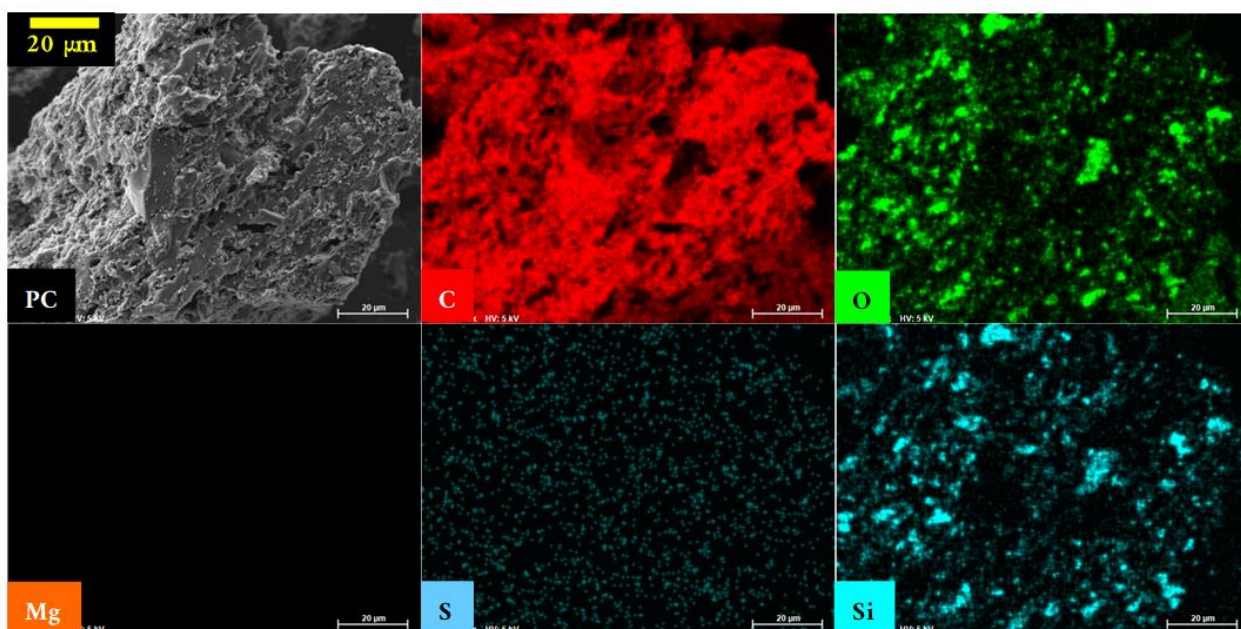


Fig. 1S. SEM and EDX mapping of the porous carbon.

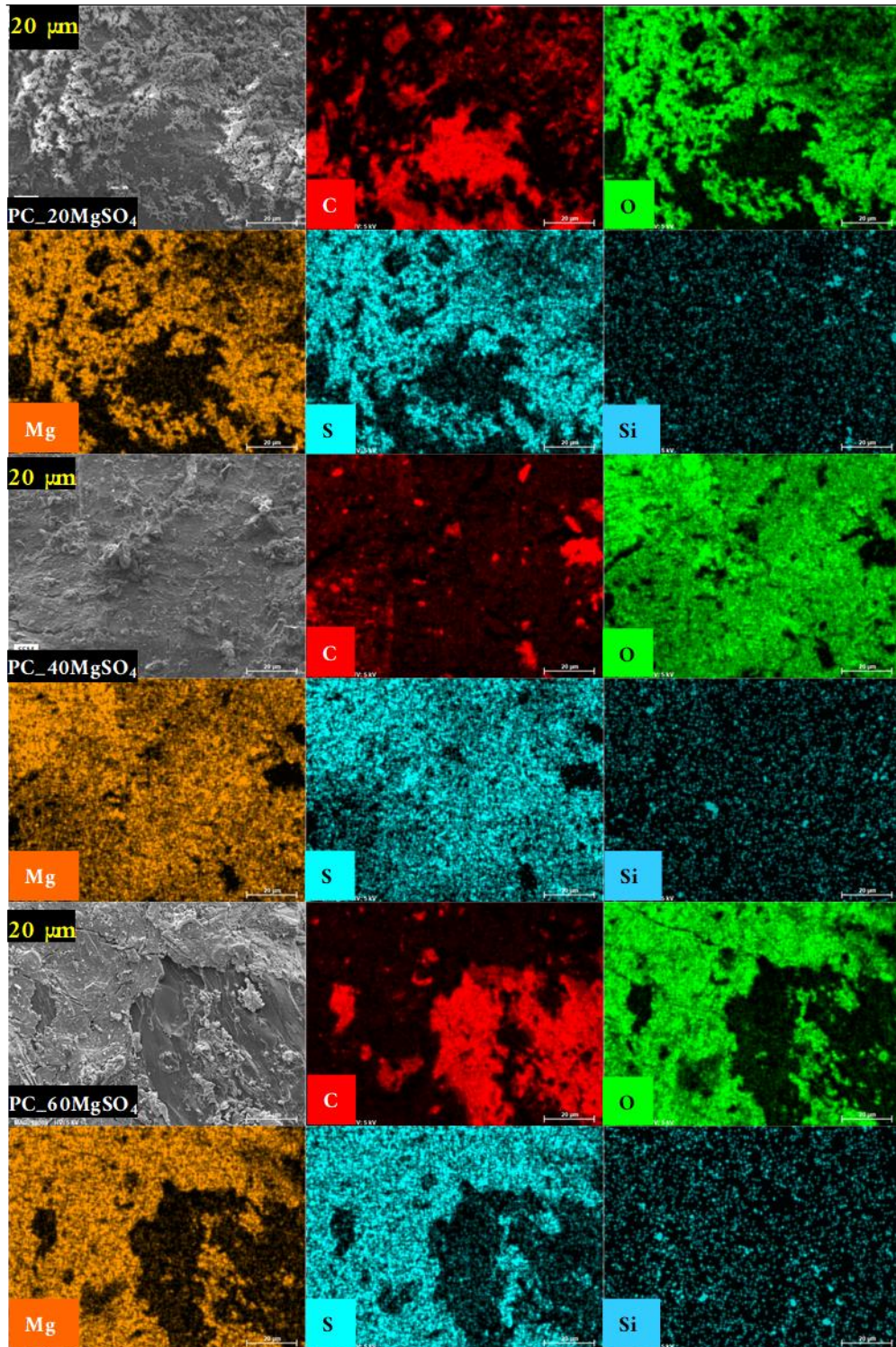


Fig. 2S. SEM and EDX mapping of composites prepared by the impregnation of mono salt MgSO_4

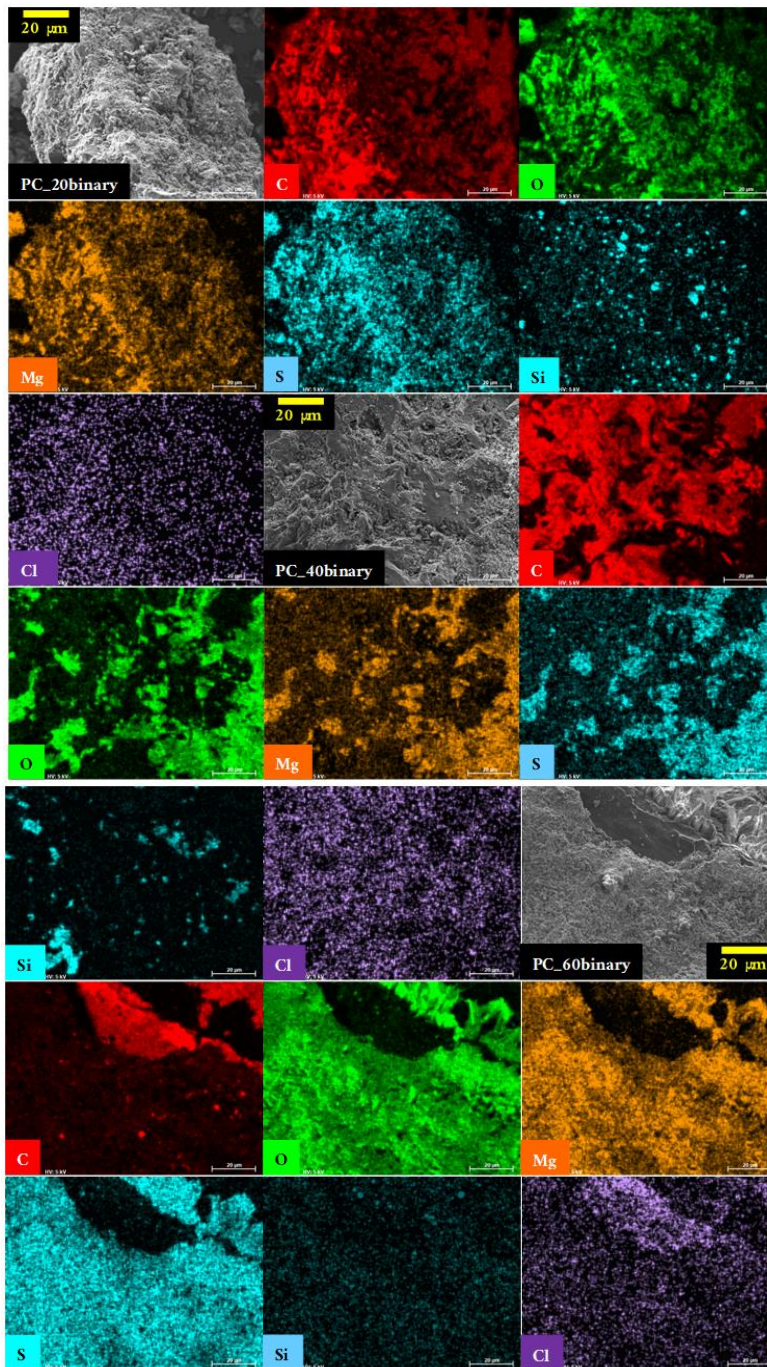


Fig. 3S. SEM and EDX mapping of composites prepared by the impregnation of binary salt (MgSO_4 and MgCl_2).

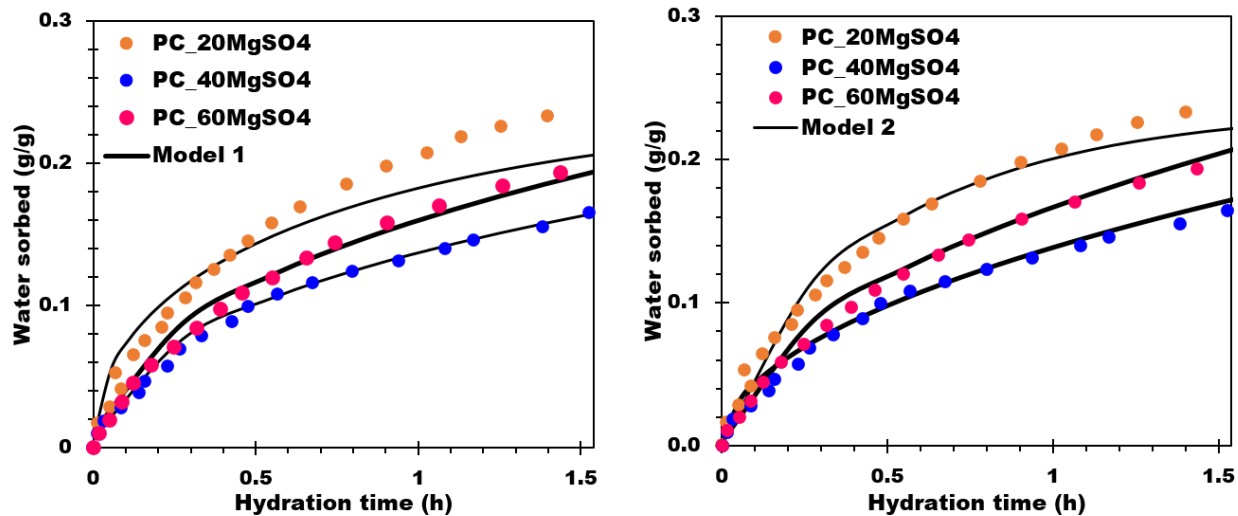


Fig. 4S. Kinetic data of mono salt impregnation fitted by Model 1 and Model 2.

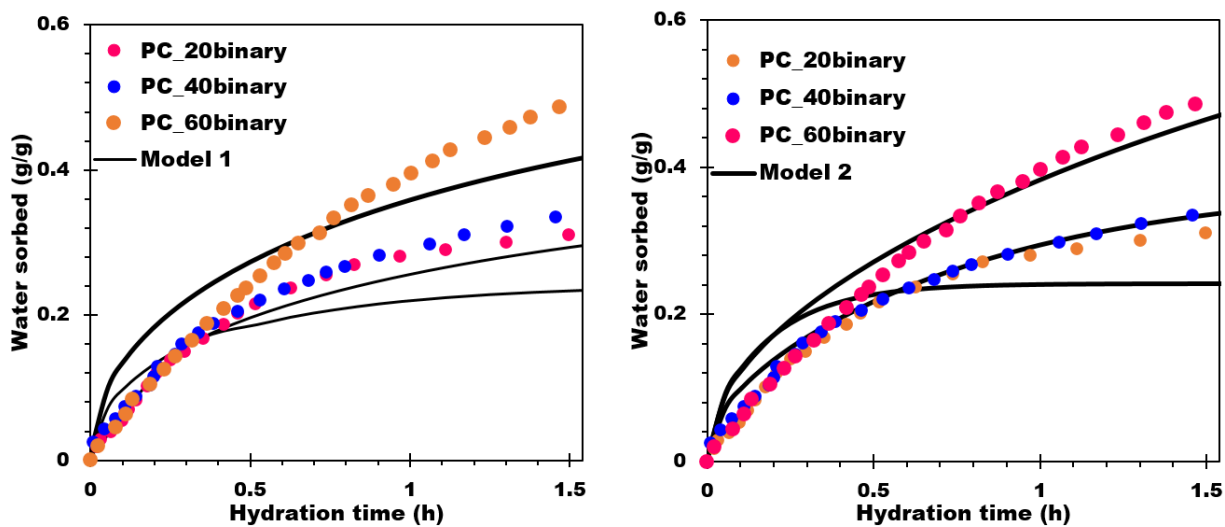


Fig. 5S. Kinetic data of binary salt impregnation fitted by Model 1 and Model 2.

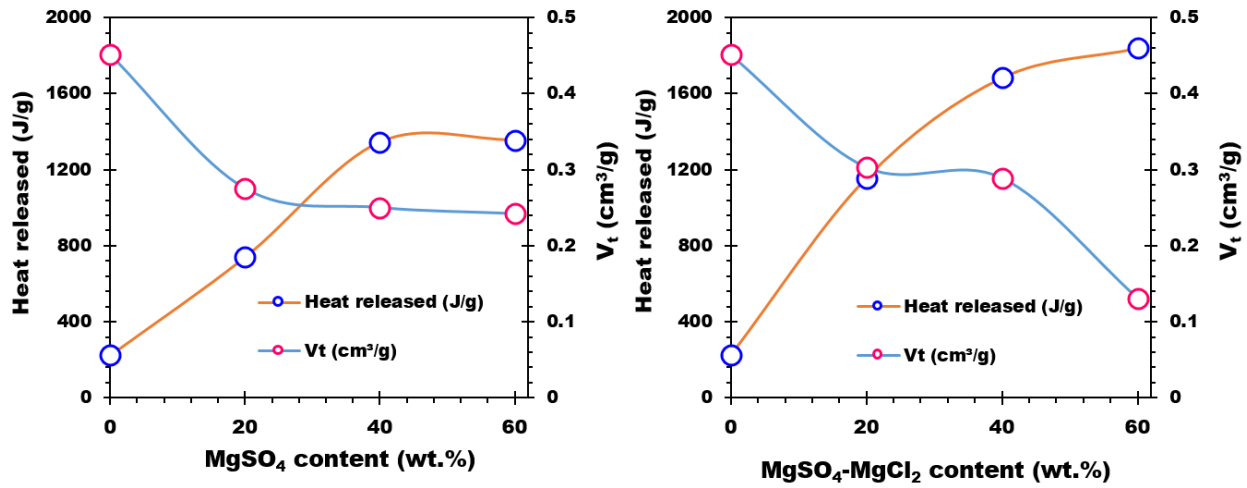


Fig. 6S. Effect of salt content on heat released and pore volume (a): Porous carbon and monosalt impregnation composites; (b): Binary salt impregnation composites

GENERAL CONCLUSION

General conclusion

Reducing fossil fuel consumption and promoting sustainable use of renewable energy sources are predominant in dealing with today's energy crisis. Thermochemical heat storage is a promising method that allows storing a large amount of energy in the form of chemical potential. Theoretically, the energy stored in this form offers little or no heat loss over time, which is very beneficial for long-term/seasonal storage applications. In this context, the objectives of the research work were primarily to evaluate and to improve the performance of the thermochemical heat storage materials with the operating conditions, as close as possible to practical applications.

Thermochemical heat storage systems are based on storing thermal energy by making use of reversible chemical reactions. With the advantages of zero-toxicity, low-cost and high energy density storage, hygroscopic salts are considered the best candidates for the applications. $\text{MgSO}_4\text{-H}_2\text{O}$ pair has high theoretical energy density (2.8 GJ/m^3) and high deliquescence relative humidity (90 % at $30 \text{ }^\circ\text{C}$), which is a potential working pair for the long-term storage systems. However, this energy density was difficult to reach due to the kinetic hindrance affecting the mass and heat transfer thus leading to poor cyclability. The synthesis of salt/support composites by impregnating a hygroscopic salt into a porous matrix is a solution to overcome the drawback of the slow hydration kinetic of MgSO_4 . Consequently, MgSO_4 -based materials have been discussed in this thesis and one of the first step was to choose an adequate porous matrix.

Ultimately, five different porous adsorbents were chosen based on their specific surface area and pore size to host MgSO_4 at different compositions: beads activated carbon, hydroxyapatite (HAP), two types of granular activated carbon, and a biochar derived from corncob. In order to understand the influence of the physicochemical properties of the adsorbents after the impregnation, characterization techniques were applied to all the materials (original support and synthesized composites). The analytical techniques employed were N_2 , CO_2 physisorption and Hg intrusion porosimetry for porous network investigation, phase analysis with X-ray diffraction, morphological investigation and chemical composition mapping by SEM coupled to EDX. Moreover, the hydration/dehydration process was carefully investigated by the study of the kinetics of the hydration. The determination of the sorption capacity and the heat released were performed; these are crucial properties to decide whether a storage material is adapted to real applications.

Activated carbon beads derived from petroleum residues were chosen as support for the first series of composites because of their high specific surface area, low cost and non-toxicity. Three composites with MgSO_4 contents of 1, 5.2, and 7.6 % were prepared. The support and the synthesized composites are microporous materials with pore sizes ranging from 0.6 to 2.0 nm. Such small pore size can prevent salt molecules from entering the pores during impregnation. The salt tends to remain on the surface of the support and block the access of the pores which affects, during the use of the storage material, the mass transfer. The water sorption results show a good hydration level ($0.33 \text{ g}_{\text{water}}/\text{g}_{\text{mat}}$) accompanied by heat of hydration of 838 J/g of composite, for the material containing 7.6 % MgSO_4 . Stability to successive cycles of hydration/dehydration has been demonstrated for 10 cycles.

Then for the first time, HAP was tested as a support for the design of a heat storage material. Two composites containing 5 and 20 % MgSO_4 were prepared. The analysis of the N_2 adsorption isotherms shows that the composites prepared with HAP are mesoporous materials with specific surfaces of the order of $100 \text{ m}^2/\text{g}$ which can facilitate the inclusion of the salt in the porosity of the matrix of the support. The storage capacity and the water adsorption capacity of the composite containing 20 % MgSO_4 were shown to be stable after 20 sorption cycles. The average energy density of the composite was measured: 472 J/g of composite.

The third series of composites was prepared using another mesoporous support: the commercial granular activated carbon L27W. A series of composites were prepared with salt contents varying between 5 and 50 % by mass. The specific surface gradually decreased by increasing the amount of salt deposited, but the porous distribution remained unchanged. This behavior suggests that the salt enters into the pores, thus decreasing the space available for the adsorption of N_2 molecules. The composite with a salt content of 30 % gave the best results in terms of storage capacity (1.3 kJ/g of composite, for a water adsorption capacity of more than 50 % by mass). Good cyclability has also been demonstrated for 8 cycles of adsorption/desorption.

The next series of composites based on MgSO_4 were prepared on a biochar derived from the pyrolysis of corncobs. Four composites with different MgSO_4 contents (ranging from 5 % to 20 % by mass) were successfully prepared. While the analyzes of the CO_2 adsorption isotherms showed that the material is mainly microporous, the analysis of Hg intrusion test shows the existence of a network of macropores. In terms of storage density, the composite containing 20 % MgSO_4 has a storage capacity of 635 J/g and a hydration level of $0.235 \text{ g}_{\text{water}}/\text{g}_{\text{mat}}$.

Finally, commercial granular activated carbon F22W was chosen as support for two series of composites: the first conventionally containing MgSO_4 (20 %, 40 % and 60 % by mass) and the other coupling two hydrated salts (MgSO_4 and MgCl_2 in a 4:1 ratio and with the same total concentrations of salts chosen for the series containing MgSO_4 alone). The analysis of the N_2 isotherms shows that all these composites are microporous materials. The specific surface area of F22W activated carbon is $962 \text{ m}^2/\text{g}$ and decreases to $405 \text{ m}^2/\text{g}$ for the mono-salt composite containing 60 % MgSO_4 and to $188 \text{ m}^2/\text{g}$ for the bi-salt composite containing 60 % of the mixture ($\text{MgSO}_4 + \text{MgCl}_2$). The water sorption results show that, for the same salt content, the presence of MgCl_2 improves the performance of the composite by 24 %. For experimental conditions of 30°C and 60 % RH, MgCl_2 (HRD at 30°C is 33 %) is present in its complete hydrated form and can potentially form a saturated solution. This solution could then serve as a vector for the successive molecules of water adsorbing on the composite that can then reach also the MgSO_4 (when initially not possible). This addition of a second salt makes possible to further exploit the storage capacity of MgSO_4 and therefore improves the performance of the composites under study.

Figure 17 below summarizes the sorption performance of all the adsorbents and synthesized composites at conditions of 30°C and 60 % RH that were studied during this thesis work. Most of the porous adsorbents and their synthesized composites showed an energy density in the range of 200 to $1000 \text{ J/g}_{\text{composite}}$. The binary composites exhibited a clear superiority over the other synthesized materials with energy densities of the composites all exceeding $1100 \text{ J/g}_{\text{composite}}$ thanks to the addition of the second hygroscopic salt MgCl_2 .

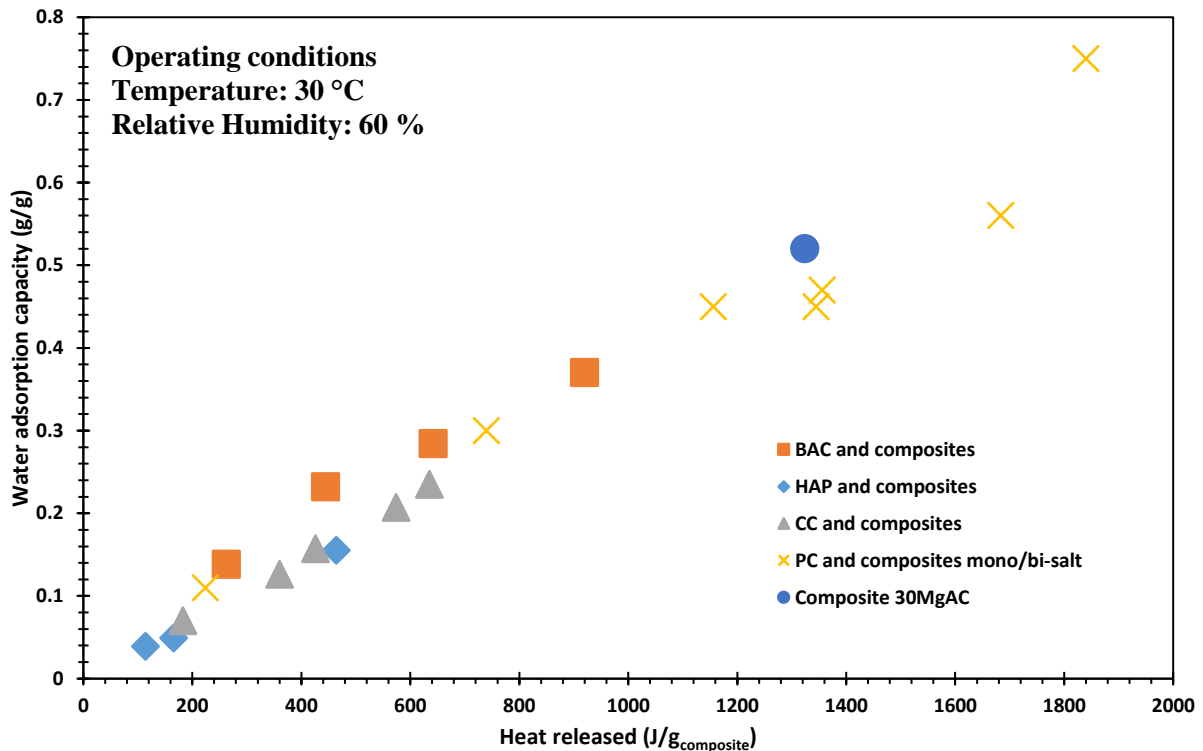


Figure 17. An overview of the performance of all the studied materials.

Future perspectives

During this thesis work, the choice of porous adsorbents with different pore distribution (micro, meso and macroporous) to be used as supports has been made. The aim was to use all the available surface to homogeneously disperse and confine a hygroscopic salt, more precisely MgSO_4 , in order to fully exploit its storage potential and to improve the performance of the overall storage system. Although the current work has shown positive results of different storage materials, several points still need to be addressed for the future development of such thermal-storage technologies using hygroscopic salt-based materials.

MgSO_4 is a hygroscopic salt with a DRH of 90 % at 30 °C and during this thesis work, the operating condition chosen was at 30 °C and a RH of 60 %. Hence, it would be significant to carry out a specific study on the influence of the RH on the performance of the composite materials. Increasing the relative humidity might increase the water adsorption capacity, thus the storage density of the studied material. It would also increase the kinetic rate during the hydration phase. More interestingly, it would be necessary to verify the behavior of the impregnated MgSO_4 at RH closest to the DRH of 90 %.

The cyclability in terms of charging/discharging has not been investigated for the composites mono/bi-salt and the corncob-based composites. Therefore, cyclability test experiments need to be conducted to examine the viability of these composites in a real-life application.

One of the highlighted results in this thesis was the addition of MgCl_2 that ultimately improved the energy density of the synthesized composites compared to the ones without the addition. Nevertheless, it is crucial to understand the mechanism behind the interactions between MgSO_4 , MgCl_2 and the water vapor. It would also be critical to synthesize other composites impregnating the same mixture of salt studied in this thesis using other porous adsorbents.

The inspiring results are obtained in this thesis with a small amount of material which is far away from a practical application. Therefore, experiments in a larger scale prototype need to be performed in order to validate the use of the studied material for practical purposes. The compactness of the fixed bed is essential and thus need to be studied carefully because it affects directly the transfer of heat and mass during the hydration and dehydration process. In addition, development of a numerical model validated by experimental results is recommended for predicting the performance of the system at different conditions.

RÉSUMÉ

1) Introduction

L'utilisation des énergies fossiles provoque des nuisances environnementales graves. Le réchauffement climatique suivi par l'élévation du niveau de la mer, la perte de biodiversité et la santé de millions de personnes dans le monde sont des conséquences sérieuses de cette surconsommation. En outre, les combustibles fossiles sont non renouvelables et les réserves sont de plus en plus réduites. Face à la raréfaction des ressources et malgré les apparences, on dispose de peu de temps pour trouver de nouvelles solutions et s'adapter à cette situation de pénurie. La transition vers des sources d'énergie renouvelable est donc cruciale.

De plus, la croissance démographique rapide au cours des dernières décennies a augmenté considérablement la demande énergétique. Avec la problématique de l'utilisation des énergies fossiles, l'implémentation de systèmes d'énergies renouvelables semble être la solution optimale pour résoudre le problème du besoin énergétique des générations futures. Parmi les différentes sources d'énergies renouvelables, l'irradiation solaire est la source d'énergie thermique la plus abondante et facile à collecter. En revanche, le caractère intermittent de cette énergie, ainsi que le déphasage de la ressource par rapport aux périodes de demandes énergétiques quotidiennes ou saisonnières sont un inconvénient important. Parallèlement, la demande d'énergie varie considérablement selon les heures du jour ou les mois. La disparité entre l'offre d'énergie et la demande nécessite donc la présence d'un système de stockage de l'énergie excédentaire qui permet de restituer cette énergie pour compenser la demande.

Par conséquent, l'intégration d'un système de stockage d'énergie thermique adéquat se révèle être une solution prometteuse pour faire face à ce décalage temporel. La chaleur sensible, la chaleur latente et la chaleur thermochimique sont les trois types d'énergies utilisées dans les systèmes de stockage de la chaleur et rapportées dans la littérature jusqu'à présent [1]. Les systèmes basés sur le stockage thermochimique de la chaleur sont les plus attractifs en termes de densité énergétique et donc d'un volume de stockage limité. De plus, le stockage thermochimique ne présente théoriquement aucune perte de chaleur au cours du processus [2]. Le principe du stockage thermochimique se base sur un procédé réversible constitué d'une réaction endothermique (charge), dans laquelle les réactifs stockant la chaleur sous forme de potentiel chimique sont séparés en utilisant la source de chaleur disponible et une réaction exothermique (décharge), pendant laquelle la chaleur est libérée grâce à la recombinaison des

réactifs. La chaleur libérée est récupérée et utilisée (pour le chauffage des bâtiments, par exemple).

La configuration la plus courante dans ce mode de stockage est basée sur les phénomènes de sorption d'un sorbat (l'eau notamment) sur un sorbant (un matériau solide). Le matériau solide doit posséder certaines caractéristiques, notamment être peu coûteux, non toxique, avoir une densité de stockage élevée, et posséder des bonnes propriétés liées aux transferts de masse et de chaleur (conductivité thermique, porosité). Le stockage par sorption diffère selon la nature du couple sorbant/sorbat et du type de liaison résultant de leur association. Les hydrates salins sont largement utilisés dans les systèmes de stockage par chimisorption, plus particulièrement par réaction chimique d'hydratation/déshydratation. Entre autres, **MgSO₄.7H₂O** est un sel hydraté avec une densité de stockage théorique de 2.8 GJ/m³ et qui valide la majorité des critères listés [3]. D'ailleurs, la température de charge est relativement basse (**150 °C**) et donc adaptée aux applications domestiques utilisant des capteurs solaires. L'autre avantage est son humidité relative de déliquescence (HRD) d'environ 90 % à **30 °C** [4] qui permet d'utiliser le matériau dans une grande gamme d'applications.

L'inconvénient de ce système est la formation d'agréats lors de la réhydratation (adsorption de l'eau) et limitant les transferts de masse qui mènent à une baisse de performance et une mauvaise cyclabilité [5]. Ainsi, la capacité de stockage n'atteint pas la valeur théorique. Pour remédier à ce problème, la solution proposée est de disperser le sel de façon homogène dans un matériau poreux présentant une bonne surface spécifique et porosité afin de produire un composite sel/support.

Pendant ces travaux de thèse, plusieurs matériaux poreux ont été testés pour déposer le sel hydraté. Les matériaux étudiés sont : les hydroxyapatites, les carbones activés et les biochars ; matériaux qui présentent des distributions de taille de pores différentes (micro, méso et macropores). Les composites ont été synthétisés par la méthode d'imprégnation par voie humide pour assurer l'homogénéité de la distribution du sel au sein de la matrice poreuse. Après un séchage à 150 °C, les composites finaux ont été caractérisés par différentes méthodes physico-chimiques pour connaître leur composition élémentaire, le type de phases présentes, leur surface spécifique ainsi que la distribution de taille des pores. Ces analyses couplées aux mesures de sorption de la vapeur d'eau nous ont permis d'évaluer le potentiel de ces matériaux dans les applications de stockage de la chaleur et de comprendre les phénomènes d'adsorption associés.

2) Résultats et discussion

Dans le manuscrit de thèse, un total de cinq types de composites à base de $\text{MgSO}_4 \cdot 7\text{H}_2\text{O}$ déposé sur différents supports (commerciaux ou préparés au laboratoire) ont été étudiés.

Chaque série de composites correspond à l'un des cinq chapitres du manuscrit. Les cinq types de matériaux apparaissent dans les chapitres en fonction de leur porosité (partant des matériaux microporeux jusqu'aux matériaux macroporeux).

Tous les échantillons ont été caractérisés en utilisant les techniques suivantes :

- Fluorescence des rayons X : pour déterminer la composition chimique de l'échantillon.
- Diffraction des rayons X : pour l'analyse des phases cristallines présentes et la détection d'éventuelles impuretés.
- Microscopie électronique à balayage couplée à l'EDX : pour visualiser la morphologie de l'échantillon et effectuer une cartographie de la composition élémentaire (distribution du sel hydraté) par spectroscopie de rayons X à dispersion d'énergie.
- Adsorption de N_2 par manométrie (- 196 °C) : pour obtenir les isothermes de sorption d'azote permettant de calculer la surface spécifique, la porosité et la distribution des tailles des pores de l'échantillon.
- Porosimétrie par intrusion de mercure : pour déterminer la distribution de tailles de pores et du volume poreux total d'un matériau macroporeux.
- Expérimentations d'hydratation/déshydratation dans un setup de thermogravimétrie-calorimètre à balayage couplée à un régulateur d'humidité : pour quantifier la quantité d'eau adsorbée et évaluer la chaleur stockée pour chaque échantillon.

Des billes de carbone activé dérivées de résidus pétroliers ont été choisies comme support pour préparer une première série de composites. Ces billes présentent une surface spécifique élevée, un faible coût et une non-toxicité. Trois composites avec des teneurs en sel MgSO_4 de 1, 5,2, et 7,6 % ont été préparés. Aucune phase secondaire n'a été détectée par DRX. L'analyse des isothermes adsorption d'azote a montré que les billes de carbone activé sont des matériaux microporeux avec une surface spécifique très élevée (de l'ordre de $1300 \text{ m}^2/\text{g}$). La distribution de tailles des pores se situe principalement entre 1 et 2 nm. Afin d'analyser plus finement la microporosité de ces échantillons, des analyses d'adsorption de CO_2 (273 K) ont également été effectuées. Elles ont permis de détecter la présence d'ultra-micropores de tailles comprises entre 0,6 et 0,85 nm. Une taille de pores si petite peut empêcher les molécules de sel de rentrer dans la matrice pendant l'imprégnation. Le sel a ainsi tendance à rester sur la surface du support et

bloquer l'accès des pores, ce qui affecte, pendant l'utilisation du matériau de stockage, le transfert de masse (migration des molécules d'eau pendant la phase d'hydratation). La cartographie EDX montre la dispersion homogène de MgSO_4 sur la surface du support, mais aucune information ne peut être déduite sur la présence de sel à l'intérieur des micropores. Les résultats de sorption d'eau montrent un bon niveau d'hydratation ($0,37 \text{ g}_{\text{eau}}/\text{g}_{\text{mat}}$) accompagné par des chaleurs d'hydratation de 920 J/g de composite, pour le matériau contenant $7,6 \%$ en masse de sel. La stabilité suivant des cycles successifs d'hydratation/déshydratation a été démontrée pour 10 cycles.

Ensuite, dans le cadre d'une **collaboration avec l'université de Milan**, nous avons testé, **pour la première fois**, de **l'hydroxyapatite** comme support pour la conception d'un matériau de stockage de la chaleur. Deux composites à base de MgSO_4 ont été préparés par imprégnation par voie humide avec 5% et 20% en masse de sel. L'analyse des isothermes d'adsorption d'azote montre que les composites préparés avec l'hydroxyapatite sont des matériaux mésoporeux avec des surfaces spécifiques de l'ordre de $100 \text{ m}^2/\text{g}$. La distribution de taille des pores se situe principalement dans le domaine mésoporeux (entre 2 et 50 nm) et à cela, de petits macropores ($50 - 100 \text{ nm}$) ce qui pourrait faciliter l'inclusion du sel dans la porosité du support. Les cartographies EDX obtenues pour les échantillons juste préparés et après 20 cycles d'hydratation/déshydratation montrent que le sel est et reste bien dispersé dans la matrice. Les résultats de sorption d'eau montrent un meilleur transfert pour les composites comparé au sel hydraté seul et au support (hydroxyapatite non imprégnée). Cette propriété est directement liée à la puissance qui peut être obtenue dans un système de stockage employant ces composites. Une bonne stabilité du composite contenant 20% en masse de sel a été prouvée en effectuant 20 cycles de sorption : la capacité de stockage et la capacité d'adsorption d'eau se sont montrées stables. La densité d'énergie moyenne du composite a été mesurée à 472 J/g de composite.

La troisième série de composites a été préparée en utilisant un autre support **mésoporeux** : il s'agit d'un **granulé de carbone activé** commercial (L27W de Norit N.V, Pays Bas). La série de composites a été préparée avec des teneurs en sel variant entre 5 et 50% en masse. Les observations par microscopie MEB montrent que le sel est déposé de façon très homogène sur la surface du carbone activé, même pour des teneurs en sel élevées (i.e. jusqu'à 40% en masse). A partir de 50% en masse de sel déposé, la dispersion est moins homogène et la présence d'agrégats de sel a été mise en évidence. La surface spécifique diminue progressivement en augmentant la quantité de sel déposée, mais la distribution poreuse reste inchangée. Ce comportement suggère que le sel est rentré dans les pores en diminuant l'espace disponible à

l'adsorption des molécules d'azote. Le composite avec une teneur en sel de 30 % en masse a donné les meilleurs résultats en termes de capacité de stockage (1,3 kJ/g de composite, pour une capacité d'adsorption d'eau de plus de 50 % en masse). Une bonne cyclabilité a également été démontrée pendant 8 cycles de sorption/désorption. Les propriétés améliorées des composites préparés à partir du carbone activé commercial rendent possible une application pratique. Pour cela, des scénarios ont été définis à partir de données expérimentales prometteuses, pour l'utilisation de ce composite dans des applications de chauffage domestique d'une habitation et de production d'eau chaude sanitaire.

Une série de composites à base de sulfate de magnésium a été préparée par imprégnation sur un **biochar** issu de la pyrolyse de **rafles de maïs**. Quatre composites comportant différentes teneurs en sel MgSO_4 (allant de 5 % à 20 % en masse) ont été préparés avec succès. Alors que les analyses des isothermes d'adsorption de CO_2 ont montré que le support est principalement microporeux, l'analyse de porosimétrie par intrusion de mercure montrent l'existence de la **macroporosité**. En analysant les cartographies EDX – (microanalyse dispersive en énergie des rayons X) des différents composites, on peut observer que pour les faibles teneurs, le sel est bien dispersé sur la totalité de la surface, externe et macroporeuse. Quelle que soit la teneur en sel, les observations (microscopie, quantité d'eau adsorbée et énergie stockée) montrent une bonne dispersion du sel à la surface et dans les macropores du matériau. En termes de performance, le composite contenant 20 % de MgSO_4 présente une capacité de stockage de 635 J/g et un niveau d'hydratation de 0,23 $\text{g}_{\text{eau}}/\text{g}_{\text{mat}}$.

Enfin, **des granulés de carbone activé commercial F22W** ont été choisis comme support en raison de leur surface spécifique élevée, de leur plus grande conductivité thermique comparée à celle d'autres matériaux adsorbants et, bien sûr, pour leur faible coût. Deux séries de composites ont été préparés : l'une contenant classiquement du MgSO_4 (20 %, 40 % et 60 % en masse) et l'autre par imprégnation de deux sels hydratés (MgSO_4 et MgCl_2 en proportion 4 :1 et avec les mêmes concentrations totales en sels choisies pour la série contenant le MgSO_4 seul). L'analyse des isothermes d'adsorption / désorption d'azote montre que tous ces composites sont des matériaux **microporeux**. La surface spécifique du carbone activé F22W est de 962 m^2/g et diminue à 405 m^2/g pour le composite mono-sel contenant 60 % de MgSO_4 et à 188 m^2/g pour le composite bi-sels contenant 60 % du mélange ($\text{MgSO}_4 + \text{MgCl}_2$). Les résultats de sorption d'eau montrent que, pour une même teneur en sel, la présence de MgCl_2 améliore les performances du composite de 24 %. Pour des conditions de réhydratation expérimentales de 30 °C et 60 % d'humidité relative, les molécules de MgCl_2 sont théoriquement sous forme

hydratées (l'humidité relative de déliquescence à 30 °C est de 33%) et pouvant potentiellement former une solution saturée. Cette solution pourrait alors servir de chemin préférentiel pour l'eau afin d'atteindre les couches inférieures de MgSO_4 (peu ou pas atteignable dans le cas du sel pur). Cet ajout d'un second sel permet d'exploiter davantage la capacité stockage du MgSO_4 et donc améliore notablement la performance des composites étudiés.

3) Conclusion générale

Avec la déplétion des sources d'énergie fossile, la transition vers des sources d'énergie plus propres et durables est cruciale et urgente. L'énergie solaire est la source la plus abondante mais il existe un déphasage entre l'offre et la demande, dû à l'intermittence du soleil. Un système de stockage de la chaleur est une solution permettant de pouvoir utiliser cette énergie lorsque les besoins sont présents. Parmi les technologies actuelles, le stockage de la chaleur thermochimique est très prometteur et présente un grand potentiel.

Ce travail de thèse se focalise donc sur la synthèse de matériaux qui peuvent être candidats pour les applications à plus grandes échelles. La phase active et aussi le matériau de cœur dans cette thèse est le sel hydraté $\text{MgSO}_4 \cdot 7\text{H}_2\text{O}$. Ce dernier est un matériau qui offre une capacité de stockage très élevé, mais qui, lorsqu'il est utilisé seul, limite les transferts de matière. La solution proposée dans cette thèse est d'imprégner le sel dans des matériaux hôtes poreux afin d'augmenter les propriétés liées au transfert de masse. Pour cela, différents matériaux poreux ont été comparés. Chaque matériau choisi présente une nature (minérale ou organique) et une distribution poreuse différentes qui impactent l'interaction avec le sel, sa dispersion et par conséquent la performance des composites synthétisés dans les cycles d'hydratation/déshydratation.

Le facteur le plus important identifié pendant ces travaux de thèse est la nécessité d'insérer les molécules de sel à l'intérieur des pores afin d'augmenter la quantité, d'utiliser toute la surface disponible et d'améliorer la dispersion. Pour trouver des corrélations entre les propriétés chimiques et morphologiques du support et les performances dans le stockage de la chaleur des composites finaux, le choix s'est focalisé sur des matériaux avec des porosités différentes (micro, méso et macroporeux). Chaque matériau a ses propres avantages. Ceux qui sont microporeux ont une grande surface spécifique, mais leurs petits pores empêchent l'insertion des molécules de sel. Les matériaux mésoporeux (ou macroporeux) ont en revanche des pores de tailles assez grands pour les accueillir. En considérant la performance de stockage des

composites synthétisés à partir de ces matériaux-là, le **carbone activé commercial F22W** est le meilleur hôte pour déposer du MgSO_4 avec une capacité de stockage allant jusqu'à 1356 J/g et un niveau d'eau adsorbée de 0,45 g/g pour le composite contenant 40 % de sel. En remplaçant 20 % du MgSO_4 imprégné par du MgCl_2 , la capacité d'adsorption du composite de bi-sel augmente de 24 %.

4) Références

1. Borri, E.; Zsembinszki, G.; Cabeza, L.F. Recent developments of thermal energy storage applications in the built environment: A bibliometric analysis and systematic review. *Appl. Therm. Eng.* **2021**, *189*, doi:10.1016/j.applthermaleng.2021.116666.
2. Zbair, M.; Bennici, S. Survey summary on salts hydrates and composites used in thermochemical sorption heat storage: A review. *Energies* **2021**, *14*, 1–33, doi:10.3390/en14113105.
3. Van Essen, V.M.; Zondag, H.A.; Cot Gores, J.; Bleijendaal, L.P.J.; Bakker, M.; Schuitema, R.; Van Helden, W.G.J.; He, Z.; Rindt, C.C.M. Characterization of MgSO_4 hydrate for thermochemical seasonal heat storage. *J. Sol. Energy Eng. Trans. ASME* **2009**, *131*, 0410141–0410147, doi:10.1115/1.4000275.
4. Okhrimenko, L.; Favergeon, L.; Johannes, K.; Kuznik, F.; Pijolat, M. Thermodynamic study of $\text{MgSO}_4 - \text{H}_2\text{O}$ system dehydration at low pressure in view of heat storage. *Thermochim. Acta* **2017**, *656*, 135–143, doi:10.1016/j.tca.2017.08.015.
5. Posern, K.; Linnow, K.; Niermann, M.; Kaps, C.; Steiger, M. Thermochemical investigation of the water uptake behavior of MgSO_4 hydrates in host materials with different pore size. *Thermochim. Acta* **2015**, *611*, 1–9, doi:10.1016/j.tca.2015.04.031.
6. Verma, R.; Nagendra, H.N.; Kasthuriengan, S.; Shivaprakash, N.C.; Behera, U. Thermal conductivity studies on activated carbon based cryopanel. *IOP Conf. Ser. Mater. Sci. Eng.* **2019**, *502*, 012197, doi:10.1088/1757-899X/502/1/012197.